Thermal-Mechanical Design of a Baffle

for the Deployable Space Telescope

J.W. Arink

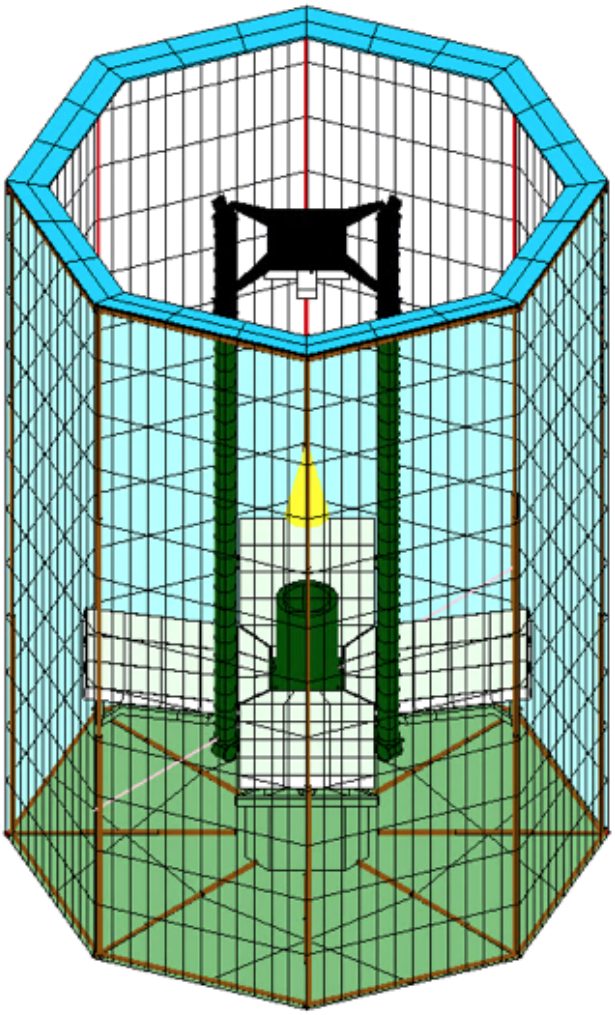

TU Delft

Thermal-Mechanical Design of a Baffle

for the Deployable Space Telescope

by

J.W. Arink

To obtain the degree of Master of Science in Aerospace Engineering
at the Delft University of Technology

Thesis Version 2.1

Student number:	4732146	
Project duration:	February 4, 2019 – October 11, 2019	
Chair:	prof. dr. ir. P.N.A.M. Visser	TU Delft
Supervisor:	dr. ir. J.M. Kuiper,	TU Delft
Supervisor:	dr. ir. M.C. Naeije,	TU Delft
External:	ir. H. Cruijssen,	Airbus Defense & Space Netherlands

Cover image: Final thermal-mechanical baffle design of the Deployable Space Telescope made by the author

TU Delft

Summary

Due to the increasing demand in high spatial resolution Earth observation telescopes, the Deployable Space Telescope (DST) has been proposed by decreasing volume, mass and costs relative to conventional telescopes. This is done by making the optical elements segmented and deployable. This, however, brings about multiple design challenges.

Firstly, the optical mirror systems need to be accurately deployed and aligned. Secondly, post-deployment deformations, mainly caused by thermo-elastic perturbations of the optical systems, shall not exceed their in-orbit drift deformation budgets. Consequently, a stable thermal environment has to be guaranteed.

To that end, a baffle has been proposed and designed as a solution to increase the thermal-mechanical stability and control of the DST sub-system temperatures and gradients. In addition to this main function, the baffle is proposed to provide another critical functionality. Namely, to attenuate and reject internal- and external stray light respectively. In addition to these two main functions, a baffle can be used to mitigate debris- and micrometeoroid impacts that would otherwise be directly exposed to the optical systems.

E. Korhonen and T. van Wees, both Aerospace Engineering master alumni students, have worked on the mechanical and thermal design and analysis of the baffle respectively. Despite the promising results, the previous thermal-mechanical design work consists of several flaws that could be corrected.

From a thermal point of view, a wrong Right Ascension of Ascending Node (RAAN) was modelled. This leads to orbits that do not experience any eclipse and thus its stability will severely decrease when placed in the right orbit with eclipse. Secondly, the stability of the thermal environment was verified against coarse-alignment budgets, which are not the most stringent thermo-elastic budgets (the in-orbit drift budgets are most stringent). Thirdly, only translational deformations were taken into account but no rotational deformations. Finally, there is a high uncertainty in the number of MLI layers to be used as this is not optimized with thermal analyses.

From a mechanical point of view, the baffle mass was 23.6 kg, thus exceeding the 15 kg budget. Furthermore, the stowed volume was 1.8 m^3, thus exceeding the 1.5 m^3 threshold requirement and the stowed eigenfrequency was $\approx$ 0 Hz due to lack of rigidity in stowed configuration. Finally, the deployment reliability was low due to many failure modes such as timely inflation of all booms, correct pressurization of the aluminium laminate and lastly the venting of the gas.

The consequence of these thermal-mechanical complications is twofold: Firstly, the thermo-elastic deformations (translation and rotation) of the M2 are 3.2 µm and 9.1 µrad respectively, which exceeds the 2.0 µm and 6.0 µrad allowed in-orbit drift budget respectively. Secondly, the baffle system requirements were not met, due to the mechanical complications.

The research question that is then asked in this thesis is: *Which modifications are required to the existing thermal-mechanical design of the baffle to create a stable thermal environment such that the related thermal-mechanical budgets are met?* Consequently, the overall design shall comply with the functional, characteristic and constraint requirements.

The answer to this question is a passively optimized thermal design using Passive Thermal Control (PTC) hardware. It has been investigated what the best baffle height, radius, shape and coatings are, as well as what the optimized MLI lay-up is based on thermal performance, debris impact mitigation, foldability, mass and structural integrity. Furthermore, additional hardware for the rejection- and attenuation of external/internal stray-light has been designed and its impact on the system design of the baffle and DST is explored. Ultimately, Active Thermal Control (ATC) has been added to the optimized passive design and is based on 8 flexible Polymide Thermofoil heaters. To comply with the functional, characteristic and constraint requirements, a completely new mechanical deployment system has been designed, consisting of telescopic booms. A trade-off between several telescopic boom concepts and the inflatable concept has been generated and the final design is chosen based on an improved performance in mass, stowed volume, stiffness, deployability and flexibility.

The result is that the newly designed baffle structure is rigid in both stowed and deployed state, offers great stiffness, contains fewer failure modes than the inflatable concept and its design is flexible. Flexibility is beneficial for the conceptual baffle design as hardware for the attenuation and rejection of stray-light can easily be added in the future. It meets all structural requirements: it has a stowed eigenfrequency of 104.7 Hz and thus ≥ 100 Hz, a stowed volume of 1.44 and thus ≤ 1.5 m^3, a mass of 12.18 kg and thus ≤ 15 kg and a 5 times higher deployed eigenfrequency than the inflatable design, yielding better resistance to operational vibrations and flutter.

The newly designed baffle does create a more stable thermal environment than the inflatable concept, as the thermo-elastic deformations are decreased: 2.7 µm and 2.6 µrad translation and rotation of M2 compared to 3.2 and 9.1 µm and µrad. However, it is concluded that an optimized PTC baffle still does not conform to the in-orbit drift budgets that are important to meet for optical stability as the effect of the eclipse is too strong.

For these reasons, Active Thermal Control (ATC) is concluded to be of crucial importance to meet the in-orbit drift budgets so that the optical performance is guaranteed. With the addition of ATC, even in the worst case the maximum athermalized translation and rotation of M2 are 0.9 µm and 2.4 µrad respectively, both less than the in-orbit drift budgets. Controlling the operation of the ATC system between +15 and +22 ° C already provides a thermal stability of the M2 optical mirror that cannot be provided with merely an optimized Passive Thermal Control (PTC) baffle as the decrease in external Solar flux due to Eclipse is too large. Furthermore, uncertainties in the design that are not accounted/simulated for can be controlled by ATC and thermal fluctuations become less stringent such that a margin in the budgets become available for structural on-board vibrations and flutter.

The work in this thesis has shown that it is feasible, at a preliminary level, to design a deployable baffle that creates a stable thermal environment to maintain in-orbit alignment and consequently guarantee the optical performance while imaging. This enables the next generation of high-resolution Earth observation space telescopes at reducing cost.

Preface

This master's thesis concludes 5 years of engineering studies in which I not only learned a whole lot of engineering hard skills, but additionally developed myself on a personal level. I have had the privilege to study in a variety of cities in different countries which all shaped me to be the engineer and man that I am today.

After having obtained my Mechanical Engineering bachelor's degree at the University of Twente in Enschede, including studying for half a year in Porto as part of my minor, I decided to move to Delft to further my studies in the field of Aerospace Engineering. All these transitions and adventures could not have been made possible without the continuous support of my parents, sister, grandparents, girlfriend, friends and our dog. Therefore, I owe this to them. For this thesis in specific, I want to express my gratitude to both of my supervisors, Hans Kuiper and Marc Naeije. Although we have only discussed the progress of my work on an occasional basis, their feedback was useful to conclude the work. Furthermore, I want to thank the rest of the DST team, and in specific V. Villalba, for his critical view on my work and discussions we have had on a regular basis.

Finally, I want to show gratitude to all the current students and recent AE alumni that I have been spending time with in the master's room on the eighth floor. Additional to mutual help with each other's thesis, we shared a great tad of laughter, frisbee sessions and coffee drink occasions.

At the point of writing this preface, I cannot say what the future holds yet, but I can say with great certainty and confidence that my time in Delft will always be remembered and cherished.

J.W. Arink
Delft, October 2019

Contents

List of Figures

List of Tables

Nomenclature

ABM	Apogee Boost Motor
AD	Array Detector
ADS	Airbus Defense and Space
AHP	Analytical Hierarchy Process
AIT	Assembly, Integration and Testing
AOC	Attitude Orbit Control
AOCS	Attitude Orbit Control Systes
ATC	Active Thermal Control
BELA	BepiColombo Laser Altimeter
BOL	Beginning Of Life
CAD	Computer Aided Design
CDHS	Command and Data Handling System
CFRP	Carbon Fibre Reinforced Plastic
CGG	Cold Gas Generator
COM	Center Of Mass
CoRDT	Constraint Requirement Discovery Tree
CORE	COmpliant Rolling-contact Element
COTS	Commercial Off The Shelf
CRDT	Characteristic Requirement Discovery Tree
CTE	Coefficient of Thermal Expansion
CVCM	Collected Volatile Condensable Materials
DM	Deformable Mirror
DOF	Degrees Of Freedom
DOF	Degrees Of Freedom
DST	Deployable Space Telescope
ECSS	European Cooperation for Space Standardization
EO	Earth Orbit
EOL	End Of Life
ESA	European Space Agency
FBD	Flexible Body Dynamics

FFBD Functional Flow Block Diagram

FM Fold Mirror

FoS Factors of Safety

FRDT Functional Requirement Discovery Tree

GMM Geometrical Mathematical Model

GSD Ground Sampling Distance

HDRM Hold Down and Release Mechanism

HST Hubble Space Telescope

HST Hubble Space Telescope

IDP Iterative Design Process

IR Infrared Radiaton

ISS International Space Station

ITAR International Traffic in Arms Regulations

JWST James Webb Space Telescope

LEOP Launch and Early Orbit Phase

LMT Local Mean Time

LSS Large Solar Simulator

LTAN Local Time of Ascending Node

LTDN Local Time of Descending Node

MLI Multi-Layer Insulation

MS Multispectral Detectors

MTBF Mean Time Between Failure

MTF Modulation Transfer Function

OBC On Board Computer

OPS Operations

OSR Optical Solar Reflector

PCM Phase Change Material

PM Primary Mirror

PMAO Primary Mirror Active Optics

PMP Parts, Materials and Processes

PMSS Primary Mirror Support Structure

PTC Passive Thermal Control

RAAN Right Ascension of Ascending Node

RDT Requirement Discovery Tree

S/C Spacecraft

SD Standard Deviation

SM Secondary Mirror

SMART Specific, Measurable, Assignable, Realistic and Time-related

SMSS Secondary Mirror Support Structure

SNR Signal-to-Noise Ratio

SPOF Single Point Of Failure

SSO Sun-Synchronous Orbit

STEM Storable Tubular Extendible Member

TB Thermal Balance

TBA To Be Analysed

TBD To Be Discussed

TCS Thermal Control System

TDI Time Delay & Integration Sensor

TM Tertiary Mirror

TML Total Mass Loss

TMM Thermal Mathematical Model

TMS Thermal Modelling Suite

TV Thermal Vacuum

VDA Vapor Deposited Aluminium

VDS Vapor Deposited Silver

Symbols

Sign	Description	Unit
B_{ij}	Gebhart factor between surface i and j	-
C_{ij}	Conductive coupling between surface i and j	$\frac{W}{K}$
D	Aperture Diameter	m
D_N	Bending stiffness / Flexural rigidity	$\frac{N}{m}$
E	Young's modulus	Pa
F	Force	N
F_{ij}	View factor between surface i and j	-
H	Height	m
I	Area moment of inertia	m^4
J_A	External Albedo heat flux	$\frac{W}{m^2}$
J_s	External Solar heat flux	$\frac{W}{m^2}$
J_{IR}	External infrared heat flux	$\frac{W}{m^2}$
L	Length	m
L_{width}	Width	m
M_z	Induced bending moment	N
N	Number of MLI layers	-
P	Fraction of MLI blanket area taken up by penetrations	-
Q_{ij}	Heat transfer between surface i and j	W
R	Resistance	Omega
R_{ij}	Radiative coupling between surface i and j	m^2
S_{spacer}	Spacer area density	$\frac{kg}{m^2}$
T_d	Deployment torque	Nm
T_m	Mean MLI blanket temperature	K
V	Volume	m^3
W	Width of one octagonal baffle side	m
ΔT_{max}	Maximum temperature gradient	° C / K
Δt_{coarse}	Time period that coarse alignment budget holds	s
Δt_{drift}	Time period that in-orbit drift budget holds	s
Ω	Right Ascension of Ascending Node (RAAN)	°
α	Absorptivity	-
α	Coefficient of Thermal Expansion	m/mK
β	Angle M2 with local X/Y-axis	°
β	Solar Beta Angle	°
ϵ	Emissivity	-
ϵ	Material strain	-
λ	Wavelength	m
ν	Poisson ratio	-
ω	Frequency	Hz
ω_n	Natural frequency / eigenfrequency	Hz
ρ	Density	$\frac{kg}{m^3}$
ρ	Radius of curvature	m
ρ	Reflectance	-
σ	Standard Deviation	–
σ	Stefan Boltzmann Constant	$\frac{W}{m^2K^4}$
σ	Material stress	Pa
τ	Transmittance	-
θ	Angular Resolution	rad

Sign	Description	Unit
c_p	Specific heat	$\frac{J}{kgK}$
k_p	Conductivity	$\frac{W}{mK}$
k_{eq}	Equivalent stiffness	$\frac{N}{m}$
m	Mass	kg
r	Radius	m
t	Wall thickness	m
y	Distance from neutral line to any other position in cross-section	m
A	Area	m^2
F	F-number (ratio between focal length and aperature diamter)	-
f	Focal length	m
h	Altitude	m
i	Inclination	°
P	Power	W
T	Temperature	K
V	Voltage	V
v	Velocity	$\frac{m}{s}$

1 Introduction

Space telescopes have been extensively used for the observation of far-off planets and other astronomical bodies, including our terrestrial planet. Visible (VIS) light telescopes ($\lambda \sim 390$ - 750 nm) are often used in Earth observation satellites for the use of weather surveys and forecasts, water and ice monitoring, fire detection, deforestation and forest degradation. [19] [34]
For many of these applications, a high spatial resolution is needed, since it allows to directly and precisely map disturbances and new infrastructure, precisely estimate the area of change, classify disturbances by type and detect fine-scale change. [34]

The spatial resolution a telescope can achieve is based on the diffraction limit of a telescope, which sets the limit on the angular resolution of a telescope. As the spatial resolution, denoted by the Ground Sampling Distance (GSD), is proportional to the angular resolution and inversely proportional to the diameter of the aperture, it can quickly be realised that a high spatial resolution requires a large aperture diameter. Additionally, for a larger aperture diameter, the focal length needs to increase as well to decrease abberations and increase optical stability in the optical system.

However, since traditional space telescopes are passive (fixed, non-moving mirrors) the problem arises that there is a geometrical limit to both these sizes and hence a limit to the spatial resolution to be reached. The geometrical limit of the aperture diameter stems from the maximum diameter to be fitted inside of the launch vehicle. Thus, when wanting to increase the spatial resolution, an increase in aperture diameter and/or focal length is needed. This results in an increase in mass and volume, which consequently results in the need to pick large (and heavy) launch vehicles to bring the payload to orbit. All this will massively increase the cost of launch and additionally sets a boundary to what spatial resolution can be reached.

To yield a high spatial resolution of 25 cm/pixel while decreasing mass, volume and costs, TU Delft is developing an active state-of-the-art Deployable Space Telescope (DST). The DST is an active telescope in the sense that its Primary Mirror (PM) unfolds from a stowed configuration to its final unfolded configuration to increase the aperture diameter and its Secondary Mirror (SM) protracts with respect to the PM to increase its focal length.

Designing a high-accuracy space telescope that is deployable while aiming for this spatial resolution brings about multiple thermal-mechanical design challenges: 1) The PM segments and SM have to be deployed with an accuracy in the order of micrometers with respect to each other before the Primary Mirror Active Optics (PMAO) system can take over, resulting in a very tight deployment error budget. 2) The structure of the PM segments and SM should withstand vibrations and corresponding deflections should not exceed the stability budgets. 3) The structure of the PM segments and SM should withstand temperature fluctuations due to transient in-orbit thermal fluxes and corresponding deformations should not exceed the thermal driftnor stability budgets.

To ensure that these temperature-dependent deformations conform to their budgets, a stable thermal environment for all optical elements is required. To this end, a baffle, which simultaneously serves as a deployable thermal shield and stray-light rejection system, has been identified to increase the thermal stability and control of DST sub-system temperatures. Therefore, this thesis focuses on the continuation of the thermal-mechanical design of the baffle to ensure a stable thermal environment so that resulting thermoelastic deformations conform to their budgets and consequently to guarantee the optical performance of the DST.

2

Overview of the Deployable Space Telescope

This chapter introduces the mission background of the DST, how the DST fits in the current market, the market needs and what the overview and working principle of the DST is. Consequently, it will be highlighted what work has already been performed regarding the DST and how the ongoing- and upcoming work on the baffle fits within the needs of the DST. Furthermore it is discussed what the thesis need and goal of the DST project are, which research questions this MSc thesis is going to answer and what the set-up of this thesis is going to look like.

2.1. DST Mission Overview and Market Needs

Many optical telescopes use visible light (λ between 390 - 750 nm) for Earth observation. This is part of remote sensing, which is the act of gaining information about a target without being in physical contact [53]. Earth observation satellites come in handy in a number of applications, e.g. weather surveys and forecasts, water and ice monitoring, fire detection, deforestation and forest degradation. [19] [34]

2.1.1. Market Needs and Thesis Fit

For many of these applications a high spatial resolution is needed, since it allows to directly and precisely map disturbances and new infrastructure, precisely estimate the area of change, classify disturbances by type and detect fine scale changes. [34] The highest spatial resolution available today is provided by WorldView-3 and WorldView-4, which have a GSD of around 31 cm/pixel. [105] The WorldView-4 is the current standard and is taken as a reference throughout this paper. An increase of this 31 cm/pixel GSD in spatial resolution will lead to an even better estimate of area of change, as well as an improvement in revision time with applications in the defense sector, amongst many.

The spatial resolution that a telescope can achieve is based on the diffraction limit of a telescope. Diffraction is a physical phenomenon in which light bends towards the shadow region of an object when it comes in contact with that object. Diffraction sets the limit to the angular resolution of a telescope, which is inversely proportional to the diameter of the aperture for a circular aperture. See Equation 2.1 below.

$$\theta = 1.220\frac{\lambda}{D} \tag{2.1}$$

In this equation, θ is the angular resolution in rad, λ is the frequency of light that is being observed in Hz and D is the aperture diameter in m. The GSD is linearly related to the angular resolution, meaning that a decrease in GSD (thus increase in spatial resolution) can be established by increasing the diameter of the aperture. Ultimately, the F-number which is defined as the ratio between the focal length and the aperture diameter ($F = \frac{\lambda}{D}$) needs to be sufficiently high to decrease the sensitivity to abberations. This means that the focal length should also increase.

Therefore, a high spatial resolution can be established in two ways: increasing the aperture diameter of the primary concave mirror and/or increasing the focal length. However, since traditional space telescopes are passive (fixed, non-moving mirrors) the problem arises that there is a geometrical limit to both these sizes

and hence a limit to the spatial resolution that can be reached. The geometrical limit of the aperture diameter stems from the maximum diameter to be fitted inside of the launch vehicle. Thus, when wanting to increase the spatial resolution, an increase in aperture diameter and/or focal length is needed, resulting in an increase in mass and volume. This results in the need to pick large (and heavy) launch vehicles to bring the payload to orbit. All this will massively increase the cost of launch, and additionally sets a boundary to what spatial resolution can be reached. Therefore, there is a market need to produce telescopes that can offer the same (or better) spatial resolution as conventionel telescopes, but for only a fraction of the price of conventional passive telescopes. This reduction in mass, volume and cost can be established by making a telescope with deployable fragmented mirrors.

To this end, the Deployable Space Telescope (DST) has been proposed by the TU Delft which acts to this need. Due to the deployability of the optical fragmented elements, several thermal-mechanical side effects arise that have to be accounted for. Namely, the optical mirror systems need to be accurately deployed and aligned. Secondly, post-deployment deformations, mainly caused by thermo-elastic perturbations of the optical systems, shall not exceed their spatial deformation budgets.

To account for these thermal-mechanical side effects, a baffle has been proposed. Its main functions are enumarated below:

1. To create a stable thermal environment by decreasing temperature fluctuations and thermal gradients
2. To attenuate and reject stray-light
3. To mitigate micrometeoroid- and debris impacts that would otherwise be directly exposed to the optical systems.

The market need statement that was discussed above is summarised below.

DST Market Need Statement *There is a need for higher spatial-temporal resolution Earth Observation telescopes to provide data at a lower price than the current standard*

The mission goal that stems from the flow of needs and the market need statement mentioned above is:

DST Mission Goal. *The DST mission goal that this thesis is supporting is to make a leap forward into developing a state-of-the-art Deployable Space Telescope for a fraction of the price of conventional space telescopes, whilst improving the spatial resolution. This improves estimates of the area of change and the mapping of disturbances for many real-life applications.*

2.1.2. DST Mission Requirements

The DST developed by the TU Delft acts on the market needs that are stated in Section 2.1.1 above, and hence aims at lowering the cost of launch plus increasing the spatial resolution. The DST is an active telescope in the sense that its primary mirror unfolds from a stowed configuration to its final unfolded configuration to increase the aperture diameter and its secondary mirror protracts with respect to the primary mirror to increase its focal length. This all while aiming for a GSD of 25 cm/pixel at an altitude of 500 km.

The rationale behind the 25 cm/pixel GSD is that it yields a slightly better GSD than that of the WorldView-3/4 (31 cm/pixel at an operating altitude of 617 km). The GSD scales linearly with the orbital height, thus $31 \cdot \frac{500}{617} \approx 25$ cm/pixel. The objectives of lowering cost and increasing spatial resolution can be translated into top-level mission requirements. These are stated in Table 2.1. These are directly taken from D. Dolkens' thesis, as he established these top-level mission requirements for his thesis. [24]
Below, a clarification of the optical terms as mentioned in the mission requirements from Table 2.1 are stated.

1. **Ground Sampling Distance (GSD).** *Refers to the distance between two pixels as measured on the ground. It is inversionally proportial to the spatial resolution: a low GSD results in a high spatial resolution. For the DST, a GSD of 25 cm, measured at 500 km altitude, means that one pixel represents an area of* 25^2 cm^2.
2. **Swath width.** *The width of the surface that is to be observed. For the DST the goal is to observe the surface of the Earth with a width of 5 km.*

ID	Requirement
REQ-1	The Ground Sampling Distance of the instrument shall be equal to 25 cm in the panchromatic band from an orbital altitude of 500 km.
REQ-2	The swath width of the instrument shall be wider than 1 km (threshold) 5 km (goal).
REQ-3	The system shall have one panchromatic channel with 25 cm GSD and four multispectral bands (blue: 450-510 nm, green: 518-586 nm, yellow: 590-630 nm, red: 632-692 nm) with 100 cm GSD.
REQ-4	The Signal-to-Noise Ratio (SNR) of the instrument shall be higher than 100 for a reflectance of 0.30 and a sun Zenith angle of 60°.
REQ-5	The nominal Modulation Transfer Function (MTF) at both the Nyquist frequency and half the Nyquist frequency shall be higher than 5% (threshold) / 15% (goal).
REQ-6	After calibration, the residual Strehl ratio of the system shall be higher than 0.80.
REQ-7	The mass of the instrument shall be lower than 100 kg (threshold) / 50 kg (goal).
REQ-8	In the stowed configuration, the volume of the instrument shall not exceed 1.5 m^3 (threshold)/ 0.75 m^3 (goal).

Table 2.1: Mission requirements, taken from D. Dolkens' thesis [24]

Mission/instrument parameter	Value	Unit
Altitude	500	km
Orbital configuration	Near-polar, sun-synchronous	-
Instrument mass	127	kg
Instrument stowed volume	0.76 x 0.76 x 1.10 m =0.64	m^3
Swath width	5	km

Table 2.2: Mission envelope with current values from early 2018 [76]

3. **Panchromatic channel.** *The channel containing a range of broad wavelengths and when coinciding with the wavelength spectrum belonging to what is known as visible light, it appears as a black-white picture.*

4. **Signal-to-Noise Ratio (SNR).** *The SNR is the level of desired signal to the level of background noise.*

5. **Modulation Transfer Function (MTF).** *The MTF is the magnitude response of the optical system to sinusoids of different spatial frequencies. [13]*

6. **Nyquist frequency.** *The highest frequency that can be achieved by a sensor, and is thus the limiting resolution of a sensor.*

7. **Strehl ratio.** *A ratio depicting the quality of the optical system in terms of abberation. When an image is perfectly unabberated, its ratio is equal to 1.*

Extending these mission requirements with instrument mass- and volume requirements will result in the following overview of the mission envelope, taken from [5], [23] and [76]. This mission overview is the current version of the value of parameters, up to early 2018 [76], stated in Table 2.2.

2.1.3. Mechanical Budgets

Using a top-down systems engineering approach, the mission requirements from Table 2.1 can be translated into mechanical budgets. These are generated to guarantee the optical performance. The need for these mechanical budgets derive from the need to reduce the optical path difference introduced by mirror misalignment and deformation. This means that these mechanical budgets have to be met in order for the optical calibration algorithm to work properly. Hence, the abberation correction system, that G. van Marrewijk has worked on during his MSc thesis [69], only works for a finite abberation in the optical system. The mechanical structure holding the mirrors in place have to designed such that the total structural integrity conforms the mechanical budgets so that limited deflections in the mechanical system can still be filtered out by the abberation correction algorithm. The top-down budgets are summarized in Table 2.3.

Element	Position X [μm]	Y [μm]	Z [μm]	Orientation X [μrad]	Y [μrad]	Z [μrad]	Radius [%]	Shape Error [nm]
Deployment/ Coarse Alignment Budget								
M1	2	2	2	2	4	50	1×10^{-3}	50
M2	15	15	10	100	100	100	1×10^{-2}	25
M3	4	4	4	10	10	50	1×10^{-3}	10
In-Orbit Drift Budget								
M1	2×10^{-2}	2×10^{-2}	2×10^{-2}	1×10^{-2}	2×10^{-2}	5	1×10^{-4}	5
M2	4	4	2	6	6	12	1×10^{-4}	5
M3	1×10^{-1}	1×10^{-1}	1×10^{-1}	1	1	5	1×10^{-4}	5
Stability Budget								
M1	5×10^{-3}	5×10^{-3}	5×10^{-3}	2.5×10^{-3}	1×10^{-2}	5×10^{-1}	n/a	n/a
M2	1	1	5×10^{-1}	1.5	1.5	3	n/a	n/a
M3	2.5×10^{-2}	2.5×10^{-2}	2.5×10^{-2}	2.5×10^{-1}	2.5×10^{-1}	1.25	n/a	n/a

Table 2.3: Mechanical top-down budgets, taken from S. Pepper's thesis [76]

Additional explanation for these budgets are needed [76]. Since the Deployment- and Coarse Alignment budgets are similar, but do not apply to the same mirrors, a distinction is made below for clarifying reasons.

1. **Deployment Budget.** *The maximum allowable deviation of the position of the optical surface from the desired datum after deployment and prior to coarse (or fine) calibration. This only applies to the deployable elements: M1 and M2.*
2. **Coarse Alignment Budget.** *The maximum allowable deviation of the position of the optical surface from the desired datum after coarse alignment. This only applies to the optics elements: M1 and M3.*
3. **In-Orbit Drift Budget.** *The maximum allowable spatial deviation of an optical surface that can occur between completion of the last active calibration procedure and the end of the next image acquisition, provided that the deviation can be considered (pseudo-)static over the period of image acquisition.*
4. **Stability Budget.** *The maximum allowable spatial deviation of an optical surface during image acquisition. Note that this only applies during image acquisition.*

Note: the In-Orbit Drift Budget is time-dependent and refers to the allowable spatial deviation over a large period of time. This period of time, Δt_{drift} is large compared to the stability budget, which is only applicable during image acquisition. Its duration is currently in the order of one second. [76] Δt_{drift} is related to the coverage rate and revision time of the DST, but no quantitative answer has been found during the literature study. To be conservative, Δt_{drift} is chosen to be equal to the entire time that the DST is able to image during the time that it is **not** in eclipse. However, the Coarse Alignment Budgets are of importance during the eclipse time, in which the DST is not able to make images. If these Coarse Alignment Budgets are not met during the eclipse, the algorithm that controls the alignment of the mirrors does not converge to a steady solution. These choices were made during a discussion with V. Villalba Corbacho, who is promoting on the thermo-mechanical design of the entire DST.

After defining the mission needs and requirements, as well as the top-level mechanical budgets to conform with the mission requirements, a detailed overview of the working principle of the DST is made. This consists of a brief explanation of the DST components and their functionality.

2.2. Working Principle DST

In this section the overall working principle of the DST is explained. There is a distinction to be made between the working principle of the DST during Launch and Early Operations (LEOP) and during operations. This distinction is made below.

1. **LEOP.** *During LEOP, the PM, SM and baffle are still in stowed position. During the early operations, when the payload is released from the launch vehicle and is inserted in the right orbital configuration, the deployment sequence of the PM, SM and baffle starts.*

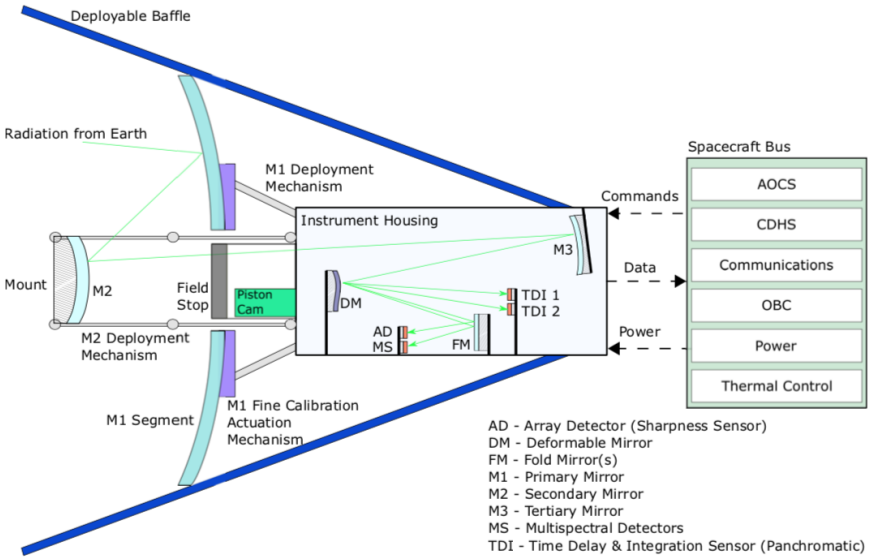

Figure 2.1: Schematic of DST and its working principle, taken from S. Pepper's thesis [76]

2. **Operational phase.** *The PM, SM and baffle are deployed and the DST can start obtaining images for EO purposes.*

This thesis will focus on the thermal-mechanical design of the baffle to create a stable thermal environment for the structures for compliance with the mechanical budgets as stated in Table 2.3. Therefore, ensuring proper deployment and thermal operation of the DST, when the PM, SM and baffle are already deployed and when the telescope can start to obtain images. This operational phase relies on proper design to comply with the budgets so that abberation correction of the system can take place to obtain high-resolution images. The requirements for this are generated in Chapter 4.
Next up, the baffle subsystem, as well as the PMSS and SMSS subsystems will be reviewed in detail. Stating the working principle and design overview of the PMSS and SMSS is important since both PMSS and SMSS are influenced by the performance of the baffle. This is also shown in the N2 chart of the DST (functional analysis method to map the architecture of the DST) in the Appendix, Figure B.1.

The DST in operational, deployed configuration uses a Korsch annular-field three mirror anastigmat optical configuration. This configuration has multiple advantages: it does not introduce any chromatic aberrations to the image, it has inherent correction of spherical aberration, coma, astigmatism and field curvature, it has a highly accessible focal plane and a large proportion of usable field. [76] Thus, the DST consists of two deployable mirrors and one stationary mirror, which is located within the S/C bus. An overview of the other components and their function are visualized in Figure 2.1 and summarized below, as well as the visualisation of the optical path.

1. **Primary Mirror Support Structure (PMSS).** *The PMSS gives support to the PM, unfolds from a stowed position to the operational position and is calibrated using a PMAO mechanism to remove discontinuous wavefront errors.*

2. **Secondary Mirror Support Structure (SMSS).** *The SMSS gives support to the SM and deploys using deployable booms to extend the focal length, without relinquishing sufficient structural stability.*

3. **Baffle** *The baffle serves two main purposes: 1. to create a thermally stable environment to guarantee that corresponding thermo-elastic deformations stay within the mechanical budgets. 2. To attenuate/reject stray-light entering the optical path. Additionally, it is be used to shield the DST from debris/micro-asteroids. However, this is not a main functionality*

4. **Instrument housing** *The instrument housing consists of the Tertiary Mirror (TM), Deformable Mirror (DM), Fold Mirror (FM), several optical detectors and sensors (AD, MS and TDI). It additionally contains a piston cam, measuring the misalignment of the PM. It is attached to the PMSS, SMSS and baffle.*

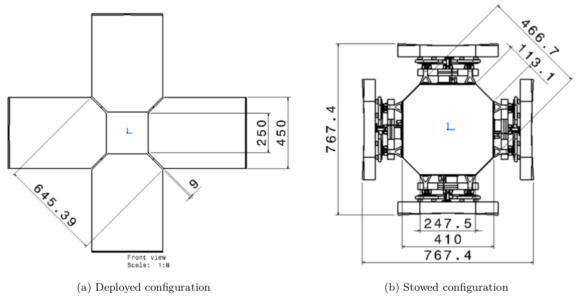

(a) Deployed configuration (b) Stowed configuration

Figure 2.2: DST bus including M1 segments, taken from T. van Wees' thesis [102]

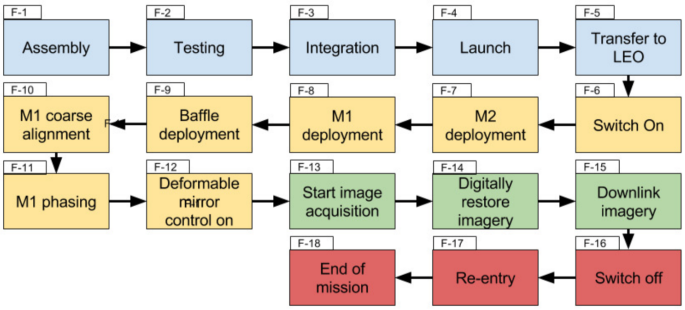

Figure 2.3: Functional Flow Block Diagram of the DST, taken from S. Pepper's thesis [76]

5. **S/C bus** *The S/C bus consists of all necessary components for the functioning of the satellite, that are not part of the payload: power-, thermal- and attitude control, communications. This is being designed by ADS Leiden.*

The S/C bus with the M1 segments, including relevant dimensions, is visualized in Figure 2.2.

The flow of operations is schematized after functionally analyzing it using a Functional Flow Block Diagram, Figure 2.3.

2.3. Primary Mirror Support Structure

The Primary Mirror Support Structure (PMSS) was initially designed by B. van Putten, but is extensively updated by M. Corvers. [22] His most recent version will be briefly paid attention to. Firstly, the general design and functionality of the PMSS with all its components is introduced and secondly the performance of the SMSS is touched upon, with a focus on the thermal performance.

2.3.1. General Design PMSS

The PMSS consists of the main support frame, whiffle plates, whiffle flexures and primary mirror actuated flexures. Below, a summation of the function of these parts are given.

1. **Support frame** *The support frame, also referred to as T-frame, gives support to all the actuated flexures, whiffle plates and whiffle flexures and eventually the PM segments itself.*

2. **Whiffle plates** *The whiffle plates form the interface between the whiffle flexures and actuated flexures.*

3. **Whiffle flexures** *The whiffle flexures are used to directly support the PM segments in a kinematic constraint manner.*

4. **Primary mirror actuated flexures** *These flexures form the basis of the Primary Mirror Active Optics (PMAO) actuation system, which have to make sure that the position and orientation of the PM segments stay within the resolution of 10 nm during calibration.*

The support frame is visualized in Figure 2.4. The pockets give space to create a kinematic interface where the primary mirror actuated flexures are placed. The whiffle flexures are a series of three flexures supporting

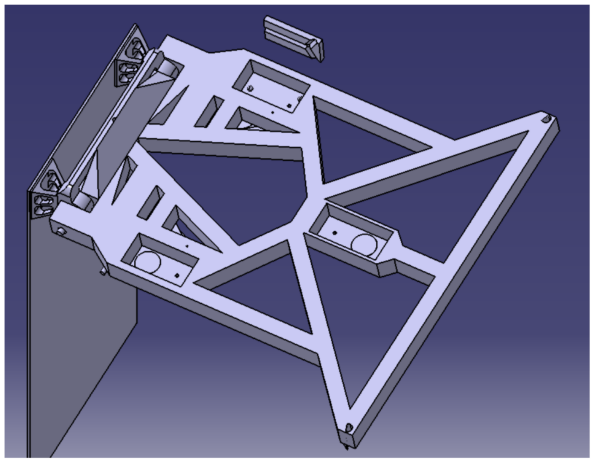

Figure 2.4: Support frame (also referred to as T-frame) of the PMSS, taken from M. Corver's thesis [22]

the PM. Having three flexures is sufficient for the removal of discontinuous wavefront errors [23], and serves as a statically determined structure. The whiffle flexures, whiffle plates and actuated flexures are made of a titanium alloy Ti-6Al-4V. This alloy was preliminarily chosen for the actuated flexure for the PMAO system, and also turned out to be a good choice when doing a more extensive design trade-off, which was part of S. Pepper's MSc Thesis. Namely, the Titanium alloy had the best overall performance except where thermal conductivity was concerned. Its mechanical performance is very good, important for flexure repeatability and surviving launch. It also performs well where dimensional stability is required. Its ability to retain these properties to high temperatures is advantageous for the LEOP use case. [76]

2.3.2. Performance PMSS

This section will state the performance of the PMSS based on the work of M. Corvers and S. Pepper. M. Corvers found out that the in-orbit drift budgets formed the toughest challenge. The mass requirement of 16 kg is not met, since the current estimate of the PMSS is 25 kg.

S. Pepper, who worked on the PMAO mechanism, made a first in-orbit drift calculation for the actuation system concerning the PM. A spacer was added to the piston to reduce the thermal expansion, based on the principle of athermalization. S. Pepper assumed a 1 K temperature gradient, due to the baffle filtering out all Solar heat flux. An addition of 15 K was added as a design uncertainty. Therefore, with a temperature margin of +- 16 K, the resulting deflection in z direction, Δ z, is 12.8 nm, which meets the in-orbit drift budget for this direction. This is only reachable with a titanium piston (low CTE) and an aluminium spacer (high CTE), acting in the opposite side to null out the effect of thermal expansion (athermalization).

Despite this in-orbit drift calculation for the PM, a complete End-To-End-Performance verification of the M1 in-orbit drift budget still needs to be performed. Also, as S. Pepper already acknowledges: "The tilt drifts have not been analysed here, nor have the effects of gradients or contributions from the deployment mechanism." [76] Furthermore, since S. Pepper's work concerned the actuation of the PM only, an in-orbit drift analysis and verification for the SM needs to be performed, since this fell out of the scope of S. Pepper's MSc Thesis.

2.4. Secondary Mirror Support Structure

The literature found on the SMSS will cover the most recent version of the design of the SMSS, without stating all preceding design iterations. The most recent version corresponds to the final design of the SMSS that A. Krikken worked on during his MSc Thesis [60], which will be discussed hereafter. Firstly, the general design and functionality of the SMSS with all its components is introduced and secondly the performance of the SMSS is touched upon, with a focus on the thermal performance.

2.4.1. General Design SMSS

The SMSS holds the SM of the DST in place. The SM is chosen to be made out of Silicon Carbide (S_iC), since it has a low CTE but high strength-to-weight ratio. [23] It has to provide a stiff support for the secondary mirror

Table 2.4: Relevant parameters of deployable booms

Parameter	Value
Diameter (D) [mm]	70
Wall thickness (t) [mm]	0.5
Total length (L) [mm]	1765.7
Midpoint hinge [mm]	658
CTE [micron/m/K]	0.8
Deployment torque (T_d) [Nm]	TBD

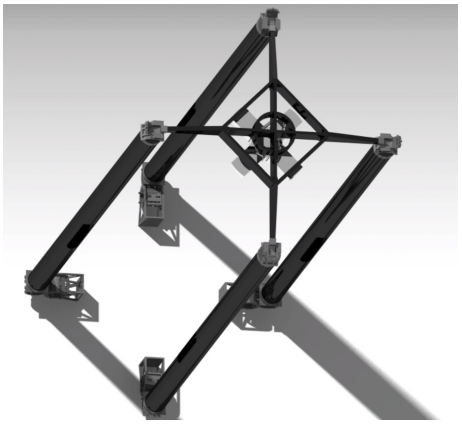

Figure 2.5: Secondary Mirror Suppport Structure

Table 2.5: Relevant parameters of CORE hinges

Parameter	Dimensions [mm]
Strip thickness	0.3
Strips total width	31
Outer radius cams	35
Inner radius cams	29.7
Fillet radius	0.5
Cam contact surface width (total)	20
Total width	54
Bolt size	M4(4)

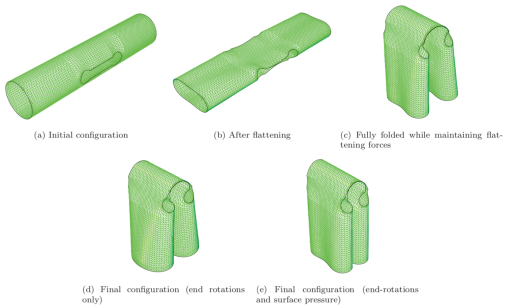

Figure 2.6: Tape Spring working principle

that complies to all budgets and the SM needs to protract with respect to the Primary Mirror (PM) to a required distance of 1.6 m between the primary mirror segments and SM, since this is beneficial for the optical system. [60] Also, the 1.6 m relative distance between the PM and SM has been a trade-off between increasing the focal length (thus increasing spatial resolution) while ensuring stability of the SM. [103] The protraction of the secondary mirror happens during LEOP. The current version of the SMSS consists of four deployable booms with tape-spring hinges, a spider structure, four top CORE hinges, four bottom CORE hinges, eight Kevlar ribbons and a hexapod structure to mount the SM to the spider, which is visualised on the render of Figure 2.5. A short explanation and characterization of all these parts of the SMSS is explained below, including their performance.

The four deployable booms that extend away from the PM have a length of 1765.7 mm. The booms host a tape-spring hinge at a position of 658 mm, measured from the bottom. In the stowed position, the tape-spring hinge folds up through a series of steps, as visualised in Figure 2.6. In terms of thermal properties, the booms have a CTE of α =0.8 micron/m/K in axial direction. Finally, all relevant parameters are mentioned in 2.4.

The mount between the SM and the spider structure consists of a hexapod structure. The hexapod structure consists of three rods and every rod has to constrain one DOF . Therefore, slots where made into these rods. This makes that the hexapod structure is fully kinematically constrained. The hexapod structure allows for relative thermal expansion of the spider and mirror, while keeping the mirror exactly constraint [60]. The material used is Aluminium 7075-T6, which has a high reduced tensile strength that is beneficial for the use of flexures. The hexapod structure in combination with the deployable boom, with a CTE of 0.8 in axial direction, yields in an athermalized system. Athermalization is an important thermal principle to be used in high-precision systems for the reduction of relative deformations due to thermal gradients.

The spider structure itself is a structure made out of CFRP and connects the deployable booms to the SM. Its has a cross shape with a circular structure in the middle and four cross beams, both to increase the stiffness. The SM is mounted on this circular structure, which has a diameter of 2/3 of the diameter of the

mirror. The reason for this is that gravity effects on the mirror are minimized, and is based on literature. [60] The part of the spider connecting to the top CORE hinges decreases in height for mass-savings and since it is not a critical load-bearing section. This is because the top CORE hinges cannot transfer a moment, meaning an internal moment of zero at the tips of the spider. The width of the spider structure is 15 mm, and is made such that no light is blocked towards the PM.

The CORE hinges, short for COmpliant Rolling-contact Element, are critical for the deployment accuracy and, together with the tape-spring mid hinge, form the basis of the folding mechanism of the deployment of the M2. These hinges show low hysteresis and friction behavior, work without lubrication, low stress behaviour and are worked out in great detail by A. Krikken [60] and M. Voorn [103]. The material of the CORE hinges is selected to be aluminium, instead of titanium (which was formerly selected). However, titanium is still used for the strips. The relevant design parameters of the hinge are shown in Table 2.5. Both surfaces of both cams are surface treated with Keronite Endure of 17 microns thick, with a layer of M_0S_2 to prevent cold welding. [60]

Finally, Kevlar ribbons are added that run from the PMSS to the top CORE hinges of the SMSS, to add stiffness to the spider structure. The ribbons have a width of 8 mm and a thickness of 1 mm, resulting in a ribbon stiffness of 750 N/mm. [60]

2.4.2. Performance SMSS

In this subsection, the performance of the SMSS will be briefly highlighted, together with how this is achieved.

The SMSS has to fulfill many mechanical requirements. These requirements concern mass (<14 kg), volume, AIT, deployment of geometries and three main accuracy budgets: deployment accuracy, in-orbit drift and stability. The mass of the total SMSS subsystem, including a 20 % safety margin, is 7.28 kg. [103] This is well below the requirement of 14 kg. Furthermore, the requirements regarding volume and deployment geometries are met, based on verification of analysis.

Regarding the accuracy budgets, A. Krikken explains that the stability budgets are met. Multiple extensive modal- and random vibration analyses were performed in his thesis which concluded that a maximum amplitude of 0.337 micron would occur, hence below the stability budgets. This is only possible with increased damping capabilities of the CFRP of the four booms and addition of ribbons.

The deployment budgets are still to be confirmed, since a thorough deployment analysis needs to be done. However, A. Krikken mentions that it is however thought that the deployment budgets can be reached, because all hinge concepts have low hysteresis, since they depend on elastic deformation (tape-spring hinge) or pure rolling contacts (CORE hinge).

Regarding thermal work, the length of the SM mount is made such that the system is athermal, so that a constant 1600 mm offset between the SM and PM is present (deployment geometry requirement). Athermalisation is a method to reduce global deflections, by making use of different materials with different Coefficients of Thermal Expansion. Applying this method to the SMSS resulted in the decision to take a length of 1765.7 mm for the CFRP booms, see Table 2.4.

2.5. Baffle

The design of the baffle was still ongoing when the auther started his thesis. The baffle proposal emerged from B. van Putten's conclusion, who did a preliminary thermal analysis on both the PMSS and SMSS. E. Korhonen designed the mechanical deployment system of the current version of the baffle as well as the thermal lay-up of materials, [58], whereas T. van Wees performed a thorough thermal analysis of the entire DST, with a special focus on the baffle. [102] The implementation of a baffle is significantly important for creating a stable thermal environment for meeting in-orbit drift and stability budgets and to attenuate and reject internal and external stray-light respectively. The baffle also has to adhere to the stowed volume requirement of 0.75 m^3 (goal) / 1.5 m^3 (threshold) and therefore it was concluded that the baffle needs to deploy as well. The baffle is currently being designed to allow for a temperature deviation of +- 1 K within the baffle, with a design uncertainty of 15 K and nominal temperature of 298 K. The current overview of the baffle, which is the latest version, is discussed below. See Figure 2.7 for an overview of the unfolded baffle.

The current overview of the baffle is broken down to a mechanical- and thermal overview respectively.

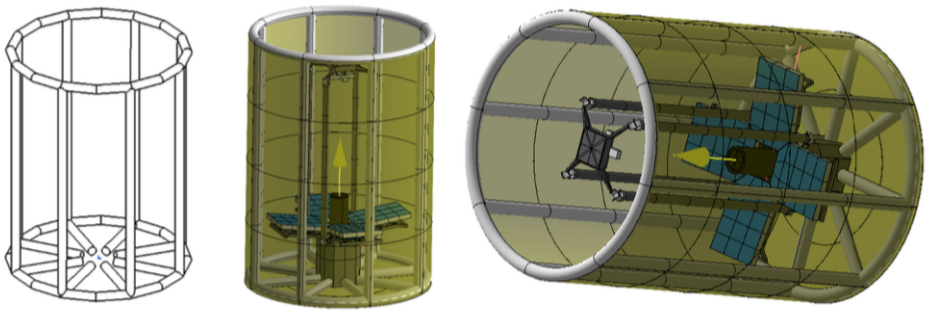

(a) E. Korhonen (b) ESATAN TMS (c) ESATAN TMS

Figure 2.7: Baffle schematic in deployed state. This is the current version of the baffle as designed and analysed by by E. Korhonen and T. van Wees respectively, [58] [102]. Taken from T. van Wees' thesis [102]

2.5.1. Mechanical Overview

The current design of the baffle consists of eight inflatable booms which deploy from an origami-like stowed state to the deployed state by means of inflation. The way inflatable structures work is by means of an inflation gas, which fills the structure like a balloon. [57] Nitrogen gas is used for the DST baffle. The advantages of inflatable structures are the high deployment ratio and simplicity of deployment mechanism and the system. However, this comes at a cost of the robustness and the insurance of the deployment of the system. This is counteracted by using a rigidisable aluminium laminate, which appeared to be the most promising mechanism in E. Korhonen's Thesis [57]. This laminate is a combination of aluminium and a polymer. Rigidization works by introducing a force that plastically deforms the aluminium, while the polymer remains elastically deformed. After the gas has vented, the laminate is prestressed with the metal layer in compression and the polymer in tension. The metal is strain hardened and any fold lines are smoothened out. [57]. The current shape is that of an octagon, which appeared to outperform the previous ellipsoidal shape. Aluminium, chosen for the structural laminate, is a widely used space material, since it is cheap, has low density and is resistant to many influences present in the space environment. However, it does have a relatively high CTE compared to other metals, but since thermal expansion of the baffle is not foreseen to affect the performance of the DST as much as thermal expansion in optical parts, it does not weigh heavy in the material choice decision making.

A mechanical overview of the current baffle including performance is given in Figure 2.8.

Mechanical Overview of Current Baffle

Geometrical Overview	Deployment Overview	Mechanical Performance
Cylindrical shape	Based on inflation and includes inflation system	Total mass of baffle system = 23.6 kg
Height = 3060 m	• Valve – and vent system	• Inflation system = 8.9 kg
Radius = 1060 mm	• 4 Cold Gas Generators	• Baffle shield = 14.7 kg
Eight booms in octagonal configuration	• Inflation gas = nitrogen	Stowed volume = 1.8 m^3
• 100 mm diameter	• Pressure sensors	First natural frequency, deployed = 0.9159 Hz
• 63 µm thick Aluminium-Kapton-Aluminium laminate	Aluminium rigidised after deployment by pressure of inflation gas	
Includes a top- and bottom torus	Origami inspired folding of MLI	
12 µm Mylar as inner lining for booms + tori to avoid leaks		

Figure 2.8: Overview of mechanical design and performance of the current baffle. Values taken from E. Korhonen- and T. van Wees' theses [58] [102]

2.5.2. Thermal Overview

Additional to the aluminium laminate, the baffle houses MLI with specific differences between the external- and internal layers, since every layer has a different function.

Inner Coating

The inner coating has to radiate heat uniformly, since it should avoid creating thermal gradients within the

baffle. This leads to a material for the internal surface/layer with a high conductivity so that heat spreads out quickly and evenly over the surface. The internal surface should however not reflect incoming stray-light and therefore has a high absorptivity and emissitivity of 0.93 and 0.83 respectively. Therefore, the inner coating is chosen to be a highly absorptive black coating to absorb as much stray-light as possible. The coating is referred to as Magic Black with an emissivity of 0.84 and absorptivity of 0.93.

Outer Coating
The external surface (Sun-facing) is made of FEP/VDA with an absorptivity of 0.14 and emissivity of 0.60, since it has to reject as much incoming Solar radiation, as concluded by E. Korhonen.

MLI Properties
Aluminized Kapton is used as the reflective shield layer. This is a very common reflector layer and resistant to a large temperature range (-250 to + 288 **continuous** exposure). The thickness is chosen to be 0.013 mm as this is based on the availability options while also taking into account the mass budget. The reflector layers are perforated to allow for venting, since perforating prevents ballooning and vent placement is critical for space optics applications to prevent contaminant deposition. [36]

As a spacer, Dacron is used. This was also chosen by E. Korhonen, since it is the most common spacer material used for MLI and is cheaper than Nomex. [58] The thickness of one layer of dacron is 0.16 mm, also based on availability and common heritage.

It must be noted that Dacron may shrink above 177 ° C, as is established in the MLI material guidelines report developed by NASA, [36]. This is lower than the operating temperature of Kapton, which is between -269 and +400 ° C, or aluminized Kapton, which is between -260 to +288 ° C continuous exposure.

These temperature levels are also input for the requirement generation, as it imposes a requirement on the baffle survival of extreme temperature limits.

Performance as Analyzed By T. van Wees
The mean temperature of the main DST elements as T. van Wees has analysed are around 300 K. The thermo-elastic translation in Z-direction of the M2 is 2.23 µm in best-case scenario of a reflected baffle design. This conforms to the coarse-alignment budget (10 µm in Z-direction), but does **not** conform to the in-orbit drift budget of 2 µm. These values are based on preliminary thermo-elastic calculations and are sensitive to changes when a proper thermo-mechanical model is present.

Furthermore, T. van Wees used a wrong RAAN for the baffle modelling, resulting in an orbit without eclipse. This means that when the baffle is put in the right orbit with eclipse, the gradients will even be worse. This is also explained in the Baffle Improvements and Recommendations section below.

A thermal overview of the current baffle including performance is given in Figure 2.9.

Thermal Overview of Current Baffle

Thermal Overview: General	Thermal Overview: MLI Properties	Thermal Performance
MLI placed outside of booms	N = 10 layers of MLI	Mean temperature of DST elements ~ 300 K
Inner coating: Magic Black	Spacer material: Dacron	Thermo-elastic deformations of M2 > 2.23 µm in z-direction (best case scenario)
• α = 0.93 & ε = 0.83	$S_{spacer} = 6.3 * 10^{-3} \frac{kg}{m^2}$	
Outer coating: FEP/VDA	Shield Material: Kapton with VDA	
• α = 0.14 & ε = 0.6	$\rho_{shield} = 1461.5 \frac{kg}{m^3}$	
	Thickness shield = 0.013 mm	
	Thickness spacer = 0.16 mm	
	Total MLI thickness of 1.99 mm	
	$\frac{N}{\Delta x} = 5780\ m^{-1}$	

Figure 2.9: Overview of thermal design and performance of the current baffle. Values taken from E. Korhonen- and T. van Wees' theses [58] [102]

2.5.3. Baffle Improvements and Recommendations

Several design improvements and recommendations are mentioned by both E. Korhonen and T. van Wees, as well as noted by the author. These are discussed in Table 2.6 below.

Table 2.6: Improvement and recommendation list for the DST baffle

Improvement and Recommendation List T. van Wees [102]
1. Wrong RAAN of orbit modelled, leading to an orbit that does not experience an eclipse
2. MLI modelled as bulk material and conductively instead of effective conductivity / emissivity. MLI is modelled in the industry (ADS) as a plate with two layers with an effective conductivity and emissivity between the outer- and inner layer and based on empirical data to also take into account stand-offs / debris penetrations and other disturbances.
3. Different HOT and COLD cases are modelled based on different Sun-Earth orientations. This is not needed, as the DST operates in a SSO, meaning that the illumination angle (beta-angle) between the Sun and the DST orbit is roughly constant so the Sun-Earth orientation remains roughly constant
4. Thermo-elastic calculations only verified against coarse-alignment budgets and not in-orbit drift / stability budgets. The 2.23 µm thermo-elastic deformation of M2 conforms to the coarse-alignment budget, but **not** to the in-orbit drift budgets
5. Only thermo-elastic translation is taken into account and not rotation
6. Optimize the length and reflective internal structure of the baffle, as the extension of 20 cm in height as well as the reflective internal structure are based on estimations
7. Add reflective top vane to improve thermal stability as well as the mitigation of stray-light. However, as this affects the deployability of the current inflation system (since vanes are rigid), other deployable systems have to be investigated
8. No thermal analysis of the stowed configuration of the DST is made
Improvement and Recommendation List E. Korhonen [58]
9. High uncertainty in number of MLI layers, so this should be optimised
10. MLI properties have to be updated in the thermal model
11. Stowed volume of 1.8 m^3 exceeds the stowed volume requirement of 0.75 m^3 (goal) as well as 1.5 m^3 (threshold)
12. Mass of 23.6 kg exceeds the 15 kg mass requirement that was assigned to the baffle
13. No structural analysis of the stowed configuration of the baffle is made

2.6. Thesis Need and Goal

The baffle recommendations and improvements as mentioned above in Section 2.5.3 conclude that there is a lot of work to be done on the thermal- and mechanical design of the baffle.

From a thermal perspective, some modelling improvements can be made, as well as optimising the number of layers of MLI needed and thorough thermo-elastic calculations that have to be compared to the in-orbit drift budgets as these are the most crucial mechanical budgets. Also no thermal analysis in stowed state is performed yet. All points on the recommendation lists will be taken into account.

From a mechanical perspective, the mass and volume budgets of the mechanical deployment system were not met. Additionally, no structural analysis in stowed state is performed. Therefore, the following thesis need statement arises:

Thesis Need. *There is a need for the continuation of the thermal-mechanical design of the baffle of the Deployable Space Telescope in both deployed and stowed configuration to create and verify a stable and feasible thermal environment for the optical instruments so that the in-orbit drift budgets will be met as well as making improvements and design changes to the deployment system to ensure that mass-, volume- and structural requirements are met*

This thesis need statement flows down into a thesis goal that forms the fundament of what the author wants to achieve within his thesis, together with the means which will be used to achieve this goal. This is specified in a Specific, Measurable, Assignable, Realistic and Time-related (SMART) manner and shown below.

Thesis Goal. *The goal of this thesis is to further continue the thermal and mechanical design of the deployed- and stowed baffle of the Deployable Space Telescope that can deploy during LEOP and can create a stable thermal environment within the baffle so that in-orbit drift- and stability budgets of the optical systems will be met, by assessing and verifying new potential methods for baffle deployability, running thermal analyses that simulate the LEOP phase and operational in-orbit phase of the baffle, identifying a feasable thermal environment that can be reached within the baffle and performing a risk assessment to determine the level of impact (major/minor) of thermal- and deployability requirements*

2.7. Research Question

The research question that derives from the thesis need, goal and aim from Section 2.6 that is going to be answered is:

1. Which modifications are required to the existing thermal-mechanical design of the baffle to create a stable thermal environment such that the related thermo-mechanical budgets are met? Consequently, the overall design shall comply with the functional, characteristic and constraint requirements.

It is important to mention that the required modifications of the design shall comply with the functional, characteristic and constraint requirements.

2.8. Thesis Deliverables

The corresponding thesis deliverables are:

1. Baffle functional-, characteristic and constraint requirements
2. Integrated thermal-mechanical baffle design that conforms to both the thermo-elastic budgets and the functional-, characteristic and constraint requirements

2.9. Thesis Methodology and Set-Up

The methodology used to systematically and quantifiably answer the questions in this thesis is depicted in Figure 2.10. This methodology is based on the the Vee model, well known in the process of product development and general systems engineering processes. In this figure, the requirement-design-verification processes are highlighted (indicated in blue), and the chapter content that captures the flow of design (in green).

Figure 2.10 states that this thesis consists of several important building blocks, each working towards realising the end goal of answering the research questions mentioned in section 2.7. First off, system requirements are generated based on theory from literature, and system architecture mapping (N2, FFBD). Based on the requirements, and the definition of the thermal performance objective, two baseline functional performances can be calculated: *Baseline 1. Thermal Performance Without Baffle* and *Baseline 2. Baffle Design from E. Korhonen.* The current work of the author will be compared/benchmarked to both these baseline performances.

Next up, the passive thermal system is designed and optimized. This yields requirements for the mechanical design which is designed thereafter. Based on the fully designed mechanical deployment system, several thermal-mechanical iterations take place. Finally, the final design is verified with the set requirements and compared to the benchmark baseline models. The overview is given in Figure 2.10.

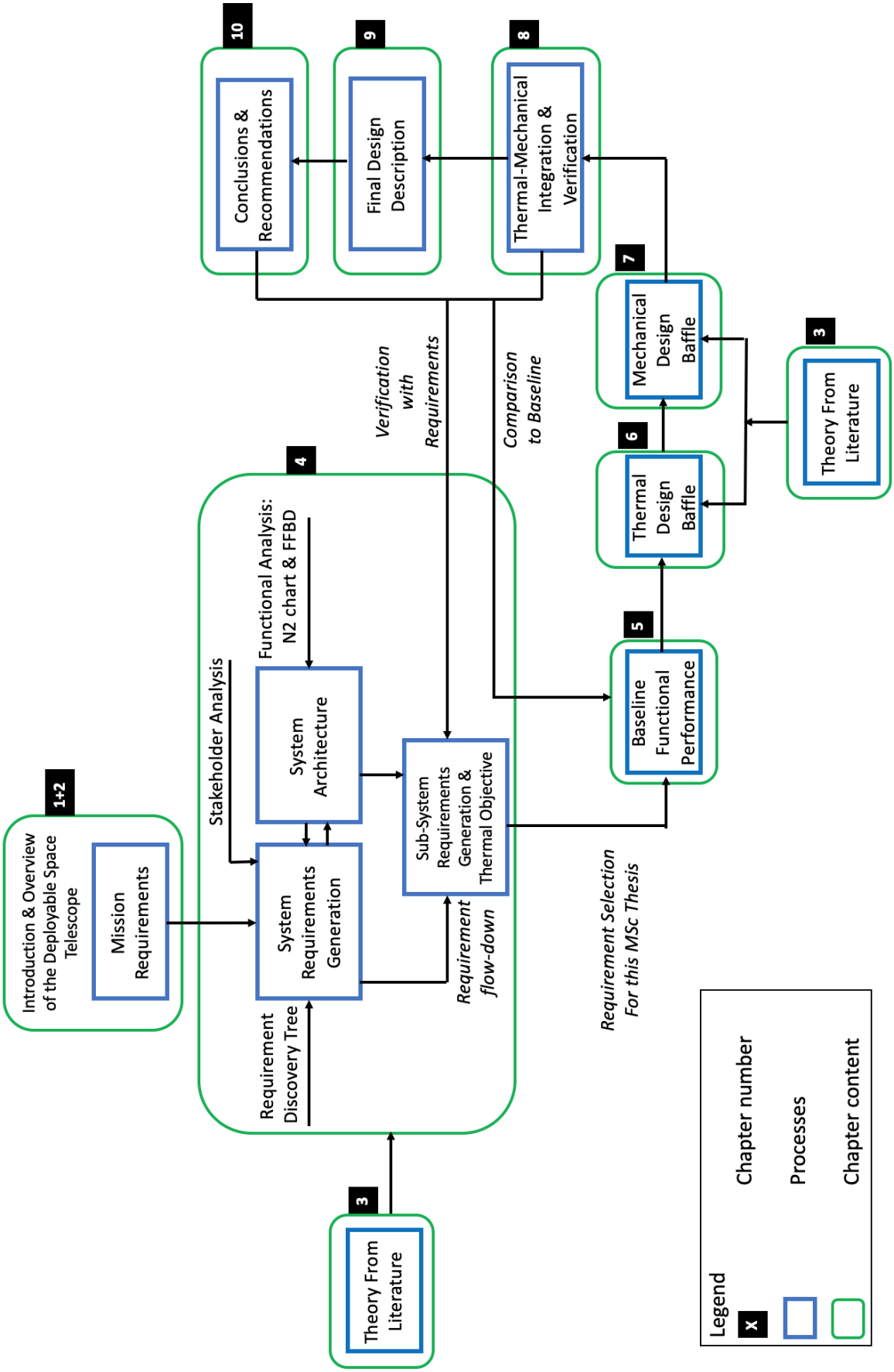

Figure 2.10: Thesis systems engineering processes (blue boxes) indicating the design flow including requirement- and verification matrix generation, the design- and verification iterative process. The chapter content (green boxes) as well as the corresponding chapter numbers are depicted as well

3

Background

This chapter summarizes relevant theoretical literature that is an input for the thermal- and mechanical design of Chapters 6 and 7 and the iterative thermal-mechanical chapter, Chapter 8.

The relevant theory for initiating the design can be categorised in eight sections. Section 3.1: DST Orbit Definition and Assumptions, Section 3.2: DST Space Environment, Section 3.3: Spacecraft Thermal Control Theory, Section 3.4: Theory about the design guidelines for thermal stability in opto-mechanical instruments, Section 3.5: Thermal Control Hardware, Section 3.6: Deployable space structures, Section 3.7: Thermal-Mechanical design uncertainties, and finally Section 3.8 that covers stray-light theory and the basic principles of stray-light attenuation/rejection. The majority of literature presented in this chapter stems from the Literature Study that was conducted before starting this MSc thesis. [3]. The most important conclusions are summarized in this chapter.

3.1. DST Orbit Definition and Assumptions

The current orbital configuration as was chosen for the DST is a Sun-synchronous orbit (SSO) at an altitude of 500 km and Local Time of Descending Node (LDTN) of 10:30 AM. The rationale for choosing this orbital configuration is summarized in Table 3.1. Furthermore, it is important to explain its characteristics, as the orbital configuration will be used as input for the thermal analyses.

SSO have the characteristic that their orbital plane rotates eastward with an angular velocity of around 360 ° per 365 days (precession rate): one full rotation per year. This is due to the Earth's oblateness and right combination of inclination and altitude. The combination of a 500 km altitude orbit with an inclination of 97.4° results in a perfect SSO. A perfect SSO therefore passes over the exact same point of the earth at the same LMT.

As a consequence of a SSO, the beta angle (the angle between the orbital plane of the DST and the vector of the Sun), remains almost constant. This yields an almost constant illumination under the same angle, that only depends on the Sun's declination. Please note that due to the small eccentricity of the Earth orbit around the Sun as well as a slight difference in the Sun's declination over the year, there is a difference in received heat flux. The constant beta angle is related to the LMT passage. Namely, for a dusk-dawn SSO for example, the beta angle is equal to 90 ° and has a crossing time at either 18:00 or 6:00 hr (around sunset or sunrise). Therefore, a dusk-dawn orbit will not experience any eclipses. This means that every 6 hours difference in LMT leads to a change in beta angle of 90 °. This translates to a change in beta angle of 22.5 ° for every 1.5 hours of change in LMT. For the DST, with a LMT is set to 10:30 AM descending node, this translates to a beta angle of -22.5 or $360 - 22.5 = 337.5°$. The RAAN (Right Ascension of Ascending Node) then is $180 - 22.5 = 157.25°$.

Table 3.1: Orbital Configuration- and Assumptions Definition

DST Orbit Definition and Assumptions		
Parameter	**Value**	**Argumentation/Comment**
Orbital Parameters Definition		
SSO	-	1. Widely used for Earth observation satellites (imaging/weather). 2. Nearly constant illumination angle of Sun when pictures are taken. 3. Nearly constant passage time of same spot on Earth [106] 4. Constant source of power solar panels
Altitude	500 km	1. Multitude of Earth observation telescopces range 443 - 550 km (ANT-1, ANT-2 and ARCTIC-1) [23]
Inclination	97.4 ∘	1. Yields a perfect SSO for an altitude of 500 km
LTDN	10:30 AM	1. Best trade-off between Europe Earth coverage and avoiding Sun glint (which is worst at 12:00 AM LTDN) [51]. 2. LTDN of 10:30 AM presents less cloud coverage than a LTAN of 1:30 PM [1]
Eccentricity	0	1. Constant velocity and orbit remains a SSO with additional constant inclination
RAAN	-22.5 ∘	1. Corresponds to LTDN of 10:30 AM
Orbital Assumptions		
Sun's right ascension & declination	0	1. Solar vector falls and vernal equinox fall together: Beta angle is now only dependent on the RAAN and orbit inclination
$\frac{di}{dt}$ and $\frac{dh}{dt}$	0	1. No change in orbital inclination and altitude: SSO remains perfect SSO
$\frac{d\beta}{dt}$	small ≈ 0	1. Beta angle also dependent on change in Sun's declination. However, change β is small for low β values.
N* of orbits modelled	1	1. Constant β angle, so constant thermal fluxes and environment 2. Significantly reduces computation time
Time steps / orbit	40	1. Default value. Leads to $\frac{T}{40} = \frac{5668}{40} = 141.7$ s / timestep
Effect On Orbital Configuration		
Beta angle (β)	-22.3 ∘	Based on $\beta = \Omega \cdot \sin i$, which only holds when Sun's right ascension and declination are 0
Orbital period	5668 s	Due to 0 eccentricity, orbital period only depends on the altitude.
Eclipse time	2102 s (37 % orbital period)	Dependent on the beta angle and height of orbit. Taken from [78]
In-Orbit Drift Budget Δt_{drift}	3566 s	Holds for Sunlit period of time.
Coarse Alignment Budget Δt_{coarse}	2102 s	Holds for period of time when DST is in eclipse.

3.2. DST Space Environment

The LEO environment that the DST is exposed to is harsh and serves many potential hazardous effects on materials. These effects include atomic oxygen, UV radiation, ionizing radiation (electrons, protons), high vacuum, plasma, micrometeoroids and debris, as well as severe temperature cycles.[46] These effects are briefly explained below, together with their effect on different materials. A full detailed analysis is made in the literature study of the author, [3]. For this thesis, the main environment types, their characteristics and solutions / mitigation strategies are summarized in Table 3.2.

Table 3.2: Orbital Configuration- and Assumptions Definition

DST Space Environment		
Environment Type	**Characteristics**	**Solutions** & **Mitigation Strategies**
Atomic Oxygen (AO)	About 96% of the LEO atmosphere consists of AO. [72] Detrimental for polymers: surface erosion, chemical composition changes, distortion of thermo-optical properties) [46]	1. AO resistant coatings such as S_iO_2 [72]
UV Radiation	Driving factor for need of thermal control. Causes degradation of material properties: polymer bonds can break, solar absorptance generally increases over time (for white paints due to change of color [66]), meaning that temperature levels increase over time [95]. This demands the usage of *end-of-life* valuesfor the absorptivity, resulting in oversized disigned components. [2]	1. Thermal control (passive and/or active) 2. Selecting appropriate coatings with similar BOL/EOL values
Ionizing Radiation	Effect on material degradation of solar cells and polymeric materials. (decreasing tensile strength) [46] Amount and intensity depends on orbital inclination, altitude and solar cycles. At higher altitude, there is a decrease in magnetic field strength of the Earth, so less protection against ionizing particles. A higher inclination will result in a higher radiation level as well,due to an increase in concentration of ionizing particles. [12]	1. (Massive) shields that absorb energy of radiation particles. 2. Active magnetic shields to deflect ergetic particles
High Vacuum	Likelihood of outgassing of the material (more severe with increasing temperature), such as polymers, cadmium, PVC, paints, composites. Threats: contamination of optical surfaces/solar panels resulting in a loss of performance, loss of dimensional stability and material property degradation. More severe in addition to atomic oxygen, UV radiation or thermal cycles. [46]	1. Thermal vacuum baking (minimum of 24 hours at a temperature above that expected in orbit or, if that is not known, at 100 °C) 2. Design vent paths 3. Be aware of line-of-sight contamination to optical surfaces. [72]
Plasma	Sources of plasma are the Ionosphere, (most important for DST), geomagnetic substorm activity and solar wind. [7] Effects: current drain on solar arrays caused by Solar array coupling to the plasma, generation and emission of plasma waves, increased surface contamination, charging effects with possible discharging [7] [59] [95]	1. Homogeneous, conducting surface lessens charge build-up [95]. 2. Proper grounding of metallic layers (MLI). 3.Using electrically conductive coatings/paints.
Debris	Orbital debris, classified in different regimes based on their size, present in mostly high inclination orbits thus important for the DST. Small particles (<1mm, majority of debris) can cause micron-size craters in surfaces. Large debris objects (>10 cm) can cause a total failure of the mission and break-up of S/C material. However low collision probability and often trackable thus not taken into account. Medium-sized debris: "The challenge to spacecraft designers" [9]: surface coating- material- window- and mirror degradation, and negatively affect thermal and optical properties.	1. Passive: normal coatings (for small particles), upgraded coatings, monolithic shields, (stuffed) whipple bumpers/shields. $t_{shield} \sim v_{impact}^{2/3}$. If $v_{impact} > 3$ km/s: whipple shield more efficient than monolithic shields. [96] [11] 2. Active: warning systems / shutters [9]
Temperature Cycles	Difference in heat flux due to shadowing. Thermal cycling temperature extremes depend on thermo-optical properties (solar absorptance and thermal emittance), view of the sun, view of Earth, view of other surfaces of spacecraft, durations of time in sunlight and in shadow, sits thermal mass and the influence of equipment or components that produce heat. [25] Material effects: thermal gradients and consequently thermo-elastic deformations, degradation of protective coatings if there is a mismatch in CTE between coating and substrate, cracking and peeling of coating pinholes. [72]	1. Right selection of absorptance and emittance of coatings. 2. Increase thermal mass. 3. Optimize geometry design for view factor tweaking

3.3. Spacecraft Thermal Control Theory

In this section, the theoretical background of satellite thermal engineering is discussed. Note that this stems from the literature study, so mainly all work from this section will be referenced back to the literature study. Additionally, only the basics and conclusive equations and theory are summed up in this section.

3.3.1. Heat Transfer Methods

Solar UV-radiation and thermal cycling due to shadowing are the driving factors for thermal control systems. This section will therefore state what the important heat transfer methods are in space, and internally within a S/C.

Radiation (External and Internal)

Radiation is the main driver of heat transfer in space, which consists of external and internal radiation. External radiation is characterised here as radiation from external bodies: the Sun and planets. The external radiation types are therefore Solar radiation, Albedo and IR radiation.

Radiation is either absorbed, reflected or transmitted by a material. The sum of the absorpted-, reflected- and transmitted radiation is always equal to 1: $\alpha + \rho + \tau = 1$. However, for an opaque material, there will be no transmission, so therefore the sum of absorption and reflection should always be equal to 1: $\alpha + \rho = 1$. The amount of reflected radiation can either be reflected in a specular, diffuse or directional manner. [21] This is also schematized in the literature study. [3]

External Radiation

External radiation is explained in detail in the literature study of the author, [3]. To conclude: Solar, Albedo and IR heat flux all depend on the view factor from the source to the impinging surface. The main view factor parameter is the orbital height. Solar heat flux also depends on the distance from the Sun to the Earth and a typical heat flux value, that will be used for the DST as well, is 1378.94 $\frac{W}{m^2}$.

The Albedo factor depends on the orbit of the S/C, and can vary between 0.05 (open ocean) and 0.6 (high cloud/icecap). The visiblity factor depends on the distance of the S/C to the Earth and the angle between the surface normal and the solar Albedo rays. It is maximum at the sub-solar point, since the angle between the surface of the earth and the Sun's rays is perpendicular. As the satellite completes its orbit and moves away from this subsolar point, the local indicent solar energy per square meter decreases with the cosine of the angle from the sub-solar point. [41] At the boundary between between the sunlit- and dark side of the Earth, this angle is 90 ° and therefore the Albedo value decreases to zero. This means that for a dusk-dawn orbit with a RAAN of 90 °, the Albedo always remains zero, since this orbit is on the vicinity of this sunlit-dark boundary line and does not experience any eclipses. The average Albedo factor is 0.304.

IR radiation is radiation emitted by the Earth, due to its effective radiating temperature, itself. Since the Earth has a lower temeprature than that of the Sun, the radiation emitted has a wavelength in the domain of the IR frequency spectrum. The effective radiating temperature of Earth is 255 K, resulting in an IR-flux for the DST of 206.1 $\frac{W}{m^2}$

In Table 3.3 these three types of external radiation are summarized.

Type	Parallel/Diffusive	Wavelength [μm]	Typical external heat flux value (J) for DST [$\frac{W}{m^2}$]
Solar	Parallel	0.5	1378.94
Albedo	Diffusive	0.5	362.81
IR	Diffusive	1-35	206.1

Table 3.3: External radiation information: Solar- Albedo- and IR-radiation

Internal radiation: From and to surfaces of S/C

Internal radiation is defined here as radiation from- and to surfaces of the S/C. Since this radiation is coming from the S/C itself, which has a relatively low (room) temperature, the frequency of the electromagnetic waves are that of the IR frequency spectrum. Based on Kirchoff's law, a good emitter is a good absorber for a specific range of wavelengths. Therefore, the absorptance of IR flux is equal to the emittance of IR flux (within a specific range of wavelenghts). For internal radiation the distances between surfaces of a S/C that emit and absorb radiation are relatively short, and include reflection, absorption and emission (and transmission for transparent materials). Internal radiation between surfaces depend on the view factor between those surfaces.

The amount of total absorbed radiation by a non-black body (=grey body) surface takes into account all reflections from other surfaces and the absorptance (= the emittance in the IR-frequency band stated by Kirchoff's law) of the surface receiving the internal radiation. The amount of absorbed radiation from surface dA_i to dA_j is stated in Equation 3.1 below, and is of similar form as that of black-body radiation given by only

view factors.

$$\mathrm{Q}_{ij} = \varepsilon_i \mathrm{A}_i \mathrm{B}_{ij} \left(\sigma \mathrm{T}_i^4 - \sigma \mathrm{T}_j^4\right) = R_{ij} \left(\sigma \mathrm{T}_i^4 - \sigma \mathrm{T}_j^4\right) \tag{3.1}$$

The result of Equation 3.1 is true due to the following symmetry rule: $\varepsilon_i A_i \mathrm{B}_{ij} = \varepsilon_j A_j \mathrm{B}_{ji}$. In Equation 3.1, B_{ij} is known as the Gebhart factor, which is the defined as the fraction of radiation emitted by surface A_i which is absorbed by surface A_j. The Gebhart factor B_{ij} between A_i and A_j is given in Equation 3.2.

$$B_{ij} = F_{ij}\varepsilon_j + \sum_{k=1}^{n} (1-\varepsilon_k) F_{ik} B_{kj} \tag{3.2}$$

In Equation 3.1, an important parameter can be distinguished, $R_{ij} = \varepsilon_i \mathrm{A}_i \mathrm{B}_{ij}$, which is the radiative coupling between two surfaces. This parameter is used in the calculation of heat balances between surfaces. The radiative coupling depends on areas, view factors, surface properties and multiple refelctions from all other surfaces.

Convection
Convection is a heat transfer method due to movement of a fluid. It is therefore abscent in the vacuum of space, but not always within the S/C internally. Some active thermal control systems, like coolers or heat exchangers, make use of some operating fluid, e.g. for the use of cooling optical instrument buses. Since this is not part of the space environment, but part of the satellite thermal control system, convection is not further discussed here.

Conduction
Conduction is of local importance and takes place within the S/C through parts and between parts that are in direct contact with each other. Conduction is expressed by Fourier's law of conduction. The conductive coupling similar to the radiative coupling for radiation heat transfer between surfaces. This is shown in Equation 3.3.

$$\mathrm{Q}_{ij} = \frac{kA}{L}(T_i - T_j) = C_{ij}(T_i - T_j) \tag{3.3}$$

In Equation 3.3 it becomes apparent that the conductive coupling between two surfaces i and j is $C_{ij} = \frac{kA}{L}$, in $[\frac{W}{K}]$.

Furthermore, contact conductance between interfaces is important to characterize. This is extensively explained in the literature study of the author and not further explained. [3]

3.3.2. Total Heat Balance

The total general heat balance for the DST can now be established. This heat balance is a balance between the external fluxes and internal fluxes. Internally, also heat dissipation can take place, which in general is the result of dissipated heat from electrical componenets. The total transient heat balance of isothermal nodes (which are assumed to be lumped parameters) is then given in 3.4. In this equation, transient means that the temperatures are dependent on time. This is the opposite of steady-state, in which the equilibrium (final) temperatures are calculated. For steady-state heat transfer, the $Q_{in} = Q_{out}$.

$$\left(mc_p\right)_i \frac{dT_i}{dt} = P_{dissipated} + \sum \left(\alpha A_S J_{\mathrm{Sun,D}} + \alpha A_A J_{\mathrm{A}} + \varepsilon A_E J_{\mathrm{IR}}\right)_i - \sum_j R_{ij}\sigma\left(T_i^4 - T_j^4\right) - \sum_j C_{ij}\left(T_i - T_j\right) \tag{3.4}$$

In Equation 3.4, m_i is the mass of the isothermal thermal node i, $(c_p)_i$ is the specific heat of the isothermal node i and $(mc_p)_i$ combined is known as the thermal mass of the isothermal node i. Equation 3.4 can be applied to a thermal network in which all couplings (radiative and conductive) of all nodes are stated.

3.4. Design Guidelines for Thermal Stability in Opto-Mechanical Instruments

For opto-mechanical instruments, like space telescopes that are mounted on support structures, thermal distortions and vibrations are crucial to take into account in the early design stage. Thermal gradients, ΔT, are related to thermo-elastic elongations/contractions.

The governing equation for thermo-elastics, for linear deformations:

$$\Delta L = \alpha \cdot L_0 \cdot \Delta T \tag{3.5}$$

In this equation, ΔL is the elongation/contraction of a material that initially has a length L_0, both in m. Furthermore, ΔT is the change in temperature in ° C and α is the Coefficient of Thermal Expansion (CTE) of that material.

For thermo-optical stability, a three-step methodology can be used as a design guideline. See Figure 3.1, taken from [40].

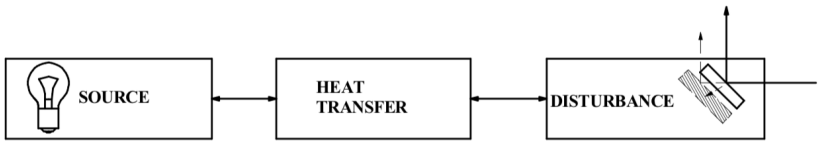

Figure 3.1: Design guideline methodology for opto-mechanical structures like the DST

In Figure 3.1, the three steps are source, heat transfer and disturbance, which will be elaborated on below.

3.4.1. Source

Source is defined as the source of heat that thermally influences the opto-mechanical instruments. This can be Solar-, Albedo- and IR radiation, as well as dissipation from electrical sub-systems or an actuator. For the DST, the primary heat sources are external heat sources: Solar-, Albedo- and IR heat fluxes, which are assumed to dominate the other types of (internal) heat transfer sources. The source is thus external, and changes during orbit due to attitude changes and the presence of an eclipse (about ≈ 38 % of the orbital period for the DST orbit). The heat source is a given, and for the DST, this cannot be mitigated. However, the *heat transfer* from the source to the system can be designed for and is explained next.

3.4.2. Heat Transfer

Heat transfer is the transfer of heat between the external sources mentioned above and "the position where it can disturb the optical performance", [40], i.e. the opto-mechanical instruments and support structures of these mirrors. This heat transfer should be minimized to ensure low ΔT, see Equation 3.6, which specifies that the change in temperature of a mechanical system is equal to the mass (thus density), specific heat and amount of heat added.

$$m \cdot c_p \cdot \Delta T = \Delta Q \rightarrow \Delta T = \frac{\Delta Q}{m \cdot c_p} \tag{3.6}$$

In this equation, m is the mass in kg, c_p is the heat capacity in $\frac{J}{kgK}$, ΔT is the change in temperature in K and ΔQ is the change in heat added to the system, in J. From this, it can be concluded that for a given change in heat source, the temperature change can be mitigated by selecting materials with a large heat capacity and/or large density, as well as ΔQ should be minimised to lower the change in temperature.

Minimising heat transfer can be controlled by proper insulation to the opto-mechanical systems (which is what the baffle will be used for), as well as locally applying high conductivity materials, which will increase the heat transfer along a material and therefore decrease thermal gradients.

3.4.3. Disturbance

Thermo-mechanical disturbances on the optical performance can be mitigated or controlled by roughly four methods: [40]

1. Using a thermal centre
2. Combination of materials with different coefficients of thermal expansion (athermalisation)
3. Low thermal expansion materials
4. Scaling effects of the optical design

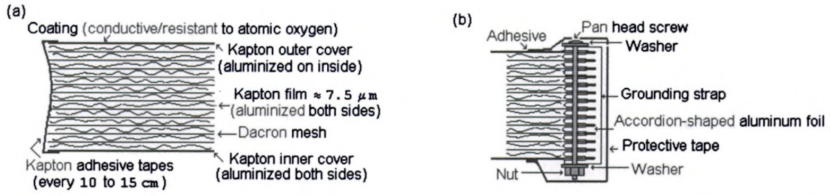

Figure 3.2: Typical lay-up of MLI: (a) typical lay-up and (b) electrical grounding. Taken from 3.2

Athermalisation is currently applied to the SMSS of the DST. Athermalisation is the process of effectively counteracting deformations by placing two opposite members, one with a long length and small CTE and the other with a small length and high CTE, with as a result a minimization of the net thermo-elastic displacement. For the SMSS this is implemented by choosing a CFRP material with low CTE for the long and slender booms and aluminium, which has a 23 times higher CTE than CFRP, for the small rods that hold the M2 in place.

Some satellites, like the Euclid, make use of adaptation rings to compensate for thermo-mechanical effects in optical elements. These adaptation rings are glued to the optical elements and are required to introduce quasi zero forces and torques to elements, preserving the shape and position in compliance with optical tolerances. [64] Another method to reduce thermo-elastic effects, is the use of low-CTE materials. Some CFRP can be designed such that the layup of the CFRP results in a near-zero CTE property.

The baffle has the highest influence on the blocking of heat transfer from external sources to the position where it can disturb the optical performance, i.e. by means of insulation and shielding. The performance of the baffle should therefore be measured by the amount of heat it can shield, or indirectly by the change of temperature it causes on the opto-mechanical structures. The thermal objective is also defined and explained in Section 4.7.

3.5. Thermal Control Hardware

3.5.1. Passive Thermal Control (PTC)

Several relevant passive thermal control systems are mentioned here that could - and already are - applied to the DST baffle.

Multi-Layer Insulation (MLI)

MLI is a stack of alternating layers of heat reflecting radiation shields with a low emissivity and low conductance spacers. [93] A typical MLI lay-up is shown in Figure 3.2. MLI thermally insulates the spacecraft with the surroundings through the use of radiation between the reflecting shields. MLI is often used as a passive thermal control system and often consists of Kapton or Mylar sheets with deposited aluminium on both sides as a heat reflecting radiation shield, seperated by Dacron layers as spacers. Dacron has a low thermal conductivity and is therefore a good isolator, since the heat transfer through conduction should be minimized. This is comparable to the MLI that is used on the Hubble telescope or JWST for example. First the working principle will be explained, then the performance parameters and finally some concerns will be touched upon.

Theoretical Idealized MLI Performance

The effective heat flow between N numbers of MLI is dependent on the temperatures of the two plates, the area and the emissivity (which are the same for both plates). [3]. Hence, selecting materials for the MLI layers with a low emissivity, will drastically reduce the net heat flow between the layers. The total effective emissivity for N numbers of MLI layers is stated in Equation 3.7:

$$\varepsilon_{eff} = \frac{1}{[N+1]\cdot[\frac{1}{\varepsilon_{outside}} + \frac{1}{\varepsilon_{inside}} - 1]} \tag{3.7}$$

When using a black material (which is a flat absorber with high solar absorptance and high IR emissivity of $\approx$ 1), an effective emissivity for 2 layers of black sheet MLI is $\approx \frac{1}{3}$. When using 5 layers of MLI with aluminium as a shield material the ideal effective emissivity becomes 0.0064. This value is in practice much higher due to degrading effects, resulting in higher values for the total emissivity in the order of 0.01. [20] The degrading effects and corresponding MLI performance is explained below.

Actual MLI Performance
The degrading effects of MLI which are the cause of the deviation of the effective emissivity to the theoretical value are [20] [3] [54]:

1. Contact → conduction
2. Perforations
3. Stand-offs, spotwelds, holes
4. Temperature levels of layers
5. Debris penetrations

Due to these reasons, empirical relations are used to calculate the effective emissivity and conductivity of MLI that take most disturbances into account and which are tested on actual satellite programs, such as the HIPPARCOS project. [20] The usage of empirical data for the calculation of effective emissivity and conductivity is supported by N. van de Pas, who is a senior thermal engineer at ADS in Leiden. Through contact N. van de Pas advised the author to model MLI as a shell with different sides: the inner layer of MLI and the outer layer of MLI. Between these layers there is an effective emissivity and conductivity and these values can be based on empirical data. The empirical relations are discovered by Doenecke [26] and used for spacecraft thermal control applications. Additional information on the Doenecke method is also found in [27]. The empirical relations found by Doenecke are:

$$\varepsilon_{eff} = \left(1.36 \cdot 10^{-4} \frac{1}{4\sigma T_m^2} + 1.21 \cdot 10^{-4} \cdot T_m^{\frac{2}{3}}\right) \cdot f_N \cdot f_A \cdot f_P \tag{3.8}$$

$$f_N = 4.5465 \cdot N^{-0.501} \tag{3.9}$$

$$f_P = 0.2685 \cdot P + 0.73 \tag{3.10}$$

$$f_A = \begin{cases} 3, & A < 0.05m^2 \\ 0.6638, & A > 3m^2 \\ 0.1^{(0.373 \cdot \log_{10} A)} & 0.05m^2 \leq A \leq 3m^2 \end{cases}$$

In these equations T_m is the mean temperature of the MLI layers:

$$4T_m^3 = \frac{T_h^4 - T_c^4}{T_h - T_c} = \left(T_h^2 + T_c^2\right) \cdot (T_h + T_c) \tag{3.11}$$

N is the number of MLI layers, P is the fraction of of blanket area taken up by penetrations and A is the exposed MLI area on which the heat transfer takes places. A typical value for f_P is on average 1, meaning that P is also equal to 1 according to Equation 3.10. [27] [26]

The effective emissivity exponentially decreases with increasing number of MLI layers. The corresponding effective conductivity then is:

$$c_{eff} = 4\varepsilon_{eff}\sigma \cdot T_m^3 \tag{3.12}$$

The uncertainty of the MLI calculation is expected to be 25% as was found in the HIPPARCOS project. This value will also be taken into account when performing a sensitivity analysis in a later stage.

It can be seen that the effective emissivity is dependent on the the mean temperature of MLI, which is dependent on the hot and cold layers of the temperature (outer and inner layers). Also note that the outer layer can either be the hot layer at some time and the cold layer at other times. Same holds for the inner layer. However, the hot and cold temperature of the inner-outer layers is on its own dependent on the effective emissivity. Schematized:

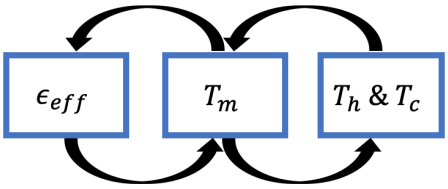

Figure 3.3: Dependence of the effective emissivity on the mean blanket temperature and hot and cold temperature of the inner/outer MLI layer. However, the hot and cold temperature, and thus the mean blanket temperature, is dependent on what the effective emissivity is. Therefore, establishing stable values for the effective emissivity/conductivity requires iteration as was also concluded in [27]

The dependence as shown in Figure 3.3 therefore results in an iterative process to establish stable values for the effective emissivity/conductivity, as was also concluded in [27].

MLI Bulk Property Calculations
The MLI bulk properties can be calculated. The bulk MLI density, $\rho_{MLI,bulk}$, calculation stems from the Cryogenic Heat Transfer book, [6], which specifically states the MLI bulk density calculation methodology. Other values, such as the specific heat (c), conductivity (k) are based on the mass rule of mixtures. Additionally, the Young's modulus (E) and Poisson ratio ν are based on the thickness rule of mixtures. The rule of mixtures can be used for composite materials and relate the properties of the individual materials to the effective properties of the bulk material. [65]

Table 3.4: MLI bulk properties based on the rule of mixtures for composites

MLI Bulk Properties				
Parameter	**Formula**	**Value**	**Units**	**Comment**
$\rho_{MLI,bulk}$	$\left(S_{spacer} + \rho_{shield} \cdot t_{shield}\right) \cdot \frac{N}{\Delta x}$	146	$\frac{kg}{m^3}$	taken from the Cryogenic Heat Transfer book, which specifically dedicates a section to the methodology of calculation MLI bulk properties. Typical values between 32 - 320 $\frac{kg}{m^3}$ [6]
$c_{MLI,bulk}$	$\left(\frac{m_{Kapton}}{m_{total}}\right) c_{p,Kapton} +$ $\left(\frac{m_{Dacron}}{m_{total}}\right) c_{p,Dacron}$	1117.5	$\frac{J}{kgK}$	Mass fraction of Kapton versus Dacron w.r.t. the total mass of MLI are: $\frac{m_{Kapton}}{m_t otal} = 0.75$ and $\frac{m_{Dacron}}{m_t otal} = 0.25$. Specific heat Kapton is 1090 $\frac{J}{kgK}$. [29] Specific heat Dacron spacer can range between 1200 - 1350 $\frac{J}{kgK}$ according to [43]. Lowest value of 1200 $\frac{J}{kgK}$ is used (worst hot case).
$k_{MLI,bulk}$	$\left(\frac{m_{Kapton}}{m_{total}}\right) C_{p,Kapton} +$ $\left(\frac{m_{Dacron}}{m_{total}}\right) C_{p,Dacron}$	0.1275	$\frac{W}{mK}$	Conductivity Kapton is 0.12 $\frac{W}{mK}$. [29] Conductivity Dacron spacer can range between 0.15, [62], to 0.24 $\frac{W}{mK}$, [101]: lowest value of 0.15 $\frac{W}{mK}$ chosen (worst case).
$t_{MLI,bulk}$	$N \cdot t_{shield} + (N+1) \cdot t_{spacer}$	TBD	m	Total MLI thickness depends on number of layers N. This is going to be analyzed within this thesis.
E_{eq}	$E_{Kapton} \cdot \frac{t_{Kapton}}{t_{Kapton}+t_{Dacron}} +$ $E_{Dacron} \cdot \frac{t_{Dacron}}{t_{Kapton}+t_{Dacron}}$	2.92	GPa	Rule of mixtures, based on volume fraction instead of mass fraction. E_{kapton} = 2.5 GPa, E_{dacron} = 2.95 GPa. [29] [43]
ν_{eq}	$\nu_{Kapton} \cdot \frac{t_{Kapton}}{t_{Kapton}+t_{Dacron}} +$ $\nu_{Dacron} \cdot \frac{t_{Dacron}}{t_{Kapton}+t_{Dacron}}$	0.40	-	Rule of mixtures, based on volume fraction instead of mass fraction. ν_{kapton} = 0.34, ν_{dacron} = 0.405. [29] [43]

In Table 3.4, S_{spacer} is mass of spacer material / unit area in $\frac{kg}{m^2}$, ρ_{shield} is density of shield material in $\frac{kg}{m^3}$, t_{shield} is thickness of radiation shields in m and $\frac{N}{\Delta x}$ is layer density. One layer, N, is defined as one layer of shield material and one layer of spacer material. [6]

Coatings
Surface finishes and coatings are used for thermal control and corrosion resistance since it can alter surface properties. Coatings change the thermo-optical properties of a surface: the $\frac{\alpha}{\epsilon}$ factor, which is the most important driver for thermal control as both the absorptance and emissivity control the temperature levels of parts of a S/C. [93]

In practice the coatings may be divided in four different segments :

	Solar Reflector	**Solar Absorber**	**Flat Reflector**	**Flat Absorber**
Property	low α, high ϵ	high α, low ϵ	low α, low ϵ	high α, high ϵ
Examples	White paint, OSR	Polished metal surfaces/coatings	Aluminium paints	Black paint

Table 3.5: Division of coatings, taken from [93]

Material	**Solar Absorptivity α**	**IR Emissivity ε**	$\frac{\alpha}{\varepsilon}$
General			
Black paint	0.96	0.75-0.88	1.09 -1.28
White paint	0.17-0.38	0.82	0.21 - 0.46
OSR	0.09	0.76	0.12
CFRP	0.92	0.82	1.12
Specific for DST (Used for Outer Coating Trade-Off)			
Aluminized Kapton (Al. outside)	0.15	0.05	3
Aluminized Kapton (Al. inside)	0.41	0.75	0.55
Black Copper	0.98	0.63	1.56
Aeroglaze L-300	0.95	0.84	1.13
Aeroglaze A971 yellow paint	0.43	0.89	0.48
Blue anodized titanium foil	0.70	0.13	5.38
Alodyne Aluminium 6061-T2	0.44	0.14	3.14
Alodyne Aluminium 2024	0.42	0.10	4.20
Aluminized Teflon foil 5 mil	0.15	0.75	0.2
Silvered Teflon foil 5 mil	0.11	0.80	0.14

Table 3.6: Relevant optical properties of widely used space coatings

Threre are different types of black- and white paints. Chemglaze Z306, which consists of polyurethane with carbon, is a standard type of black paint and e.g. Vantablack is a relatively new researched black paint. An example of a white paint is SG121FD, which consists of a Silicone binder and encapsulated Zinc Oxide pigment. OSRs, which are solar reflectors, consist of a thin sheet of glass or quartz, silverized/aluminized on one side one one side by vacuum evaporation. The side that is silverized/aluminized is placed on the desired S/C exterior wall with conduction adhesive. This helps to control temperatures locally in areas where high dissipation takes place, such as batteries, output multiplexier. [93]

Different surface finishes can be used which thermal properties and more. *Black anodizing* films have a high absorptance and emmitance and are used for areas, where high heat dissipation takes place, to minimise temperature gradients. However, since they have high weight loss and volatile condensed materials percentage, their use in optical systems is prevented, thus making it non-ideal for the use of the interior of the baffle of the DST. *Hard anodizing* improves abrasion resistance and prevents for cold welding. *White anodizing* provides a film with low absorptance, <0.2, and high emittance, >0.8, therefore making it a solar reflector. Reynolds Metals Co. developed a white anodising process, which consists of "mixed electroly system of double salts of titanium/zirconium, polyhydric alcohol, carboxylic acid and sulphuric acid". [93]

Aluminized polyimide is also often used as a layer for coating, however the outer coating the polyimide is not aluminized, but the inside is. A well known example of a polyimide is Kapton, and is often used for MLI.

An overview of common coatings is summarized in Table 3.6.

3.5.2. Active Thermal Control (ATC)

There are many active thermal control methods and hardware versions. For the DST, in which deployability is required, some active thermal control methods which involve deployable hardware is considered here, thus only relevant for the DST baffle.

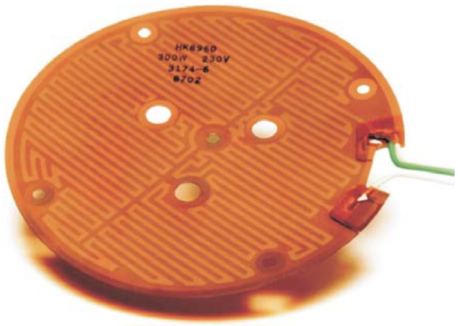

Figure 3.4: Polymide Thermfoil heater schematized

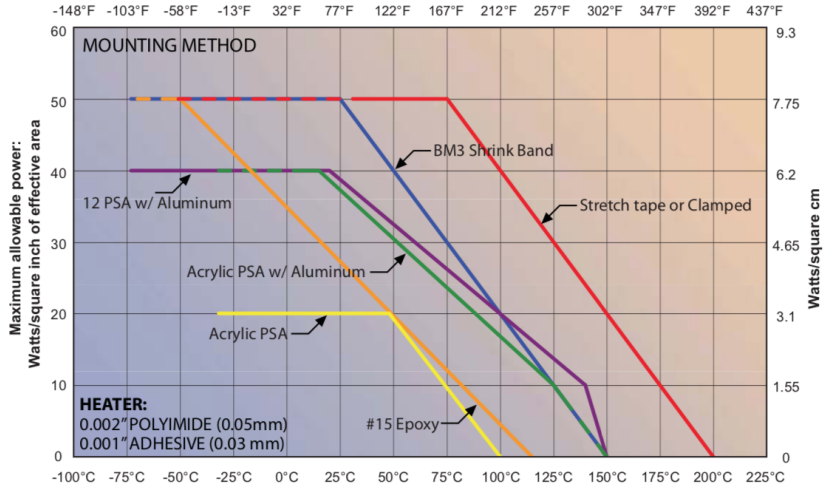

Figure 3.5: Dependence of service temperature- and mounting technique on power density of Polymide Thermofoil heaters

Heaters

Several heaters can be used to heat a component through dissipation. The temperature is monitored with a thermistor/thermostat and based on these values temperature actuation is performed.

A type of heater that is a good candidate (if active thermal control is needed) are Polymide Thermfoil heaters, since they are flexible with a minimum bending radius of 0.8 mm, are well embedded in Kapton (for the DST baffle MLI) and have a large temperature operation limit of -200 to + 200 ° C. [70] This heater is displayed in Figure 3.4. These heaters can provide a maximum power of around 750 W and minimum power of around 1 Watt, depending on the size of the heater. It also depends on the mounting technique and operation temperature.[70] The dependence on service temperature and mounting technique is given in Figure 3.5. From this figure it can be seen that the average power density is around 5 $\frac{W}{cm^2}$, but depends on the service temperature and mounting technique. Therefore, in order to use Polymide Thermofoil heaters for the DST baffle, care must be taken what the service temperature is of the inner layer of the baffle and what mounting technique will be used.

The average power can be calculated using:

$$P = \frac{V^2}{R} \tag{3.13}$$

In which V is the voltage in V, and R is the resistance in Ohms and P the power in Watts.

3.6. Deployable Space Structures

In the literature study of the author, [3], a detailed overview of potential deployable structures is made. The most important findings are briefly summarized in this thesis.

3.6.1. Telescopic Booms

James Webb Space Telescope (JWST) uses telescopic booms to deploy its Sun shield. The telescopic boom is shown in Figure 3.7, which is designed by Northrop Grumman. These telescopic booms are actuated by means of strain energy Storable Tubular Extendible Member (STEM) booms. The mid-boom STEM deployment actuator of the JWST is visualized in Figure 3.6.

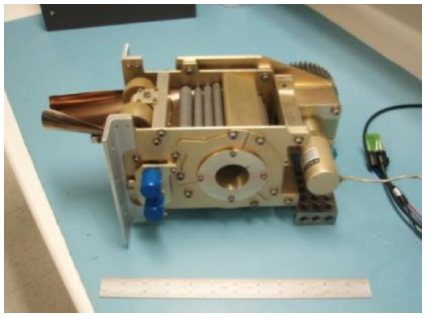

Figure 3.6: JWST mid-boom deployment actuator

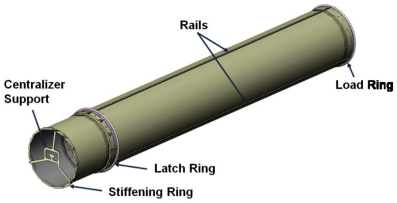

Figure 3.7: Telescopic Tubular Mast, designed by Northrop Grumman

Telescopic booms seem promising, as they have flight heritage in space, use reliable strain based energy springs/booms for deployment (also for the JWST Sun shield) and can provide a large deployment ratio. Telescopic booms can be used for both the radial and axial deployment of such a system, while other deployment techniques might not.

3.6.2. Sarrus Linkage

A Sarrus linkage uses a conventional scissor-linkage mechanism, which can be useful for the deployment of antennas or other hardware. It is proven to be a widely used and reliable deployment technique, so it is worth stating its heritage.

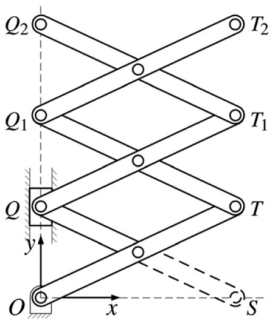

Figure 3.8: Sarrus Linkage

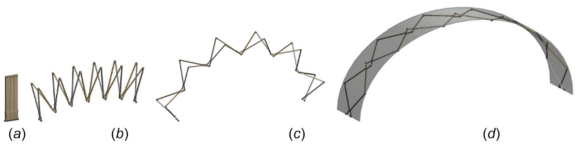

Figure 3.9: Bennet Linkage

Sarrus linkages are however tough to implement for a baffle, as the baffle needs to have a deployment ratio in both radial and axial direction.

3.6.3. Bennet Linkage

Lu et al, [68], have used the conventional bennet links to tessellate a half cylindrical shape into polygonal shapes. This could potentially be a solution for the deployment of the baffle which decreases mass, volume and increases deployment reliability. It is based on revolute joints.

The same problem with Bennet linkages apply as for the Sarrus linkage: it is difficult to yield a large deployment ratio in 2 dimensions, which is needed for the baffle. The current baffle height is around 3 m with a radius of around 1 m, while the stowed volume cannot exceed 1.5 m^3. The deployment volume ratio is thus around $\frac{\pi 1^2 \cdot 3}{1.5} = 6.28$. The radial deployment would work but axial deployment (to reach to a height of 3 m from a stowed height of $\approx$ 1 m) is extremely difficult.

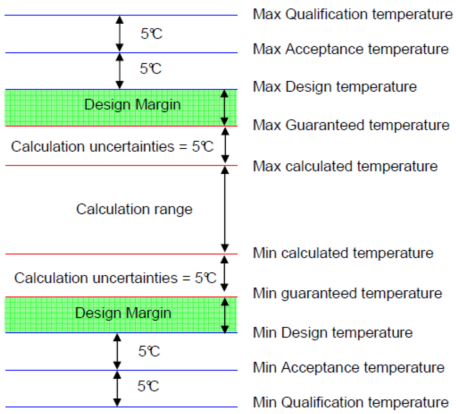

Figure 3.10: Appropriate temperature design margins, taken from [74]

3.7. Thermal-Mechanical Design Uncertainties

When design a thermal-or mechanical system, uncertainties have to be taken into account which could lead to an accumulated deviation from the designed performance. Especially for the early design phase and Phase-A studies, this is crucial as the design is immature and still in feasibility stage or preliminary design phase. Safety margins are therefore applied to take these uncertainties into account. These may differ for different applications, and a distinction between thermal- and mechanical uncertainty margins is made.

3.7.1. Thermal Design Uncertainties

For a TCS, different uncertainty margins for different design phases hold. In general, a 5 degrees temperature calculation uncertainty margin is applied, as dictated by NASA. This is also visualized in Figure 3.10 [74] Furthermore, for acceptance and qualification, additional margins of 10 - 15 degrees are applied, but for the DST preliminary design the calculation uncertainties of 5 degrees as pictured in Figure 3.10 will be applied.

3.7.2. Mechanical Design Uncertainties

For mechancial systems, the mass uncertainty of preliminary space structure designs is often 25 % for Phase-A/B phase design. [55] [32] This value will also be chosen for the mass budget uncertainty of the DST baffle.

3.8. Basic Principles of Stray-Light Attenuation/Rejection

Although the focus of this thesis does not lay on stray-light analysis, it is important to characterize what the basic principles of attenuating/rejecting stray-light are. These can be implemented in the design and a proper stray-light analysis can be made by someone else to verify the functionality of its design. First of all, stray light is defined as "light that reaches the detector, which is at a wavelength other than that which is intended to be measured" [98]. To this end, it is important to classify various types of stray light.

3.8.1. Stray-Light Classification

Various types of stray-light are classified here. These all stem from literature: [98].

Diffusive Stray Light

Light that is diffusely reflected by structures or imperfect mirror surfaces inside the housing, consequently hitting the detector array at all or many pixels. Absorptive coatings reduce the diffusive reflection.

Specular Stray Light

Light that is specularly reflected by structures or imperfect mirror surfaces inside the housing, consequently hitting the detector array at all or many pixels. Absorptive coatings reduce the specular reflection.

Out Of Range Stray Light

Light with a wavelength that is out of the wavelength range of the telescope and gives rise to a signal at some wavelengths which is inside the measurement range wavelength. For the DST this is typically infrared (IR)

from the Earth's radiation (due to its 255 K temperature) and ultraviolet radiation (UV) from the Earth Albedo and/or Sun.

3.8.2. Interior Design

Stray light can be controlled by means of using appropriate coatings for the interior layer of the DST baffle. The interior of the baffle can be made, and is made in the current version, of a highly absorptive black painted surface, since it then does not reflect much radiation. This is also done for the Hubble Space Telescope (HST) baffle: the interior of the Light Shield and baffles consist of black painted surfaces (Chemglaze Z306 diffuse blackpaint), due to its high absorptivity (low reflectivity). [16] How absorptivity and reflectivity are related is stated in Equation 3.14 (for a transparent material) and 3.15 (for an opaque material).

$$a + \rho + \tau = 1 \tag{3.14}$$

$$a + \rho = 1 \tag{3.15}$$

Hence for an opaque material, the reflectivity is low when the absorptivity is high and vice-versa.

Low reflectivity (high emissivity and high absorptivity) black surfaces have a number of applications, such as mitigating and reducing stray-light in baffles, light shields and cold stops in infrared detector assemblies. [77] Also, in the literature study of the author, [3], it is found that "the design of the baffle needs to very carefully weigh the benefits of diffuse versus specular vane surfaces. For example, diffuse surfaces tend to be more susceptible to outgassing and particulate contamination of nearby surfaces than do specular. However, with the specular approach slight design errors or manufacturing tolerances can be more critical."[77]

Additionally, it was shown that after thousands of hours the IR emmitance and Solar absorptance of the black paint degraded with less than 2 %, due to Atomic Oxygen and long solar UV exposure. [16]

3.8.3. Adding Baffles (Truncated Cones/Vanes)

In addition to choosing appropriate interior coatings, baffle vanes or truncated cones can be applied that have to be reflective such that it reflects incoming stray-light under some incident angle. Terebizh, [97], defined as a rule of thumb for baffle design for Cassegrain telescopes that two truncated cones can be used to block direct light in reflectors of open structures. The two truncated trones should be situated near the primary and secondary mirror, which prevents direct light from any incident angle, as well as reflected light from the tube from reaching the focal plane. [97]

Furthermore, the BepiColombo Laser Altimeter (BELA) has used a reflective baffle which "both reduce straylight to the best possible extent and minimize the heat load to the spacecraft" [91]. Therefore, this might be a suitable solution for the DST baffle, since it yields both stray-light mitigation and reducing external heat sources for the creation of a more stable thermal environment. Its thermo-optical requirements are.

Table 3.7: Summarized requirements for the stowed configuration, including verification methods used

Requirements From Literature [97] [91]
1. The baffle shall provide an aspect angle of ≤ 35 deg
2. The reflection efficiency of the baffle in the solar spectrum between 200-2500 nm shall be > 93 %
3. The reflection efficiency of the baffle in the thermal IR range between 2.5-8 μm shall be > 98 %

4

Requirement Generation

This chapter contains the generation of requirements stated as a first thesis deliverable. Verification of the thermal-mechanical design is then performed by verifying the performance to these set requirements.

The requirements that are derived in this chapter hold for the baffle system and hence are referred to as baffle system requirements. There is a distinction to be made between three types of baffle system requirements:

- Functional / input-output requirements (capabilities)
- Non-functional requirements / system objectives (characteristics)
- Constraints

4.1. Requirement Generation Plan

Before realising the three types of baffle system requirements mentioned above, a brief plan of approach will be explained, referred to as the Requirement Generation Plan. The plan is explained in Figure 2.10 under the Chapter 4 content and consists of a stakeholder analysis, functional analysis (N-squared diagram and a FFBD) as a means to map the architecture of the baffle and a requirement discovery tree to be used for all three system requirements as mentioned above. These are stated in chronological order and is paid attention to in the following sections.

4.2. Stakeholder Analysis

A stakeholder analysis is crucial as it states which stakeholders (active/passive) are of interest to the DST. These stakeholders can then be transformed into engineering characteristics that apply to the entire DST system and the baffle sub-system, which is needed to find the non-functional characteristic requirements (second type of system requirement).

The stakeholder analysis, shown in Figure 4.1, has already been performed for the entire DST by S. Pepper in his MSc thesis, [76]. It is assumed that the stakeholders from this analysis are stakeholders of the baffle system as well. ADS Leiden as a prime contractor and remaining sub-system design company are added in the organisational boundary for plenitude- and clarification reasons. The technical system boundary are active stakeholders that directly affect the design of the DST. The organisational boundary is defined as those who design and manage the DST, which is the reason why ADS Leiden is added as the remaining sub-system design company that takes care of the S/C bus design. The total system boundary are passive stakeholders that indirectly influence the design, analysis, manufacturing, testing and qualification of the DST. These constitute mostly of regulations and space standards.

4.3. Mapping the Baffle Functional Architecture

Defining the architecture of the entire DST is crucial to find all relevant thermal, mechanical, optical, electrical and environmental interfaces to other sub-systems, such as the PMSS or instrument housing, as well as

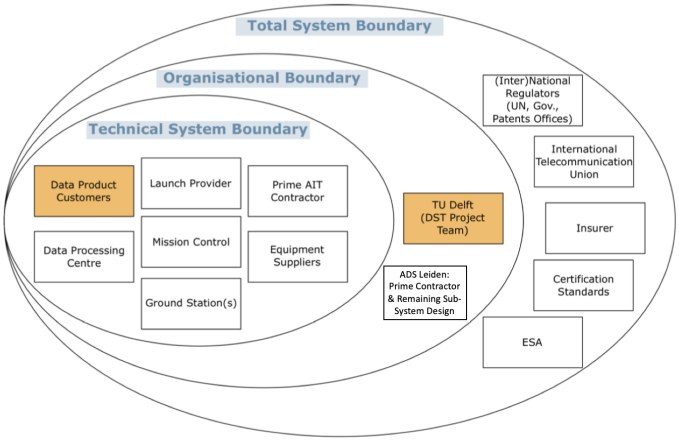

Figure 4.1: Stakeholder analysis for the DST, made by S. Pepper. [76]

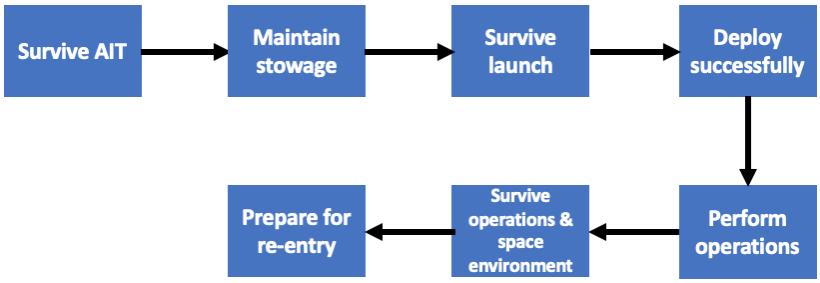

Figure 4.2: Functional Flow Block Diagram, visualizing the flow of functions in sequential order.

the flow of sequence of functions. The architecture of the DST has been established by means of creating a N-squared diagram as a group deliverable and is show in the Appendix, Figure B.1.

However, mapping the interfaces between functions of the baffle sub-system is crucial as well, as it defines what the system must be capable of doing. This is done by decomposing the system's top-level function, which define which functions influence others and of what nature these interfaces are. Decomposition of the top-level functions, together with the interfaces between these functions, opens up the generation of requirements. This is the main reason why the architecture is mapped to a functional level.

The architecture is established by two functional analysis methods: the N-squared diagram and the Functional Flow Block Diagram (FFBD). These are generated and discussed below.

4.3.1. Functional Flow Block Diagram (FFBD)

Using a FFBD is useful to map the flow of sequence of functions, contrary to the N-squared diagram. Characterizing the flow of sequence helps to understand which functions the baffle need to perform in what sequence (flow). The disadvantage of this is that there is no indication of time between two sequenced functions, which is especially desired between launch survival and successful deployment (and deployment initiation). This is because the DST, including stowed baffle, is exposed to radiation from the Sun, Albedo and Earth IR during the time between launch survival and initiation of baffle deployment. This time is important to simulate the *transient* temperature behaviour of the stowed baffle including sub-components, as well as the other DST systems (SMSS, PMSS, PMAO system elements, etc). The FFBD is shown in Figure 4.2.

4.3.2. N-squared (N^2) Diagram

An N-squared diagram is useful to map the interfaces between functions, but does not give information on the flow of sequence of these functions. The flow of functions is discussed in the FFBD. The N-squared diagram of the baffle is shown in Figure 4.3 and consists of the functions on the diagonal and the corresponding output-input in green and input-output in yellow. The functional interfaces are of type Mechanical (M), Thermal (T) or Optical (O). A combination of the above means a coupled effect, e.g. TM: Flutter means that flutter is a

Survive AIT	M: Fit on DST M: Attachment to Sub-Systems	M: Fit on DST MT: Thermal-Structural Integrity (Degradation)	M: HDRM Electrical Initiation				
	Maintain Stowage	MT: Maintain Configuration T: Thermal Strain Energy	M: Potential Strain Energy, HDRM functionality, Stiffness, Creep				
		Survive Launch	M: Vibrations, Pressure, G-load, Fairing Separation T: Aerothermal Heating	M: Vibrations, Pressure, G-load T: Aerothermal Heating	M: Vibrations, Pressure, G-load T: Aerothermal Heating		
			Deploy Successfully	M: Configuration M: Vibrations, Shocks, Buckling	M: Configuration M: Vibrations	M: Configuration M: Structural Integrity	
				Create Stable Thermal Environment	M: Configuration, Vibrations T: Stability, Uniformity, Gradients		
				T: Radiation (reflections)	Mitigate Stray Light		
				T: Radiation MTO: AO, Outgassing, Debris, Property Degradation MT: Configuration, Vibrations, Flutter	T: Radiation M: Configuration, MTO: AO, Outgassing, Debris, Property Degradation	Survive OPS & Space Environment	
							Prepare for Re-Entry

Figure 4.3: N-squared diagram: Input/Output interfaces between functions of the baffle. The functions stem from the FFBD, Figure 4.2

thermo-mechanical coupled problem.

The N-squared diagram shows that there is an interesting input-output loop between maintaining stowage, surviving launch, successful deployment, creating stable thermal environment, mitigating stray-light and surviving OPS & space environment.

Succesful deployment depends on the ability of the baffle system to maintain stowage and launch survival. Maintaining stowage depends on the functionality of the HDRM, strain energy stored in the deployable booms (if these are used) and mechanical integrity such as creep and stiffness. Launch survival depends on the thermal heating and mechanical vibration loads that occur during launch. Therefore, both are an input to succesful deployment.

The output of the deployment is the configuration (placement) of the baffle, which is the driver for the passive thermal control of the baffle. Namely, the deployed volume (and thus area) of the baffle has a direct relation with the surface area to dissipate heat to space. Mechanical vibrations and local buckling, which can result in wrinkle formation of thermal sheets, has also an effect on the creation of hotspots. Hotspots are spots in which local overheating occurs. [94] The level of deployment success affects the survival of OPS and space environment, since any form of decrease in structural integrity due to deployment will decrease the survival chance. The output of this survival is hence the performance affection due to environmental effects, such as AO, debris and outgassing, as well as operational effects, such as induced vibrations due to angular accelerations of the reaction wheel (part of AOCS) or radiative couplings between the solar panels and baffle.

4.4. Requirement Discovery Tree (RDT)

A RDT is used for the generation of requirements and discovery of the flow-down and interfaces between functions of the baffle. Three types of RDT's are used: a Functional RDT, Characteric RDT and Constraint RDT.

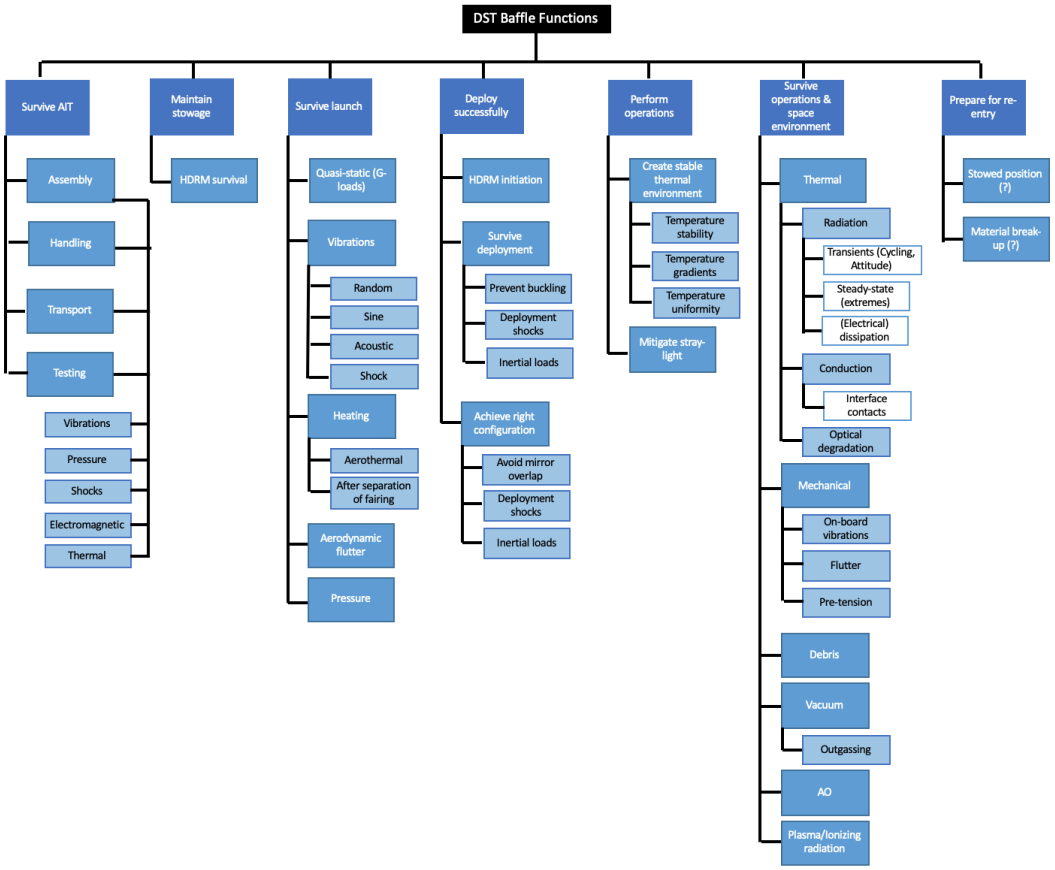

Figure 4.4: Functional Requirement Discovery Tree (FRDT) for the baffle. The main functions are equal to the sequential functions of the Functional Flow Block Diagram.

4.4.1. Functional Requirement Discovery Tree (FRDT)

The FRDT shown in Figure 4.4 breaks down all main baffle functions from the FFBD into sub-functions. The main baffle functions are visualized in Figure 4.4 at the top in dark blue and correspond to the sequential functions of the FFBD. The sub-functions of these main baffle functions will be transformed to system requirements (capabilities) that have to be complied to in Section 4.5.1. Compliance to the main functional capabilities can only be reached by compliance to ALL sub-function capabilities.

4.4.2. Characteristic Requirement Discovery Tree (CRDT)

The characteristics stem from the total-, organisational and technical system boundaries in the stakeholder analysis, which comprise mainly of regulations and certification standards. Cost is a characteristic, as it flows down from the market need (hence as well stakeholder analysis) and the mission goal to produce a space telescope with an equal (or better) spatial resolution as conventional telescopes, but at a fraction of conventional telescopes. Therefore, cost is a system characteristic and not a system contraint. There is also some overlap in characteristics. The material degradation regulation is noted in the ECSS and provides support to the reliability characteristic as well.

The ECSS, short for European Cooperation for Space Standardization, is a set of defined, coherent standards to be used in European space activities. The ECSS defines standards for roughly three categories: space project management, space product assurance and space engineering. The ECSS space engineering - and space product assurance standards are to be used for the safety and reliability of the DST baffle, since these standards define the space environment (ECSS-E-ST-10-04C) [85], thermal control + exchange of thermal analysis data (ECSS-E-ST-31-04C and ECSS-E-ST-31C) [84], fracture control (ECSS-E-ST-32-01C) [82], structural finite element models (ECSS-E-ST-32-03C), space engineering materials (ECSS-E-ST-32-08C) [89], general structural requirements (ECSS-E-ST-32C) [83], requirements for mechanisms (useful for the HDRM mechanism, ECSS-E-ST-33-01C) [88], and potential informative standards on explosive subsystems if that

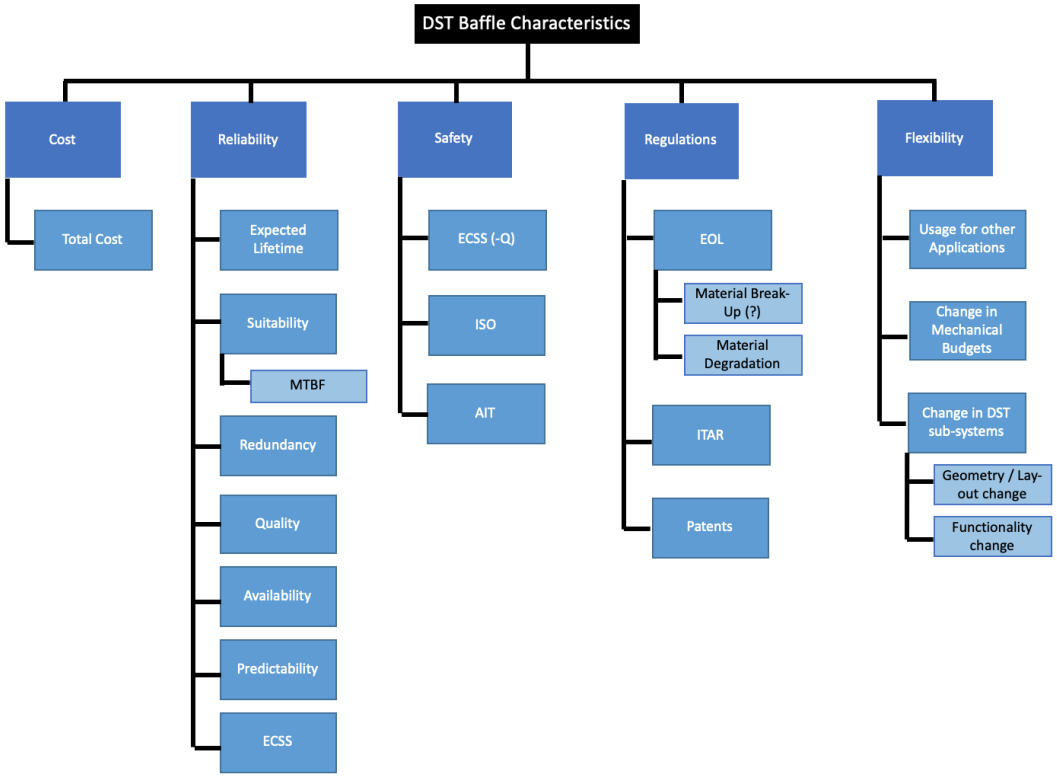

Figure 4.5: Characteristic Requirement Discovery Tree (CRDT) for the baffle. These characteristics stem from the stakeholders that were analysed in the stakeholder analysis.

will be used as part of the HDRM inititation of the baffle deployment (ECSS-E-ST-33-11C) [90]. Verification guidelines (ECSS-E-ST-10-02A), [33], also defines a crucial set of standards to be used for the verification of the baffle design.

4.4.3. Constraint Requirement Discovery Tree (CoRDT)

The constraints also stem from the technical-, organisational and total system boundaries of the stakeholder analysis and comprise of the interest of AIT (AIT contractor, equipment suppliers), interest of launcher selection and provider, compliance with the other sub-systems of the DST that are being designed within the DST project team and Airbus as the prime contracter.

4.5. System Requirement Generation

Now that the three RDT's are generated, as well as the architecture through N-squared and FFBD functional analyses, the system requirements are to be generated. Requirements are not static and could be altered. However, a proper and well traceable requirement list serves as a baseline for the design of the baffle and the verification thereof. Requirements are indicated with 'shall', and goals (or nice-to-haves) are indicated with 'should'.

The system requirements are subdivided in the three categories as mentioned before: functional-, characteristics- and constraint requirements. In this section these requirements will be independently generated in different sections and merged in the end to form the totality of system requirements. Note, the requirements will be labeled by identifiers, but no visible distinction in identifier between functional-, characteristics- and constraint requirements will become apparent. This is to be consistent with the requirements generated for other sub-systems of the DST by other members of the DST project team.

As these three types of system requirements hold for different parts of the mission as established in the RDT's, a distinction between the different mission functions is made and discussed below.

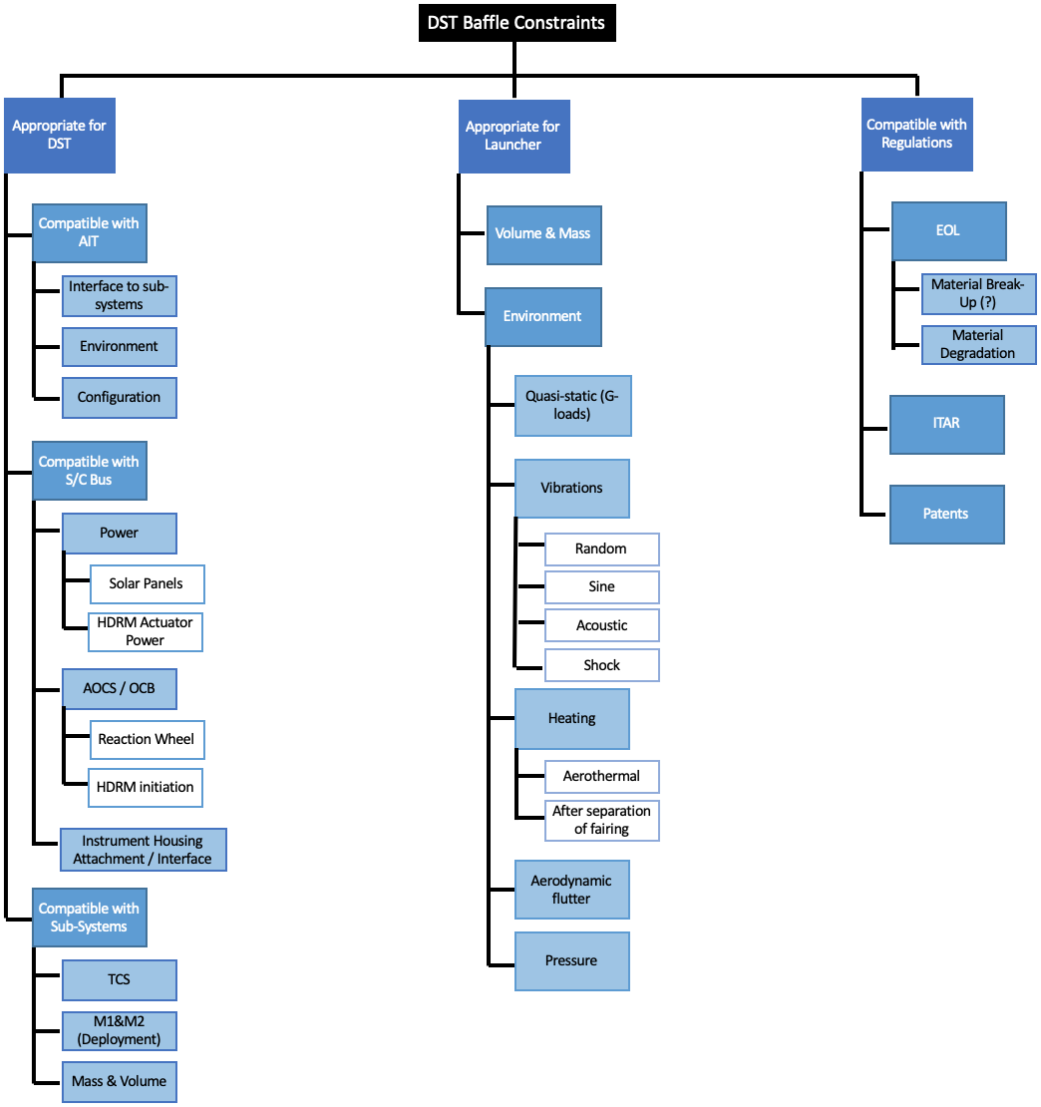

Figure 4.6: Constraint Requirement Discovery Tree (CoRDT) for the baffle. These characteristics stem from the stakeholders that were analysed in the stakeholder analysis.

4.5.1. Functional Requirements (Capabilities)

The FRDT in Figure 4.4 shows that there are 7 main baffle functions that the baffle has to comply with. As these are divided into sub-functions, requirements for each sub-function are generated and discussed for all 7 main baffle functions below. The functional requirements are shown in the Appendix, Table C.1, C.2 and C.3.

AIT Survival

The FRDT in Figure 4.4 highlights that the baffle shall survive all processes of AIT: assembly, integration, handling, transport and testing. Survival is crucial for both stowed and deployed configuration and is therefore integrated in the first requirement (properly stated in Table C.1). This contains survival of vibrations, pressures, shocks, thermal- and electromagnetic loads that can take place during different phases of AIT, such as assembly, integration, handling, transport and testing.

Maintain Stowage

Maintaining stowage is an import function of the baffle, for pre-launch and during launch, until deployment is initiated. Maintaining stowage is linked directly with the capability of the HDRM to survive until deployment is initiated. This is then linked to the survival of the structural integrity of the baffle during stowage, due to effects like creep. Additionally, storage conditions shall not cause any degradation of the thermal hardware.

[84] These are embedded in functional requirements, as can be seen in Table C.1.

Launch Survival
Surviving launch as a baffle function is directly translated to a functional requirement. The baffle system is not deployed yet during launch, so the baffle in stowed configuration shall survive launch, as a main requirement. The daughter requirements for this is the survival of different launch loads, such as quasi-static G-loads, vibrations, heating, aerodynamic flutter and pressure.

The quasi-static G-load that occur is a 30g load, applied simultaneous in a combination of two different axes: x- and y-, x- and z- and y- and z- axes, to represent the worst-case scenario and to include the possiblity of shear deformations during launch. [76] This is translated to three seperate requirements, as is done for other DST sub-systems like the PMAO. [76]

The ability of the baffle to survive vibrations during launch also translates into several daughter requirements. One daughter requirement of this is that the minimum natural frequency of the stowed baffle structure should be at least 100 Hz. Experts at ADS Leiden designated this requirement, along with the 30g bi-axial quasi-static loading to account for worst-case vibrations. [76]

Although S. Pepper mentions that loads imposed by the thermal environment and additional safety factors are included in the 30g quasi-static load requirement [76], an additional requirement is set up to account for the heating after the seperation of the fairing. As soon as the fairing is seperated, the stowed DST, including stowed baffle is exposed to a a heat flux of on average 1135 $\frac{W}{m^2}$, as the altitude at which the fairing of a rocket is jettisoned depends on the aerothermal flux limit. [37] Therefore, this serves as an additional launch requirement.

Other thermal requirements that are important stem from A. Krikken's thesis, who worked on the design of the SMSS. These requirements are based on the principle of preventing creep; slow deformations due to persistant mechanical stresses. A. Krikken formulated two requirements that the baffle has an influence on, of which the first holds for the stowed configuration: [60] [102] The bulk temperature of the SMSS booms shall not exceed 373K during stowage. The second requirement, which refers to the survival of the SMSS booms in deployed, operational configuration, is mentioned under the Operations- and Space Environment Survival header.

Successful Deployment
Successful deployment is a key functionality for the baffle and has many interfaces with operations (creating stable thermal environment and mitigating stray light), as well as surviving the operations and space environment, see the N-squared diagram in Figure 4.3. Generating functional requirements that guarantee the success rate of the deployment, from initiation to deployed configuration including survival, is key. The top functional requirement for this is the overarching requirement that the baffle shall deploy succesfully. This shall be initiated by an actuation command to the HDRM that initiates the deployment of the baffle.

The baffle shall also survive deployment, which is crucial to the structural and thermal integrity, which can affect the performance of the operations as well as the survival of the space environment and/or operations. When the baffle deploys to the correct configuration, but the thermal shield is distorted, hot spots can occur for example. Hot spots are wrinkle spots in which local overheating occurs. Therefore, the following daughter requirements are necessary to dictate: The baffle shall survive local- and global buckling loads, the baffle shall survive deployment schocks, the baffle shall deploy in TBD s within the acceleration range of TBD $\frac{\mathrm{m}}{\mathrm{s}^2}$, the baffle shall prevent the creation of hot-spots and the baffle shall survive mechanism heat dissipation.

Furthermore, the baffle shall achieve a deployed configuration that conforms to the operational requirements with a position accuracy of TBD m. [88] The position accuracy is important, since it drives the thermal- and structural performance. Having an offset in deployed configuration means an offset in area that can be used to radiate heat to space, and this linearly deviates the temperature levels the baffle will encounter. A daughter requirement that is important to conform to is that the baffle geometry shall not obstruct any telescope elements and not interfere with the optical performance. Blocking the visual light spectrum that will fall on the optical elements will tremendously affect the optical performance of the DST and therefore shall be avoided at all cost. Additionally, the baffle shall not impede the deployment of the primary- and secondary mirror, by ensuring that the baffle shall deploy before the primary- and secondary mirror.

Perform Operations
Performing operations successfully considers the creation of a stable thermal environment within the baffle, as well as the mitigation of stray light. This MSc thesis mainly focuses on the thermal-mechanical design

of the baffle and therefore puts its focus on the creation of a stable thermal environment. A stable thermal environment is defined as a thermal environment of which the resulting thermo-elastic effects on the mirror support structures do not exceed the mechanical budgets for the mirrors, with a nominal temperature range between -20 and +50 degrees C (253-323 K). These mechanical budgets are displayed in Figure 2.3. The rationale behind these requirements are mentioned below.

Thermo-elastic effects are briefly discussed in Section 3.4 and are extremely important to characterize the thermal performance of the baffle. Temperature variations and gradients that critical structures are exposed to throughout an orbit result in these thermo-elastic displacements. The most important thermal budgets are those for the M2, since for the M2 and SMSS, no active optical system based on actuation commands is present, unlike for the M1. Additionally, the spider of the M2 is least protected by the baffle and the length of the SMSS CFRP booms are extremely high to meet the required focal length, which both contribute to making the M2 a critical system. The thermal design objective will also be explained later in this chapter.

The reason for these nominal chosen temperatures, is that for visible light space telescopes, like the DST, the thermal performance is **not** distorted by its own thermal heat. However, this is the case when dealing with an infrared telescope. Consequently, for infrared telescopes the temperatures of the mirrors and support structures are immensely low in order to reduce infrared heat. Ideally these temperatures are 0 K ($Q = \sigma \epsilon T^4$). Thus, for the DST, which is not an infrared telescope, the optical elements do not suffer from thermal infrared distortion and nominal temperature ranges are found to be sufficient when complying with a temperature range of -20 to +50 ° C, since these temperatures are survival temperature margins of standard space equipment. [45] Electrical components have in general a non-operating temperature range of -25 to +51 ° C and an operating temperature range of -10 to + 45 ° C. [75] The set limit of -20 to +50 ° C is therefore a good first estimate and used as a nominal temperature requirement, which is a safe temperature margin as material properties, such as CFRP properties used for the PMSS and SMSS, are in general valid within a range of -50 to +250 degrees C (glass transition temperarature). This holds for the tensile strength for example. [38]

It must be noted that mitigating stray light is also an essential function but extensive ray-tracing stray light analyses will be left as a recommendation for another MSc student.

Thus, the main operational function of the baffle is to create a stable thermal environment, which flows down into several daughter functions, as discovered in the FRDT in Figure 4.4: temperature stability, temperature gradients and temperature uniformity. Temperature stability can be expressed as a temporal stability of a node, i.e. the change of temperature as a function of time, and the overall stability between a bandwith of an upper- and lower boundary limit. Temperature uniformity and gradients are both expressed as the spatial derivation of temperature in a point at a given time, i.e. expressed in K/m, according to ECCS-E-ST-31C thermal general requirements. [84] These requirements are stated in Table C.2.

Furthermore, the baffle shall maintain its operational functionality in both extreme cases of BOL- and EOL optical material properties.

The baffle shall also mitigate stray-light in deployed configuration, which puts a requirement to the internal layer of the baffle: the internal layer shall absorb at least 90 % of incident radiation, in both Solar- and IR spectrum. This absorption coefficient is based on the absorption of the internal surface of the Hubble Space Telescope (HST). [3]. The HST uses Chemglaze Z306 diffusive black paint as a means of controlling stray light, since having a surface with high Solar absorptance and emissivity will yield a low reflection. Chemglaze Z306 has a Solar absorptance of 0.95 and emissivity of 0.9. Stray light can also be mitigated by applying truncated cones: one near the primary mirror and one near the secondary mirror. This has been proposed by Terebizh for the application of Cassegrain telescopes (like the DST), since it prevents direct light from any incident angle, as well as reflected light from the tube from reaching the focal plane. [97] However, since requirements shall not contain solutions, the application of a truncated cone is not transformed to a requirement. This is merely a solution to the requirement that the baffle shall mitigate stray-light.

Operations- and Space Environment Survival

Surviving the operations and space environment means surviving a variety of loads ranging from in-orbit thermal-, mechanical- and environmental loads or hazards.

The thermal loads are mainly focused around thermal radiation, but also includes conduction and the effect of optical (as well as thermal and mechanical) degradation of material properties. The fundament of thermal requirements stem from the ECSS Thermal Control general requirements. [84]

The parent functional requirement is that the baffle shall survive the operations- and space environment in deployed configuration. The operational loads have to be added to the in-orbit environmental loads, as a worst case. Temperature dissipation for example has to be added to the thermal heat from the environ-

ment (Sun, Albedo, Earth IR, radiative- and conductive couplings), since otherwise the results are extremely inaccurate.

In terms of environmental loads, the baffle shall survive the impact of medium sized debris, $1 < d <$ 100mm in the order of TBD. It is chosen that medium sized debris shall be accounted for, unlike small debris $d <$ 1mm or large debris $d >$ 100mm, since small debris survival, the majority of debris impacts, can be accounted for by normal coating and shielding protection. Large debris can severly damage the S/C, but the collision probability is low and debris with a large diameter are often trackable and collision can be prevented by active attitude/altitude control. [3] Surviving medium sized debris, and the impact and consequences thereof bring about multiple daughter requirements, that are listed in Table C.2. These requirements are taken from the ECSS facture control standards, [82], since debris can cause fractures and fracture control has to be implemented as well as mitigating the possibility of fracture initiation.

Another vital requirement to survive the space environment, especially for space telescopes that use sensitive optical elements, is that the materials to be used for the baffle shall limit outgassing to a TML of < 1 % and CVCM of < 0.01 %. These values are standard for S/C. [88] [3] [14]

Additionally, spacecraft suffer from electrical-charge buildup due to space plasmas when orbiting in a region with high density space plasma. Midaltitude to geosynchronous altitude Earth orbits and high-inclination low-Earth orbits are negatively affected by this. This electrical-charge buildup can lead to static discharge effects through the surface. [42] Therefore, the baffle shall be resistant to AO and plasma/ionizing radiation. This could for example be done by making use of a protective outer coating that is resistant to AO, however this is a solution to the requirement that the baffle shall be resistant to AO and plasma/ionizing radiation and therefore not added as a requirement. Furthermore, the baffle shall be electrically bonded (grounded) to the S/C bus to avoid electrical charging.

The baffle shall survive extreme thermal operational- and environmental loads in deployed configuration, both with BOL- and EOL thermo-optical properties. This requirement does not set a temperature limit on the MLI layers, since this was not yet designed. Since the baffle lay-up is characterized (by E. Korhonen, see 2.5.2), it is possible to set an objective requirement towards the maximum temperature. The maximum Dacron operational temperature of 177 ° C is used for this. The minimum temperature requirement is that of aluminized Kapton under continuous exposure: -250 ° C. This means that the baffle shall survive extreme hot and cold temperatures between -250 ° C and +177 ° C respectively.

The baffle design shall use the parameters for operational orbits, as specified by ECSS-E-ST-31C, Section 4.1.4. [84]. The parameters that this functional requirement entails are stated in the ECSS TCS: [84]

- Orbit radii (height) and eccentricity
- Inclination
- Ascending node angle
- Maximum eclipse duration
- S/C orientation w.r.t sun and planets
- Relative movement of spacecraft items with respect to the main spacecraft body.

Part of the operations is also the ABM firing. During the operation of the thruster, plume interactions occur with other S/C sub systems. As the baffle is the outer part of the S/C that has a direct line of sight to the propulsion unit, care must be taken to avoid too large heat fluxes and corresponding temperature levels due to plume interaction. This can create thermal instability and nonuniformity which has to be mitigated so that the functional requirements on temperature stability-, uniformity-, gradients and levels are not violated. A seperate requirement that corresponds to the mitigation of this phenomenon is established, as can be seen in Table C.3, but the interface between thruster firing and the baffle may also be mitigated by adding an extra margin of safety to the external absorped heat fluxes that the baffle encounters.

The baffle shall survive the mechanical operational- and environmental loads in deployed configuration. This can be established by the requirement that the baffle shall survive on-board vibrations of TBD due to the reaction wheel in deployed configuration, the baffle shall mitigate the effect of thermal flutter in deployed configuration and the baffle shall survive vibration fatigue due to on-board vibrations and thermal flutter.

These in-orbit dynamic loads all require the baffle to have a certain stiffness, which is linked to the eigenfrequency of the deployed baffle. Therefore, the baffle shall have a minimum first eigenfrequency ≥ 0.9 Hz in deployed configuration, as well as a structural bending damping factor of TBD. The first eigenfrequency (natural frequency) of 0.9 Hz in deployed configuration stems from E. Korhonen's thesis [58]. E. Korhonen concluded that her inflatable deployment design could withstand operational structural loads due to reaction-wheel vibrations and slew-rate rotations, and the inflatable system has an eigenfrequency of 0.92 Hz. Thus, a minimum eigenfrequency of 0.9 Hz (rounded off) is assumed to be enough to meet on-board vibrations and slew rate rotations.

An additional thermal requirement as set by A. Krikken in his thesis, [60], is that the bulk temperature of the SMSS booms
shall not exceed 473 K when deployed. This is a requirement that is vital for the thermal control system and is therefore also mentioned in T. van Wees' thesis [102]. This requirement is essential for the baffle, as the baffle is the major thermal control system of the DST.

4.5.2. Non-Functional Requirements (Characteristics)

Characteristic requirements are discovered by the CRDT, Figure 4.5. All sub-characteristics bring about multiple characteristic requirements, that are touched upon and explained below. The characteristic requirements table is shown in the Appendix, Table C.4.

Cost

The cost of the baffle is a characteristic, as explained in Section 4.4.2. The total cost is important and will be taken as a requirement, since it includes all costs that occur during the mission lifetime.

Reliability

Reliability is sub-divided into several sub-characteristics of the baffle: expected lifetime, suitability, redundancy, quality, availability and ECSS standards to be used for designing a reliable baffle.

The expected lifetime is defined as the expected operational lifetime in which the baffle shall survive the operations and space environment. As for every other DST sub-system, this is set to 5 years. This then depends on the MTBF, which should be a minimum of 5 years for single point of failure components. A single point of failure is a component that will stop the entire system from working when that single point of failure component stops working. Therefore, any single point of failure can only happen after a MTBF of 5 years, since it otherwise would stop the baffle from functioning.

Before this requirement can be stated, all single point of failure modes of the baffle, and its sub-components, shall be identified. This is stated as a particular design requirement for mechanisms, but will be applied to the whole baffle system including its HDRM mechanism to assess its reliability. [88] [84]

This flows into the sub-characteristic of redundancy as a means of designing a reliable space system. Designing a space system that requires maintance during operations is not feasible and hence should be accounted for. This imposes the requirement that operational maintenance on any part of the baffle during in-orbit phases shall be avoided. [84] Therefore, each single point of failure should be eliminated by using redundant components. The word 'should' is used, since it is not a strict requisite.

Furthermore, ECSS-E-ST-33-01C states that "unless redundancy is achieved by the provision of a complete redundant mechanism, active elements of mechanisms, such as sensors, motor windings, brushes, actuators, switches and electronics, shall be redundant." [88]

In terms of availability, quality and reliability, the baffle shall use space qualified parts, materials and procesess (PMP), conforming to ECSS-Q-ST-70. [87] [84]

Another form of design reliability is the conformance of the requirements (verification) by thermal analyses and testing. This is defined as predictability and is stated in the ECSS standard for thermal control requirements, [84]: The TCS shall be designed such that conformance to performance requirements can be demonstrated by thermal analyses and thermal test. Designing a baffle that allows for thermal testing (TV or TB), sets a constraint to the deployed volume of the baffle, since a too large volume of the baffle impedes the process of thermal testing, if not makes it impossible, since the volume to be fitted inside a TV/TB chamber is finite. This volume requirement is noted in the constraint requirements.

Safety

Safety entails applying Factors of Safety (FoS) , which are mentioned in the ECSS Structural factors of safety for spaceflight hardware standard, ECSS-E-ST-32-10. [86] The most important FoS are directly mentioned in

the characteristic requirement table, Table C.4.

Regulations
As far as regulations go that stem from the total-, organisational and technical system boundaries in the stakeholder analysis, ITAR related regulations are mandatory. That is, the entire DST shall not use any ITAR controlled components or technologies. Additionally, As S. Pepper mentions in his MSc thesis, the DST shall not comply with national and international regulations during AIT activities, launch, operations and EOL. Obviously, both of these requirements hold for the baffle sub-system as well.

Flexibility
Flexibility is a characteristic that the baffle shall incorporate in the design. In general, every TCS shall incorporate a certain level of flexibility, as defined in the ECSS-E-ST-31C thermal control requirements standards, namely: "The TCS design shall incorporate flexibility to accommodate modifications of requirements imposed on the TCS during the project development phase" and "the TCS design shall incorporate flexibility to offer trimming capabilities to accommodate late requirement updates." [84], Section 4.4.7 page 30. Both of these requirement shall hold for the baffle sub-system.

4.5.3. Constraint Requirements
Constraint requirements are categorised in three sections, as the CoRDT shows in Figure 4.6: appropriate for DST, appropriate for launcher and compatible with regulations. Constraint requirements for these three categories will be derived and explained below. The constraint requirements table is shown in the Appendix, Table C.5.

Appropriate for DST
The baffle needs to be appropriate for the DST and therefore yields some constraint requirements that need to be met in order to be compatible with AIT, the S/C bus and other DST sub-systems.

Compatability with AIT is important for the baffe design. In general, the baffle shall be compatible with operation on ground in ambient and thermal vacuum conditions. This is important for mechanisms and is taken from the ECSS mechanism standards, but holds for the baffle as well. [88] Additionally, as described under the reliability characteristic requirement in Section 4.5.2, the deployed baffle should be able to fit inside a TV/TB chamber, hence setting a constraint requirement on the allowable volume of the deployed configuration of the baffle. For this maximium allowable volume, the usable volume of the Large Space Simulator (LSS) at ESTEC is taken as a reference: 10 m by 15 m. Note that this maximum volume is a constraint requirement regarding the allowance for testing, but in practice the baffle will me made much shorter, since structural requirements will become dominant when increasing the baffle size.

Compatability with the S/C bus and other sub-systems is important for the deployed configuration of the baffle, since for every thermal control system, many mechanical interface requirements are mandatory. An important one that can directly be applied is the interface attachment to the instrument housing. Therefore, the baffle shall include fixation and mounting techniques.

Furthermore, it is important that the baffle in stowed configuration does not require any power during launch, as to prevent electrical discharge effects, or other potentially catastropic phenomena.

Moreover, the baffle functional capabalities shall be compatabile with the power and radiation exchange of the solar panels. The solar panels will be designed by ADS Leiden, but do have to be included in the GMM and TMM. Ignoring the effect of radiation exchange and power dissipation on the baffle operational functionality can lead to a large offset in temperature levels, uniformity and stability of the baffle.

Finally, the mass and stowed volume of the baffle are immensively important constraint requirements. One volume requirement is the clearance of the baffle in operational deployed state with the DST sub-systems. Namely, the baffle shall have a clearance of 200 mm in deployed configuration between M1 and any point of the baffle. This requirement stems from an internal discussion with the DST team and is also mentioned by E. Korhonen [58].

Other mass and volume constraint requirements are discussed below when talking about appropriate constraint requirements for the launcher.

Appropriate for Launcher
The DST, including the baffle, shall be appropriate for the launcher. This flows down in several sub-requirements that define what appropriate or compatability with the launcher means. Compatibility entails the volume-

and mass budgets of the baffle in both stowed and deployed configuration. The volume of the deployed configuration is not a constraint, since this is functional requirement as this volume has an influence on the thermal heat rejection capabilities. However, the volume that the baffle needs to reach in stowed configuration in the launcher is a constraint. The dimensions of stowage stem from the parent requirement on instrument stowed volume of the mission requirements mentioned in Table 2.1: REQ-8 - In the stowed configuration, the volume of the instrument shall not exceed 1.5 m^3 (threshold) / 0.75 m^3) (goal). This mission requirements comes from D. Dolkens, who initiated the DST thermo-optical baseline design. The treshold mass budget of 1.5 m^3 is based on half the mass budget of the expected volume of a conventional 25 cm GSD telescope (which is 3 m^3, using the Zemax model. [23] The stowed goal requirement is then half of the treshold, just like the mass budget requirement.

Since the baffle drives the volume budget in stowed requirement as it is an external shield for the DST in both stowed and deployed configuration, this volume requirement also holds for the baffle itself: The volume of the baffle shall not exceed 1.5 m^3 (threshold) / 0.75 m^3) (goal) when in stowed configuration. Note that this is requirement is solution free, and thus does not impose requirements on what the diameter or area must be. Also note that the current estimate of the instrument stowed volume is 0.76 m x 0.76 m x 1.10 m = 0.64 m^3, see Table 2.2.

Furthermore, next to the stowed volume, the mass is an important constraint requirement as mentioned above. Based on a literature review on deployable light shields, E. Korhonen found that assigning a mass budget of 15 kg to the baffle seems reasonable. [58] This is a fraction of the mass budget of the DST, which was set to 100 kg, since then it can still be classified as a microsatellite. However, the 100 kg mass budget for microsallites holds for the entire satellite, including S/C bus and propellant. Since the DST is just the payload of a satellite system, a 50% payload mass fraction is taken, which decreases the mass budget from 100 kg to 50 kg. As this is a challenging task, this is set as a goal, while a threshold mass budget of 100 kg was set (see Table 2.1). [23]

Compatible with Regulations
Compatability with regulations are equal to the regulations mentioned under in the characteristic requirement generation section and are therefore also displayed in Table C.4.

4.6. Requirement Selection for this MSc Thesis

This section contains the selection of requirements that are to be verified within this MSc thesis. These requirements are of importance for the thermal performance and the effect of deployability- and the survival of the operations and space environment on the thermal performance, and could therefore be referred to as killer requirements for the operational phase and are selected from all functional-, characteristic- and constraint requirements that were developed in the last sections. These selected killer requirements are then translated to a bottom-up design objective, stated in Section 4.7.

The underlying reason for verifying these set of requirements is that the author wants to focus on the functional operation of creating a stable thermal environment, using a deployable baffle. The remaining requirements that are not selected to be verified during this thesis are left as a recommendation.

The full requirement list that correspond to the System Requirement Generation Section, Section 4.5, are shown in Table C.1, C.2, C.3, C.4 and C.5 in the Appendix, but for this thesis, the selected requirements are those of Table 4.1, 4.2 and 4.3.

4.7. Thermal Objective Definition Based on Selected Requirements

The design objective that is going to be realised within this MSc thesis is a thermal design optimization of the baffle, of which the objective used for the optimization process flows down from the optical performance that needs to be ensured in its operational state. This objective stems from the BAF-T-01 functional requirement, Table 4.1. Namely, optical path difference due to mirror misalignment and deformation should be reduced. For this, mechanical budgets have been established using a top-down systems engineering approach, as shown in Table 2.3, that highlight three types of allowed budgets: a deployment/coarse alignment budget, an in-orbit drift budget and a stability budget, as was defined in Section 2.1.3. The most stringent budgets that the baffle has an influence on are the In-Orbit Drift Budget and the Coarse Alignment Budget, since both are time-dependent budgets that hold for a large period of time, as explained in Chapter 2. The In-Orbit Drift Budget it is defined as the allowable spatial deviation of an optical surface (M1, M2 or M3) between comple-

Table 4.1: Baffle Functional Requirements for this Thesis: Survive Launch, Successful deployment and Perform Operations.

ID	Description
Survive Launch	
BAF-MEC-03	The baffle shall survive the launch in stowed configuration.
BAF-MEC-03-01	The baffle shall survive a quasi-static load of 30g applied simultaneously to the x- and y- axes in the launcher coordinate frame in the stowed configuration during launch.
BAF-MEC-03-02	The baffle shall survive a quasi-static load of 30g applied simultaneously to the x- and z- axes in the launcher coordinate frame in the stowed configuration during launch.
BAF-MEC-03-03	The baffle shall survive a quasi-static load of 30g applied simultaneously to the y- and z- axes in the launcher coordinate frame in the stowed configuration during launch.
BAF-MEC-03-04	The baffle shall have a minimum first eigenfrequency of 100 Hz in stowed configuration
BAF-T-04	The stowed baffle shall survive a heat flux of 1135 $\frac{W}{m^2}$ immediately after separation of the fairing.
M2-T-01	The bulk temperature of the booms shall not exceed 373K during stowage.
Successful Deployment	
BAF-MEC-04	The baffle shall deploy succesfully.
BAF-MEC-04-03	The baffle shall survive deployment.
BAF-MEC-04-03-01	The baffle shall survive local- and global buckling loads.
BAF-MEC-04-03-02	The baffle shall survive deployment shocks and vibrations.
BAF-MEC-04-03-04	The baffle shall mitigate the creation of hot-spots such that it shall not result in consequential structural- or thermal damage that does not conform to the operational requirements.
BAF-MEC-04-04	The baffle shall achieve a deployed configuration that conforms to the operational requirements with a position accuracy of TBD m.
BAF-MEC-04-04-02	The baffle geometry shall not obstruct any telescope elements and not interfere with the optical performance
BAF-MEC-04-04-02-01	the baffle shall have a clearance of 200 mm in deployed configuration between M1 and any point of the baffle.
BAF-MEC-04-05	The baffle shall not impede the deployment of the primary- and secondary mirror.
BAF-MEC-04-05-01	The baffle shall deploy before the primary- and secondary mirror
Perform Operations	
BAF-T-01	The baffle shall create a stable thermal environment for all sub-systems, so that the mechanical displacement budgets will be met
BAF-T-01-01	The temperatures of all sub systems within the baffle shall remain within a stability bandwith of 253-323 K.
BAF-T-01-02	The baffle shall maintain its operational functionality in both extreme cases of BOL- and EOL thermo-optical material properties.
BAF-O-01	The baffle shall mitigate stray-light in deployed configuration.
BAF-O-01-01	The internal layer of the baffle shall absorb at least 90 % of incident radiation in both UV- and IR wavelength spectra.

Table 4.2: Baffle Functional Requirements for this Thesis: Survive Operations and Space Environment.

ID	Description
Survive OPS & Space Environment	
BAF-MEC-07-01	The operational loads shall be added to the in-orbit loads.
BAF-MEC-07-02	The baffle shall survive the impact of medium sized debris, $1 < d < 100$mm.
BAF-MEC-07-03	The materials to be used for the baffle shall limit outgassing to a TML of < 1 % and CVCM of < 0.01 %.
BAF-MEC-07-04	The baffle shall be resistant to AO and plasma/ionizing radiation.
BAF-MEC-07-04-01	The baffle shall avoid electrical charging.
BAF-T-02	The baffle shall survive the thermal operational- and environmental loads in deployed configuration.
BAF-T-02-01	The baffle shall survive extreme hot and cold temperatures between -250 ° C and +177 ° C respectively.
BAF-T-02-02	The baffle shall survive the thermal loads both with BOL- and EOL optical properties.
BAF-MEC-07-06	The baffle shall survive the mechanical operational- and environmental loads in deployed configuration.
BAF-MEC-07-06-01	The baffle shall survive on-board vibrations of TBD due to the reaction wheel in deployed configuration.
BAF-MEC-07-06-02	The baffle shall mitigate the effect of thermal flutter in deployed configuration.
BAF-MEC-07-06-03	The baffle shall survive vibration fatigue due to on-board vibrations and thermal flutter
BAF-MEC-07-06-03-01	The baffle structure shall have a minimum first eigenfrequency ≥ 0.9 Hz in deployed configuration.
M2-T-02	The bulk temperature of the booms shall not exceed 473K when deployed.

Table 4.3: Baffle Characteristic and Constraint Requirements for this Thesis

ID	Description
Cost	
BAF-SYS-01	The total cost of the baffle shall be no more than TBD over the mission lifetime of the DST.
Safety	
BAF-SYS-02	The baffle shall have an operational expected lifetime of 5 years.
BAF-SYS-02-01	All single point of failure modes of the baffle and its sub-components shall be identified.
BAF-SYS-02-02	The baffle shall have a MTBF of at least 5 years for single point of failure components.
BAF-SYS-02-03	All single point of failures should be eliminated by redundant components.
BAF-SYS-03	Active elements of mechanisms, such as sensors, motor windings, brushes, actuators, switches and electronics, shall be redundant if a mechanism is is not completely redundant.
BAF-SYS-04	The baffle shall use space qualified parts, materials and procesess (PMP).
BAF-SYS-05	The baffle shall be designed such that conformance to performance requirements can be demonstrated by thermal analyses and thermal test.
BAF-SYS-06	Verification by analysis shall take into account uncertainties: a 5 degrees temperature calculation uncertainty margin and 25 % mass uncertainty.
BAF-SYS-07	The baffle shall be designed using factors of safety (FoS) conform with ECSS-E-ST-32-10.
BAF-SYS-07-01	The baffle shall use a minimum yield stress safety factor (FoS) of 1.25 for standard metallic materials
BAF-SYS-07-02	The baffle shall use a minimum ultimate stress safety factor (FoS) of 1.5 for standard metallic materials
BAF-SYS-07-03	The baffle shall use a minimum buckling safety factor (FoS) of 2 for standard metallic materials
BAF-SYS-07-04	The baffle shall use a minimum fatigue safety factor (FoS) of 4 for standard metallic materials
Regulations	
BAF-SYS-08	The baffle shall not use any ITAR controlled components or technologies
BAF-SYS-09	The baffle shall not comply with national and international regulations during AIT activities, launch, operations and EOL.
Flexibility	
BAF-SYS-10	The baffle design shall incorporate flexibility to accommodate modifications of requirements imposed on the TCS and deployement system during the project development phase
BAF-SYS-11	The baffle design shall incorporate flexibility to offer design trimming capabilities to accommodate late requirement updates.
Constraints	
BAF-SYS-12	The volume of the baffle shall not exceed 1.5 m^3 (threshold) / 0.75 m^3 (goal) when in stowed configuration.
BAF-SYS-13	The stowed baffle shall not require any power during launch
BAF-SYS-14	The operational functionality of the baffle, as well as the ability to survive the operations and space environment shall be compatible with the power- and radiation exchange of the solar panels.
BAF-SYS-15	The baffle in deployed configuration should fit inside a TV/TB chamber to allow for thermal testing.
BAF-SYS-15-01	The maximum volume of the baffle in deployed configuration shall conform to the usable volume of the Large Solar Simulator from ESA/ESTEC: 10 m diameter and 15 m height
BAF-SYS-16	The mass of the entire baffle including deployment mechanism shall not exceed 15 kg
BAF-SYS-17	The baffle shall be given sufficient structural support by other sub-systems.
BAF-SYS-18	The baffle shall be manufacturable with compliance to the availability of parts and materials.

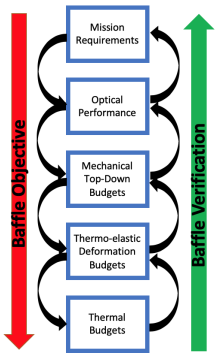

Figure 4.7: Baffle design objective flow-down and bottom-up verification of design

Element	Position X [μm]	Position Y [μm]	Position Z [μm]	Orientation X [μrad]	Orientation Y [μrad]	Orientation Z [μrad]	Radius [%]	Shape Error [nm]
Deployment/ Coarse Alignment Budget								
M1	2	2	2	2	4	50	1×10^{-3}	50
M2	15	15	10	100	100	100	1×10^{-2}	25
M3	4	4	4	10	10	50	1×10^{-3}	10
In-Orbit Drift Budget								
M1	2×10^{-2}	2×10^{-2}	2×10^{-2}	1×10^{-2}	2×10^{-2}	5	1×10^{-4}	5
M2	4	4	2	6	6	12	1×10^{-4}	5
M3	1×10^{-1}	1×10^{-1}	1×10^{-1}	1	1	5	1×10^{-4}	5

Figure 4.8: In-Orbit Drift Budgets for the M2, which are chosen to be the most stringent mechanical top-down budget. The thermo-elastic deformation budget is initially set to be equal to these mechanical top-down budgets.

tion of the last active calibration procedure and the end of the next image acquisition, therefore referring to a time-dependent spatial deviation of the three mirror elements. Furthermore, this in-orbit drift budget has to be maintained for a large time period. The conservative estimate that was made in Chapter 2 is that this time period is equal to the time that the DST is able to obtain images, which is equal to the Sunlit period of its orbit when the DST is **not** in eclipse. In Section 3.1, this time-period is defined as well as further orbital assumptions.

The Coarse Alignment Budget holds for the period of time that the DST is in eclipse, and this time period is also defined in Section 3.1.

The spatial deviation of the M2 is the most stringent in-orbit budget that needs to be controlled by the baffle, because of a multitude of reasons:

1. For the M2 and SMSS, no active optical system that controls the 6DOF of the M2 based on actuation commands is present, unlike for the M1
2. The spider of the SMSS is least protected by the baffle and therefore a highly critical system that needs thermal control
3. The length of the SMSS deployed CFRP booms make it thermally sensitive, since thermo-elastic elongations are linearly related to the length of the booms.
4. As analyzed by T. van Wees, [102], the thermo-elastic translation in Z-direction of M2 is > 2.23 µm and exceeds the in-orbit drift budget in best case scenario of a reflected baffle and no orbital eclipse

Therefore, to control the spatial deviation of the M2, a thermo-elastic budget is established that is directly flown-down from the mechanical In-Orbit Drift - and Coarse Aligment Budgets. This thermo-elastic budget is defined as a fraction of both In-Orbit Drift - and Coarse Aligment Budgets. Initially, this thermo-elastic budget is set to be **equal** to the In-Orbit Drift - and Coarse Aligment Budgets of M2 for the time periods that both these budgets hold, meaning that the spatial deviation of the M2 is totally devoted to the deformations associated to thermal gradients. The final thermal budgets are then derived from these thermo-elastic budgets. The summary of these thermo-elastic budgets for the M2 is shown in Figure 4.8.

To verify the thermal design of the baffle and assess its thermal performance, the thermal budgets that the baffle achieves flows back to the thermo-elastic deformation budgets, mechanical in-orbit budget and consequently the optical performance of the telescope. This is a bottom-up verification procedure, based on a top-down design objective. This objective- and verification flow is depicted in Figure 4.7.

4.7.1. Thermal Budgets: Thermal Gradient Requirements

The thermal budgets are thermal gradient requirements and are based on the principle of athermalization (already explained in Section 3.4). This is visualized in Figure 4.9 and consists of a translational deformation (left figure) and rotational deformation (right figure) of M2.

The thermo-elastic deformation in z-direction due to thermal gradients is counteracted by choosing a CFRP material with low CTE for the long and slender booms and aluminium, which has a 23 times higher CTE than CFRP, for the small rods that hold the M2 in place.

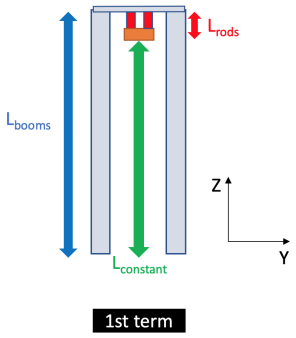

Figure 4.9: Athermalization process to counteract thermo-elastic deformations due to thermal gradients. Used for translational term of thermal design objective related to in-orbit drift Z-position budget.

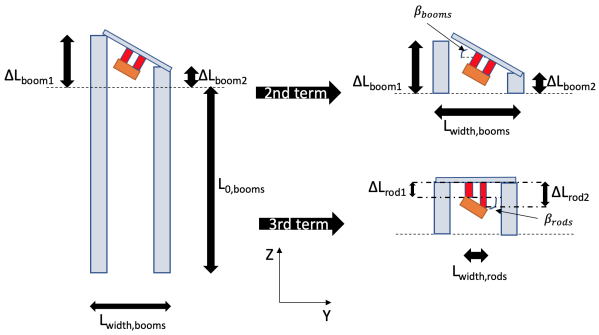

Figure 4.10: Used for rotational term of thermal design objective, related to in-orbit drift X/Y-orientation budget.

The rotational term of the CFRP booms and the aluminium rods respectively stem from the mechanical in-orbit orientation drift budget of M2. Namely, according to Table 2.3 the M2 orientation budget in both X and Y direction is 6 μrad, which is the most stringent rotational budget, compared to an orientation budget of 12 μrad for the Z direction. This rotation is caused by a difference in ΔT between two CFRP booms, and between two aluminium rods respectively. This is visualized for the booms in Figure 4.10, and is similar for the rods. The mathematical expression for the angle β_{booms}, which is the angle that the M2 makes with the local Y-axis due to deformations of the booms as defined in Figure 4.10, is given in Equation 4.1 below.

$$\beta_{booms} = \tan^{-1}\left(\frac{\Delta L_{boom1} - \Delta L_{boom2}}{L_{width,booms}}\right) = \tan^{-1}\left(\frac{\alpha_{CFRP} * L_{0,booms}(\Delta T_{boom1} - \Delta T_{boom2})}{L_{width,booms}}\right) \tag{4.1}$$

The rotation caused by local deformations in the rods, β_{rods} can be derived. The objective is to minimize both these angles. For β_{booms}, it can be concluded that the difference in thermal gradient between two CFRP booms with the largest- and smallest change in length should be minimized as well: $\Delta T_{boom,max} - \Delta T_{boom,min}$ as small as possible. Ideally, they are equal, so that $\Delta T_{boom,max} = \Delta T_{boom,min}$ and $\Delta L_{boom,max} = \Delta L_{boom,min}$, leading to no rotation around the X and/or Y axis. Equation 4.1 also holds for the minimization of β_{rods}, resulting in a similar rotational thermal objective: minimizing $\Delta T_{rod,max} - \Delta T_{rod,min}$.

For a perfectly athermalized system in which there is no net translation:

$$\begin{aligned} &\alpha_{booms} L_{booms} \Delta T_{booms,avg} - \alpha_{rods} L_{rods} \Delta T_{rods,avg} = 0 \rightarrow \\ &\left(\frac{\Delta T_{booms,avg}}{\Delta T_{rods,avg}}\right)_{perfect,athermal} = \frac{\alpha_{rods} L_{rods}}{\alpha_{booms} L_{booms}} = 1.483 \end{aligned} \tag{4.2}$$

However, the budgets are that of the in-orbit drift budget (2 µm):

$$\begin{aligned} &\alpha_{booms} L_{booms} \Delta T_{booms,avg} - \alpha_{rods} L_{rods} \Delta T_{rods,avg} = \pm 2\mu m \rightarrow \\ &\left(\frac{\Delta T_{rods,avg}}{\Delta T_{booms,avg}}\right)_{perfect,athermal} \cdot \frac{\Delta T_{booms,avg}}{\Delta T_{rods,avg}} - 1 = \frac{2 * 10^{-6}}{\alpha_{rods} L_{rods} \Delta T_{rods,avg}} \rightarrow \\ &\frac{\Delta T_{booms,avg}}{\Delta T_{rods,avg}} = 1.483 \cdot \left(\frac{\frac{\pm 2 * 10^{-6}}{\alpha_{rods} L_{rods}}}{\Delta T_{rods,avg}} + 1\right) = 1.483 \cdot \left(\frac{\pm 0.96}{\Delta T_{rods,avg}} + 1\right) \end{aligned} \tag{4.3}$$

Using Equation 4.3 the upper and lower boundaries for the $\frac{\Delta T_{booms,avg}}{\Delta T_{rods,avg}}$ to conform to the 2 µm budget are then:

$$\begin{aligned} &\left(\frac{\Delta T_{booms,avg}}{\Delta T_{rods,avg}}\right)_{upper,boundary} = 1.483 \cdot \left(\frac{+0.96}{\Delta T_{rods,avg}} + 1\right) \\ &\qquad\qquad \& \\ &\left(\frac{\Delta T_{booms,avg}}{\Delta T_{rods,avg}}\right)_{lower,boundary} = 1.483 \cdot \left(\frac{-0.96}{\Delta T_{rods,avg}} + 1\right) \end{aligned} \tag{4.4}$$

The difference in both Equations 4.2 and 4.3 is that for an athermalized system with zero net translation (Equation 4.2), a ratio of 1.483 appears which holds for *any* value of $\Delta T_{booms,avg}$ and $\Delta T_{rods,avg}$. However, since the translation does not have to be zero, but can expand with a maximum of 2 µm, an insolvible equation with two parameters appears that depend on both the ratio of $\frac{\Delta T_{booms,avg}}{\Delta T_{rods,avg}}$, but also $\Delta T_{rods,avg}$ itself. Note that if in Equation 4.3 the budget goes down to 0 µm (perfectly athermalized), then the temperature gradient ratio $\frac{\Delta T_{booms,avg}}{\Delta T_{rods,avg}}$ becomes equal to 1.483 again and is independent on the individual values of $\Delta T_{booms,avg}$ or $\Delta T_{rods,avg}$.

The conclusion of this is that it is not possible to establish a single requirement on what $\frac{\Delta T_{booms,avg}}{\Delta T_{rods,avg}}$ shall be to meet the in-orbit drift budget of 2 µm which is valid for all analysis cases, since according to Equation 4.3 this again depends on the individual contribution of $\Delta T_{rods,avg}$. Therefore, for all individual analysis cases, the requirement on what $\frac{\Delta T_{booms,avg}}{\Delta T_{rods,avg}}$ shall be, and in what range, is calculated and therefore differs from all analysis cases (since $\Delta T_{rods,avg}$) is different for differerent analyses. This plus other thermal requirements for the booms and rods to conform to the in-orbit drift budget (both translation of 2 µm and rotation of 6 µrad) are summarized in Table 4.4.

Table 4.4: Thermal requirements for individual contributions of booms and rods, as well as their athermalized behaviour. Holds for both translation and rotation budgets

Parameter	**Booms**	**Rods**	**Units**
Length (L)	1.7657	0.0907	m
CTE (α)	$0.8 * 10^{-6}$	$23.1 * 10^{-6}$	m/mk
Width (L_{width})	0.54	0.11	m
Thermal Gradient Requirements			
Translation: $L_{max} = 2\,\mu m$			
$\Delta T_{max} = \frac{\Delta L_{max}}{\alpha * L}$	1.4	0.96	° C / K
$(\frac{\Delta T_{booms,avg}}{\Delta T_{rods,avg}})_{perfect,athermal}$	1.483		-
$(\frac{\Delta T_{booms,avg}}{\Delta T_{rods,avg}})_{upper,boundary}$	$1.483 \cdot (\frac{+0.96}{\Delta T_{rods,avg}} + 1)$		-
$(\frac{\Delta T_{booms,avg}}{\Delta T_{rods,avg}})_{lower,boundary}$	$1.483 \cdot (\frac{-0.96}{\Delta T_{rods,avg}} + 1)$		-
Rotation: $\beta_{max} = 6\,\mu rad$			
$\Delta T_{max} = \frac{\tan(\beta) \cdot L_{width}}{\alpha * L_0}$	2.3	0.3	° C / K

In this table, L is the entire length of the boom and rods in m, CTE is their coefficients of thermal expansion in m/mK and L_{width} is the width between two booms or two rods respectively in m and visualized in Figure 4.10. The L_{width} is only of importance for the calculation of the rotational budget: β_{booms} and β_{rods}. Both values have to be below β_{max}.

It is thus concluded that in order to meet the in-orbit drift budgets, the thermal gradient requirements of Table 4.4 shall be met.

However, for an optimized system, the thermal gradients shall be minimized. The thermal objective that is then used for optimization is composed out of the three factors mentioned earlier: one translational factor and two rotational factors. The total objective is then the summation of all:

Thermal Design Objective:
Minimizing $\frac{\Delta T_{booms,avg}}{\Delta T_{rods,avg}} + (\Delta T_{boom,max} - \Delta T_{boom,min}) + (\Delta T_{rod,max} - \Delta T_{rod,min})$

4.7.2. Overview of Design Objective, Design Constraints and Sensitivity to Objective

A well traceable overview of the above stated thermal design objective and corresponding constraints is shown in this section, as well as a variety of sensitive parameters that affect the thermal design objective. The design constraints are based on the selected functional-, characteristic- and constraint requirements for this MSc, Table 4.1, 4.2 and 4.3 and the sensitive parameters are mostly derived from the N-squared diagram, Figure 4.3, and the CRDT, Figure 4.5. Note that the constraints, as defined in this section, are not similar

to the constraint requirements, but are design constraints that limit the number of parameter combinations feasible to optimize the design objective. The overview is given in Figure 4.5.

Table 4.5: Baffle Thermal Design Objective, Design Constraints and Sensitivity

Thermal Design Objective	
Minimizing $\frac{\Delta T_{booms,avg}}{\Delta T_{rods,avg}} + (\Delta T_{boom,max} - \Delta T_{boom,min}) + (\Delta T_{rod,max} - \Delta T_{rod,min})$	
Design Constraints	**Requirement ID**
1. The temperature gradient requirements of Table 4.4 shall be met	Table 4.4
2. The temperatures of all sub systems within the baffle shall remain within a stability bandwith of 253-323 K.	BAF-T-01-01
3. The bulk temperature of the booms shall not exceed 473K when deployed.	M2-T-01
4. The baffle shall maintain its operational functionality in both extreme cases of BOL- and EOL optical material properties.	BAF-T-01-02
5. The baffle structure shall have a minimum first eigenfrequency ≥ 0.9 Hz in deployed configuration.	BAF-MEC-07-06-03-01
6. The baffle shall mitigate stray-light in deployed configuration	BAF-O-01
7. The internal layer of the baffle shall absorb at least 90 % of incident radiation in both UV- and IR wavelength spectra.	BAF-O-01-01
8. The baffle shall be resistant to AO and plasma/ionizing radiation	BAF-MEC-07-04
9. The total cost of the baffle shall be no more than TBD over the mission lifetime of the DST	BAF-SYS-01
10. The baffle shall use space qualified parts, materials and processess (PMP) and shall be manufacturable with compliance to the availability of parts and materials	BAF-SYS-04/18
11. The baffle shall not use any ITAR controlled components or technologies	BAF-SYS-07
12. The maximum volume of the baffle in deployed configuration shall conform to the usable volume of the Large Solar Simulator from ESA/ESTEC: 10 m diameter and 15 m height	BAF-SYS-15-01
13. The mass of the entire baffle including deployment mechanism shall not exceed 15 kg	BAF-SYS-16
14. The volume of the baffle shall not exceed 1.5 m^3 (threshold) / 0.75 m^3 (goal) when in stowed configuration	BAF-SYS-16
15. The baffle avoid electrical charging.	BAF-MEC-07-04-01
16. The baffle geometry shall not obstruct any telescope elements and not interfere with the optical performance	BAF-MEC-04-04-02
Sensitivity to Thermal Design Objective	
1. Verification by analysis shall take into account uncertainties	BAF-SYS-06
2. The operational functionality of the baffle, as well as the ability to survive the operations and space environment shall be compatible with the power- and radiation exchange of the solar panels.	BAF-SYS-13
3. The baffle design shall incorporate flexibility to accommodate modifications of requirements imposed on the TCS during the project development phase	BAF-SYS-09
4. The baffle design shall incorporate flexibility to offer trimming capabilities to accommodate late requirement updates.	BAF-SYS-10
5. The baffle shall mitigate the creation of hotspots such that it shall not result in consequential structural- or thermal damage that does not conform to the operational requirements.	BAF-MEC-04-03-04
6. The baffle shall achieve a deployed configuration that conforms to the operational requirements with a position accuracy of TBD m.	BAF-MEC-04-04

5

Baseline Functional Performance

After the requirements and thermal performance objective have been established in Chapter 4, Section 4.7, the functional performance of two baseline designs can be simulated and analyzed. The two baseline designs are: **Baseline 1. Without Baffle** and **Baseline 2. Baffle Design from E. Korhonen**. The current work of the author will be compared/benchmarked to both these baseline performances. Each baseline is explained in the subsequent sections, but the thermal performance of both baselines are summarized in the final Performance of Baseline 1 & 2 section: Section 5.3.

5.1. Baseline 1. Without Baffle

Now that the thermal objective and the orbit is defined, a nominal model can be established that contains the DST *without* addition of a baffle. This way, a first baseline model is created that can be used to compare the upcoming design iterations of the author with addition of the baffle. The thermal performance as defined by the thermal objective should improve when adding a baffle, since otherwise adding one does not yield any benefit but only disadvantages. The model of the full DST is made by T. van Wees who worked on the complete TCS for the DST and is shown in Figure 5.1. In Figure 5.2, this model is displayed in its orbital configuration using the orbital parameters established in Section 3.1.

For both baselines, the nominal temperatures of the DST sub-systems and baffle itself (only for baseline 2 ofcourse) are simulated, as well as the transient temperature gradients.

Figure 5.3 shows the temperature profile of the booms over the course of 3 orbits. Note that for every orbit the temperature profile is the same, indicating that one orbit is sufficient to model the thermal behaviour of the DST, as was already assumed in Section 3.1. In Figure 5.3 it can furthermore be seen that the $T_{boom,max} - T_{boom,min} = 22.9$, as Table 5.1 indicates. It can also be seen that the maximum and minimum temperature of the booms, used to calculate part of the thermal objective, is the same for **both** the Sunlit period and Eclipse

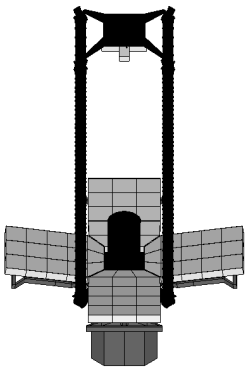

Figure 5.1: DST model *without* the addition of a baffle, initial model made in ESATAN-TMS by T. van Wees, [102], but minor modifications made by the author.

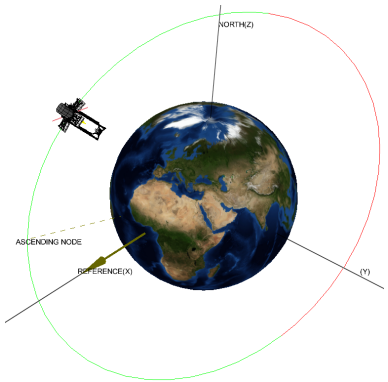

Figure 5.2: Orbital configuration of DST model *without* the addition of a baffle. The red part of the orbit highlights the eclipse.

period. Consequently, the thermal gradients and corresponding thermo-elastic deformations are the same, even though Δt_{drift} and Δt_{coarse} are different (3566 s vs 2102 s as established in Section 3.1). As the in-orbit drift budget is most stringent, this budget therefore serves as the determining budget that has to be adhered to.

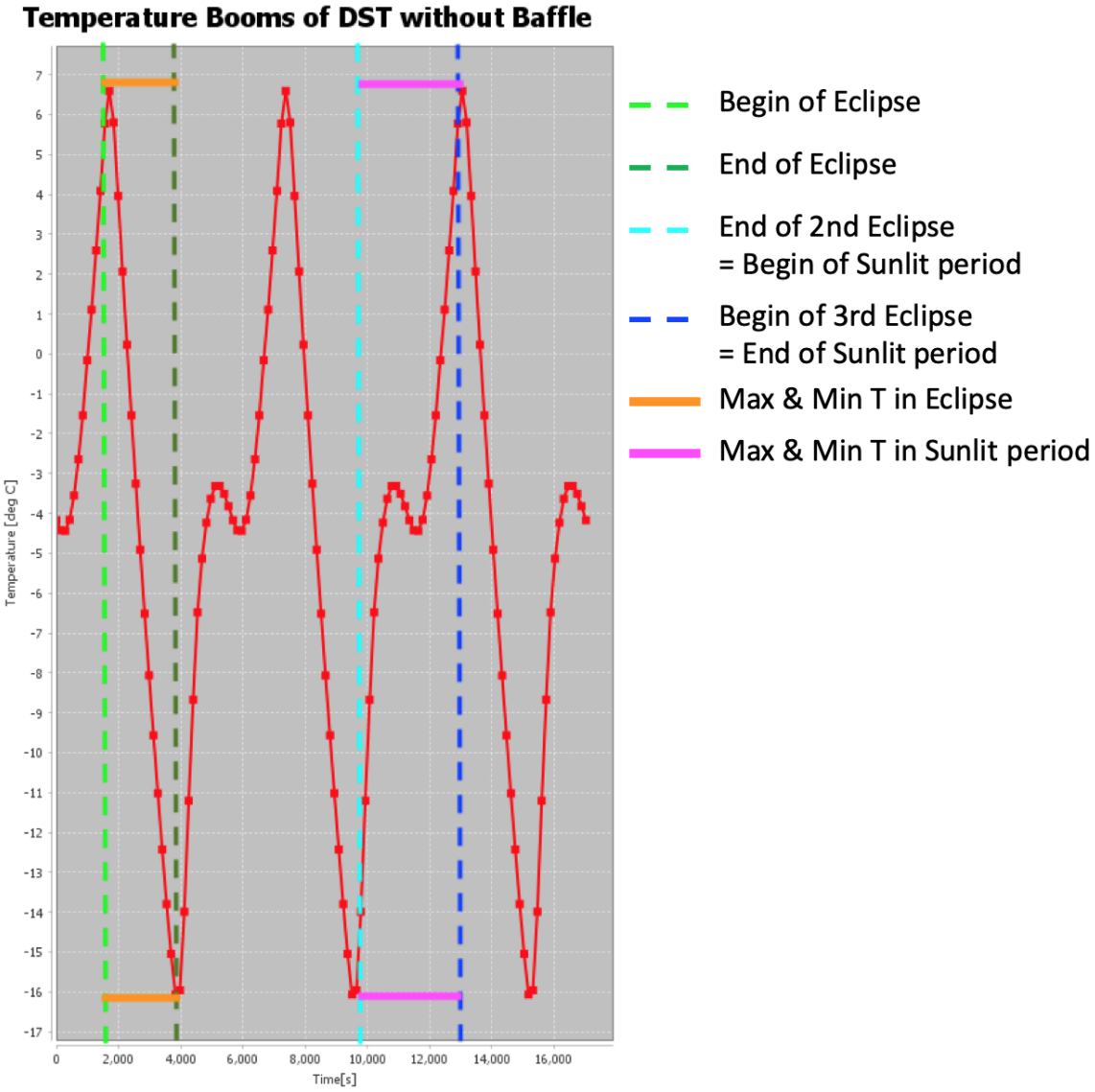

Figure 5.3: Temperature profile of the booms. It can be seen that the $T_{boom,max} - T_{boom,min} = 22.9$, as Table 5.1 indicates. Furthermore, it can be seen that the maximum and minimum temperature of the booms, used to calculate part of the thermal objective, is the same for **both** the Sunlit period and Eclipse period. This means that the thermal gradients and corresponding thermo-elastic deformations are the same, even though Δt_{drift} and Δt_{coarse} are different (3566 s vs 2102 s as established in Section 3.1). As the in-orbit drift budget is most stringent, this budget serves as the determining budget that has to be adhered to.

The in-orbit drift budget serves as the most stringent and determining budget that has to be adhered to: maximum translation of 2 µm and rotation of 6 µrad

5.2. Baseline 2. Baffle Design from E. Korhonen

Next to baseline 1 of the DST without baffle, the previously designed baffle by E. Korhonen, [58] [102], has to modelled in the correct orbit and its performance has to be assessed. Its performance will serve as the

second baseline to which the baffle design of the author will be compared to. Chapter 2 already gave an overview of the current version of the baffle, *without* stating the rationale behind specific design choices as well as specific design information. Therefore, this will be discussed in this section. All design choices are made by E. Korhonen and will therefore only referred to once in this section: [58]. Specific information about the thermal analyses made by T. van Wees' can be found in his master's thesis: [102]. The design overview and performance will result in a second baseline for comparison with the design of the author.

5.3. Performance of Baseline 1 & 2

Baseline 1 Performance: Without Baffle
The temperature data corresponding to the DST without addition of the baffle is shown in Table 5.2. In this table it becomes apparent that for the *nominal temperatures*, the temperatures in red are not adhering to the temperature constraint of BAF-T-01-03. This constraint states that all sub-system temperatures shall remain within a bandwith of 253 - 323 K. The temperatures in orange are barely conforming to this constraint without any safety margin, meaning that due to design uncertainties this will not hold anymore. Furthermore, the *temperature gradients* that are in red are not acceptable, since these gradients cause thermo-elastic deformations well above the requirements. This verification is described below and summarized in Table 5.1.

Furthermore, it can be seen in Table 5.1 above, none of the thermo-elastic requirements for baseline 1 are met. This proves the necessity of implementing a baffle that shields most of the external heat fluxes and can create a stable thermal environment for the rest of the sub-systems.

Baseline 2 Performance: E. Korhonen Design
The thermal performance of E. Korhonen's baffle design is evaluated by T. van Wees. However, his evaluation was done for a different orbital configuration that did not match with the LMT of 10:30 AM requirement. The orbital configuration and assumptions are defined in Section 3.1 and these will be used as input for the assessment of the performance of the baseline design. The same input as for the thermal performance without baffle is used, and the same input will be used for future thermal analyses, so that objective comparison and judgement can be applied.

It can be seen in Table 5.2 that the nominal temperatures all adhere to the BAF-T-01-03 requirement, for both the DST sub-systems as well as the baffle itself. The minimum temperature requirement is that of aluminized Kapton under continuous exposure: -250 ° C.

M2-T-01 is adhered to as even in the worst case without a baffle the temperature levels of the booms are < 373 K.

Table 5.1: Thermo-elastic deformations for baseline 1 and 2

	In-Orbit Drift Budget (requirement)	**Thermo-Elastic Deformation Booms**	**Thermo-Elastic Deformation Rods**	**|Athermalized M2|**
Baseline 1. Without Baffle				
Translation [µm]	2	32.4	42.1	9.7
Rotation [µrad]	6	8.3	928.3	920.1
Baseline 2. E. Korhonen design				
Translation [µm]	2	5.4	2.2	3.2
Rotation [µrad]	6	35.9	44.9	9.1

Table 5.2: Temperature data corresponding baseline 1, Figure 5.1, and baseline 2. For **Nominal Temperatures**: Temperatures in red are not adhering to the temperature constraint of BAF-T-01-03, which states that all sub-system temperatures shall remain within a bandwith of 253 - 323 K. Temperatures in orange: nominal case still adheres to the above requirement, but due to design uncertainties and temperature, this will not hold. For **Temperature Gradients**: Those in red are not acceptable, since these gradients cause thermo-elastic deformations well above the requirements, see Table 5.1

Nominal Temperatures.				
Sub-System	**Max Temp. (° C)**	**Min Temp. (° C)**	**Requirement**	**Reference**
Baseline 1. Without Baffle				
M2	49.9	44.5	$-20°C < T < 50°C$	BAF-T-01-03
Spider	4.8	-7.9	$-20°C < T < 50°C$	BAF-T-01-03
PMSS	32.3	3.6	$-20°C < T < 50°C$	BAF-T-01-03
M1	76.9	75.8	$-20°C < T < 50°C$	BAF-T-01-03
Top Hinge	15.5	-10.0	$-20°C < T < 50°C$	BAF-T-01-03
Booms	7.5	-15.2	$-20°C < T < 50°C$	BAF-T-01-03
Baseline 2. E. Korhonen design				
M2	25.0	24.3	$-20°C < T < 50°C$	BAF-T-01-03
Spider	16.8	-5.5	$-20°C < T < 50°C$	BAF-T-01-03
PMSS	-5.3	-5.7	$-20°C < T < 50°C$	BAF-T-01-03
M1	-4.9	-4.9	$-20°C < T < 50°C$	BAF-T-01-03
Top Hinge	4.7	-7.6	$-20°C < T < 50°C$	BAF-T-01-03
Booms	-2.0	-5.7	$-20°C < T < 50°C$	BAF-T-01-03
Baffle Bottom Outside Avg	-7	-134	$-250°C < T < 177°C$	BAF-T-02-01
Baffle Bottom Inside Avg	-5.1	-5.8	$-250°C < T < 177°C$	BAF-T-02-01
Baffle Side Outside Avg	-62	-106	$-250°C < T < 177°C$	BAF-T-02-01
Baffle Side Inside Avg	-5.2	-11.0	$-250°C < T < 177°C$	BAF-T-02-01
Temperature Gradients				
Thermal Objective Terms	**Value**	**Requirement**	**Unit**	**Reference**
Baseline 1. Without Baffle				
$\Delta T_{booms,avg}$	22.9	≤ 1.4	° C	Table 4.4
$\Delta T_{rods,avg}$	20.0	≤ 0.96	° C	Table 4.4
1. $\frac{\Delta T_{booms,avg}}{\Delta T_{rods,avg}}$	1.15	Between 1.4 - 1.6. Perfect athermal = 1.483	-	Table 4.4
2. $T_{boom,max} - T_{boom,min}$	4.1	≤ 2.3	° C	Table 4.4
3. $T_{rod,max} - T_{rod,min}$	49.4	≤ 0.3	° C	Table 4.4
Thermal Design Objective (1+2+3)	54.7	-	° C	-
Baseline 2. E. Korhonen design				
$\Delta T_{booms,avg}$	3.8	≤ 1.4	° C	Table 4.4
$\Delta T_{rods,avg}$	1.0	≤ 0.96	° C	Table 4.4
1. $\frac{\Delta T_{booms,avg}}{\Delta T_{rods,avg}}$	3.7	Between 0.1 - 2.8. Perfect athermal = 1.483	-	Table 4.4
2. $T_{boom,max} - T_{boom,min}$	13.7	≤ 2.3	° C	Table 4.4
3. $T_{rod,max} - T_{rod,min}$	2.4	≤ 0.3	° C	Table 4.4
Thermal Design Objective (1+2+3)	19.7	-	° C	-

6

Thermal System Design and Performance

This chapter contains the thermal design and performance. The optimization process can begin by changing parameters that influence the thermal design objective. The parameters that are going to be changed are of geometrical nature: shape and height of the baffle, as well as material- and coating selection: different outer coatings that yield a different ratio of absorptance to emittance and a combination with different lay-ups of the MLI material (number of layers, material usage, density of material and thicknesses) that are captured in a single parameter known as the effective emissivity and effective conductivity, as explained in the theory from literature chapter, Chapter 3. After this, a preliminary sensitivity analysis is conducted and HiPeR- as well as other stray light control systems and orbital debris control mitigation systems are implemented.

6.1. Thermal Design Flow Chart

The thermal design flow chart has been established and can be seen in Figure 6.1.

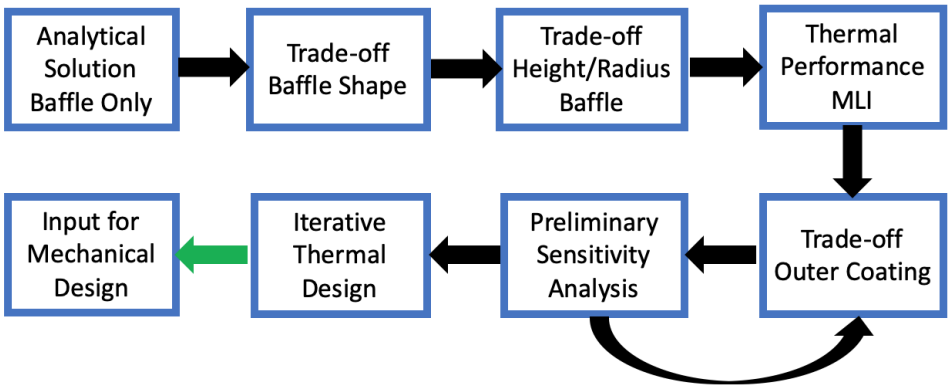

Figure 6.1: Thermal Design Flow Chart

6.2. Analytical Solution of Cylindrical Baffle: Serving as Validation of Thermal Results

In this section, the analytical solution of a cylindrical baffle is calculated, which will be used to validate the ESATAN-TMS results. The entire nodal network will be explained, including all heat loads and radiative/-conductive couplings. The baffle is modeled using four nodes and is given in Figure 6.2. The rest of the sub-systems are not modeled, since analytical view factors to complex geometries (like the secondary mirror or concave mirrors) are hard to calculate or even non-existent. ESATAN-TMS uses Monte-Carlo ray-tracing to calculate view factors from every node to all other nodes in which rays are fired from each surface in a random distribution. However, for this method, the ray-tracing method from ESATAN-TMS is compared to the analytical model in which view factors between the four nodes are calculated based on geometry ratios

found in literature on view factor data. This validation gives sound evidence that results of more complex geometries modeled in ESATAN-TMS are also physically accurate.

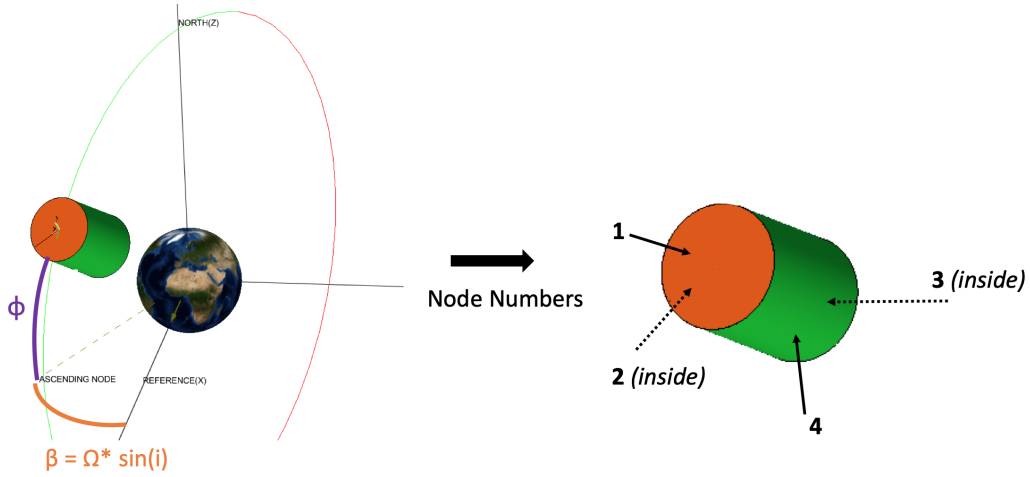

Figure 6.2: Orbital configuration of the analytical model. This is the same orbital configuration as for all future thermal analyses and stated in 3.1

In Figure 6.2, β is the Sun's beta angle, Ω is the RAAN, i is the inclination angle, and Φ is the latitude of the DST. Note that the beta angle remains constant, but the latitude is time-dependent and changes for every orbital time step.

The right figure in Figure 6.2 displays the node numbers used in the model: node 1 and 2 are the the outside- and inside of the bottom of the baffle respectively, node 3 and 4 are the inside- and outside of the side of the cylindrical baffle. The reason that node 1-2 and 3-4 are not the same (and hence will not display the same temperature), is because the baffle is made of MLI. This means that there is an effective emissivity and conductivity between the inside-and outside of the baffle and therefore different temperature values for both sides.

6.2.1. Nodal Network Reduction

The nodal network for this 4 node thermal model is given in Figure 6.3, including first set of reductions.

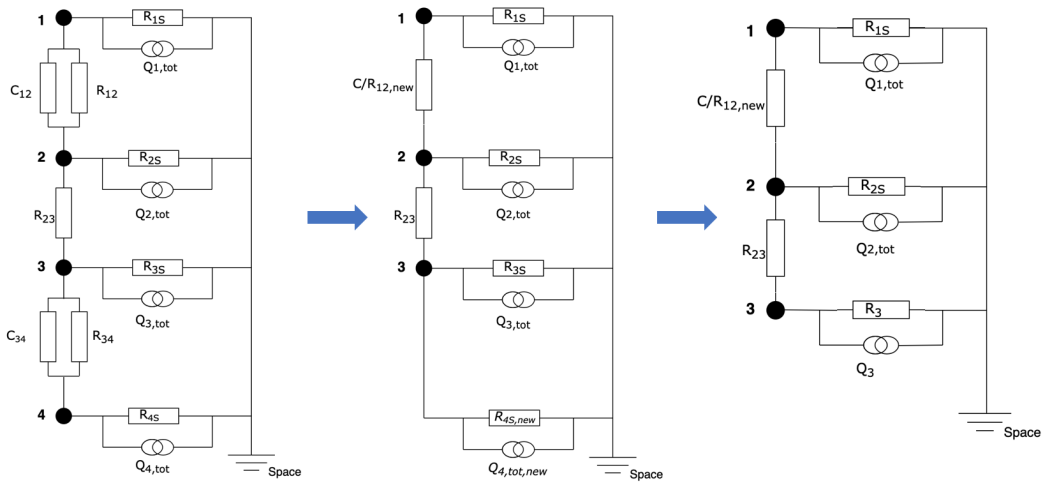

Figure 6.3: Nodal network of the four node thermal analytical model. Including first reduction.

Table 6.1: Nodal Network corresponding to Figure 6.3

Radiative Couplings	**Heat Fluxes Couplings**
Full Nodal Network: Figure 6.3, left figure	
$R_{1S} = \epsilon_1 \cdot A_1 \cdot B_{1S} = \epsilon_1 \cdot A_1$	$Q_{1,tot} = \alpha_1 \cdot A_1 \cdot J_S \cdot \cos(\beta) \cdot \cos(\Phi)$
$R_{2S} = \epsilon_2 \cdot A_2 \cdot B_{2S}$	$Q_{2,tot} = \alpha_2 \cdot A_2 \cdot J_A \cdot \cos(\beta) \cdot \cos(\Phi) + \epsilon_2 + A_2 + J_{IR}$
$R_{3S} = \epsilon_3 \cdot A_3 \cdot B_{3S}$	$Q_{3,tot} = 0$
$R_{4S} = \epsilon_4 \cdot A_4 \cdot B_{4S} = \epsilon_4 \cdot A_4$	$Q_{4,tot} = \alpha_4 \cdot A_{4,half} \cdot J_S \cdot \sin(\beta) = 0.5 \cdot \alpha_4 \cdot A_4 \cdot J_S \cdot \sin(\beta)$
$R_{12} = \epsilon_{eff,1\to2} \cdot A_1$	
$C_{12} = c_{eff,1\to2} \cdot A_1$	
$R_{23} = \epsilon_2 \cdot A_2 \cdot B_{23}$	
$R_{34} = \epsilon_{eff,3\to4} \cdot A_3$	
$C_{34} = c_{eff,3\to4} \cdot A_3$	
First Reduction, elimination of node 4: Figure 6.3, middle figure	
$R_{4S,new} = \frac{(R_{34}+C_{34}) \cdot R_{4S}}{R_{34}+C_{34}+R_{4S}}$	$Q_{4,tot,new} = \frac{(R_{34}+C_{34})}{R_{34}+C_{34}+R_{4S}} \cdot Q_{4S}$
Second Reduction, combining heat fluxes and radiative couplings: Figure 6.3, right figure	
$R_3 = R_{3S} + R_{4S,new}$	$Q_3 = Q_{3,tot} + Q_{4,tot,new}$

In this table, ϵ is the emissivity of a surface, A is the area of the surface, B_{ij} is the Gebhart factor from surface i to surface j and indicates the view factor including reflections, α is the absorptivity of a surface, β is the Sun's beta angle and equal to $\Omega \cdot sini$, ϕ is the latitude of the DST at a given orbital time, J_S is the Solar flux and equal to 1387.94 $\frac{W}{m^2}$, J_A is the Albedo flux and equal to 365.15 $\frac{W}{m^2}$ and J_{IR} the infrared flux and equal to 203.9 $\frac{W}{m^2}$. Also note that $A_{4,half}$ is only half of the area of A_4, since the solar heat flux only illuminates half of the cylinder. Therefore: $2 \cdot A_{4,half} = A_4$. Furthermore: $A_1 = A_3 = \pi \cdot R^2$ and $A_2 = A_4 = 2 \cdot \pi \cdot R \cdot H$, in which R is the radius of the cylinder and H is the height of the cylinder, both in m. Further reductions:

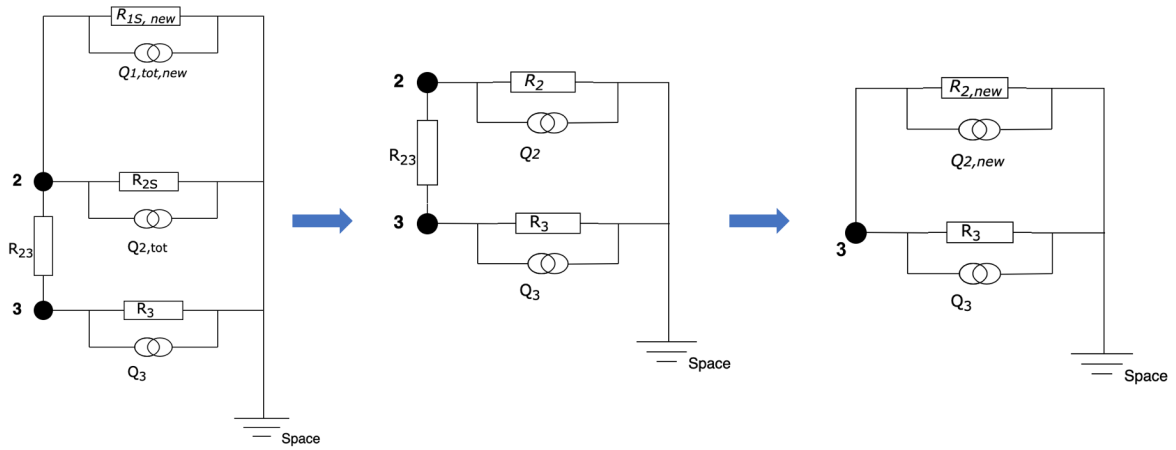

Figure 6.4: Nodal network of the four node thermal analytical model. Including first reduction.

Table 6.2: Nodal Network corresponding to Figure 6.4

Radiative Couplings	**Heat Fluxes Couplings**
Fourth reduction, star-point elimination of node 1: Figure 6.4, left figure	
$R_{1S,new} = \frac{(R_{12}+C_{12}) \cdot R_{1S}}{R_{12}+C_{12}+R_{1S}}$	$Q_{1,tot,new} = \frac{(R_{12}+C_{12})}{R_{12}+C_{12}+R_{1S}} \cdot Q_{1,tot}$
Fifth Reduction, combining heat fluxes and radiative couplings: Figure 6.4, middle figure	
$R_2 = R_{1S,new} + R_{2S}$	$Q_2 = Q_{1,tot,new} + Q_{2,tot}$
Sixth Reduction, star-point elimination of node 2: Figure 6.4, right figure	
$R_{2,new} = \frac{R_{23} \cdot R_2}{R_2+R_{23}}$	$Q_{2,new} = \frac{R_{23}}{R_{23}+R_2} \cdot Q_2$

And the last reduction to obtion one total radiative coupling to space and one total heat flux absorbed on node 3 is:

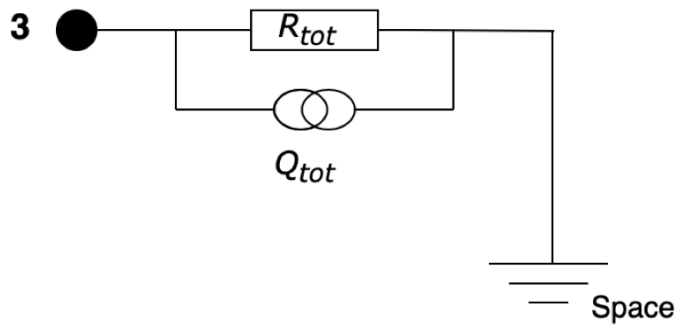

Figure 6.5: Nodal network of the four node thermal analytical model. Including first reduction.

Table 6.3: Nodal Network corresponding to Figure 6.5

Radiative Couplings	**Heat Fluxes Couplings**
Last reduction, combining heat fluxes and radiative couplings: Figure 6.5	
$R_{tot} = R_{2,new} + R_3$	$Q_{tot} = Q_{2,new} + Q_3$

6.2.2. Gebhart- and View Factor Calculations

The radiative couplings in Table 6.1 consist of emissitivity values, areas and Gebhart factors. These Gebhart factors are a function of the radiation view factor between two surfaces as described in Chapter 3. These need to be calculated in order to compute the thermal response. The view factors for a hollow cylinder can be analytically expressed as a function of height and radius.

View Factors

The view factor between the inner surface of a cylinder to itself (node 3 to node 3 in this case) is given in Equation 6.1, and taken from p. 7.84 from the Handbook of Heat Transfer. [80]

$$F_{33} = 1 + H - \left(1 + H^2\right)^{1/2} \tag{6.1}$$

The view factor between the bottom of a cylinder to the inner surface (node 2 to node 3 in this case) is given in Equation 6.2, also taken from the source stated above, [80].

$$F_{23} = 2H\left[\left(1 + H^2\right)^{1/2} - H\right] \tag{6.2}$$

In both these equations, H is the ratio between the height to the radius of the cylinder: $H = \frac{h}{2r}$.

The view factor from the inner surface to the inner bottom of a cylinder, F_{32} results from the following symmetry rule: $F_{ij} \cdot A_i = F_{ji} \cdot A_j$. Applying this rule to obtain F_{32}:

$$F_{32} = \frac{A_2}{A_3} \cdot F_{23} \tag{6.3}$$

Table 6.4: Summary of view factors as calculated above

F	**1**	**2**	**3**	**4**	**S**
1	0	0	0	0	1
2	0	0	F_{23}	0	$1 - F_{23}$
3	0	$F_{23} \cdot \frac{A_2}{A_3}$	F_{33}	0	$1 - F_{23} \cdot \frac{A_2}{A_3} - F_{33}$
4	0	0	0	0	1
S	0	0	0	0	1

Table 6.4 contains the summary of the view factors.

Gebhart Factors
The Gebhart factors, that are a function of the above view factors, are generally defined as in Equation 3.2 of Chapter 3. Applying this formula to the Gebhart factors in this problem:

$$B_{2S} = F_{2S} + (1-\epsilon_3)\cdot F_{23}\cdot B_{3S} \tag{6.4}$$

$$B_{3S} = F_{3S} + (1-\epsilon_2)\cdot F_{23}\cdot \frac{A_2}{A_3}\cdot B_{2S} + (1-\epsilon_3)\cdot F_{33}\cdot B_{3S} \tag{6.5}$$

$$B_{23} = F_{23}\cdot\epsilon_3 + (1-\epsilon_3)\cdot F_{23}\cdot B_{33} \tag{6.6}$$

$$B_{33} = F_{33}\cdot\epsilon_3 + (1-\epsilon_2)\cdot F_{23}\cdot \frac{A_2}{A_3}\cdot B_{23} + (1-\epsilon_3)\cdot F_{33}\cdot B_{33} \tag{6.7}$$

In all Gebhart equations above, other Gebhart factors appear and therefore these have to be uncoupled and rewritten. There are four equations and 4 unknown Gebhart factors, so this is a solvable system. Uncoupling all Gebhart factors lead to the following result:

$$B_{2S} = [F_{2S} + \frac{(1-\epsilon_3\cdot F_{23}\cdot F_{3S})}{1-F_{33}\cdot(1-\epsilon_3)}]/[1-\frac{(1-\epsilon_3)\cdot(1-\epsilon_2)\cdot\frac{A_3}{A_2}\cdot F_{32}^2}{1-F_{33}\cdot(1-\epsilon_3)}] \tag{6.8}$$

$$B_{3S} = \frac{F_{3S} + (1-\epsilon_2)\cdot F_{32}\cdot B_{2S}}{1-F_{33}\cdot(1-\epsilon_3)} \tag{6.9}$$

$$B_{23} = [F_{23}\cdot\epsilon_3 + \frac{(1-\epsilon_3\cdot F_{23}\cdot F_{33}\cdot\epsilon_3)}{1-F_{33}\cdot(1-\epsilon_3)}]/[1-\frac{(1-\epsilon_3)\cdot(1-\epsilon_2)\cdot\frac{A_3}{A_2}\cdot F_{32}^2}{1-F_{33}\cdot(1-\epsilon_3)}] \tag{6.10}$$

$$B_{33} = \frac{F_{33}\cdot\epsilon_3 + (1-\epsilon_2)\cdot F_{32}\cdot B_{23}}{1-F_{33}\cdot(1-\epsilon_3)} \tag{6.11}$$

6.2.3. Steady State Solution

The steady state temperature of node 3 given that the heat flux absorbed on node 3, Q_{tot}, is constant is given in Equation 6.12 below.

$$Q_{tot} = R_{tot}\cdot\sigma\cdot T_3^4 \rightarrow T_3 = \frac{Q_{tot}}{R_{tot}\cdot\sigma}^{1/4} \tag{6.12}$$

In which Q_{tot} is the total heat input as summarized in Table 6.3:

$$\begin{aligned} Q_{tot} = Q_{2,new} + Q_3 = \frac{R_{23}}{R_{23}+R_2}\cdot Q_2 + Q_3 = \frac{R_{23}}{R_{23}+R_2}\cdot(Q_{1,tot,new} + Q_{2,tot}) + Q_{3,tot} + Q_{4,tot,new} = \\ \frac{R_{23}}{R_{23}+R_2}\cdot(\frac{R_{12}+C_{12}}{R_{12}+C_{12}+R_{1S}}\cdot Q_{1,tot} + Q_{2,tot}) + Q_{3,tot} + \frac{R_{34}+C_{34}}{R_{34}+C_{34}+R_{4S}}\cdot Q_{4S} = \\ \frac{R_{23}}{R_{23}+R_2}\cdot(\frac{R_{12}+C_{12}}{R_{12}+C_{12}+R_{1S}}\cdot Q_{1,tot} + Q_{2,tot}) + Q_{3,tot} + \frac{R_{34}+C_{34}}{R_{34}+C_{34}+R_{4S}}\cdot Q_{4S} \end{aligned} \tag{6.13}$$

And R_{tot} the total radiative coupling from node 3 to space:

$$\begin{aligned} R_{tot} = R_{2,new} + R_3 = \frac{R_{23}\cdot R_2}{R_{23}+R_2} + R_{3S} + R_{4S,new} = \frac{R_{23}\cdot(R_{1S,new}+R_{2S})}{R_{23}+R_{1S,new}+R_{2S}} + R_{3S} + \frac{(R_{34}+C_{34})\cdot R_{4S}}{R_{34}+C_{34}+R_{4S}} = \\ \frac{R_{23}\cdot(\frac{(R_{12}+C_{12})\cdot R_{1S}}{R_{12}+C_{12}+R_{1S}}+R_{2S})}{R_{23}+\frac{(R_{12}+C_{12})\cdot R_{1S}}{R_{12}+C_{12}+R_{1S}}+R_{2S}} + R_{3S} + \frac{(R_{34}+C_{34})\cdot R_{4S}}{R_{34}+C_{34}+R_{4S}} = \\ \frac{\epsilon_2 A_2 B_{23}\cdot(\frac{(\epsilon_1 A_1^2\cdot(\epsilon_{eff,1\rightarrow2}+c_{eff,1\rightarrow2}))}{A_1\cdot(\epsilon_{eff,1\rightarrow2}+c_{eff,1\rightarrow2}+\epsilon_1)}+\epsilon_2 A_2 B_{2S})}{\epsilon_2 A_2 B_{23}+\frac{\epsilon_1 A_1^2\cdot(\epsilon_{eff,1\rightarrow2}+c_{eff,1\rightarrow2})}{A_1\cdot(\epsilon_{eff,1\rightarrow2}+c_{eff,1\rightarrow2}+\epsilon_1)}+\epsilon_2 A_2 B_{2S}} + \epsilon_3 A_3 B_{3S} + \frac{\epsilon_4 A_4 A_3\cdot(\epsilon_{eff,3\rightarrow4}+c_{eff,3\rightarrow4})}{\epsilon_4 A_4 + A_3\cdot(\epsilon_{eff,3\rightarrow4}+c_{eff,3\rightarrow4})} \end{aligned} \tag{6.14}$$

And σ is the Stefan-Boltzmann Constant: $\sigma = 5.67 \cdot 10^{-8} \frac{W}{m^2 \cdot K^4}$.

In Equation 6.12, the heat input is equal to the heat output: $Q_{in} = Q_{out} = Q_{tot} = R_{tot} \cdot \sigma \cdot T_3^4$, meaning that $\Delta Q = 0$. However, for the transient solution, the heat input is not equal to the heat output, resulting in a ΔQ. Due to Newton's law of cooling, the rate of heat loss is proportional to the difference in temperature of a body and thus an exponential decay in temperature is expected. This is futher explained in the transient solution section, Section 6.2.4.

6.2.4. Transient Solution

The transient heat transfer solution follows from Equation 3.6, but is stated below for simplicity:

$$m \cdot c_p \cdot \frac{dT}{dt} = dQ \rightarrow dT = \frac{dQ}{m \cdot c_p} \cdot dt \tag{6.15}$$

Using a first order approximation, the temperature of node 3 at time $n+1$ is equal to:

$$\Delta T = \frac{\Delta Q}{m \cdot c_p} \cdot \Delta t \rightarrow T_{3,n+1} = T_{3,n} + \Delta t \cdot \frac{Q_{tot,n+1} - R_{tot,n+1} \cdot \sigma \cdot T_{3,n}^4}{m \cdot c_p} \tag{6.16}$$

In both Equations 6.15 and 6.16, $T_{3,n+1}$, $Q_{tot,n+1}$ and $R_{tot,n+1}$ are the temperature, total heat input and radiative coupling of node 3 at an increase of one timestep $n+1$ respectively. Furthermore, $T_{3,n}$ is the temperature of node 3 of the previous timestep n. It is assumed that the mass and specific heat are a constant and do not change over time. For the given set of parameters as highlighted in Table 6.5, the following transient response appears as seen in Figure 6.6.

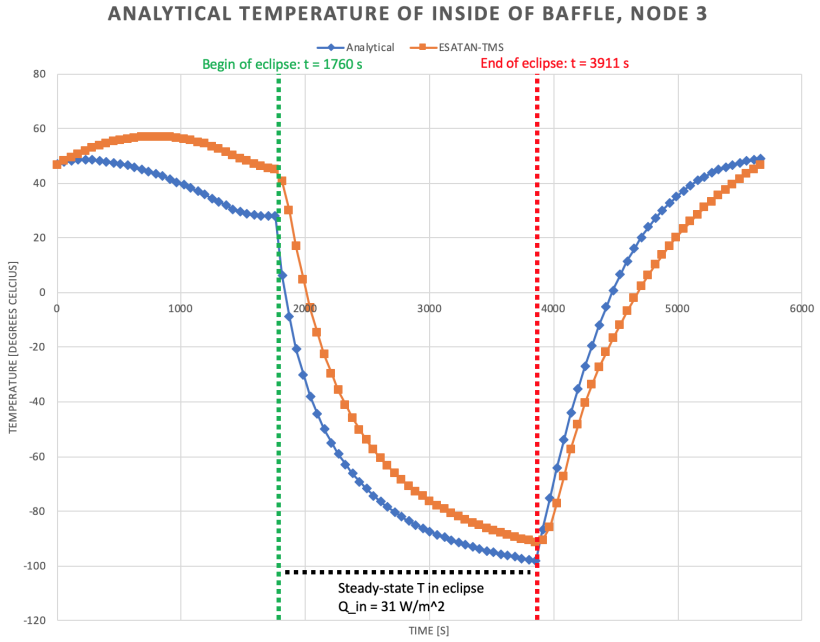

Figure 6.6: Transient thermal response of node 3 (inner layer of MLI). Note that at around $t = 1760$ s, the eclipse starts. An exponentail decay in temperature towards the steady state temperature of -100.8 ° C is visible. The eclipse ends around $t = 3911$ s

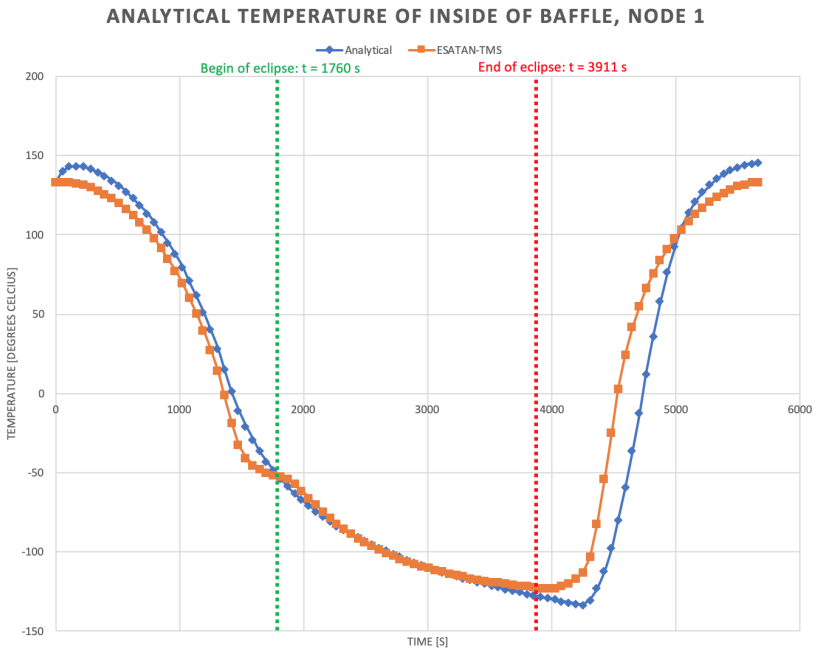

Figure 6.7: Transient thermal response of node 1 (outer layer of bottom). The eclipse starts again around $t = 1760$ and ends around $t = 3911$ s. However, since node 3 is always illuminated by the Sun up to the point of eclipse while for node 1 that is not the case, it is less obvious to see the start and end of the eclipe in the graph for node 1.

Table 6.5: Input data for transient thermal response

Input Parameter	**Value**
Orbital Parameters	
Orbital Height	500 km
Inclination	97.4 °
RAAN	-22.5 °
β	-22.3 °
Heat Input Values	
J_S	1387.94 $\frac{W}{m^2}$
Albedo Factor	0.306
J_A	365.15 $\frac{W}{m^2}$
J_{IR}	203.9 $\frac{W}{m^2}$
Emissivity Values	
ϵ_1 and ϵ_4	0.14
ϵ_2 and ϵ_3	0.84
Absorptivity Values	
α_1 and α_4	0.19
α_2 and α_3	0.93
Effective Conductivity & Emissivity	
$\epsilon_{eff,1\to2}$ and $\epsilon_{eff,3\to4}$	0.01894 (matching with 5 layers of MLI)
$C_{eff,1\to2}$ and $C_{eff,3\to4}$	0.1097 (matching with 5 layers of MLI)
Geometrical Values	
Height Cylinder	2.725 m
Radius Cylinder	1 m
MLI thickness corresponding to 5 layers	0.7812 mm
Density of Material	146 $\frac{kg}{m^3}$
Heat Capacity of Material	1117.5 $\frac{J}{kgK}$

6.2.5. Observed Differences Analytical- and ESATAN-TMS Model

There are some observed differences between the analytical model and the ESATAN-TMS model, especially for node 3 (inner layer of MLI of cylindrical part) as can be seen in Figure 6.6. These differences are due to a number of different reasons:

1. Node 1: Node 1 is flat surface of which the $Q_{1,tot} = \alpha_1 \cdot A_1 \cdot J_s \cdot cos(\beta) \cdot cos(\Phi)$ holds with great confidence. Furthermore, the radiated heat to space, $R_1S = \epsilon_1 \cdot A_1$ does not depend on any Gebhart factors, since no other node is seen by node 1. This is different for node 3: it depends on the Gebhart factor between node 2 and 3 and its corresponding view factor from node 2 to node 3. There is also a discrepancy between the analytical and ESATAN view factors: $F_{23,analytical} = 0.893$ and $F_{23,ESATAN} = 0.931$.

2. Node 3: The temperature levels of node 3 are dependent on the temperature levels of node 4 (outer cylindrical MLI) and the effective emissivity/conductivity through the MLI, as well as the coupling of node 2 to node 3. In general, the interior temeperatures (node 3 and node 2) are therefore less predictable.

3. Node 3: Up to the point when the eclipse starts ($t = 1760$ s), the heat input is different by a factor of 1.3. Since the external heat fluxes are the same for both models, this difference must be due to a difference in absorption for both models, which results in the following point below.

4. Node 3: Different angle calculation meaning that the heat flux impinging on a surface (especially on the cylindrical outer surface 4) is different, and not equal to the cosine of the normal to the surface. Since this impinging angle is calculated using Monte-Carlo Ray Tracing in ESATAN-TMS, this is difficult to validate.

5. General: Different integration schemes are used. For the analytical model, a first order Euler forward scheme is used, which is only a first order accurate to solve differential equations (Δ t), whereas ESATAN-TMS uses a more accurate integration scheme with iterations to account for inaccurate first estimate of initial temperature $T_{3,n}$. Therefore, a different exponential decay to the final end-point is visible. Note that the end-point at $t = 5668$ s are equal for both models and the general trend line for both node 1 and node 3 is equal

Now that the ESATAN-TMS model is defined (orbital configuration, MLI, geometry) and is validated against analytical data, the ESATAN-TMS software is proven to be correct and accurate and can be used to run more complex thermal analyses that also take all other DST sub-systems into account. Since the DST consists of many geometries with various complex shapes, view factor data for these shapes do not exist and therefore ESATAN-TMS must be used to calculate view factors between all nodes using a Monte Carlo Ray-Tracing method.

6.3. Trade-off Shape

The shape of the baffle has been extensively traded off by E. Korhonen based on mass, reliability and stiffness and also by T. van Wees based on thermal performance. [58] [102]

Both decided to go with a cylindrical shape, but due to mechanical deployability, the cylinder is polygonized to an octagonal shape. However, since E. Korhonen made a trade-off based on only mechanical parameters without looking at the thermal performance, and T. van Wees made a trade-off based on only the thermal performance without looking at mechanical parameters (deployability, stiffness, mass), the trade-off is briefly revised to take into account both thermal- and mechanical performance. Furthermore, the thermal performance is assessed based on the thermal objective as established in Section 4.7, instead of arbitrary nominal temperature data.

Only the cylindrical- and cubical baffle shape are taken into consideration for this brief trade-off, since the cubical baffle performed best in E. Korhonen's trade-off after the the cylindrical baffle.

6.3.1. Thermal Performance

The thermal performance objective is evaluated for three different outer coatings, to assess the impact of different parameters that influence the choice of shape on thermal performance.

The input parameters are the same as those from Table 6.5, only the outer coating ϵ_1, α_1, ϵ_4 and α_4, are not the same as the values from this table.

Shape	Coating	$\frac{\alpha}{\epsilon}$	$\frac{\Delta T_{booms,avg}}{\Delta T_{rods,avg}}$ [-]	$\Delta T_{booms,max} - \Delta T_{booms,min}$ [°C]	$\Delta T_{rods,max} - \Delta T_{rods,min}$ [°C]	Thermal Performance Objective [°C]
Cylinder			8.6	11.3	4.4	24.2
Cubical	Black Copper	1.56	3.3	11.7	23.3	38.3
Cylinder			8.6	11.0	4.1	23.7
Cubical	a = 0.15 and e = 0.083	1.81	3.0	11.8	23.1	37.9
Cylindrical			7.9	9.9	5.6	23.4
Cubical	Aluminized Kapton	3	8.6	9.0	6.4	24.0

Figure 6.8: Shape comparison for different outer coatings. For all different outer coatings, the cylindrical baffle performs best, yielding a lower value for the thermal performance objective.

The thermal performance of the cylindrical shape is better than the cubical shape in all three cases. A cylindrical shape is chosen and preferred over a cubical shape, since its thermal performance is better: it yields a lower value for the thermal performance objective, evaluated for different outer coatings: 24.2 ° C instead of 38.3 ° C for a black copper outer coating with $\frac{\alpha}{\epsilon} = 1.56$, 23.7 ° C instead of 37.9 ° C for an $\frac{\alpha}{\epsilon} = 1.81$ and 23.4 ° C instead of 24.0 ° C for aluminized Kapton as the outer coating with an $\frac{\alpha}{\epsilon} = 3$. This means that the gradients of the booms and rods are lower for a cylindrical shape than for a cubical shape.

Note that the thermal performance objective in all three cases is already much better than that of the DST without baffle, Table 5.2: 24 °C versus 54.7 °C .

6.3.2. Mechanical Performance

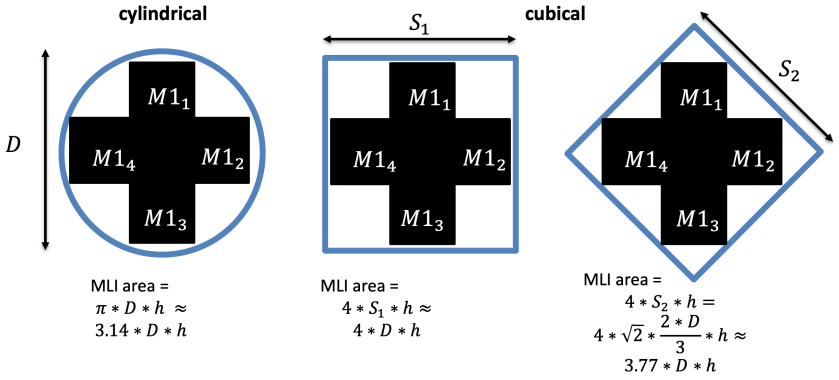

Figure 6.9: Mechanical performance

Based on the mechanical performance, it can be seen in Figure 6.9 that a cylindrical baffle always yields a lower value for the area of MLI needed to shield the DST. This saves mass, and hence results in a lower eigenfrequency for the mechanical system ($\omega_n = \sqrt{\frac{k_{eq}}{m_{eq}}}$). The mass savings is around $1 - \frac{3.77}{3.14} = 16.7\%$ in best case scenario when the cubical baffle is 45 degrees rotated.

Furthermore, E. Korhonen found that the cylindrical (triangulated to octagonal shape) has a higher eigenfrequency than the cubical concept: 1.53 Hz and 1.27 Hz respectively, based on preliminary ANSYS modal analyes. [58] Moreover, the cylindrical model is worked out in quite some detail by both authors mentioned above and therefore, choosing a cylindrical shape yields a better functional baseline for comparison with different mechanical deployment concepts that are going to be worked out in Chapter 7.

To conclude, all trade-off criteria (thermal performance, mass, stiffness) are in favor of the cylindrical shape. Therefore no need for a thorough trade-off is needed using the AHP, since the cylindrical baffle outperforms the cubical baffle for any given weight factor combination. Also, as mentioned above, more design information is available for the cylindrical baffle, since E. Korhonen's and T. van Wees' thermal-mechanical design is based on a triangulated cylindrical (octagonal) shape. Consequently, the cylindrical shape is again chosen to be worked out in more detail.

6.4. Trade-off Height and Radius

6.4.1. Trade-off Height

The height of the baffle is important for the thermal performance, since the height of the baffle determines the view factor F_{33} and F_{23}. In Equations 6.1 and 6.2 it can be deduced that the height of the baffle has a quadratic relationship to the view-factors, meaning that this will also be expected.

Several heights are examined of which the lowest boundary height is 2.5 m and the highest is 2.9 m. The minimum height of 2.5 m still covers the SMSS spider, but without much margin as can be seen in Figure 6.10. Therefore, this is taken as the minimum height for the various height analyses. The maximum height of 2.9 m is established since a decrease in thermal performance was already observed for this height and further increased heights. Namely, for a height of 2.9 m the temperature of the M2 is 50.3 - 52.3 ° and therefore already exceeds the BAF-T-01-03 requirement that imposes that all DST sub-systems shall stay within the temperature limit of -20 to +50 °C. This temperature result is shown in Table F.4 in the Appendix. The results of a height of 2.5 m, 2.9 m, 2.65 m and 2.725 m are also put in tabular form in the Appendix: Table F.1, F.2 and F.3. The only variable for these analyses is the height. The outer coating is fixed and is chosen to be a coating that is often used for the sake of simplicity: aluminized Kapton with an absorptivity of 0.15 and emissivity of 0.05 ($\frac{\alpha}{\epsilon} = \frac{0.15}{0.05} = 3$).

The non-linear, quadratic impact of the baffle height on the thermal performance is indeed visualized in Figure 6.12. In this figure it can be seen that a height of 2.5 m is too little as its thermal performance objective is highest. A height of 2.9 m also already degrades the thermal performance. The most optimal solution is that of 2.65 and 2.275 m. For these two values, as well as for the maximum and minimum height of the baffle the performance is summarized in Table 6.6.

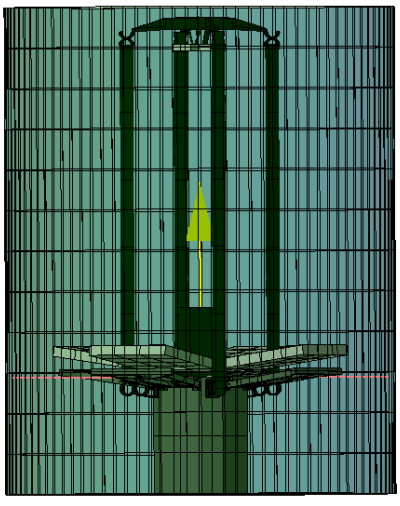

Figure 6.10: Baffle height of 2.5 m modelled in ESATAN-TMS. As can be seen, the SMSS spider is barely protected, meaning that a lower height than 2.5 m is not sufficient.

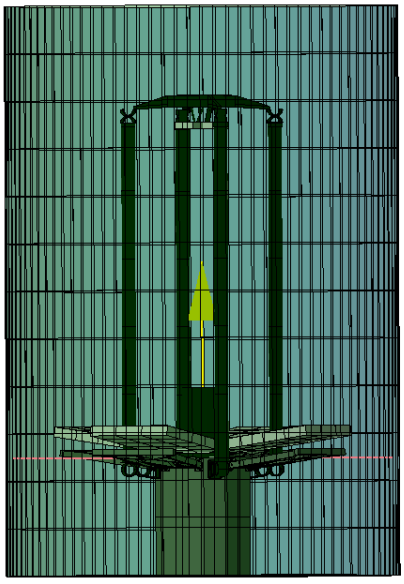

Figure 6.11: Baffle height of 2.9 m modelled in ESATAN-TMS. This is taken as the highest baffle height value to be taken into account as decreasing thermal performance with higher baffle heights was already visible (as well as a further decrease in structural integrity for further increasing baffle heights.)

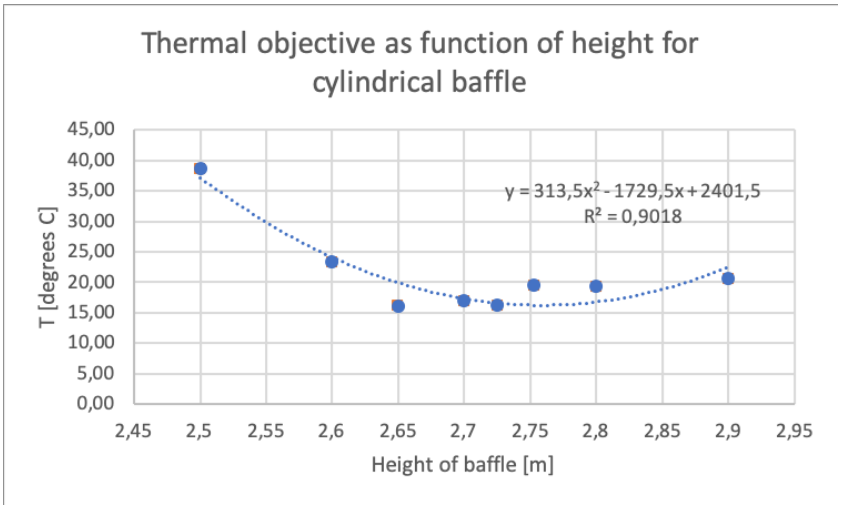

Figure 6.12: Thermal performance objective as a function of height for a cylindrical baffle

Table 6.6: Thermo-elastic deformations of the cylindrical baffle for height of 2.5, 2.65, 2.725 and 2.9 m.

	In-Orbit Drift Budget (requirement)	**Thermo-Elastic Deformation Booms**	**Thermo-Elastic Deformation Rods**	**|Athermalized M2|**
Height = 2.5 m				
Translation [µm]	2	26.0	21.2	4.5
Rotation [µrad]	6	22.9	534.4	511.5
Height = 2.65 m				
Translation [µm]	2	25.7	5.8	19.8
Rotation [µrad]	6	13.7	82.2	69.5
Height = 2.725 m				
Translation [µm]	2	25.7	7.2	18.5
Rotation [µrad]	6	9.9	135.8	125.8
Height = 2.9 m				
Translation [µm]	2	24.9	8.6	16.3
Rotation [µrad]	6	19.4	169.9	150.5

None of the heights conform to the in-orbit requirements of 2 µm max translation and 6 µrad max rotation. However, one height is better than the other. Namely, it can be seen that a height of 2.5 m is too low as it barely protects the SMSS rods: the thermal gradient of the rods for a baffle height of 2.5 m is extremely high, namely 10.1 ° C, which leads to a translation of the rods of 21.2 µm as can be seen in Table 6.6. The difference in gradient for different rods is 28.1 ° C, which leads to a corresponding rotation of 534.4 µrad. The athermalized rotation (since the booms also rotate) is 534.4 - 22.9 = 511.5 µrad, which exceeds the 6 µrad budget by a great margin. Therefore, a height of 2.5 m is too low. This is also observed already as the thermal performance objective is higher than those of 2.65, 2.725 and 2.9 m.

The thermal performance objective for a height of 2.9 m is also higher than for a 2.65 and 2.725 m baffle height. This is because the thermal performance objective consists of the summation of $\frac{\Delta T_{booms,avg}}{\Delta T_{rods,avg}} + T_{boom,max} - T_{boom,min} + T_{rod,max} - T_{rod,min}$. The last two terms of this objective are higher than for a height of 2.65 and 2.725 m. This leads to a too high rotation in the booms, the rods and its athermalized result: 19.4 µrad, 169.9 µrad and 150.5 µrad respectively. This is however lower than the 511.5 µrad athermalized rotation of the 2.5 m baffle, but still much higher than the 69.5 µrad rotation and 125.8 µrad rotation for the 2.65 m and 2.725 m baffle heights. Also, a 2.9 m baffle height results in too high nominal temperatures as was already discussed. The M2 already exeeds the requirement that its temperature shall be between -20 to +50 °C, since its minimum temperature is 50.3 °C. Thus, a baffle height of 2.9 m is too high, also from a structural integrity and mass point of view.

It is thus concluded that the lowest and tallest height are not good candidates, but the 2.65 and 2.725 m are. The difference between a 2.65 m and 2.725 m baffle height is:

1. Baffle height of 2.65 m has lower thermo-elastic athermalized rotation: 69.5 µrad instead of 125.8 µrad for the 2.725 m baffle height.
2. Baffle height of 2.725 m has lower athermalized translation: 18.5 µm instead of 19.8 µm for the 2.65 m baffle height.
3. Baffle height of 2.65 m yields a lower mass than 2.725 m of $\rho A \Delta L$ and also lower volume.
4. Baffle height of 2.65 m yields better structural integrity, since eigenfrequency $\sqrt{\frac{k_{eq}}{M_{eq}}}$ will increase as the mass decreases and also the stiffness increases at the same time.
5. For baffle height of 2.65 m less deployment force is needed

For these reasons, a baffle height of 2.65 m is chosen. This is different than the 3.06 m that E. Korhonen has designed, but is an improvement for the same structural-, mass- and volume reasons as enumarated above. The full thermo-elastic results + nominal temperatures for this height are summarized in Table 6.7. This holds for a cylindrically shaped baffle with outer coating of aluminized Kapton outer coating and 3 number of MLI layers, as the outer coating and number of MLI layers is not optimized yet.

Table 6.7: Cylindrical Baffle - Height of 2.65 m

Nominal Temperatures.				
Sub-System	**Max Temperature (° C)**	**Min Temperature (° C)**	**Requirement**	**Reference**
M2	26.5	25.9	$-20°C < T < 50°C$	BAF-T-01-03
Spider	21.5	12.7	$-20°C < T < 50°C$	BAF-T-01-03
PMSS	48.0	36.0	$-20°C < T < 50°C$	BAF-T-01-03
M1	40.3	40.2	$-20°C < T < 50°C$	BAF-T-01-03
Top Hinge	26.3	9.0	$-20°C < T < 50°C$	BAF-T-01-03
Booms	36.0	18.0	$-20°C < T < 50°C$	BAF-T-01-03
Temperature Gradients				
Thermal Objective Terms	**Value**	**Requirement**	**Unit**	**Reference**
$\Delta T_{booms,avg}$	18.2	≤ 1.4	° C	Table 4.4
$\Delta T_{rods,avg}$	2.8	≤ 0.96	° C	Table 4.4
1. $\frac{\Delta T_{booms,avg}}{\Delta T_{rods,avg}}$	6.5	Between 1.0 - 2.0 . Perfect athermal = 1.483	-	Table 4.4
2. $T_{boom,max} - T_{boom,min}$	5.2	≤ 2.3	° C	Table 4.4
3. $T_{rod,max} - T_{rod,min}$	4.3	≤ 0.3	° C	Table 4.4
Thermal Design Objective (1+2+3)	16.1	-	° C	-

6.4.2. Trade-off Radius

The radius of the cylinder must be minimized to avoid heat flow from different angles to enter the interior of the baffle. The larger the radius, the more heat can slip in. The constraint to the minimal radius is the allowed clearance between the DST sub-systems (mainly M1) and the baffle. The requirement is that there is a minimum clearance of 200 mm between M1 and any point of the baffle in deployed configuration - BAF-MEC-04-04-02-01. Given that the arc length of M1 is 750 mm, this leads to a minimum radius of 950 mm, which leads to 1000 mm radius when taking an extra margin of safety into account. Therefore, no trade-off is made, as the minimal usable radius yields the best solution.

6.5. Thermal Performance MLI (Effective Emissivity/Conductivity)

The thermal performance of MLI is discussed in this section. First of all, the method of modelling MLI is explained and consequently the results are shown.

Note that an in-depth trade-off between number of layers is **not** made in this section, since it depends on many mechanical parameters like mass, strucutral integrity, stowed volume (due to packing efficiency) and reliability of deployment and debris mitigation. These factors depend on the mechanical design of the deployment mechanism, which is not yet defined. The mechanical design is part of Chapter 7 and therefore a proper trade-off is made in the mechanical-thermal design integration chapter, Chapter 8. In this chapter only the thermal performance of MLI is discussed.

6.5.1. MLI Modelling

This section describes how MLI is modelled. The effective emissivity and conductivity as well as material bulk properties such as density, specific heat and conductivity are modelled.

Effective Emissivity and Conductivity Modelling

The effective emissivity and conductivity is modelled based on the Doenecke method, explained in Section 3.5. The reason for this choice is that this method has been experimentally validated and takes into account degrading effects (debris penetrations, contact conductance, temperature levels of layers). Furthermore, N. van de Pas, a senior thermal engineer at ADS Leiden, recommended to use experimental data. This is additionally being supported by old Fokker Space documents, in which similar methods are explained. The uncertainty of the MLI calculation, which is taken into account for the sensitivity analysis, is expected to be 25% as was found in the HIPPARCOS project. [20]

Bulk Material Properties MLI

For the bulk material properties empirical data based on literature is used, similar to how the effective emittance and conductance is calculated. The bulk density of MLI is based on MLI literature data. The bulk specific heat and bulk conductivity of MLI is based on the rule of mixtures for composites. This rule of mixtures can be used as MLI is effectively a composite, composed of Dacron and aluminized Kapton. The formulas to calculate these material properties are explained in the theory chapter, Section 3.5.1. The evaluated values are summarized in Table 6.8 below.

Table 6.8: MLI bulk property values

MLI Values		
Parameter	**Value**	**Units**
$\rho_{\text{Bulk MLI}}$	146	$\frac{kg}{m^3}$
$C_{\text{p, Bulk MLI}}$	1117.5	$\frac{J}{kgK}$
$k_{\text{p, Bulk MLI}}$	0.1275	$\frac{W}{mK}$

As mentioned in Section 3.5.1, typical values of MLI bulk density lie around 32 to 320 $\frac{kg}{m^3}$, so the calculated 146 $\frac{kg}{m^3}$ conforms to these values. [6]

6.5.2. Thermal Performance MLI

Now that it is clear how the MLI is modelled in terms of bulk material properties (bulk conductivity, specific heat and density) as well as effective emissivity and conductivity the thermal performance can be evaluated.

The effective emissivity- and conductivity for 2 to 6 number of layers of MLI is shown in Figure 6.13. Note that this holds for the cylindrical baffle with height of 2.725 m and radius of 1 m, as according to Equation 3.8 it depends on the area.

Number of layers	Effective Emissivity	Effective Conductivity
2	0.0260	0.1651
3	0.0212	0.1347
4	0.0184	0.1167
5	0.0164	0.1043
6	0.0150	0.0952

Figure 6.13: Effective emissivity and conductivity for the cylindrical baffle as a function of number of MLI layers

When plotting these effective emissivity values, an exponential relation between the effective emissivity (and thus effective conductance as well) and the number of MLI layers is visible. This is the direct consequence of using Doenecke's empirical formula for a fixed temperature layer:

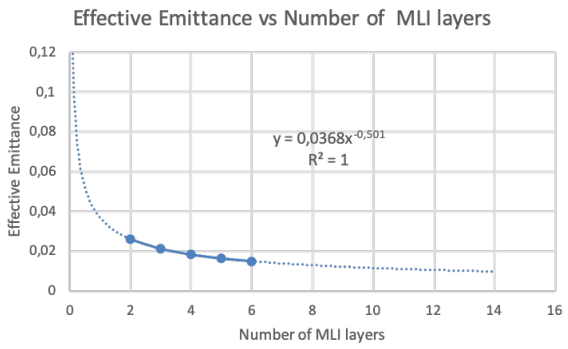

Figure 6.14: Exponential relation between the effective emissivity and number of MLI layers. This is apparent is Doenecke's empirical formula.

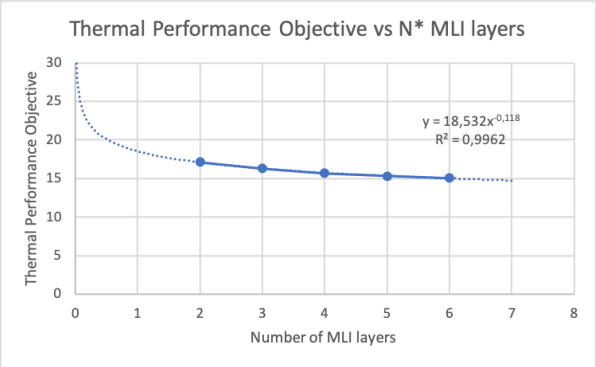

Figure 6.15: Thermal performance objective as function of number of MLI layers. Also an exponential decay is apparent, however the power of function is different (-0.118) than for Doenecke's effective emissivity relation (-0.501).

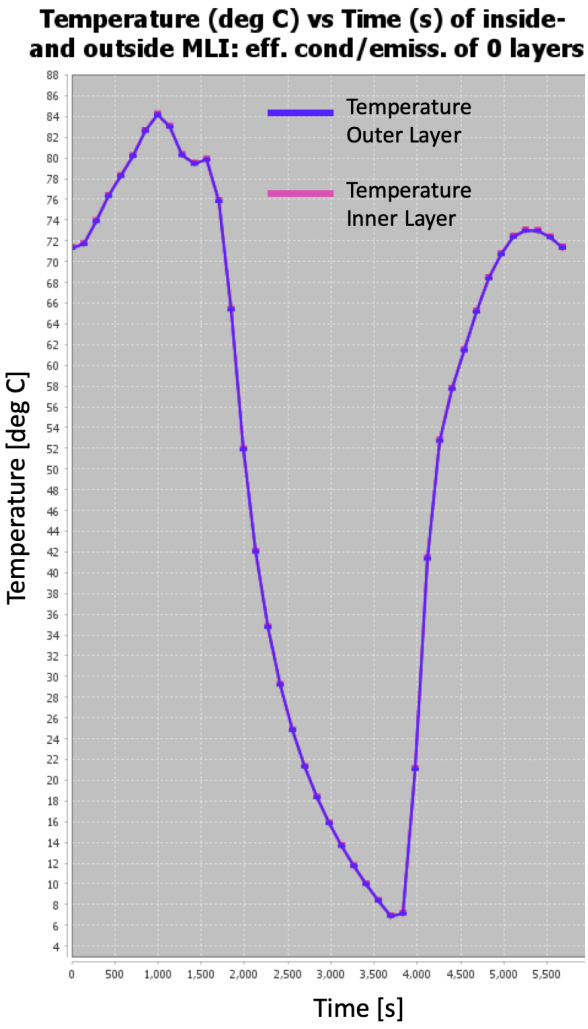

Figure 6.16: Temperature levels of inner- and outer layer of baffle for 0 layers of MLI = high effective emissivity and conductivity

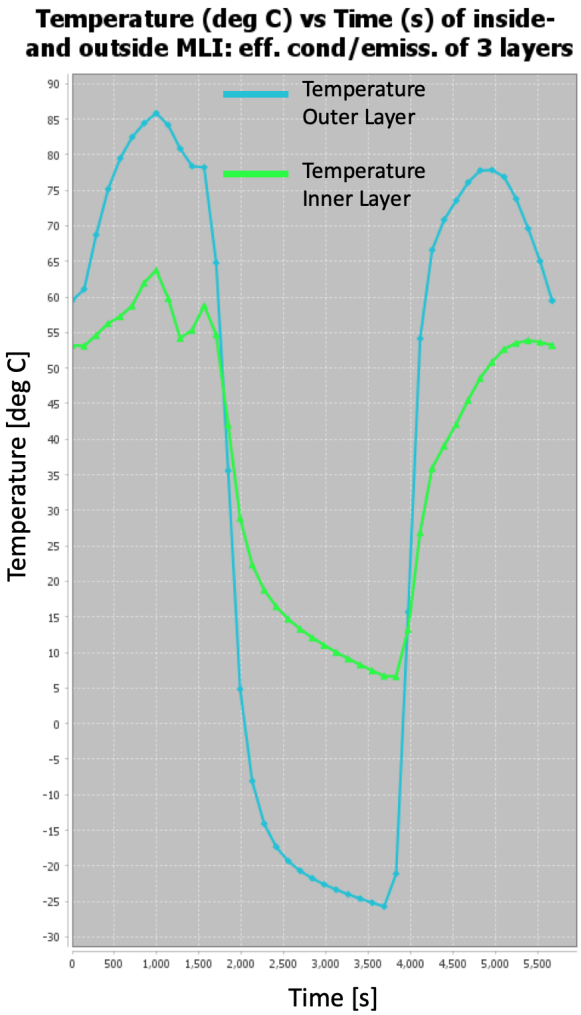

Figure 6.17: Temperature levels of inner- and outer layer of baffle for 3 layers of MLI = low effective emissivity of 0.0212 and effective conductivity of 0.1347

It can be seen that the thermal performance always increases with increasing number of MLI layers. However, there is a physical limit to the number of MLI layers that can be used due to mass (and corresponding eigenfrequency influence), stowed volume and foldability. All these other limitations are not known yet since

the mechanical design has to be designed still.

The choice on the number of layers of MLI therefore depends on a multitude of factors, such as the thermal performance, mass, structural integrity, mechanical folding reliability and debris mitigaiton reliability. As all other criteria depend on the design of the mechancial system, the trade-off for the amount of MLI layers is made in Chapter 8. Also, the amount of MLI layers is likely going to be changed after the mechanical design is mature. For now, three layers of MLI with an effective emissivity of 0.0212 and effective conductivity of 0.1347 are chosen as a baseline for further thermal analyses in this chapter and after the deployment system has been designed, the mass + structural integrity + foldability is known, meaning that the number of MLI layers can be chosen. The number of MLI layers based on proper argumentation is therefore part of the thermal-mechanical integration chapter: Chapter 8.

From Equation 3.8 it can be seen that when having zero layers ($N = 0$), the effective emissivity and consequently the effective conductivity approach infinity. This means that the outer an inner layer temperature are the same. This is shown in Figure 6.16 for a very high effective emissivity and conductivity of around 100. This can be compared to the temperature of the inner- and outer MLI layers when using 3 layers of MLI which leads to an effective emissivity and conductivity of 0.0212 and 0.1347 respectively.

The corresponding mass for MLI with a bulk density of 146 $\frac{kg}{m^3}$, 3 layers (so thickness = $6.79 \cdot 10^{-4}$ m), baffle height of 2.65 m and radius of 1 m is 1.96 kg. This mass is also used as input for the mechanical design.

6.6. Outer Coating

The various coatings that are going to be verified are chosen based on their variety of $\frac{\alpha}{\epsilon}$ values and are common for satellite use. Therefore, a complete range of usable outer coatings for the DST baffle is summarized in Table 3.6, as part of the Theory from Literature chapter, Chapter 3.

6.6.1. Outer Coating Performance

Figure 6.18 shows the thermal performance objective as a function of different $\frac{\alpha}{\epsilon}$ of all coatings that are mentioned in Table 3.6. The thermal performance objective, to summarize, is an objective that is **only** based on thermal gradients and corresponding thermo-elastic deformations, since the aim of the baffle is to create a stable thermal environment and for that the in-orbit drift budgets of 2 µm translation and 6 µrad rotation have to bet met.

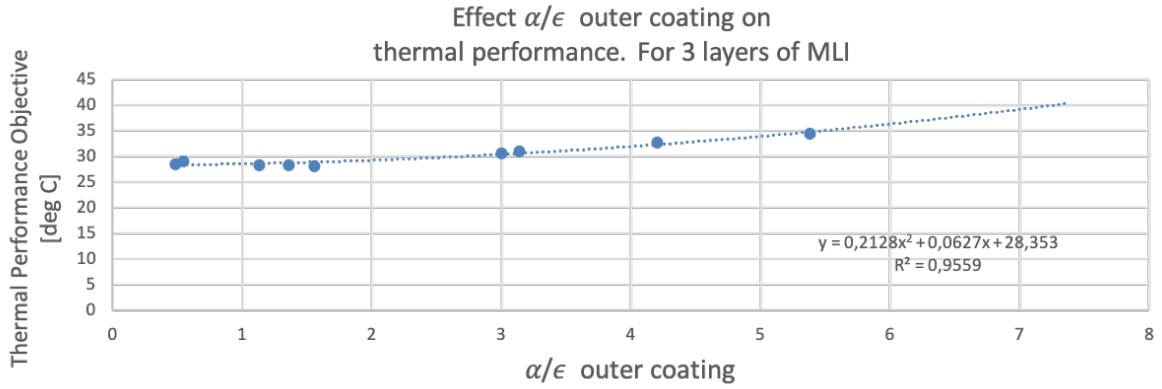

Figure 6.18: Thermal performance objective as a function of different $\frac{\alpha}{\epsilon}$ for different coatings. It can be seen that the thermal performance objective barely changes for different coatings, since different $\frac{\alpha}{\epsilon}$ values do not affect the **temperature gradients, Δ T** of the booms.

As can be seen in Figure 6.18 there is barely a difference in thermal performance objective for different $\frac{\alpha}{\epsilon}$ outer coatings. This means that the outer coating has no significant effect on the thermal gradients and corresponding thermo-elastic deformations of the booms and rods of the SMSS.

Therefore, the choice of what outer coating does not depend on the thermal gradients, but depends on the nominal temperatures of the DST sub-systems that the baffle protects as well as the baffle nominal temperatures as well. This outer coating choice is explained next.

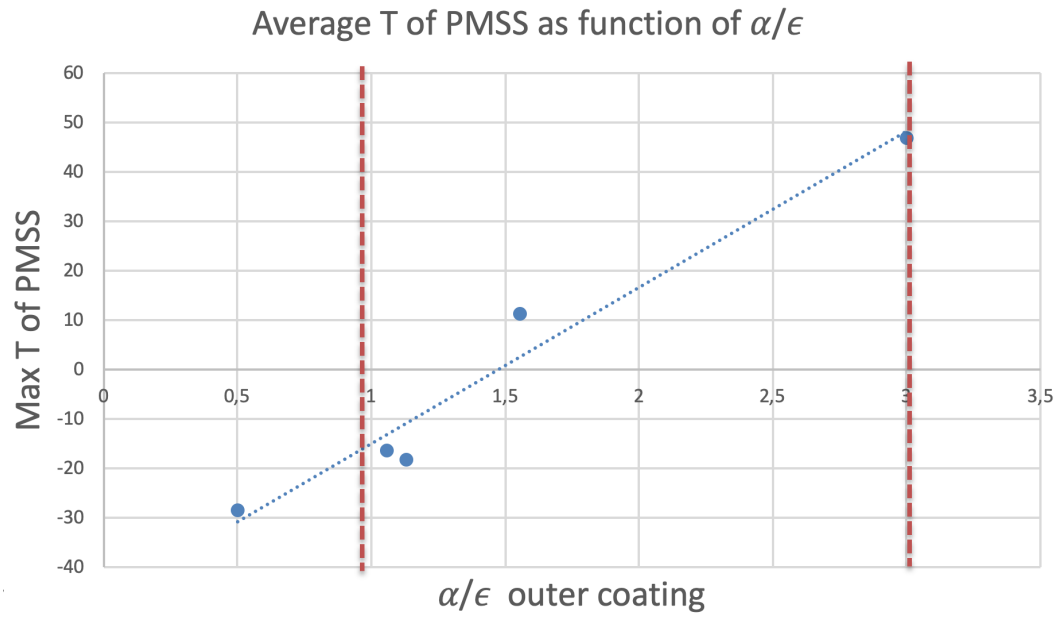

Figure 6.19: Linear relatinoship between nominal temperatures of PMSS, the most critical system in terms of nominal temperature levels, and the absorptance/emissivity ratio of the outer coating

6.6.2. Outer Coating Choice

It was found that the outer coating does not have a big influence on the thermal gradients and thus the thermal performance objective. However, the outer coating of the MLI does have a big influence on the nominal temperatures as it regulates how much bulk heat comes in. The nominal temperatures are important since they are constraint by requirement BAF-T-01-03. This requirement, as well as other requirements that the outer couting shall adhere to are summarized below:

1. The temperatures of all sub-systems within the baffle shall remain within a stability bandwidth of 253.25 - 323.25 K (-20 to +50 °) - BAF-T-01-03
2. It shall be a metallized coating of 99.99 % pure metal, vacuum-deposited onto the polymer film substrate with satisfactory adhesion [36]
3. The coating shall be available to procure and use.
4. The outer coating shall prevent outgassing (The materials to be used for the baffle shall limit outgassing to a TML of < 1 % and CVCM of < 0.01 %. - BAF-MEC-07-03)
5. The outer coating shall be resistant to AO and shall be grounded to prevent electrical-charge buildup effects - BAF-MEC-07-04 and BAF-MEC-07-04-01
6. The baffle shall survive the thermal loads both with BOL- and EOL thermo-optical properties - BAF-T-02-02

1. Nominal Temperatures

The most crucial nominal temperature is that of the PMSS, since this exceeds -20 ° C for coatings with a low $\frac{\alpha}{\epsilon}$ value. Based on Table 6.7 it can also be seen that the PMSS yields high values, higher than the other sub-systems. This is probably due to the fact that the PMSS has a direct view factor to the inner bottom of the baffle, and as the inner bottom of the baffle has only an effective emissivity/conductivity to the outer bottom (with extreme temperatures), the IR flux from the bottom is directly impinged on the PMSS, which is then directly absorbed as the PMSS uses a CFRP thermo-optical coating with both an α and ϵ of 0.88.

The nominal temperature of the PMSS is figured for coatings with different $\frac{\alpha}{\epsilon}$ coatings. As can be seen a linear relationship exists between the average temperature of the PMSS and the outer coating choice of the baffle. The red lines indicate the requirement BAF-T-01-03 boundary: -20 and +50 ° C.

As can be seen, the outer coating shall roughly be between $1 \leq \frac{\alpha}{\epsilon} \leq 3$ so that the PMSS remains in the -20 to +50 ° bandwidth. Therefore, one of the requirements is that the outer coating shall have an absorptivity $1 \leq \frac{\alpha}{\epsilon} \leq 3$.

For these reasons, aeroglaze A971 yellow paint, blue anodized titanium foil, alodyne aluminium 6061-T2, alodyne Aluminium 2024 and Aluminized Kapton will not be selected as they all have an $\frac{\alpha}{\epsilon} < 1$ or $\frac{\alpha}{\epsilon} > 3$.

Also, the properties of aluminized Kapton with aluminium on the inside highly depends on the film thickness.. An uncertainty in thickness due to machining errors or erosion, results in unexpected absorptivit and emissivity values. So aluminized Kapton with aluminium on the inside will not be chosen additinal to the fact that its $\frac{\alpha}{\epsilon} < 1$ for all thicknesses.

2. Metallized Coating

All coatings from Table 3.6 are metallized, thus adhere to requirement 2 in the enumeration list above. However, not all coatings have sufficient adhesion. Aeroglaze L300 does not have proper adhesion and should be used with Pyrolac P123 Primer to increase adhesion. Also black copper is known to decrease its adhesion due to thermal cycling: "Thermal cycling enlarges cracks and decreases adhesion of the coating according to the scratch-test measurements. Anodic films may crack because of two different phenomena: the difference in the coefficient of thermal expansion between substrate and coating and the drying of the coating." [44] Both coatings will thus not be used.

3. Availability

Aeroglaze L300, which is a black coating with good properties, is difficult to procure in Europe, making it a difficult coating to use and therefore not chosen.

4. Outgassing

Aeroglaze L-300 yields a TML of 1.7%, which is higher than the requirement that states that TML < 1.0%. This is thus not a good coating to use.

Also Aeroglaze Z306 has a CVCM of 0.02%, which also exceeds the 0.01% requirement, making it unusable for the DST baffle.

5. AO Resistance and Grounding

A few thermal finishes, such as Z307 black paint, PCBZ white paint, and black Kapton are already conductive enough so that electrical-charge buildup effects will not results in catastrophic effects.

6. BOL-EOL Properties

Surface finishes that are not affected by UV or charged particles, such as polished metals, will still suffer absorptance increases because of contamination. For such materials, degradation rates similar to those for quartz mirrors should be used if the surface has a low beginning-of-life absorptance. White paints, such as S13GLO, are affected most strongly by UV radiation and charged particles, and their absorptance may rise from around 0.20 to 0.70 in just a few years. Black paint and other high-absorptance surfaces generally do not degrade much from space-environment exposure. Any change in black paint is more likely to be a slight reduction in absorptivity of a few percentage points from UV bleaching over time. [42] This means that white paints will not be used for the DST baffle, since its EOL differs too much from its BOL value. As the stable thermal environment is crucial for the DST, white paints will not be considered. Also, coating thickness can change the solar absorptance, and in particular for white paints. [42]

The only coating that adheres to the requirements at this point is aluminized kapton with aluminium on the outside, because aluminized kapton with aluminium on the outside has:

1. Same BOL-EOL → useful for creation of a stable thermal environment for the complete lifetime duration
2. AO resistant since it is already conductive enough to prevent electrical charge buildup effects
3. A lot of flight heritage, since this is the go to material for MLI as also for coatings (JWST Sun shield uses the same outer coating)
4. It prevents outgassing
5. $\frac{\alpha}{\epsilon} = \frac{0.15}{0.05} = 3$, so meets the requirement that the temperatures of all sub-systems within the baffle shall remain within a stability bandwidth of 253.25 - 323.25 K (-20 to +50 °) - BAF-T-01-03. However, the max

nominal PMSS temperature is +47 °, meaning that when performing a sensitivity analysis it most likely exceeds the +50 requirement.

The choice for now is aluminized Kapton with aluminium on the outside due to the above mentioned reasons. However, as the PMSS temperature is +47 ° C and barely meets the -20 to +50 ° C requirement, a preliminary sensitivity analysis needs to be performed to find out if the maximum PMSS temperature exceeds this BAF-T-01-03 requirement. If so, then a new coating has to be chosen that has a different $\frac{\alpha}{\epsilon}$ ratio, but has the same characteristics.

6.7. Preliminary Sensitivity Analysis

For the preliminary sensitivity analysis we are only interested in the nominal temperatures in the worst case compared to the nominal case. Namely, if the PMSS temperature of +47 ° C will exceed the +50 ° requirement. If so, a new outer coating must be chosen.

The various parameters that are going to be varied for the sensitivity analysis are summarized in Table 6.9. The uncertainty margins for each parameter from Table 8.15 are explained below and are generally based on BOL-EOL discrepancies, machining uncertainties, modelling uncertainties and deployment accuracy uncertainties.

Effective Conductivity and Emissivity: Uncertainty Margin Rationale
The uncertainty margin of the effective emissivity of the MLI is 25 % and is stated in the "Background for Thermal Modeling of Multi Layer Insulation Blankets" document. The experimental data used in this document was applied to the HIPPARCOS project in 1985 and "from the experience gained in the HIPPARCOS project, especially the Payload part, one can expect, using this method, an uncertainty of 25% in the assessment of the MLI thermal performance." [20]

The effective conductivity scales linearly with the effective emissivity ($c_{eff} = 4\epsilon_{eff}\sigma T^3$), meaning that the uncertainty margin of the effective conductivity is also 25 %.

Uncertainties in effective emissivity/conductivity are due to conductivity uncertainties, penetrations due to debris that do not conform to the f_P value, machining errors and other disturbances that are either not taken into account in the Doenecke formula or deviate from its calculated value.

MLI Density: Uncertainty Margin Rationale
The density is quite well known and based on the equations in Table 3.4. The bulk density is a linear function of the shield thickness, density of the shield, mass of spacer and layer density. These mass and thickness values are also well known, but due to machining errors and uncertainties a total uncertainty margin of 20 % is applied.

Specific Heat: Uncertainty Margin Rationale
The specific heat uncertainty is based on [6] : 15%.

Conductivity: Uncertainty Margin Rationale
It is hard to predict the uncertainty margin for the in-plane conductivity of MLI, therefore a conservative margin of 20 % is applied.

Inner Coating Absorptivity / Emissivity: Uncertainty Margin Rationale
The inner coating of the MLI is a black coating with absorptance of 0.93 and emissivity of 0.87. For black coatings, the absorptance does not increase much over its lifetime. In fact, it even decreases the absorptance a bit due to bleaching effects [2] [3]. Additionally, it is not directly exposed to Solar radiation, but it is to Albedo, which is by definition a third of the Solar radiation strength. This is not much, but the absorptance is still dependent on surface finishes. Therefore a lower value for the absorption uncertainty margin is chosen: 5 %.

The emissivity of the magic black coating is expected to not change much either, even less than the absorptivity: "Coating materials can suffer irreversible degradation of the physical characteristics (optical, thermal, electrical and mechanical) which these materials were designed to have. The general result of these processes is an increase in solar absorptance with little or no effect on infrared emissivity." [66] However, since the emissivity is still prone to manufacturing uncertainties, a uncertainty margin of 5% is chosen as well.

Outer Coating Emissivity / Absorptivity: Uncertainty Margin Rationale
The outer coating is directly exposed to UV radiation from the sun under different angles as well as AO which can cause thermo-optical property degradation, whilst the inner coating is not (only Albedo / IR). The ratio in solar flux between Solar and reflected Albedo is around 0.306 (see Table 6.5), meaning that its uncertainty increases roughly scales with the same factor. For this reason, an uncertainty margin for both emmissivity and absorptivity of the outer coating is 15 %.

Table 6.9: Sensitivity analysis input parameters, including uncertainty margins and corresponding hot and cold worst cases

Parameter	**Uncertainty Margin**	**Worst Hot Case**	**Worst Cold Case**	**Nominal Value**	**Worst Hot Case Value**	**Worst Cold Case Value**
MLI parameters for sensitivity analysis						
Effective Conductivity [$\frac{W}{K}$]	25%	High	Low	0.1347	0.168375	0.101025
Effective Emissivity [-]	25%	High	Low	0.0212	0.0265	0.0159
Density [$\frac{kg}{m^3}$]	20%	Low	High	146	116.8	175.2
Specific Heat [$\frac{J}{kgK}$]	15%	Low	High	1117.5	949.9	1285.1
Conductivity [$\frac{W}{mK}$]	20%	Low	High	0.1275	0.102	0.153
Inner Coating α [-]	5%	High	Low	0.93	0.977	0.884
Outer Coating α [-]	15%	High	Low	0.19	0.219	0.162
Outer Coating ϵ [-]	15%	Low	High	0.14	0.119	0.161

Table 6.10: Nominal temperatures for the nominal- worst hot- and worst cold case as analyzed with a preliminary sensitivity analysis. Outer coating is aluminized Kapton.

Nominal Case.				
Sub-System	**Max Temp. (° C)**	**Min Temp. (° C)**	**Requirement**	**Reference**
M2	30.9	29.3	$-20°C < T < 50°C$	BAF-T-01-03
Spider	22.0	12.7	$-20°C < T < 50°C$	BAF-T-01-03
PMSS	47.0	35.2	$-20°C < T < 50°C$	BAF-T-01-03
M1	41.0	40.9	$-20°C < T < 50°C$	BAF-T-01-03
Top Hinge	28.0	9.0	$-20°C < T < 50°C$	BAF-T-01-03
Booms	40.0	22.0	$-20°C < T < 50°C$	BAF-T-01-03
Baffle Bottom Outside Avg	195	-32	$-250°C < T < 177°C$	BAF-T-02-01
Baffle Bottom Inside Avg	82	4	$-250°C < T < 177°C$	BAF-T-02-01
Baffle Side Outside Avg	74	-32	$-250°C < T < 177°C$	BAF-T-02-01
Baffle Side Inside Avg	57	-4	$-250°C < T < 177°C$	BAF-T-02-01
Worst Hot Case.				
Sub-System	**Max Temp. (° C)**	**Min Temp. (° C)**	**Requirement**	**Reference**
M2	37.1	35.1	$-20°C < T < 50°C$	BAF-T-01-03
Spider	27.0	16.4	$-20°C < T < 50°C$	BAF-T-01-03
PMSS	60.0	44.5	$-20°C < T < 50°C$	BAF-T-01-03
M1	50.2	50.0	$-20°C < T < 50°C$	BAF-T-01-03
Top Hinge	32.1	14.0	$-20°C < T < 50°C$	BAF-T-01-03
Booms	48.2	38.2	$-20°C < T < 50°C$	BAF-T-01-03
Baffle Bottom Outside Avg	210	-20	$-250°C < T < 177°C$	BAF-T-02-01
Baffle Bottom Inside Avg	98	10	$-250°C < T < 177°C$	BAF-T-02-01
Baffle Side Outside Avg	87	-25	$-250°C < T < 177°C$	BAF-T-02-01
Baffle Side Inside Avg	67	0	$-250°C < T < 177°C$	BAF-T-02-01

It can clearly be seen in Table 6.10 that in the worst hot case the temperature of the PMSS and M1 exceeds the maximum +50 ° C requirement. Also, the temperature of bottom of the cylindrical baffle is 195 ° C in nominal case, which exceeds the requirement imposed on the baffle itself that states that the temperature of the MLI shall be between -250 and +177 ° C, since those are the temperatures that Kapton and Dacron can

continuously be exposed to. In the hot case, this bottom temperature increases to +210 ° C, which is even worse.

Based on the preliminary sensitivity analysis, it can be concluded that the outer coating of aluminized Kapton with aluminium on the outside is not sufficient as it yields too high temperatures in the worst case for the PMSS and M1. Additionally it exceeds the continuous Kapton and Dacron exposure temperature requirement of -250 to +177 ° C, since in nominal case the bottom of the baffle is 195 ° C and in worst hot case even rises to +210 ° C .

6.8. Re-choosing Outer Coating

It is found that the alpha/emissivity ratio of aluminized Kapton should be lowered, to account for worst cases found in the preliminary sensitivity analysis. Therefore, a new coating must be chosen with a lower $\frac{\alpha}{\epsilon}$ lower than that of aluminzed Kapton (which is 3), but however has to same nice characteristics as that of aluminized Kapton with aluminium on the outside. Those are: same EOL as BOL, prevents outgassing, has flight heritage, is available, is resistant to AO and is electrically grounded and shall be a metallized coating.

With these requirements, the new chosen coating is SiOx/VDA/Kapton. It is a simple solution, since only SiOx has to be added to aluminized Kapton with aluminium on the outside as a protective layer with different thermo-optical properties. The $\frac{\alpha}{\epsilon} = \frac{0.19}{0.14} = 1.37$.

The SiOx/VDA/Kapton coating shows very good thermo-optical properties, that remain stable throughout its operational lifetime. It is resistant against AO, since it erodes uniformly, with minor differences in its thermo-optical - and radiative properties. This was tested for a SiOx/VDA/Kapton coating that was flying on a 480 km LEO orbit with an inclination of 28.5 degrees for 10 months. The lay-up of this coating is shown in Figure 6.20. [81] Also, it prevents outgassing, is easily embedded in MLI and has flight heritage as mentioned above and its thermo-optical properties as a function of wavelengths remain solid. Especially its infrared emittance, at wavelengths more than 700 nm.

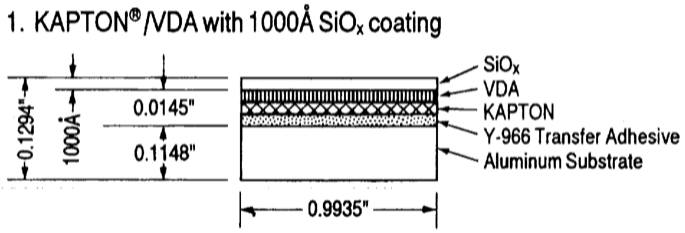

Figure 6.20: Lay-up of SiOx/VDA/Kapton coating, taken from [81]. This coating will also be used for the outer layer of the baffle.

The thermal performance of the integrated SiOx/VDA/Kapton coating is examined. For this also a preliminary sensitivity analysis is ran using the same variables as Table 6.9. Now we are interested in both the nominal temperatures as well as the gradients, in both worst hot and worst cold conditions, different than for the aluminized Kapton (aluminium outside) sensitivity analysis as there the only point of interest was if the temperatures would stay within the -20 to +50 ° bandwidth for the worst hot case.

6.8.1. Nominal Temperatures

The nominal temperatures of the DST are important to adhere to their nominal temperature requirement BAF-T-01-03 and BAF-T-02-01, even in the worst hot and cold cases.

In Table 6.11 it can be concluded that in both worst cases the temperature requirements are met. In the worst hot case, the maximum temperature of the baffle is that of the outside bottom: 148 ° C, which is well below the 177 ° C requirement. The lowest temperature, which is the case for the worst cold case, is also that of the outside of the MLI bottom: -92 ° C, which is far above the minimum temperature of -250 ° C to which aluminized Kapton can be continously exposed (BAF-T-01-03). All DST sub-systems are well within the $-20°C < T < 50°C$ range. The worst hot and cold cases are therefore not crucial for the nominal temperature levels, but are expected to influence the gradients in the booms and rods a lot, which influences the thermo-elastis of the athermalisation system. The thermo-elastics sensitivity analyis results is shown below and these are the results for the same worst hot and cold models as for the nominal temperatures from Table 8.16.

Since this is not the case for the aluminized Kapton (aluminium outside) coating, the change to a SiOx/VDA/Kapton coating is a good choice.

It is shown that the nominal temperature levels of the DST sub-systems for the SiOx/VDA/Kapton conform to requirement BAF-T-01-03 and requirement BAF-T-02-01, which is not the case for the aluminized Kapton (al. outside) coating. Additionally, the temperature gradients in the booms and rods and their difference is better than for the aluminized Kapton coating. As can be seen in Table 6.12 the nominal average temperature gradients in the booms is 14.5 ° C, which is better than the 18.2 ° C for the aluminized Kapton coating (see Table 6.7). Also, for SiOx/VDA/Kapton the average temperature gradient in the rods is 2.7 ° C instead of 2.8 ° C for aluminized kapton. The difference in temperaruture gradient of the booms ($T_{boom,max} - T_{boom,min}$) is 3.0 instead of 5.2 ° C. Only the difference in temperature gradient of the rods is a bit higher for SiOx/VDA/Kapton: 6.3 instead of 4.3 ° C.

Table 6.11: Nominal temperatures of DST sub-systems and baffle in both nominal- worst hot- and worst cold case. Outer coating is now SiOx/VDA/Kapton

Nominal Case.				
Sub-System	**Max Temp. (° C)**	**Min Temp. (° C)**	**Requirement**	**Reference**
M2	12.4	11.3	$-20°C < T < 50°C$	BAF-T-01-03
Spider	8.9	1.0	$-20°C < T < 50°C$	BAF-T-01-03
PMSS	12.6	5.0	$-20°C < T < 50°C$	BAF-T-01-03
M1	14.4	14.3	$-20°C < T < 50°C$	BAF-T-01-03
Top Hinge	15.0	-2.0	$-20°C < T < 50°C$	BAF-T-01-03
Booms	16.0	2.0	$-20°C < T < 50°C$	BAF-T-01-03
Baffle Bottom Outside Avg	130	-80	$-250°C < T < 177°C$	BAF-T-02-01
Baffle Bottom Inside Avg	44	-28	$-250°C < T < 177°C$	BAF-T-02-01
Baffle Side Outside Avg	24	-66	$-250°C < T < 177°C$	BAF-T-02-01
Baffle Side Inside Avg	32	-26	$-250°C < T < 177°C$	BAF-T-02-01
Worst Hot Case.				
Sub-System	**Max Temp. (° C)**	**Min Temp. (° C)**	**Requirement**	**Reference**
M2	16.5	15.1	$-20°C < T < 50°C$	BAF-T-01-03
Spider	12	3.2	$-20°C < T < 50°C$	BAF-T-01-03
PMSS	21.5	11.5	$-20°C < T < 50°C$	BAF-T-01-03
M1	21.1	21.0	$-20°C < T < 50°C$	BAF-T-01-03
Top Hinge	18.0	0.0	$-20°C < T < 50°C$	BAF-T-01-03
Booms	22.0	5.5	$-20°C < T < 50°C$	BAF-T-01-03
Baffle Bottom Outside Avg	148	-72	$-250°C < T < 177°C$	BAF-T-02-01
Baffle Bottom Inside Avg	56	-25	$-250°C < T < 177°C$	BAF-T-02-01
Baffle Side Outside Avg	37	-60	$-250°C < T < 177°C$	BAF-T-02-01
Baffle Side Inside Avg	40	-24	$-250°C < T < 177°C$	BAF-T-02-01
Worst Cold Case.				
Sub-System	**Max Temp. (° C)**	**Min Temp. (° C)**	**Requirement**	**Reference**
M2	9.6	8.7	$-20°C < T < 50°C$	BAF-T-01-03
Spider	7.0	-0.2	$-20°C < T < 50°C$	BAF-T-01-03
PMSS	6.0	0.1	$-20°C < T < 50°C$	BAF-T-01-03
M1	9.4	9.3	$-20°C < T < 50°C$	BAF-T-01-03
Top Hinge	12.5	-3.1	$-20°C < T < 50°C$	BAF-T-01-03
Booms	12.0	-0.5	$-20°C < T < 50°C$	BAF-T-01-03
Baffle Bottom Outside Avg	110	-92	$-250°C < T < 177°C$	BAF-T-02-01
Baffle Bottom Inside Avg	32	-28	$-250°C < T < 177°C$	BAF-T-02-01
Baffle Side Outside Avg	11	-74	$-250°C < T < 177°C$	BAF-T-02-01
Baffle Side Inside Avg	25	-25	$-250°C < T < 177°C$	BAF-T-02-01

6.8.2. Thermo-Elastics

Table 6.12: Temperature gradients for thermo-elastics. Outer coating is now SiOx/VDA/Kapton

Nominal Case				
Thermal Objective Terms	**Value**	**Requirement**	**Unit**	**Reference**
$\Delta T_{booms,avg}$	14.5	≤ 1.4	° C	Table 4.4
$\Delta T_{rods,avg}$	2.7	≤ 0.96	° C	Table 4.4
1. $\frac{\Delta T_{booms,avg}}{\Delta T_{rods,avg}}$	5.4	Between 0.96 - 2.0. Perfect athermal = 1.483	-	Table 4.4
2. $T_{boom,max} - T_{boom,min}$	3.0	≤ 2.3	° C	Table 4.4
3. $T_{rod,max} - T_{rod,min}$	6.3	≤ 0.3	° C	Table 4.4
Thermal Design Objective (1+2+3)	14.7	-	° C	-
Worst Hot Case				
Thermal Objective Terms	**Value**	**Requirement**	**Unit**	**Reference**
$\Delta T_{booms,avg}$	16.5	≤ 1.4	° C	Table 4.4
$\Delta T_{rods,avg}$	3.2	≤ 0.96	° C	Table 4.4
1. $\frac{\Delta T_{booms,avg}}{\Delta T_{rods,avg}}$	5.2	Between 1.0 - 1.9. Perfect athermal = 1.483	-	Table 4.4
2. $T_{boom,max} - T_{boom,min}$	3.5	≤ 2.3	° C	Table 4.4
3. $T_{rod,max} - T_{rod,min}$	7.3	≤ 0.3	° C	Table 4.4
Thermal Design Objective (1+2+3)	16.0	-	° C	-
Worst Cold Case				
Thermal Objective Terms	**Value**	**Requirement**	**Unit**	**Reference**
$\Delta T_{booms,avg}$	12.8	≤ 1.4	° C	Table 4.4
$\Delta T_{rods,avg}$	2.3	≤ 0.96	° C	Table 4.4
1. $\frac{\Delta T_{booms,avg}}{\Delta T_{rods,avg}}$	5.6	Between 0.9 - 2.1. Perfect athermal = 1.483	-	Table 4.4
2. $T_{boom,max} - T_{boom,min}$	2.7	≤ 2.3	° C	Table 4.4
3. $T_{rod,max} - T_{rod,min}$	5.3	≤ 0.3	° C	Table 4.4
Thermal Design Objective (1+2+3)	13.6	-	° C	-

Table 6.13: Thermo-elastic deformations for nominal case, cylindrical baffle with height of 2.65 m. Outer coating is now SiOx/VDA/Kapton

	In-Orbit Drift Budget (requirement)	**Thermo-Elastic Deformation Booms**	**Thermo-Elastic Deformation Rods**	**|Athermalized M2|**
Translation [µm]	2	20.4	5.6	14.8
Rotation [µrad]	6	7.8	119.8	112.0

The nominal temperatures of the baffle and the DST sub-systems all adhere to their nominal temperature requirements. Now, the gradients need to be lowered so that the corresponding thermo-elastic deformations (both translation and rotation) conform to the in-orbit drift budget requirements of 2 µm and 6 µrad respectively. For these a multitude of design changes are implemented which are mentioned in the next section.

6.9. Iterative Thermal Design

The baffle height, radius, MLI lay-up (number of MLI layers still needs to be traded-off but is done in Chapter 8) and outer coating are chosen, based on the thermal gradients (relating to the thermal performance objective) as well as nominal temperatures. However, the thermo-elastic deformations are still exceeding the thermo-elastic budgets of 2 µm in translation and 6 µrad in radiation. These need to be lowered.

The thermal gradients of the DST sub-systems are dependent on the transient temperature performance of the inner layer of the baffle: if the inner layer shows large gradients (meaning big difference between maximum and minimum temperature over the course of one orbit), then the inner sub-systems including booms and rods that are designed to make the SMSS athermal also show large gradients. To decrease the temperatures of the booms and rods, the heat input to these system need to be lowered ($\Delta T = \frac{\Delta Q}{m \cdot c_p}$). The ΔQ mainly comes from the radiative coupling between the inner layer of the baffle and the sub-systems, which is equal to $Q_{ij} = \epsilon \sigma T^4$. Therefore, the gradient (maximum - minimum temperature) of the inner temperature of the baffle characterizes the stability of the DST sub-systems and need to be as low as possible.

A few methods to decrease the temperature of the inner layer of MLI is to increase the mass or specific heat of MLI which shows in the analytical model, see Equation 6.16. Mass can be increased by increasing the density or by adding more MLI layers (which increases thickness and thus mass). Specific heat is a material parameter and is hard to increase, as Kapton and Dacron already have outstandingly high specific heats of around 1000 $\frac{J}{kgK}$, whereas aluminium for example has a lower specific heat of around 880 $\frac{J}{kgK}$. Since (i) the MLI specific heat is already high and (ii) the mass is constrained by the mass budget, the structural integrity and volume, these parameters will not be tweaked.

Another method is to change the thermal parameters of the sub-systems that influence the thermo-elastics. Especially that of the boom, since its current temperature gradient is 14.5 °C. If it is possible to decrease this gradient, then the ratio $\frac{\Delta T_{booms,avg}}{\Delta T_{rods,avg}}$ also decreases, which increases the ability to make the system athermal. Furthermore, the difference in temperatures of the different booms will decrease as well, so that the corresponding rotation caused by a difference in deformation of the booms decreases.

For this a multitude of design changes are implemented that are summarized below.

1. Increasing specific heat, conductivity and coating of boom, but still leave it to be a CFRP material so that mainly the thermal properties are altered

2. Discretizing the nodal model in ESATAN-TMS: the booms change from 5 nodes to 25 nodes

3. Addition of truncated cone

6.9.1. Increasing Properties- and Discretization of Booms

The increased CFRP properties of the boom are:

1. Coating CFRP altered to absorb as little heat as possible, but still adhering to the stray-light requirement: $\frac{\alpha}{\epsilon} = \frac{0.9}{0.99} = 0.91$.

2. Specific heat of CFRP from 880 to 1037 $\frac{J}{kgK}$, based on [35]

3. Conductivity of CFRP from 55 to 180 $\frac{W}{mK}$, based on [99]

See Table 6.14 for the nominal temperatures of the various DST sub-systems and the baffle itself and see Table 6.15 for the corresponding thermo-elastic deformations.

Table 6.14: Temperature data corresponding to the iterated DST baffle with improved properties for the boom. For **Temperature Gradients**: Those in red are not acceptable, since these gradients cause thermo-elastic deformations well above the requirements, see Table 6.15

Nominal Temperatures.				
Sub-System	**Max Temp. (° C)**	**Min Temp. (° C)**	**Requirement**	**Reference**
M2	9.5	8.4	$-20°C < T < 50°C$	BAF-T-01-03
Spider	7.6	4.7	$-20°C < T < 50°C$	BAF-T-01-03
PMSS	10.7	7.2	$-20°C < T < 50°C$	BAF-T-01-03
M1	13.8	13.7	$-20°C < T < 50°C$	BAF-T-01-03
Top Hinge	19.0	4.5	$-20°C < T < 50°C$	BAF-T-01-03
Booms	11.0	8.0	$-20°C < T < 50°C$	BAF-T-01-03
Baffle Bottom Outside Avg	131	-82	$-250°C < T < 177°C$	BAF-T-02-01
Baffle Bottom Inside Avg	46	-28	$-250°C < T < 177°C$	BAF-T-02-01
Baffle Side Outside Avg	25	-65	$-250°C < T < 177°C$	BAF-T-02-01
Baffle Side Inside Avg	26	-21.8	$-250°C < T < 177°C$	BAF-T-02-01
Temperature Gradients				
Thermal Objective Terms	**Value**	**Requirement**	**Unit**	**Reference**
$\Delta T_{booms,avg}$	3.0	≤ 1.4	° C	Table 4.4
$\Delta T_{rods,avg}$	2.4	≤ 0.96	° C	Table 4.4
1. $\frac{\Delta T_{booms,avg}}{\Delta T_{rods,avg}}$	1.3	Between 0.9 - 2.1. Perfect athermal = 1.483	-	Table 4.4
2. $T_{boom,max} - T_{boom,min}$	0.4	≤ 2.3	° C	Table 4.4
3. $T_{rod,max} - T_{rod,min}$	3.9	≤ 0.3	° C	Table 4.4
Thermal Design Objective (1+2+3)	5.5	-	° C	-

Table 6.15: Thermo-elastic deformations after iterative process: cylindrical baffle with height of 2.65 m, outer coating of SiOx/VDA/Kapton, discretized booms and improved thermal properties

	In-Orbit Drift Budget (requirement)	**Thermo-Elastic Deformation Booms**	**Thermo-Elastic Deformation Rods**	**|Athermalized M2|**
Translation [µm]	2	4.2	5.0	0.8
Rotation [µrad]	6	1.0	73.8	72.8

As can be seen, the baffle is made athermal in the translational direction: this means that the summation of the deformation of the booms and rods is lower than the maximum allowed deformation of 2 µm. This is the effect of the improved boom properties: higher conductivity and specific heat and lower absorption properties.

The difference in gradient of the rods is still high and these need to be lowered. This might be possible by adding a truncated cone at the top that reflects some of the critical IR and Albedo radiation from the Earth. This is discussed in the next section.

6.9.2. Addition of Truncated Cone

A truncated cone is useful for both stray-light mitigation (first baseline design) as was mentioned by [97], as well as blocking and reflecting critical IR/Albedo flux from the Earth that would otherwise be absorbed by the spider, SMSS or other syb-systems.

The truncated cone has to adhere to the requirements as mentioned in the theory section, Table 3.7. Additional requirements as were generated in Chapter 4 are also added:

Table 6.16: Summarized requirements for the stowed configuration, including verification methods used

Requirement ID	Requirement
Requirements From Literature [97] [91]	
-	The baffle shall provide an aspect angle of ≤ 35 deg
-	The reflection efficiency of the baffle in the solar spectrum between 200-2500 nm shall be > 93 %
-	The reflection efficiency of the baffle in the thermal IR range between 2.5-8 µm shall be > 98 %
Additional Requirements (Summarized From Requirements Generation Chapter 4)	
BAF-MEC-04	The baffle shall deploy succesfully.
BAF-SYS-16	The mass of the entire baffle including deployment mechanism shall not exceed 15 kg
BAF-MEC-07-06-03-1	The baffle structure shall have a minimum first eigenfrequency ≥ 0.9 Hz in deployed configuration
BAF-MEC-04-04-02	The baffle shall not obstruct any telescope elements and not interfere with the optical performance

Therefore, as a first estimate a Vapor Deposited Silver coating with absorptivity of 0.04 and emissivity of 0.02 is applied, as it adheres to the second and third requirement from the truncated cone requirement list above. A first estimate for the material is aluminium as was also suggested by T. van Wees, [102], and is based on low density, machinability, high strength and stiffness and low outgassing performance. A first estimate for the aspect angle is chosen to be 1.5 degrees. The thickness is only 1 mm, resulting in a truncated cone mass of 1.61 kg.

The design of the truncated cone is not optimized in this part, as it is highly dependent on the mechanical deployment system and its mass, deployment shape and volume. The optimization is part of the thermal-mechanical integration in Chapter 8.

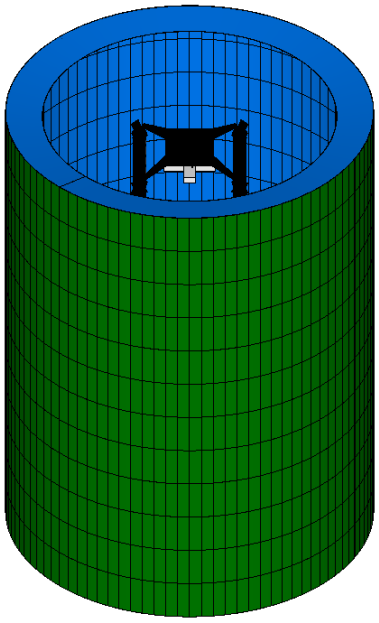

Figure 6.21: Iterated baffle with addition of a truncated cone near M2, side view

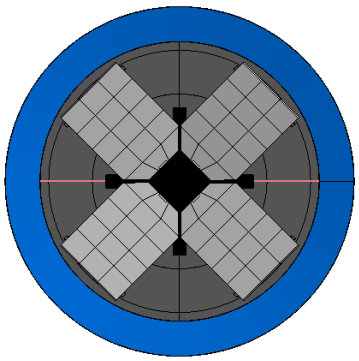

Figure 6.22: Iterated baffle with addition of a truncated cone near M2, top view

It can be seen that even for a low aspect angle truncated cone of 1.5 degrees, there is a slight decrease in rotation of the rods. It decreases the athermalized rotation of M2 from 72.8 µrad to 64.4 µrad. Additionally, it slightly decreases the athermalized translation from 0.8 µm to 0.5 µm. Obviously, the perfect angle needs to be chosen and this needs to be optimized, but all this depends on how the baffle will deploy and what is allowed in terms of mass, volume, structural integrity and ofcourse deployability ability, so this will be done in Chapter 8.

Table 6.17: Thermo-elastic deformations after iterative process: cylindrical baffle with height of 2.65 m, outer coating of SiOx/VDA/Kapton, discretized booms, improved thermal properties AND addition of truncated cone.

	In-Orbit Drift Budget (requirement)	**Thermo-Elastic Deformation Booms**	**Thermo-Elastic Deformation Rods**	**|Athermalized M2|**
Without Truncated Cone				
Translation [µm]	2	4.2	5.0	0.8 µm
Rotation [µrad]	6	1.0	73.8	72.8
With Truncated Cone				
Translation [µm]	2	4.4	4.9	0.5
Rotation [µrad]	6	0.7	66.2	65.4

6.10. Summary Thermal Design and Performance

In this section the thermal performance will be summarized as well as its mass budget and impact on the mechanical design.

6.10.1. Thermal Performance

The complete thermal performance of the DST baffle with the above mentioned attributes is summarized below in Table 6.18. Note that the gradients in Table 6.18 and the complete Table 6.19 are the same as Table 6.17. The only addition are the nominal temperatures of the various DST sub-systems, as well as the nominal temperature of the truncated cone and baffle itself.

Table 6.18: Temperature data corresponding to the iterated DST baffle with improved properties for the boom. For **Temperature Gradients**: Those in red are not acceptable, since these gradients cause thermo-elastic deformations well above the requirements, see Table 6.19

Nominal Temperatures.				
Sub-System	**Max Temp. (° C)**	**Min Temp. (° C)**	**Requirement**	**Reference**
M2	7.9	6.7	$-20°C < T < 50°C$	BAF-T-01-03
Spider	6.9	4.1	$-20°C < T < 50°C$	BAF-T-01-03
PMSS	10.6	7.1	$-20°C < T < 50°C$	BAF-T-01-03
M1	14.1	14.1	$-20°C < T < 50°C$	BAF-T-01-03
Top Hinge	18.3	4.4	$-20°C < T < 50°C$	BAF-T-01-03
Booms	11.4	8.4	$-20°C < T < 50°C$	BAF-T-01-03
Truncated Cone	27.2	27.1	$-20°C < T < 50°C$	BAF-T-01-03
Baffle Bottom Outside Avg	131	-82	$-250°C < T < 177°C$	BAF-T-02-01
Baffle Bottom Inside Avg	46	-28	$-250°C < T < 177°C$	BAF-T-02-01
Baffle Side Outside Avg	25	-64	$-250°C < T < 177°C$	BAF-T-02-01
Baffle Side Inside Avg	26.7	-20	$-250°C < T < 177°C$	BAF-T-02-01
Temperature Gradients				
Thermal Objective Terms	**Value**	**Requirement**	**Unit**	**Reference**
$\Delta T_{booms,avg}$	3.1	≤ 1.4	° C	Table 4.4
$\Delta T_{rods,avg}$	2.3	≤ 0.96	° C	Table 4.4
1. $\frac{\Delta T_{booms,avg}}{\Delta T_{rods,avg}}$	1.3	Between 0.9 - 2.1. Perfect athermal = 1.483	-	Table 4.4
2. $T_{boom,max} - T_{boom,min}$	0.3	≤ 2.3	° C	Table 4.4
3. $T_{rod,max} - T_{rod,min}$	3.4	≤ 0.3	° C	Table 4.4
Thermal Design Objective (1+2+3)	5.1	-	° C	-

Table 6.19: Thermo-elastic deformations after iterative process: cylindrical baffle with height of 2.65 m, outer coating of SiOx/VDA/Kapton, discretized booms and improved thermal properties and addition of truncated cone.

	In-Orbit Drift Budget (requirement)	**Thermo-Elastic Deformation Booms**	**Thermo-Elastic Deformation Rods**	**|Athermalized M2|**
Final Thermal Design				
Translation [µm]	2	4.4	4.9	0.5
Rotation [µrad]	6	0.7	66.2	65.4
Baseline 1. Without Baffle				
Translation [µm]	2	32.4	42.1	9.7
Rotation [µrad]	6	8.3	928.3	920.1
Baseline 2. E. Korhonen design				
Translation [µm]	2	5.4	2.2	3.2
Rotation [µrad]	6	35.9	44.9	9.1

General Conclusions for Thermal Performance

As can be seen, all the nominal temperatures of all sub-systems adhere to the -20 to +50 ° C requirement of BAF-T-01-03. Additionally, the temperatures of the baffle adhere to requirement BAF-T-02-01.

The temperature gradients of the individual booms and rods do not adhere to their requirement of a max ΔT of 1.4 and 0.96 ° C. However, the athermalized result (translation) does comply to the requirement since the $\frac{\Delta T_{booms,avg}}{\Delta T_{rods,avg}}$ = 1.3 and lies between the 0.9 and 2.1 requirement ratio. The corresponding athermalized translation is then 0.5 µm. Furthermore, the gradient difference in booms also conforms to the requirement: 0.3 ≤ ° C, resulting in a rotation that is below 6 µrad for the booms only. Unfortunately, the gradient difference of the rods exceeds its requirement, since 3.4 > 0.3 ° C. The resulting rotation of the rods is 66.2 µrad, which exceeds the requirement of 6 µrad by a great margin. The athermalized rotation is still too high: 66.2 µrad - 0.7 µrad is 65.4 µrad in best case scenario.

The thermal gradients of the DST sub-systems are dependent on the transient temperature performance of the inner layer of the baffle: if the inner layer shows large gradients (meaning big difference between maximum and minimum temperature over the course of one orbit), then the inner sub-systems including booms and rods that are designed to make the SMSS athermal also show large gradients. To decrease the temperatures of the booms and rods, the heat input to these system need to be lowered ($\Delta T = \frac{\Delta Q}{m \cdot c_p}$). The ΔQ mainly comes from the radiative coupling between the inner layer of the baffle and the sub-systems, which is equal to $Q_{ij} = \epsilon \sigma T^4$. Therefore, the gradient (maximum - minimum temperature) of the inner temperature of the baffle characterizes the stability of the DST sub-systems and need to be as low as possible. This could be improved and iterated, but first it is chosen to work out the mechanical deployment system, as this is likely changing the thermal performance. After the mechanical deployment system has been designed, a thermal-mechanical integration is made and the design will be iterated.

6.10.2. Mass Budget

Table 6.20: Mass budget after preliminary thermal design has been established

Mass Calculation	
Sub-System	**Mass (kg)**
MLI	1.96
Truncated Cone M2	1.61
Baffle Structure	TBD
Deployment Actuation System	TBD
Total Mass	3.57
Safety Margin	25%
Total Mass Including Safety Margin	4.46
Mass Thermal System $M_{thermal}$	4.46
Mass Mechanical System $M_{mechanical}$	TBD
Mass Requirement	15

As can be seen in Table 6.20, the total mass including safety margin of 25 % is 4.46 kg. This includes only the thermal system mass $M_{thermal}$ (MLI shield + truncated cone mass for stray-light purposes), since the mechanical design still has to be designed. The $M_{thermal}$ is, next to the deployed configuration, input for the mechanical design and its influence is discussed in the next section, Section 6.10.3.

6.10.3. Effect of Thermal Design Choices on Mechanical Design

The effect of thermal design choices on mechanical design is roughly displayed in the N2 diagram in Figure 4.3. To sum up:

1. Deployed thermal configuration → Requirements for deployment system from stowed to deployed configuration
2. Mass of thermal sub-systems (MLI + truncated cone) → Structural integrity (eigenfrequency)- and mass budget of 10.54 kg for baffle structure and deployment actuation system

The deployed thermal configuration in operational state is crucial to determine how the baffle should deploy to this configuration and the mass of the MLI shield + truncated cone near M2 influence the eigenfrequency of the system and sets a limit to the mass budget of the baffle structure and deployment actuation system that will be designed in Chapter 7. The mass budget limit for $M_{mechanical}$ is now equal to $15-4.46 = 10.54$ kg. The above mentioned thermal influence on mechanical design is schematized in Figure 6.23.

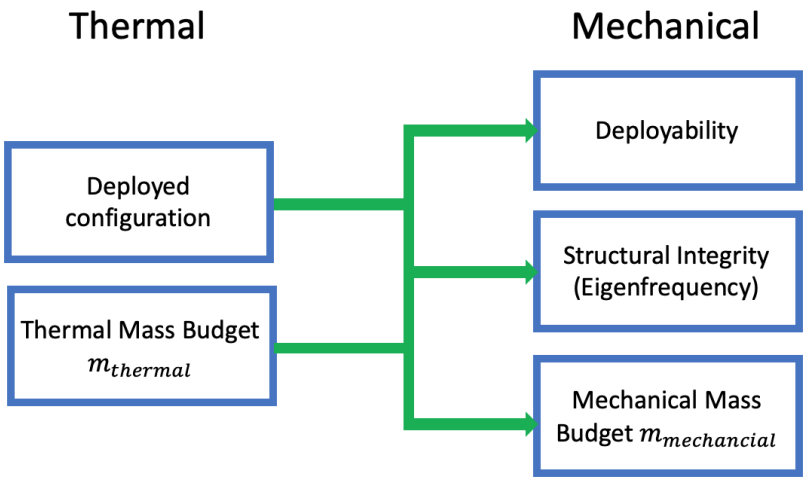

Figure 6.23: Influence of the thermal design on the mechanical design. These thermal design choices are input to start the mechanical design process, Chapter 7

7

Mechanical System Design and Performance

This chapter focuses on the mechanical deployment design.

7.1. Mechanical Design Flow Chart

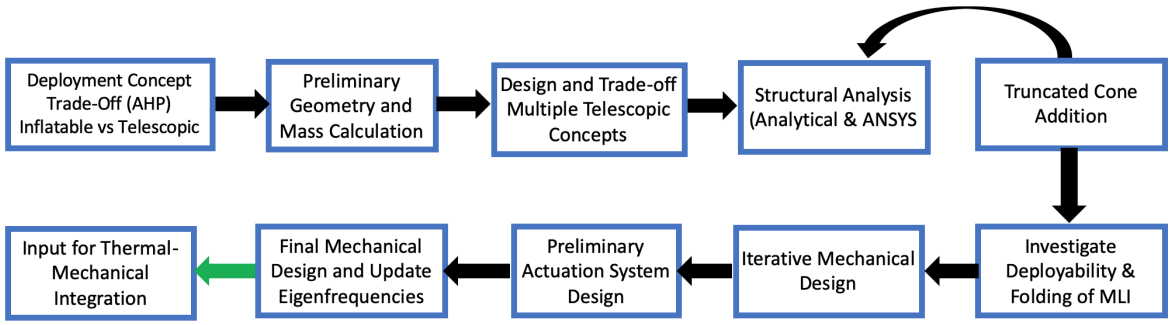

Figure 7.1: Flow chart of mechanical design

7.1.1. Requirements: Input For Mechanical Design

The requirements and constraints for the mechanical deployment system are summarized here that hold for a proper mechanical design of the baffle.

The geometry in operational phase of the baffle is known based on thermal requirements that were found in the Thermal System Design and Performance chapter, Chapter 6. Additionally, these requirements are supplemented with other requirements and constraints for the mechanical deployment system that were already generated in the requirements generation chapter, Chapter 4. These mechanical requirements are summarized in Table 7.1.

Table 7.1: Summarized requirements for the stowed configuration, including verification methods used

Requirement ID	Requirement
Requirements From Thermal Design, Chapter 6	
-	The baffle in operational state shall have a cylindrical shape with a height of 2.65 m and radius of 1 m
-	Preliminary thermal mass $M_{thermal}$ of 4.46 kg shall be taken into account for the mechanical deployment design
Additional Mechanical Requirements (Summarized From Requirements Generation Chapter 4)	
BAF-SYS-11	The volume of the baffle shall not exceed 1.5 m^3 (threshold) / 0.75 m^3 (goal) when in stowed configuration
BAF-SYS-16	The mass of the entire baffle including deployment mechanism shall not exceed 15 kg
BAF-MEC-07-06-03-1	The baffle structure shall have a minimum first eigenfrequency ≥ 0.9 Hz in deployed configuration
BAF-MEC-03-01/02/03	The baffle shall survive a quasi-static load of 30g applied simultaneously to the x-y/x-z/y-z axes in the launcher coordinate frame in the stowed configuration during launch
BAF-MEC-03-04	The baffle shall have a minimum first eigenfrequency of 100 Hz in stowed configuration
BAF-MEC-04	The baffle shall deploy succesfully
BAF-MEC-04-04-02	The baffle shall not obstruct any telescope elements and not interfere with the optical performance
BAF-MEC-04-05-01	The baffle shall deploy before the primary- and secondary mirror
BAF-SYS-17	The baffle shall be given sufficient structural support by other sub-systems.
BAF-SYS-02-03	All single point of failures should be eliminated by redundant components
BAF-SYS-03	Active elements of mechanism, such as actuators, shall be redundant

7.2. Trade-Off Inflatable vs Telescopic Systems Using the AHP Method

The reason for changing the inflation deployment system as designed by E. Korhonen is that the stowed volume goal budget of $0.75m^3$ is not met, nor the stowed volume treshold budget of $1.5m^3$. See requirement BAF-SYS-11. Furthermore, the inflation concept was observed to be too complex, and it lacks structural integrity in stowed baffle configuration. Therefore a new deployment system trade-off is made in this section.

E. Korhonen already made a concept trade-off using the Analytical Hierarchy Process (AHP) in her thesis regarding what deployment system yields the optimal performance, based on several criteria. The goal is to find the best deployment system with the optimal performance. The alternatives are the inflation concept that E. Korhonen designed and the telescopic deployment system that is going to be examined.

The criteria E. Korhonen used in her trade-off were mass, stowed volume, deployment complexity, deployed stiffness and heritage. However, there are two major parts that have room for improvement and therefore need to be updated. Namely, three other criteria that are linked to the requirements have to be added and the weighting of the criteria should be changed. First off, the three criteria that need to be added are stowed stiffness, deployment control and flexibility. These are explained below.

Stowed stiffness is important, since the stiffness of the deployment mechanism of the baffle in stowed state relates to the natural frequency (eigenfrequency) of the stowed baffle. The natural frequency of the stowed baffle needs to exceed 100 Hz, as can be seen in the functional requirement table, Table C.1. This requirement is crucial to survive LEOP and has been discussed with ADS and the project team to account for worst-case loading, including thermal loads and additional safety factors in a conservative manner.

Deployment control needs to be added to the criteria list as well, since it relates to the accuracy of the final deployed configuration. If the control of deployment is high, the designed configuration is achieved more accurately, which benefits the thermal control system, since, as could be seen in the previous chapter, a change in deployed height results in a change in view factors and consequently a change in radiation exchange and alteration of the thermal performance objective.

Flexibility, the third criterion that needs to be added, is important, since the baffle shall incorporate flexibility to accommodate modifications of requirements, as well as design trimming capabilities: requirement BAF-SYS-09/10. This includes the later addition of stray-light cones (additional to the truncated cone). Also, if the truncated cone configuration needs to be changed based on stray-light analyses, this should be made possible by already incorporating flexibility in the design so that future changes like this can be made.

Advantages	Disadvantages	Mitigation / Solution
High stiffness, both deployed and stowed	High mass	Constraint requirement, < 15 kg
Flexible: ability to use any coating or additional materials	Low storage efficiency	Constraint requirement, < 0.75 m^3
Deployment can be strain energy based (no external power input)	Constant diameter	Telescopic deployment in both radial and axial directions
Controlled deployment with high accuracy to reach final configuration	No thermal shielding heritage found, which questions the feasibility	Used for solar sails, solar arrays and instrument booms. Used on JWST Sunshield
Simple		
Able to shield telescope in stowed configuration as well		
Good customizability of thermal properties		
Good stray light mitigation ability, due to controlled, solid shape and ease of adding vanes		

Table 7.2: Advantages, disadvantages and mitigation/solution strategies of the telescopic deployment system. Partially found by E. Korhonen and taken from her thesis, [58]

The second part that has room for improvement are the weight factors E. Korhonen used. These weight factors are based on pair-wise comparison between the criteria. For five criteria, like the amount E. Korhonen used, there are $\frac{5!}{2!\cdot(5-2)!} = 10$ pair-wise combinations that all have to be evaluated relatively. When including the three factors mentioned to get a total of eight criteria, the number of combinations go up to 28, which also increases the amount of scoring weight factors to 28.

The reason the telescopic deployment mechanism is chosen as the second concept to perform the trade-off study on is that E. Korhonen investigated the use of a telescopic boom structure and found many advantages and relatively few disadvantages of the system. These are summarized in Table 7.2 below. From the disadvantages, the constant diameter is one that can be disregarded, because it is possible to design a telescopic boom system that can both expand in radial (diameter) direction and in axial direction. This makes it a 2-DOF deployment.

Low storage efficiency and high mass might be a disadvantage, but as long as the mass and volume both agree with the set requirements (mass of less than 15 kg for the entire baffle and stowed volume of $0.75m^3$ (goal)), these disadvantages can be disregarded too.

It is true that a telescopic deployment system has not been used for a thermal deployable shield, but a lot of research on deployable, telescopic booms have been performed for solar arrays, solar sails, drag sails and instrument booms. [10] Also, Northrop Grumman is working on the design of several telescopic mechanism, like the Telescopic Tubular Mast, which will be used to deploy the Large Sunshield of the James Webb Space Telescope (JWST). [73] This all improves the feasibility tremendously.

7.2.1. Performing the trade-off using the AHP method

The goal of this trade-off is to find the best deployment system with the most optimal performance based on a trade-off of different criteria. The alternatives are the inflatable deployment system and the telescopic deployment system. The criteria with corresponding weights, step 1 as seen above, follow from all 28 pair-wise comparisons between all criteria and are seen in Table 7.3. There are two weight factors, 1 and 2, since the pair-wise comparison between the criteria is changed for the second weight factor to see the sensitivity to the result when swapping the importance of the stowed stiffness and the deployment complexity. The consistency of the weights vector based on the pair-wise comparisons is characterized by the consistency ratio. As a rule of thumb, the consistency ratio should be lower than 10%. [107]. For the first set of weight factors, the consistency ratio $CR = 9.0\%$, thus yielding a consistent trade-off.

The relative importance of each criterion is summarized in in Table 7.3 in order of most important (1) to least important (8). Additionally, the final scoring weight factors are explained in Table 7.4 in which the best performing concept is summarized. The scoring weight factors are also explained below.

The scoring weight factors off all alternatives for each criterion are displayed in Table 7.4. The total scores are calculated by multiplying the vector of scoring weight factors by the criteria weight vector. As can be seen, the telescopic deployment system is objectively better performing that the inflation deployment system. Therefore, this telescopic boom system is chosen to be worked out in detail.

Note that the full, detailed description of criteria and weight factors for both inflatable and telescopic concepts is given in Chapter D, Section I.

Criteria	Criteria Weights 1	Importance 1	Criteria Weights 2	Importance 2
Mass	0.214	2	0.079	6
Deployment Complexity	0.135	3	0.092	5
Stowed Volume	0.291	1	0.277	1
Feasibility based on heritage	0.027	8	0.05	7
Stiffness Deployed	0.109	4	0.176	3
Stiffness Stowed	0.08	6	0.184	2
Deployment Control	0.103	5	0.109	4
Flexibility	0.041	7	0.032	8
Total	1		1	

Table 7.3: Criteria weight factors as part of the Analytical Hierarchy Process (AHP)

Table 7.4: Scoring weight factors of all alternatives for each critertion as part of the Analytical Hierarchy Process (AHP).

Criteria	Inflation	Telescopic	Summarized Argumentation (Detailed Argumentation in Appendix: Chapter D Section I
Mass	0.362	0.638	Inflatable: 23.6 kg thus >15 kg. Telescopic: ≤ 15 kg. Weight factors determined by the ratio.
Deployment Complexity	0.334	0.666	Inflatable: 4 CGG's, filter, valve, pressure sensors. Telescopic: STEM booms (flight heritage) + redundancy (only 2DOF)
Stowed Volume	0.334	0.666	Inflatable: 1.8 m^3. Telescopic: 0.94 m^3 (first estimate)
Heritage	0.5	0.5	Inflatable: Inflatable Antenna Project (Proven in 1996), Echo II Telescopic: JWST Sun Shield / Northrop Grummann booms
Deployed Stiffness	0.167	0.833	Inflatable: ≈ 0.9 Hz. Telescopic: ≈ 4.5 Hz (5 times higher)
Stowed Stiffness	0.1	0.9	Inflatable: ≈ 0 Hz (not rigid) Telescopic: ≥ 100 Hz.
Deployment Control	0.5	0.5	Roughly equal complications: Inflatable: inflation velocity discrepancy, rigidization, pressurization, pre-tension. Telescopic: jamming (friction), uncertainty STEM booms
Flexibility	0.2	0.8	Inflatable: future addition (stray-light) hardware needs to be inflatable. Telescopic: rigid in both stowed-deployed state (facilitates addition of hardware)
Total Score 1	**0.33**	**0.67**	
Total Score 2	**0.30**	**0.70**	

7.3. Preliminary Geometry and Mass Calculation

In this section the preliminary mass and required geometry of the telescopic deployment system are calculated, which are input for the generation of several telescopic concepts in the next section.

7.3.1. Telescopic Boom Deployment Ratio

Based on the requirements on stowed configuration and deployed configuration, a first estimate in deployment ratio is established. See Table 7.5.

Required Deployment Ratio for Telescopic Boom Deployment System	
Requirements	
Maximum stowed volume	0.75 m^3 (goal) / 1.5 m^3 (treshold)
Total mass	15 kg
Deployed radius	1 m
Deployed height	2.65 m
Stowed Parameters Corresponding to Requirements	
Maximum stowed radius	0.5 m
Maximum stowed height	0.955 m
Deployment ratio in axial direction	2.775
Deployment ratio in radial direction	2

Table 7.5: Required deployment ratio from stowed to deployed configuration of baffle in order to meet both the deployed configuration requirement (cylindrical shape of 2.65 m height and 1 m radius) and stowed configuration requirement (max stowed volume of 0.75 m^3 (goal))

The stowed parameters corresponding to the deployment requirements are simply calculated for a cylindrical shape with radius R in m and height H in m: $V_{stowed,goal} = \pi \cdot R^2 \cdot H$

When the maximum stowed goal volume of 0.75 m^3 is taken and a stowed radius of 0.5 m is assumed (since this would result in a radial deployment ratio of 2), a stowed height of 0.955 m would be required. A stowed height of 0.955 m gives an axial deployment ratio of $\frac{2.65}{0.955} = 2.775$. For telescopic tubes a deployment ratio of whole numbers is required (since every telescopic element with length L fits inside another telescopic element with length L yielding a deployment ratio of $L \cdot N_{elements}$), therefore the axial deployment ratio is changed from 2.775 to 3, meaning that precisely 3 telescopic tubes are needed to deploy in axial direction.

This results in a stowed height of not 0.955 m, but of $\frac{2.65}{3} = 0.884$ m.

Deployment	Total Deployed length (m)	Deployment ratio	Length per boom (m)
Axial direction	2.65	3	0.884
Radial direction	1	2	0.5

Table 7.6: Conclusion of deployment ratio and length per boom for a cylindrical baffle to conform to the stowed goal volume requirement of 0.75 m^3

7.3.2. Preliminary Geometry Calculation of Telescopic Structure

With the realisation that a telescopic boom system can only deploy in radial and axial direction when the cylindrical shape is triangulated into a polygonal shape, a preliminary geometry calculation of the baffle structure used as input for the design has to be established. Furthermore, the radial deployment is bounded by the interfacehouse, since the baffle shall be given sufficient structural support, likely from the interface housing. This is stated in requirement BAF-SYS-17. Therefore, the length of the *radial* booms change. The lengths that the radial structure need to have in both stowed and deployed configuration are schematized in Figure 7.2 and 7.3, to match the deployment ratio of 2 as stated in Table 7.6 of the previous section. An octagonal system is used to polygonize the cylindrical shape (with 8 booms) that was concluded to be the best shape from a thermal perspective. An octagonal shape has been used for the inflatable concept as desigend by E. Korhonen as well. [58] This facilitates future thermal performance comparison.

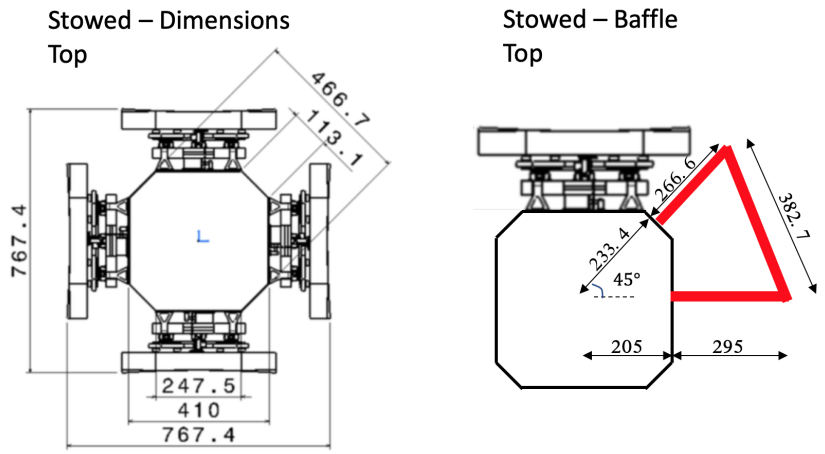

Figure 7.2: Maximum octagonal length of booms in stowed configuration to conform to the total **stowed** radial length of 500 mm (205+295 = 233.4+266.6 = 500 mm). All values are in mm.

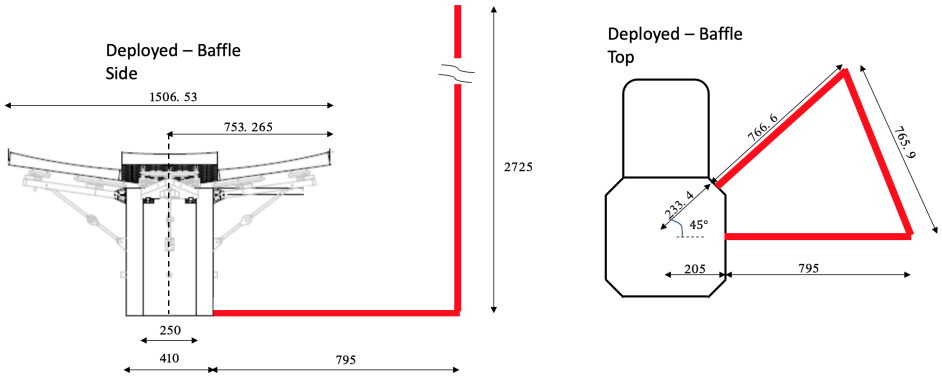

Figure 7.3: Required octagonal length of booms in deployed configuration to conform to the total **deployed** radial length of 1000 mm (205+795 = 233.4+766.6 = 1000 mm). All values are in mm.

As can be seen, since the booms need to be attached to the instrument housing, the **maximum stowed** boom length in radial direction is 295 mm (boom parallel to mirror) / 266.6 mm (diagonal boom between 2 mirrors) to conform to the **maximum** stowed length of 500 mm.

The **required deployed** boom length in radial direction is 795 mm (boom parallel to mirror) / 766.6 mm (diagonal boom between 2 mirrors) to reach a total radius of 1 m.

However, the deployment ratio is not the same as it was before when the instrument housing was *not* taken into account. The new deployment ratio is equal to $\frac{795}{295} \approx 3$. This is because the boom length in deployed configuration is 795 mm / 766.6 (requirement) and the maximum boom length in stowed configuration is 295 / 266.6 mm. For a deployment ratio of 3 the new boom lengths (parallel to mirror *and* diagonal between 2 mirrors) in radial direction then become 0.265 m and 0.256 m respectively. In the axial direction, the deployment ratio of 3 with individual lengths of 0.884 m per telescopic boom still suffices, leading to the total deployed height requirement of $3 \cdot 0.884 = 2.65$ m.

The support structure booms from one end of a boom to the end of the sequential boom is 382.7 mm and 765.9 mm. Since this is almost equal to a deployment ratio of $\frac{765.9}{382.7} \approx 2$, two booms are chosen for this deployment. All above mentioned results are summarized in Table 7.7 below.

Deployment	Total Deployed length (m)	Deployment ratio	Length per boom (m)
Axial direction	2.65	3	0.884
Radial direction - parallel	0.795	3	0.265
Radial direction - diagonal	0.7666	3	0.256
Support	0.7659	2	0.3827

Table 7.7: Overview of lengths per boom in both radial and axial direction. In axial direction, these values are the same as Figure 7.6, but the radial direction is now polygonized to an octagonal shape (8 boooms) and the instrument housing is taken into account for attachment of the baffle booms.

7.3.3. Preliminary Mass Calculation of Telescopic Structure

One of the disadvantages named by E. Korhonen about the telescopic deployment system is the large mass of the baffle structure it would have. Therefore, it is important to do a preliminary mass calculation before designing the system to see what the mass will be of a telescopic boom system. The octagonal system as was found in the Preliminary Geometry Calculation section, Section 7.3.2, is used for the mass calculation.

It will be assumed that the booms have the shape of a hollow cylinder as this is the typical shape of telescopic elements. This could later be changed to a hollow square if need be. Also, Northrop Grumman developed a hollow cylindrical telescopic mast. [73]

The assumed material is aluminium, with a density of 2770 $\frac{kg}{m^3}$. This will give a good first estimate of mass, since aluminium is often the go to material in aerospace applications due to its relatively low density compared to other metals and high stiffness. If it turns out that the mass budget is exceeded, lighter materials such as Carbon Fibre Reinforced Plastics (CFRP) may be used, that additionally offer equal or even better stiffness. Also, cold welding might be a problem, but will for now be assumed to not play a role in the early determination of mass. See Table 7.8 for the overview of the preliminary mass calculation.

							Volume per element ($*10^{-5}$) [m^3]			Mass per element [kg]			
	Number of booms	Number of telescopic elements	Radius booms [m]	Thickness booms [m]	Length booms [m]	Density [$\frac{kg}{m^3}$]	1	2	3	1	2	3	Total mass [kg]
Radial	4	3	0.01	0.001	0.256	2770	1.53	1.21	1.61	0.042	0.038	0.033	0.48
Radial diagonal	4	3	0.01	0.001	0.265	2770	1.58	1.25	1.67	0.044	0.039	0.034	0.50
Axial	8	3	0.01	0.001	0.884	2770	5.28	4.17	5.55	0.147	0.116	0.154	3.44
Support Top	8	2	0.006	0.001	0.368	2770	1.28	1.28		0.018	0.018		0.57
Support Bottom	8	2	0.008	0.001	0.368	2770	1.74	1.74		0.024	0.024		0.77
													5.66

Table 7.8: Quick estimate of mass, to make sure that the mass constraint requirement will be met

The total preliminary mass using an octagonal shape for the telescopic deployment system and aluminium as the material for all elements is around 5.66 kg. Since the budget for the deployment actuation system and baffle structure was set to 10.54 kg in the Thermal Conclusion section, Section 6.10, this leaves enough margin for design iterations and mass allocation for the deployment actuation system, attachment methods and other unforeseen hardware additions. Therefore, (i) the mass of the telescopic booms does not exceed the budget and falls well within the mass constraint requirement of 15 kg and (ii) the mitigation strategy that stated that the mass requirement is just a constraint that has to be adhered to that was made in the trade-off between the inflation system and telescopic deployment system holds. This gives enough certainty that a telescopic deployment system is feasible from a mass and volume perspective, since both mass- and volume requirements of 15 kg and 0.75 m^3 are adhered to up to this point.

Next up, several telescopic deployment concepts can be worked out in further detail, of which one is chosen based on the same criteria as for the trade-off with the inflatable concept: deployed stiffness, stowed

stiffness, deployment complexity, deployment control, stowed volume, mass, flexibility and heritage. These concepts are based on radial deployment.

7.4. Design and Trade-Off of Multiple Telescopic Concepts

Now that the preliminary geometry calculation has been established including a check for mass, several telescopic concepts can be worked out using CATIA, a Computer Aided Design (CAD) program. These concepts are used for a new trade-off from which one is picked and worked out in further detail, including full structural analysis in ANSYS.

Concept 1. Telescopic Only Concept

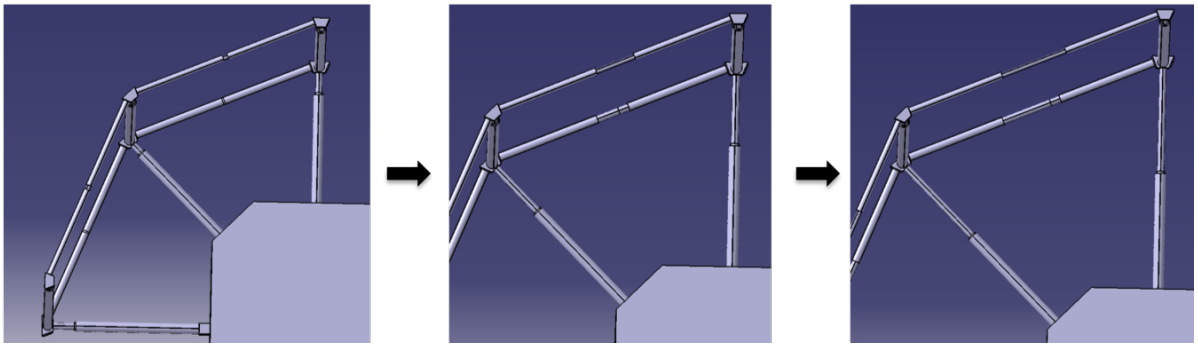

Figure 7.4: Concept 1: Telescopic Only concept using only telescopic booms for radial deployment (prismatic joints) and no hinges (revolute joints)

Concept 2. Mid-Hinge + Side-Hinge Concept

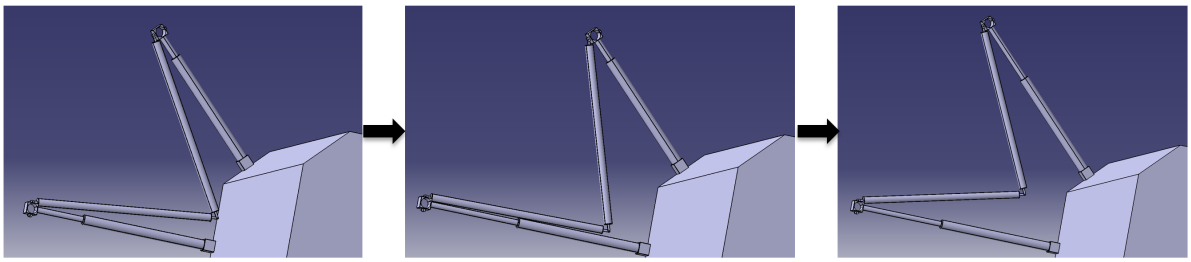

Figure 7.5: Concept 2: Mid-hinge concept using only a revolute joint (hinge) in the middle of each support boom

Concept 3. Telescopic + Mid-Hinge + Side-Hinge Concept

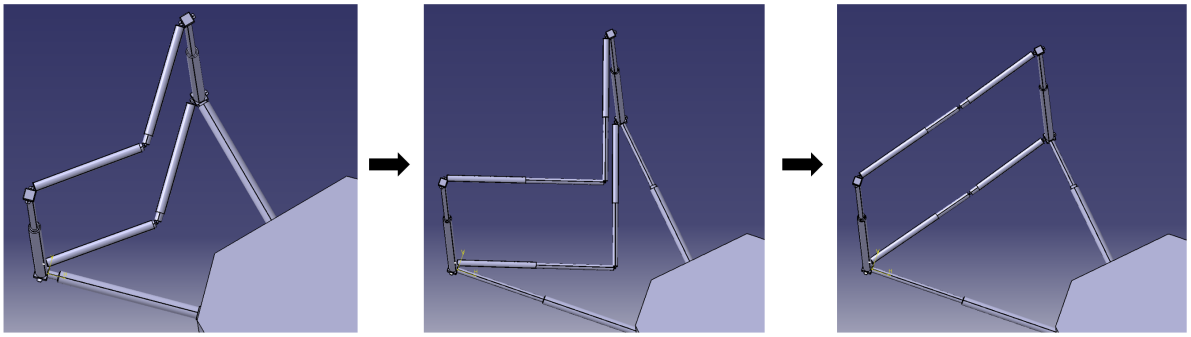

Figure 7.6: Concept 3: telecopic + mid-hinge concept using both telescopic booms and a mid-hinge. The booms that are attached to the hinge are telescopic booms.

Concept 4. Side-Hinge Concept

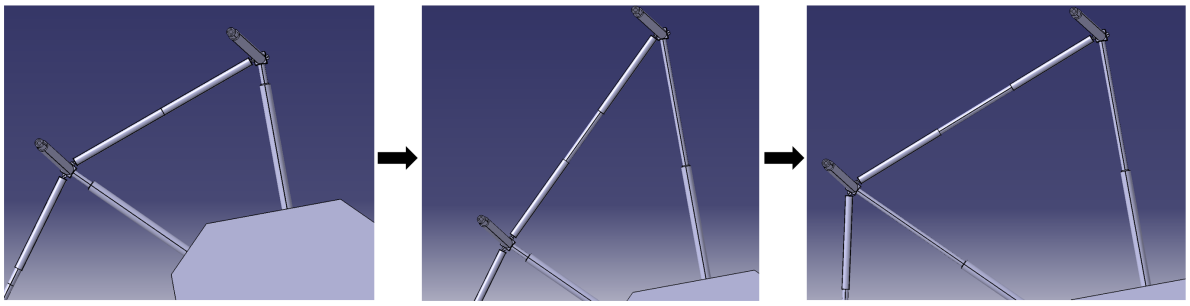

Figure 7.7: Concept 4: side-hinge concept in which the hinges are located on the side near the axial booms

7.4.1. Trade-Off

The four telescopic deployment concepts are traded off in this section based on deployed/stowed stiffness, deployment complexity, deployment control, stowed volume, mass, flexibility and heritage. These concepts are based on radial deployment. Stowed and deployed stiffness are taken as one criterion, as The scoring weight factors are calculated using the AHP method, similar to the trade-off between general telescopic systems and the inflatable concept in the beginning of this chapter. These are explained below. Due to the naming convention (because of the concept similarity), the concepts are referred to using their indices number: concept 1, 2, 3 and 4.

Table 7.9: Scoring weight factors of all alternatives for each critertion as part of the Analytical Hierarchy Process (AHP).

Criteria	**Summarized Argumentation (Detailed Argumentation in Appendix: Chapter D Section II)**
Mass	Mass baffle structure roughly equal, but actuation system for different concepts is not. Concept 1: 1-DOF system in radial direction so 1 actuator needed. Concept 2/3: > 8-DOF in radial direction (extra mid-hinge control) thus > 8 actuation systems. Concept 4: 8-DOF in radial direction thus 8 actuation systems
Deployment Complexity	Relates to amount of failure modes of the system (need to be low as possible) Concept 2/3 more complex due to extra DOF of mid-hinge. Concept 1: only 1 actuator needs to work (redundancy). Concept 4: 8-DOF system and ALL 8 actuation systems need to work, as otherwise the intended deployed shape cannot be reached
Stowed Volume	Concept 2 worst: > 0.75 m^3 as middle of support structure is not telescopic. All other concepts < 0.75 m^3 and thus perform equally well.
Heritage	Equal for all concepts: prismatic- and revolute joints have been used in the space industry
Deployed/Stowed Stiffness	Concept 1: Telescopic structure only, only 1 telescopic support boom, extremely rigid (same stowed and deployed configuration) Concept 2: Mid-hinge which decreases stiffness. Concept 3: Both telescope and 3 hinges for support structure = worse than concept 2. Concept 4: Only two side-hinges so higher stiffness than concept 2 and 3, but worse than concept 1.
Deployment Control	Concept 4 better than 1: every boom needs to be actuated and less friction in support structure due to side-hinge. Concept 2/3 equally bad due to mid-hinge.
Flexibility	Concept 1: same stowed and deployed configuration due to its rigidity. This facilitates future addition of (stray-light) hardware. Concept 4: More flexible than concept 2/3 but worse than concept 1. Concept 2/3: least flexible (equally), again due to > 8-DOF

All scoring weight factors are summarized in Table 7.10 and the final score is also added. Note that the criteria weights are the same as for the first AHP trade-off between the inflatable concept and general telescopic systems. This criteria weight table is shown in 7.3.

Table 7.10: Scoring weight factors of all alternatives for each critertion as part of the Analytical Hierarchy Process (AHP).

Criteria	1. Telescopic Only	2. Mid-Side Hinge	3. Telescopic + Mid-Side-Hinge	4. Side-Hinge	Total
Mass	0.586	0.088	0.088	0.238	1
Deployment Complexity	0.586	0.088	0.088	0.238	1
Stowed Volume	0.318	0.046	0.318	0.318	1
Heritage	0.25	0.25	0.25	0.25	1
Deployed Stiffness	0.565	0.118	0.055	0.262	1
Stowed Stiffness	0.565	0.118	0.055	0.262	1
Deployment Control	0.208	0.089	0.089	0.614	1
Flexibility	0.614	0.089	0.089	0.208	1
Total Score 1	**0.457**	0.086	0.153	0.304	1

As can be seen concept 1, the fully telescopic concept, is best and will therefore be worked out in more detail.

Note that the full, detailed description of criteria and weight factors for all four telescopic concepts is given in Chapter D, Section II.

7.4.2. Conclusion Telescopic Concepts Trade-Off & Final Telescopic Design

The concept that consists of only rigid telescopic elements without any hinges performs best and is chosen based on an extensive AHP trade-off as summarized in Table 7.10. The design of this concept will therefore be finalized and structural analyses will be performed.

The design of the telescopic booms is based on the Telesopic Tubular Mast, designed by Northrop Grumman. They are working on the design of several telescopic mechanisms, like the Telescopic Tubular Mast, which will be used to deploy the Large Sunshield of the James Webb Space Telescope (JWST). This therefore increases the reliability of deployment. [73]

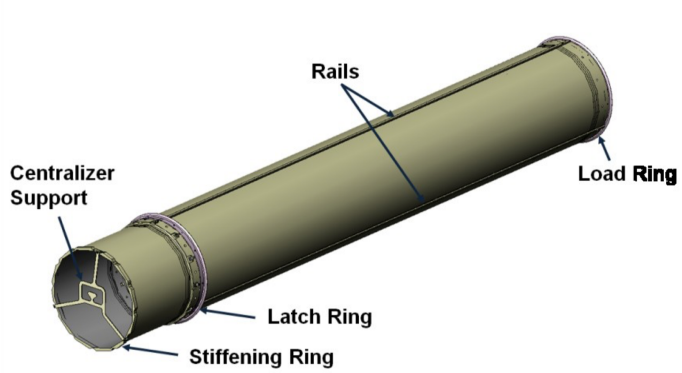

Figure 7.8: Telescopic Tubular Mast, developed by Northrop Grumman Aerospace [73]. Its main features are sliding rails to prevent rotation and increase deployed stiffness, a centralized support to improve buckling prevention and a latch ring to latch/lock the booms in deployed state

The Telescopic Tubular Mast as designed by Northrop Grumman (see Figure 7.8) uses a hollow cylindrical shape for its telescopic booms with the addition of three sliding rails placed 120 degrees apart. Its use is to prevent rotation of the booms and to increase deployed stiffness. Furthermore, it has a latch ring used for latching and locking the booms once deployed and a stiffened ring with centralized support to increase stiffness and buckling resistance.

The rails are also used for the baffle telescopic concept for the same reasons as the Telescopic Tubular Mast: prevent rotation and increase deployed stiffness. The design of the baffle telescopic booms is shown in Figure 7.9 and 7.10. Note that, next to the sliding rails, there is a cold stop at the end when the boom is fully extracted. The cold stop constraints that the telescopic boom can only move along a predefined length. Also, the contact surface of the booms is not equal to the entire circumference of the cylinder, but only of two contact points: at the end of each boom.

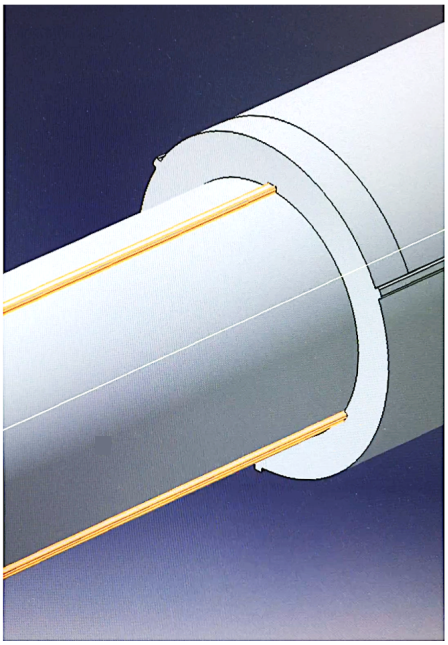

Figure 7.9: Telescopic boom designed for the DST baffle, also consisting of three sliding rails placed 120 degrees apart, a cold stop at the end so booms can only translate for a defined length, and two surfaces of contact only meaning that not the entire telescopic boom length is in contact with its embedded telescopic boom. The inner boom is placed on the inside here for visualization purposes, as is also the case during operations.

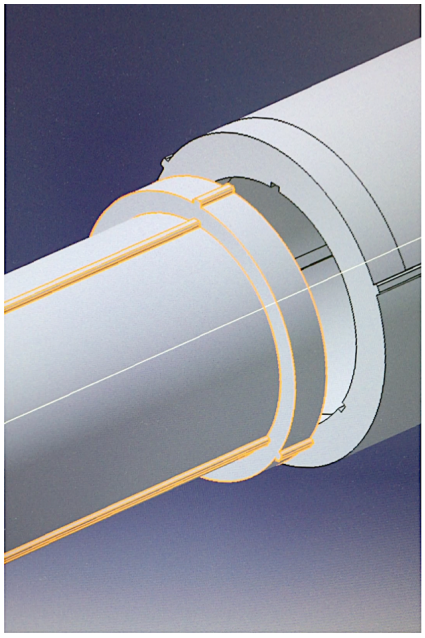

Figure 7.10: Telescopic boom designed for the DST baffle, also consisting of three sliding rails placed 120 degrees apart, a cold stop at the end so booms can only translate for a defined length, and two surfaces of contact only meaning that not the entire telescopic boom length is in contact with its embedded telescopic boom. The inner boom is now placed on the outside here for visualization purposes, but obviously this is not possible in operations due to the cold stop.

The final design as made in CATIA is shown in Figure 7.11 and 7.12 below. These are input for the structural analysis.

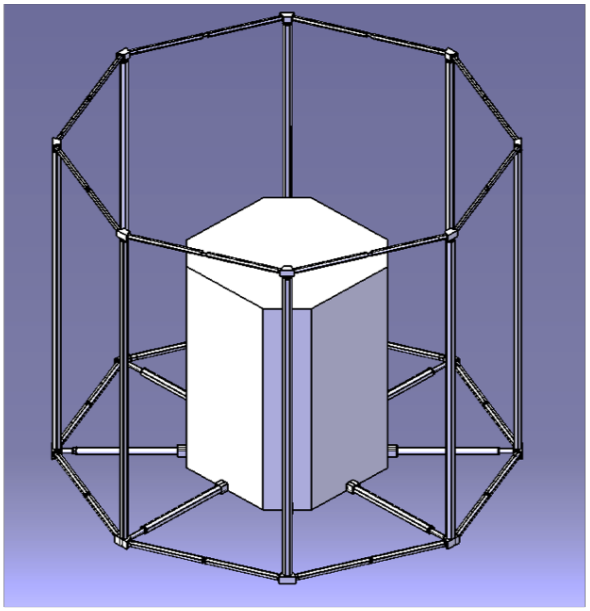

Figure 7.11: **Stowed** configuration of the chosen telescopic concept without mid-hinge. This model serves as input for the structural analysis

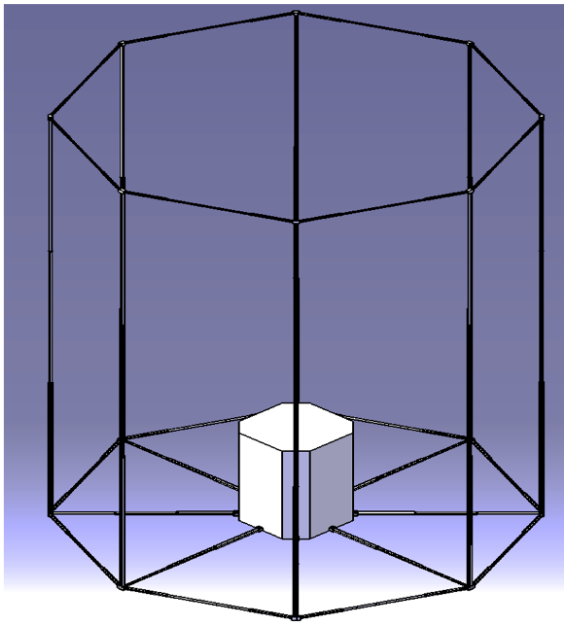

Figure 7.12: **Deployed** configuration of the chosen telescopic concept without mid-hinge. This model also serves as input for the structural analysis

7.5. Structural Analysis

The structural analysis will be performed for both the stowed and deployed configuration seperately, as for both states its structural integrity shall conform to the set requirements to survive LEOP and continuous operations. Furhtermore, structural analyses will be performed for the radial- and axial configuration seperately because ANSYS has limitations on the number of elements that can be used for the student edition. However, this is not a problem as the main modes will be the axial and radial mode shapes which can be uncoupled and treated seperately. Both configurations are shown in Figure 7.13 and 7.14.

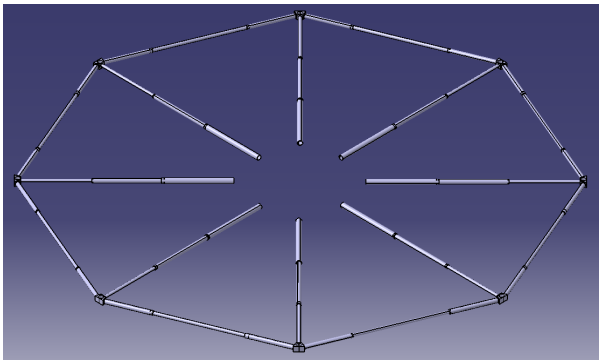

Figure 7.13: **Radial** configuration of the telescopic baffle

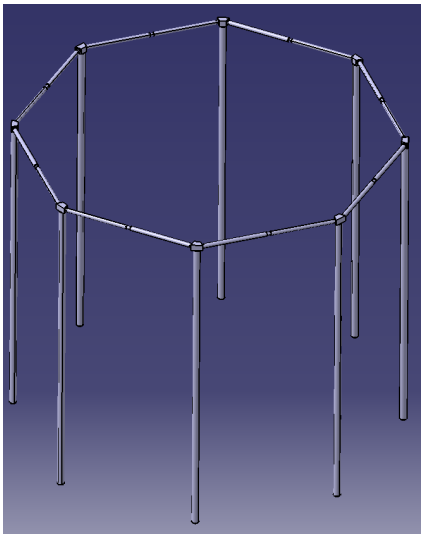

Figure 7.14: **Axial** configuration of the telescopic baffle

7.5.1. Structural Analysis - Stowed Configuration

For the stowed configuration there are a number of important requirements the baffle structure shall adhere to. These, including verification methods, are summarized below in Table 7.11:

Table 7.11: Summarized requirements for the stowed configuration, including verification methods used

Summarized Stowed Baffle Requirements + Verification Methods		
Requirement ID	**Requirement**	**Verification Method**
BAF-MEC-03-04	The baffle shall have a minimum first eigenfrequency of 100 Hz in stowed configuration	**Ver. 1.** Modal analyses (by hand and ANSYS)
BAF-MEC-03-01/02/03	The baffle shall survive a quasi-static load of 30g applied simultaneously to the x-y/x-z/y-z axes in the launcher coordinate frame in the stowed configuration during launch	**Ver. 2.** 30g quasi-static load to COM in all 12 combinations. **Ver. 3.** Buckling analysis due to 30g load

The eigenfrequency in stowed configuration is calculated first.

Ver. 1. Eigenfrequency Calculation - Stowed Configuration

The eigenfrequency of a system depends on the equivalent mass and equivalent stiffness of a system. For the baffle, which consists of 8 radial telescopes and 8 axial telescopes (of which each telescope consists of 3 booms each), both parameters are schematized in Figure 7.15. The main modes of vibration that are likely to be dominant are the bending vibrations.

Therefore the equivalent bending stiffness of both radial- and axial configuration can be approximated by a mass-spring system of which all 8 telescopes have their own bending stiffness and the equivalent stiffness is simply the addition of all individual stiffnesses. See Figure 7.15.

The corresponding equation to calculate the eigenfrequency is shown in Table 7.12.

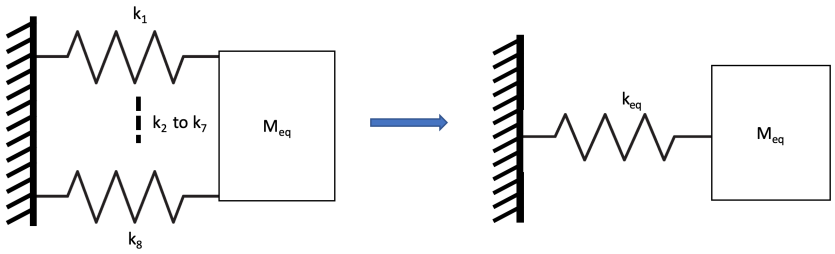

Figure 7.15: Equivalent bending stiffness

Table 7.12: Parameters to calculate the eigenfrequency. Note that these hold for the **stowed** configuration

Calculation of Eigenfrequency		
Parameter	**Formula**	**Units**
ω_n	$\frac{1}{2\pi}\sqrt{\frac{k_{eq}}{M_{eq}}}$	Hz
k_{eq}	$8 * k_{\text{radial booms}} = 8\frac{3EI}{L^3}$	$\frac{N}{m}$
I	$\frac{\pi}{4}\cdot(r_{out}^4 - r_{in}^4)$	m^4
$M_{\text{axial eq}}$	$0.2427\cdot M_{\text{booms,own weight}} + 0.2427\cdot M_{\text{MLI}} = 0.2427\cdot(\rho AL\cdot 8 + M_{\text{MLI}})$	kg
Without Truncated Cone		
$M_{\text{radial eq}}$	$0.2427\cdot M_{\text{booms,own weight}} + M_{\text{axial}} + M_{\text{support bottom}} + M_{\text{support top}} + M_{\text{MLI}} =$ $0.2427\rho AL\cdot 8 + M_{\text{axial}} + M_{\text{support bottom}} + M_{\text{support top}} + M_{\text{MLI}}$	kg
With Truncated Cone		
$M_{\text{radial eq}}$	$0.2427\rho AL\cdot 8 + M_{\text{axial}} + M_{\text{support bottom}} + M_{\text{support top}} + M_{\text{MLI}} + M_{\text{Truncated Cone}} =$ $0.2427\rho AL\cdot 8 + 2.29 + 0.39 + 0.53 + 1.96 + 2.766$	kg

In Table 7.12, E is the Young's modulus of the booms in Pa, I is the area moment of Inertia in m^4 and L is the length of the booms in m. This equation holds for both the radial- and axial configuration. The only parameter that changes for both configurations is the length L of the booms. The area moment of inertia is that of a hollow cylindrical cross-section. In stowed configuration there are three telescopic booms shoved together. The equivalent area moment of inertia of 3 booms which are stacked is simply to summation of the three. Only, each boom has a different outer and inner radius.

Furthermore, the equivalent mass of the own weight of the booms is equal to $0.2427\cdot M_{\text{booms,own weight}}$. The 0.2427 factor stems from [50] and is applied to the calculations here. Furthermore, ρ is the density of the material in $\frac{kg}{m^3}$, A is the area of the hollow cylindrical cross-section and equal to $A = \pi\cdot(r_{out}^2 - r_{in}^2)$ in m^2.

Radial Configuration - Stowed Eigenfrequency

The equivalent mass is not the same for radial- and axial configuration. Namely, for the radial configuration, the mass consists of the own weight of the radial booms as well as the added distributed mass of the axial booms that have to be added to the radial booms as a point mass at the end of the boom length, taken from [50]. Also, the MLI mass needs to be added as a point mass at the end of each beam, as this is where the MLI is located. For now, the truncated cone and MLI mass is disregarded from the design so that easy verification with ANSYS can be made, but will be added to the baffle structure in Section 7.6. This will then change the equivalent mass of the radial configuration, but this is touched upon in Section 7.6.

With aluminium as a material for the booms with a Young's modulus of $7.1\cdot 10^10$ Pa and density of 2780 $\frac{kg}{m^3}$ and thus a Young's modulus over density ratio of $\frac{7.1\cdot 10^10}{2780} = 2.6\cdot 10^7\ \frac{m^2}{s^2}$, a stowed length of the baffle of around 0.256 m and mass of the axial beams and upper support booms of of 3.44 and 0.57 kg respectively (see Table 7.8), the eigenfrequency of the stowed radial state is:

$$\omega_n = \frac{1}{2\pi}\sqrt{\frac{24EI/L^3}{0.2427\cdot\rho AL\cdot 8 + M_{\text{axial}} + M_{\text{support bottom}} + M_{\text{support top}}}} = 54.92\text{Hz} \tag{7.1}$$

This result is validated in ANSYS. If the results are similar, then modal modelling is correct and the impact of changes in the thermal- or mechancial design on the structural integrity can quickly be analysed based on the above equations.

The result of the modal analysis in ANSYS for the radial configuration is 57.53 Hz. This is very close to the 54.92 Hz calculated analytically. The difference can be explained due to an increase in stiffness of the actual model as it consists of a cold stop at the end of the tube with increasing thickness.

However, the eigenfrequency is too low and it needs to increase to 100 Hz to meet the requirement. The eigenfrequency will even be lower due to the addition of MLI and the truncated cone mass. The eigenfrequency of the baffle structure in radial configuration with the addition of MLI with a mass of 1.96 kg, and a truncated cone with a mass of 1.61 kg, the eigenfrequency decreases from 54.92 Hz to 40.24 Hz.

Therefore, the stiffness needs to increase and/or the mass needs to decrease to make sure that this eigenfrequency already meets the 100 Hz requirement. Based on simple calculations it is found that the ratio $\frac{E}{\rho}$ needs to increase to $\geq 1 \cdot 10^8 \ \frac{m^2}{s^2}$. Therefore, aluminium as a material needs to be changed to a material that has this characteristic. Due to this conclusion, the material for the baffle structure is changed from aluminium to a M55J which is an high-modulus epoxy CFRP with an $\frac{E}{\rho}$ of $\frac{5.4 \cdot 10^{11}}{1910} = 2.8 \cdot 10^8 \ \frac{m^2}{s^2}$. This is better than aluminium, which has an $\frac{7.1 \cdot 10^{10}}{2780} = 2.6 \cdot 10^7 \ \frac{m^2}{s^2}$. M55J is also mainly used in the Aerospace industry. [100]

The eigenfrequency needs to be ≥ 100 Hz: the stiffness to mass ratio ($\frac{E}{\rho}$) needs to increase to $\geq 1 \cdot 10^8 \ \frac{m^2}{s^2} \rightarrow$ *Change aluminium to high modulus M55J CFRP to conform to the stowed eigenfrequency requirement*

There are additional reasons why M55J is a better material than aluminium. These are summarized below:

Table 7.13: Advantages of using M55J CFRP over aluminium for the baffle telescopic boom structure

	M55J CFRP Advantages
1	Lower mass and higher Young's modulus than aluminium: $\frac{E}{\rho} = 2.8 \cdot 10^8$ vs $2.6 \cdot 10^7 \ . \frac{m^2}{s^2}$. → Lowest eigenfrequency increases to ≥ 100 Hz and the mass of the baffle decreases: 5.66 kg to 3.90 kg.
2	Not sensitive to cold-welding between the telescopic parts
3	M55J has a negative CTE, meaning that due to temperature gradients the boom does not expand but contract. This therefore does not hinder but only facilitates the deployment and no extra clearance between the telescopic elements is needed.

Table 7.14: Advantages of using M55J CFRP over aluminium for the baffle telescopic boom structure

M55J CFRP Properties		
Property	**Value**	**Unit**
Density	1911	$\frac{kg}{m^3}$
Specific Heat	711.8	$\frac{J}{kgK}$
Conductivity	155.6	$\frac{W}{mK}$

The new stowed eigenfrequency of the radial configuration with the updated Young's modulus and density of M55J is now 138.1 Hz. The validated ANSYS result is 142.1 Hz, so again close. For both these analyses the mass of the MLI is added of 1.96 kg as a distributed mass on all 8 boom tips. The truncated cone is not added for the analytical-ANSYS comparison, but this does not matter as the mass of the trucated cone will again also be added as a distributed mass at the boom tips. The 142.1 Hz eigenfrequency result from ANSYS is shown in Figure 7.16. Indeed, the first mode shape is a bending mode shape as was already predicted.

Axial Configuration - Stowed Eigenfrequency

For the axial configuration as schematazed in Figure 7.14, the same equations apply. What changes is the length of the stowed booms from 0.256 m to 0.884 m, as well as the equivalent mass. For the model with only the addition of MLI but without truncated cone, the equivalent mass is:

Note that for the axial booms the mass of the MLI is not added as point mass distributed at the end of all 8 booms as is the case for the radial booms, but is now added as a distributed mass mass, since MLI is placed along the entire length of the axial booms. Therefore, the distributed fraction of 0.2427 is added as well, just like for the distributed own weight of the booms. [50]

The calculated eigenfrequency of the axial booms in stowed configuration is then 122.0 Hz. However, the validation in ANSYS yields extremely different values of 321.9 Hz. The minimum eigenfrequency is thus not based on the bending of all 8 axial booms together as was expected, but is now based on local bending of the upper support structure at a specific location. This is also visualized in figure 7.17. However, this is only benificial from a structural integrity point of view, as the eigenfrequency is extremely high. The axial configuration will therefore not be the critical/determining configuration in **stowed** state. It is important to note that this conclusion only holds for the stowed state, as for the deployed state, the global bending mode is expected as the deployed axial boom length with a deployment ratio of 3 is $3 \cdot 0.884 = 2.65$ m. This length drastically detoriates the eigenfrequency, since the stiffness scales with the length to the power 3: $k = \frac{EI}{L^3}$. Therefore, the eigenfrequencies of the axial booms might be the determining factor for the deployed configuration, but are not for the stowed configuration. In stowed configuration the radial configuration is the critical configuration yielding a lower eigenfrequency, mainly due the addition of mass of MLI, truncated cone **and axial boom mass** as distributed point masses on all 8 radial booms at the end of the booms.

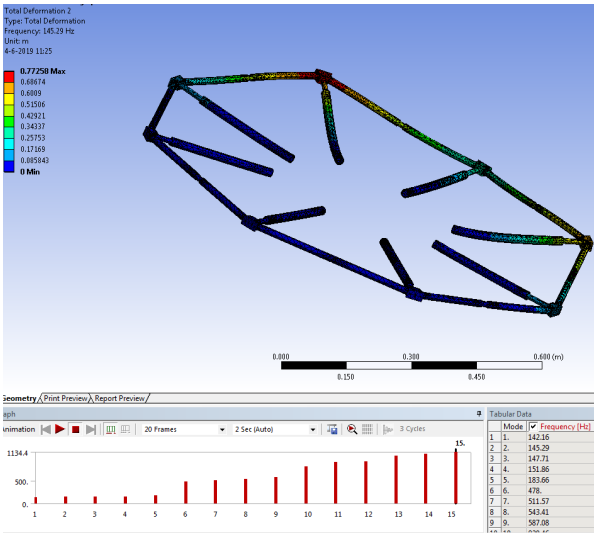

Figure 7.16: Eigenfrequency of stowed radial configuration with added mass of MLI. Minimum eigenfrequency is 142.1 Hz as expected

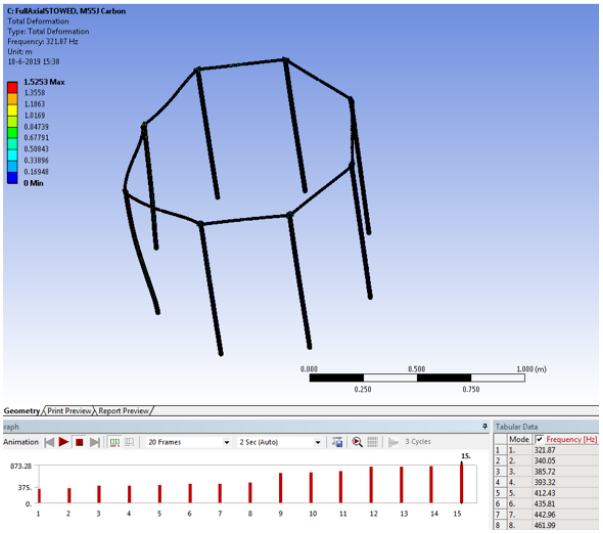

Figure 7.17: Eigenfrequency of stowed axial configuration with added mass of MLI. Minimum eigenfrequency is 321.9 Hz, which was not expected. The calculated value is 122.0 Hz, but is for a different mode shape. Apparently, local bending happens only with a much greater eigenfrequency.

The summary of the eigenfrequencies for both radial and axial configuration in stowed configuration are summarized in Table 7.15 below:

Table 7.15: Results modal analysis in ANSYS and by hand

Ver. 1. Modal Analysis - Stowed Configuration			
Parameter	**Requirement**	**Analytical Result**	**ANSYS Result**
First Eigenfrequency Radial [Hz]	≥ 100	138.1	142.1
First Eigenfrequency Axial [Hz]	≥ 100	122.0	321.9 (different mode shape)

Ver. 2. Quasi-Static Load of 30G in X-Y/X-Z/Y-Z - Stowed Configuration

BAF-MEC-03-01/02/03 require that the baffle shall survive a quasi-static load of 30g applied simultaneously to the x-y/x-z/y-z axes in the launcher coordinate frame in the stowed configuration during launch. The consequence of this is that 12 different quasi-static analyses have to be performed as there are 12 different coordinate combinations. The quasi-static load that is being applied is 30g which is equal to $30 \cdot 9.81 = 294.3$ $\frac{m}{s^2}$. It is thus an acceleration, but this results in a force (load) as mass in being accelerated. Furthermore, the 30g load has to be applied to the COM of the baffle structure.

The requirement is that the maximum von Mises stress is lower than the tensile strength of M55J, which is $2 \cdot 10^9$ Pa. For safety reasons, a factor of safety of 1.5 is used. This is also one of the generated requirements: BAF-SYS-07. The requirement then is that the maximum von Mises stress is $\leq 1.3 \cdot 10^9$ Pa.

Table 7.16: Quasi-static 30g load applied to the COM of the baffle structure, for both the radial and axial configuration in 12 different X-Y/X-Z/Y-Z combinations

Parameter	**Requirement**	**Result**			
X/Y					
		+X / +Y	**+X / -Y**	**-X / +Y**	**-X / -Y**
Radial					
Max. Von Mises Stress [Pa]	$< 1.3 \cdot 10^9$	$2.23 \cdot 10^7$	$3.37 \cdot 10^7$	$3.37 \cdot 10^7$	$2.23 \cdot 10^7$
Max. Total Deformation [m]	-	$9.79 \cdot 10^{-6}$	$8.69 \cdot 10^{-6}$	$8.69 \cdot 10^{-6}$	$9.79 \cdot 10^{-6}$
Axial					
Max. Von Mises Stress [Pa]	$< 1.3 \cdot 10^9$	$5.65 \cdot 10^7$	$3.28 \cdot 10^7$	$3.28 \cdot 10^7$	$5.65 \cdot 10^7$
Max. Total Deformation [m]	-	$1.17 \cdot 10^{-4}$	$1.32 \cdot 10^{-4}$	$1.32 \cdot 10^{-4}$	$1.17 \cdot 10^{-4}$
X/Z					
		+X / +Z	**+X / -Z**	**-X / +Z**	**-X / -Z**
Radial					
Max. Von Mises Stress [Pa]	$< 1.3 \cdot 10^9$	$1.39 \cdot 10^8$	$1.26 \cdot 10^8$	$1.26 \cdot 10^8$	$1.39 \cdot 10^8$
Max. Total Deformation [m]	-	$3.49 \cdot 10^{-4}$	$3.44 \cdot 10^{-4}$	$3.44 \cdot 10^{-4}$	$3.49 \cdot 10^{-4}$
Axial					
Max. Von Mises Stress [Pa]	$< 1.3 \cdot 10^9$	$4.42 \cdot 10^7$	$4.42 \cdot 10^7$	$4.42 \cdot 10^7$	$4.42 \cdot 10^7$
Max. Total Deformation [m]	-	$8.82 \cdot 10^{-5}$	$8.82 \cdot 10^{-5}$	$8.82 \cdot 10^{-5}$	$8.82 \cdot 10^{-5}$
Y/Z					
		+Y / +Z	**+Y / -Z**	**-Y / +Z**	**-Y / -Z**
Radial					
Max. Von Mises Stress [Pa]	$< 1.3 \cdot 10^9$	$1.38 \cdot 10^8$	$1.26 \cdot 10^8$	$1.26 \cdot 10^8$	$1.38 \cdot 10^8$
Max. Total Deformation [m]	-	$3.47 \cdot 10^{-4}$	$3.45 \cdot 10^{-4}$	$3.45 \cdot 10^{-4}$	$3.47 \cdot 10^{-4}$
Axial					
Max. Von Mises Stress [Pa]	$< 1.3 \cdot 10^9$	$2.69 \cdot 10^7$	$2.36 \cdot 10^7$	$2.36 \cdot 10^7$	$2.69 \cdot 10^7$
Max. Total Deformation [m]	-	$7.58 \cdot 10^{-5}$	$7.63 \cdot 10^{-5}$	$7.63 \cdot 10^{-5}$	$7.58 \cdot 10^{-5}$

From Table 7.16 it can be concluded that the baffle structure adheres to the 30g quasi-static load requirement, as the largest stress is $1.39 \cdot 10^8$ Pa and holds for the radial configuration when the 30g load is applied in the +X/+Z or -X/-Z direction. These are the same due to symmetry as is the case for other combinations as well. The maximum stress in the baffle structure is an order of magnitude lower than the requirement of $\leq 1.3 \cdot 10^9$ Pa. This does therefore not impose any problems on the structural integrity during launch due to the quasi-static 30g load.

The corresponding total deformations are in the order of magnitude of 10^{-4} m. The largest deformation is 0.4 mm. There is no strict requirement for the maximum deformation of the baffle. Only in deployed configuration there is a strict requirement on the maximum deformation: clearance of 200 mm must be maintained between baffle and mirror elements. This does not hold for the stowed configuration, but even if it did, the 0.4 mm deflection does not detoriate the conformance to this requirement.

Ver. 3. Buckling Due To 30g Load - Stowed Configuration

Buckling due to the quasi-static load might be an issue as the baffle booms consist of thin walls. For hollow cylinders with a large ratio of radius to wall thickness $\frac{R}{t}$, buckling might be critical. The telescopic booms have a mediocre radius/wall thickness ratio, but the buckling load multiplier will still be analyzed. The buckling load multiplier is a multiplication factor that indicates with what factor the actual load must be multiplied before the critical buckling load is reached, which is the point when buckling happens.

Ver. 3. Buckling Due To 30g Load - Stowed Configuration - Analytical Approximation

Based on the small-deflection theory, the critical stress in thin-walled cylinders is [8]:

$$\sigma_x = \frac{E \cdot t}{r \cdot \sqrt{3 \cdot (1 - \nu^2)}} \tag{7.2}$$

In which E is the Young's modulus in Pa, t is the wall thickness in m, r is the radius of the cylinder in m and ν is the Poisson ratio. Applying Equation 7.2 to the DST baffle telescopic booms with a wall thickness of 1 mm,

a radius of 10 mm (worst case, largest $\frac{r}{t}$ ratio), a Young's modulus of M55J of $5.4 \cdot 10^{11}$ Pa and a Poisson's ratio of 0.3, the following critical stress appears:

$$\sigma_x = \frac{5.4 \cdot 10^{11} \cdot 0.001}{0.01 \cdot \sqrt{3 \cdot (1 - 0.3^2)}} = 3.3 \cdot 10^{10} \text{Pa} \tag{7.3}$$

It can be seen from this equation that in the worst case of a hollow cylinder with r = 10 mm and t = 1 mm, the critical stress before buckling starts is only $3.3 \cdot 10^{10}$ Pa. This is two orders of magnitude higher than the maximum von mises stress caused by the 30g quasi-static load of $1.39 \cdot 10^{8}$ Pa. The buckling load multiplier is then:

$$B_{\text{buckling load multiplier}} = \frac{3.3 \cdot 10^{10}}{1.39 \cdot 10^{8}} = 237 \tag{7.4}$$

However, in the "critical stress of thin-walled cylinders in axial compression' document published by the National Advisory Committee for Aeronatics, it is mentioned that the actual critical stress is much lower of that of Equation 7.2: 15 to 50 %. This is found through experimental research. [8] Even when the actual critical buckling stress is 15 % (worst case) of the calculated critical buckling stress it is still more than an order of magnitude of higher than the 30g load due to launch. Based on simple hand calculations it can thus be concluded that buckling will not be critical for the baffle structure. This is validated with ANSYS buckling analyses.

Ver. 3. Buckling Due To 30g Load - Stowed Configuration - ANSYS
By performing buckling analyses in ANSYS it was found out that the maximum load buckling multiplier is -579 for the radial structure in the +Y / -Z direction. This means that the 30g needs to be multiplied 579 times before buckling becomes crucial. The negative sign of the buckling multiplier indicates that the load must be reversed for buckling. For the radial structure this makes sense, as buckling becomes crucial for compressive loads, which is the case for the -Y direction. The Z direction for the radial booms is bending in transverse direction and thus less crucial than in-plane compressive loads. The -579 value is also two order of magnitudes higher and only twice that of the calculated 237 which holds for the worst case in which the largest radius and smallest thickness is used.

Summarized:

Table 7.17: Ver. 3. Buckling Due To 30g Load - Stowed Configuration. Results from both analytical approximations- and ANSYS simulations

Ver. 1. Modal Analysis - Stowed Configuration			
Parameter	**Requirement**	**Analytical Result**	**ANSYS Result**
Buckling Load Multiplier [-]	≥ 2	237	-579 (minus, so buckling load is reversed)

It can thus be concluded based on analytical-, experimental and ANSYS analyses and data that buckling is not critical for the baffle telescopic booms that make up the baffle structure. This is mainly due to the mediocre ratio between the radius and thickness and due to the high Young's modulus of the M55J CFRP.

It can also be concluded that the eigenfrequencies of the stowed configuration all conform to the ≥ 100 Hz requirement as is summarized in Table 7.15.

Therefore, both BAF-MEC-03-04 and BAF-MEC-03-01/02/03 are met and structural integrity in stowed configuration is guarenteed. The same eigenfrequency analysis shall be performed for the deployed configuration to also find out if the structural integrity conforms the requirements that hold for the deployed configuration.

7.5.2. Structural Analysis - Deployed Configuration

For the deployed configuration there are also a number of important requirements the baffle structure shall adhere to. Summarized:

Table 7.18: **Summarized requirements for the deployed configuration, including verification methods used**

Summarized Stowed Baffle Requirements + Verification Methods		
Requirement ID	**Requirement**	**Verification Method**
BAF-MEC-07-06-03-01	The baffle structure shall have a minimum first eigenfrequency ≥ 0.9 Hz in deployed configuration	**Ver. 4.** Modal Analysis (By hand + ANSYS)
BAF-MEC-04-03	The baffle shall survive deployment	**Ver. 5.** Modal Analysis ($\omega_n \geq$ Inflatable Concept ≥ 0.9 Hz)
BAF-MEC-04-03-02	The baffle shall survive deployment shocks and vibrations	**Ver. 6.** Modal Analysis ($\omega_n \geq$ Inflatable Concept ≥ 0.9 Hz)
BAF-MEC-04	The baffle shall deploy succesfully	**Ver. 7.** Flexible Body Dynamics

These requirements can be verified by performing modal analyses to get the eigenfreqencies of the deployed system, and by performing Flexible Body Dynamics analyses in which the deployment is simulated.

The eigenfrequency in deployed configuration is calculated first.

Ver. 4/5/6. Eigenfrequency Calculation - Deployed Configuration

The eigenfrequency can be calculated using the same equations as for the stowed state. The difference in eigenfrequency calculation between the deployed- and stowed configuration is that the area moment of inertia and the lengths change.

The area moment of inertia is derived in the Appendix, I of Chapter E. Using this area moment of inertia for the deployed booms, the eigenfrequencies are calculated, again analytically and in ANSYS. The results are shown in Table 7.19, which also includes the stowed eigenfrequencies from the previous section.

Table 7.19: Results modal analysis in ANSYS and by hand

Parameter	**Requirement**	**Analytical Result**	**ANSYS Result**
Ver. 1. Modal Analysis - Stowed Configuration			
First Eigenfrequency Radial [Hz]	≥ 100	138.1	142.1
First Eigenfrequency Axial [Hz]	≥ 100	122.0	321.9 (different mode shape)
Ver. 4/5/6. Modal Analysis - Deployed Configuration			
First Eigenfrequency Radial [Hz]	≥ 0.9	12.79	22.99
First Eigenfrequency Axial [Hz]	≥ 0.9	12.39	11.06

The eigenfrequencies in deployed state are ofcourse lower than that of the stowed state due to the increase in length. It was already concluded that the stiffness decreases with the length to the third power: $k = \frac{EI}{L^3}$, so this effect is clearly visible in the eigenfrequency values. Also note that the mass of the MLI / truncated cone remains the same in both stowed- and deployed state and are still added as a distributed mass at the end of the radial beams or as a distributed equivalent own weight for the axial telescopic booms. Also, both eigenfrequencies are roughly similar, but the axial eigenfrequency is now dominant and thus the determining factor for the deployed state. This was already predicted in the previous section.

Deployed eigenfrequency: determined by axial configuration. Stowed eigenfrequency: determined by radial configuration.

Both eigenfrequencies meet the ≥ 0.9 Hz requirement that was generated in Chapter 4. The 0.9 Hz requirement stems from E. Korhonen's thesis [58] as E. Korhonen concluded that her inflatable deployment design could withstand operational structural loads due to reaction-wheel vibrations and slew-rate rotations, and the inflatable system has an eigenfrequency of 0.92 Hz. Thus, a minimum eigenfrequency of 0.9 Hz (rounded off) is assumed to be enough to meet on-board vibrations and slew rate rotations. Therefore, it can be concluded that the structural integrity of the designed telescopic baffle structure can also survive operations such as slew rate rotations, on-board vibrations (reaction-wheel) and such.

Ver 7. Flexible Body Dynamics

Flexible Body Dynamics (FBD) analyses can be used to simulate the deployment of the telescopic baffle structure. In FBD analyses, the booms are simulated as non-rigid flexible beams which can bend and elongate and therefore obstruct the deployment. For every timestep the stiffness matrices are calculated ($\frac{EA}{L}$ and

$\frac{EI}{L^3}$) and the corresponding deflections are added to the kinematics of the system. In the case that the deflection of the support structures exceeds their requirement based on the deployed force of the radial booms, the deployment fails. This is due to the kinematics which are affected in great extent by the deflection of the support structure. FBD is also used to get a first order approximation of the force that is needed to deploy the baffle. Therefore, this is a crucial step in analyzing the deployment success.

The setup of this analysis including preliminary results is shown in Figure 7.18. It can be seen that the outer booms including support structures are made flexible and hence are meshed. These booms are included FBD. The bigger telescopes are not meshed. These are rigid and therefore excluded from the FBD analysis.

Based on the preliminary FBD analysis, the maximum equivalent von Mises stress is in the order of magnitude of 10^6 Pa and hence does not exceed the tensile strength requirement for M55J: $\leq 1.3 \cdot 10^9$ Pa. However, care must be taken that these analyses have to be continued in more depth. Also, the axial deployment has to be analyzed, but since the baffle first deploys radially, this was chosen to be simulated first. Additionally, the radial support is most critical as it consists of telescopic support structures that are flexible, deploy with a velocity of $\sqrt{2}$ times the velocity of the radial booms itself and could potentially jam the deployment. For the axial deployment, this is less critical as it only consists of axially deploying telescopes.

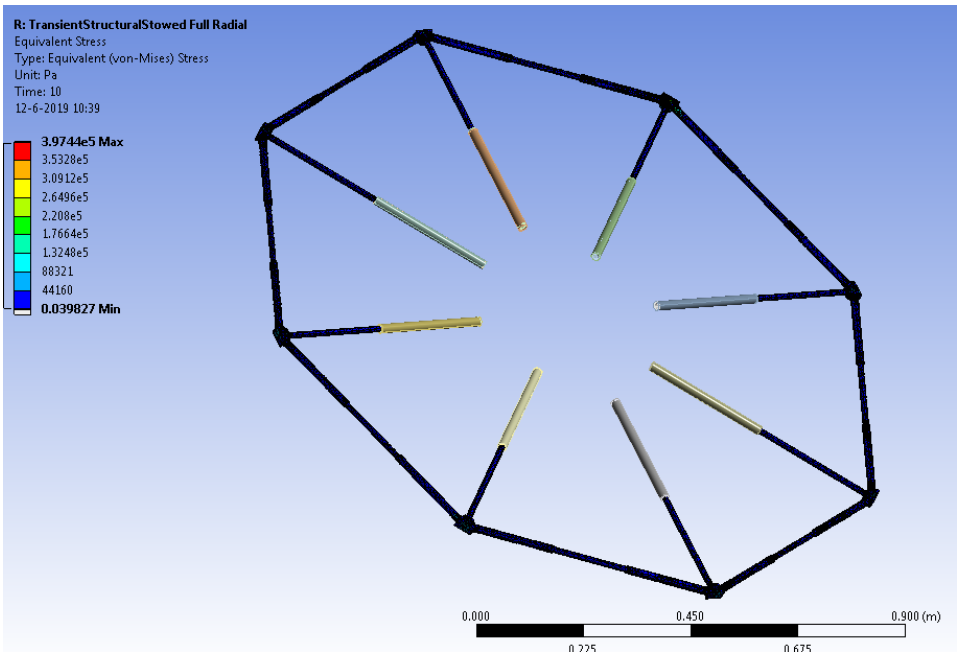

Figure 7.18: Flexible Body Dynamics in Radial Configuration. The mass of the MLI is added a a distributed mass at the tip of each boom.

Table 7.20: Results Flexible Body Dynamics analysis in ANSYS

FBD analysis for radial deployment, including MLI mass and distributed mass of axial booms			
Parameter	**Value**		
Max. Von Mises Stress [Pa]	$4.88 \cdot 10^5$	$7.31 \cdot 10^6$	$6.58 \cdot 10^6$
Load Type	Velocity [$\frac{m}{s}$]	Velocity [$\frac{m}{s}$]	Acceleration [$\frac{m}{s^2}$]
Load Value	0.02	0.068	0.106
Load Applied	2 opposite booms	2 opposite booms	1 boom
Total Simulation Time [s]	10	10	3

Furthermore, a first order estimate of the force based on the Flexible Body Dynamics (FBD) analysis can be made which is needed to deploy the system.

The force needed to deploy the telescopic booms on Earth normally depends on the friction induced by the normal loads caused by the gravity field. However, in space, gravity is low: $9.8 \cdot 10^{-6}$ $\frac{m}{s^2}$ and denoted as

micro-gravity. However, inertia due to mass is still present as was concluded by prof. dr. ir. J.L. Herder, meaning that there will still be friction. The friction levels due to deployment are hard to predict and uncertain which also reduce the reliability of the system. However, the lack of deployment reliability due to friction caused by inertia could be mitigated by using a multitude of distributed actuation systems. This will also be applied when designing the actuation system since it results in redundancy and an increase in deployment reliability.

The deployment force is equal to the deployment acceleration times the mass that it accelerates. For the radial deployment, the acceleration is equal to 0.106 $\frac{m}{s^2}$ and the mass is equal to the mass of the radial booms and the lower support structure as well as the axial booms and MLI mass: 8.2 kg (uncertainty margin of 50% added to account for truncated cone mass). The force needed to accelerate 8.2 kg with an acceleration of 0.106 $\frac{m}{s^2}$ is around 0.9 N. This force can definately be provided with a strain based actuation boom (STEM for example).

In terms of friction, Delrin-Acetal can be used for the inner layers of the telescopic booms. This has been applied to a 1U cubesat with similar characteristics as the DST baffle structure: extandable boom structure of low mass and high stiffness, composed of 20 mm diameter composite booms (so same as 10 mm radius as is the case for the largest baffle structure booms) but with even lower thickness than the DST baffle booms: 0.3 mm only. For this design it is stated that "where low friction is required (e.g. components that interface with the composite boom), delrin-acetal is used instead." [79]

However, Delrin-Acetal only has a Young's modulus of $3 \cdot 10^9$ Pa, and its density is 1410 $\frac{kg}{m^3}$. This means that the ratio of $\frac{E}{\rho} = \frac{3 \cdot 10^9}{1410} \approx 2 \cdot 10^6$, which is well below the $1 \cdot 1 \cdot 10^8$ requirement which is required to make the telescopic booms have a stowed eigenfrequency ≥ 100 Hz. Therefore, Delrin-Acetal will not be used as a material for the booms, but might in the future be useful as a coating, if possible. This is left as a recommendation. Its operation temperature is -40 ° C to +120 ° C, so if it could be used as a coating, then it also has to adhere to these temperature limits. [28]

7.6. Addition of Truncated Cone

The truncated cone as was found in Chapter 6 to be benificial for the thermal gradients, is also modelled in CATIA. It will be attached to the upper support structures / axial telescopic booms and will therefore have a similar telescopic deployment as the bottom- and top support structures. The truncated cone has a wall thickness of 1 mm and is made of the same material as the baffle booms: M55J with a density of 1910 $\frac{kg}{m^3}$. The truncated cone is displayed in both stowed and deployed configuration for one eighth of the total truncated cone shape in Figure 7.19.

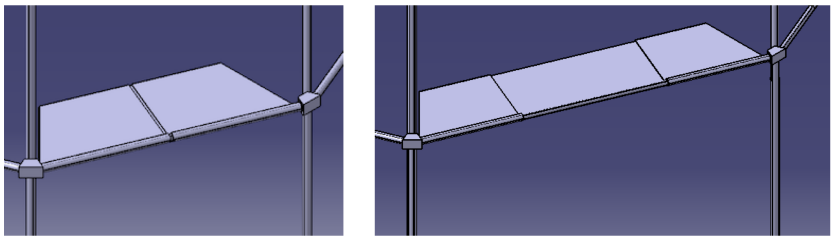

Figure 7.19: Stowed and deployed model of one side of the truncated cone as designed in CAD

The mass was estimated to be 1.62 kg earlier, but due to the telescopic nature of the truncated cone more volume has to be added. The current mass of the telescopic truncated cone is 2.77 kg, which holds for the entire truncated cone, so eight times that of Figure 7.19.

The eigenfrequency in stowed radial configuration (most crucial state as the stowed axial configuration has a higher eigenfrequency of 321.9 Hz as was analyzed in ANSYS) will change due to the mass addition of the truncated cone.

Table 7.21: Results modal analysis when a truncated cone is added. Results are analytically calculated by hand

Parameter	Requirement	Analytical Result
Ver. 1. Modal Analysis - Stowed Configuration - Without Truncated Cone		
First Eigenfrequency Radial [Hz]	≥ 100	138.1
Ver. 1. Modal Analysis - Stowed Configuration - With Truncated Cone		
First Eigenfrequency Radial [Hz]	≥ 100	108.2

7.7. Foldability of MLI

The telescopic deployment system is now designed and the stowed and deployed configuration with corresponding dimensions are known. A first order stowage design for the MLI can be made. The MLI will be folded based on the origami technique as indicated by E. Korhonen. [58] In this section, it is calculated what the packing thickness of MLI is as a function of the number of folds. Packing thickness relates to the minimum total thickness of MLI when folded in which the internal stress does not exceed the Yield point of the MLI composite. This is to ensure that plastic deformation will **not** occur. In Figure 7.20 several origami folding patters are visualized.

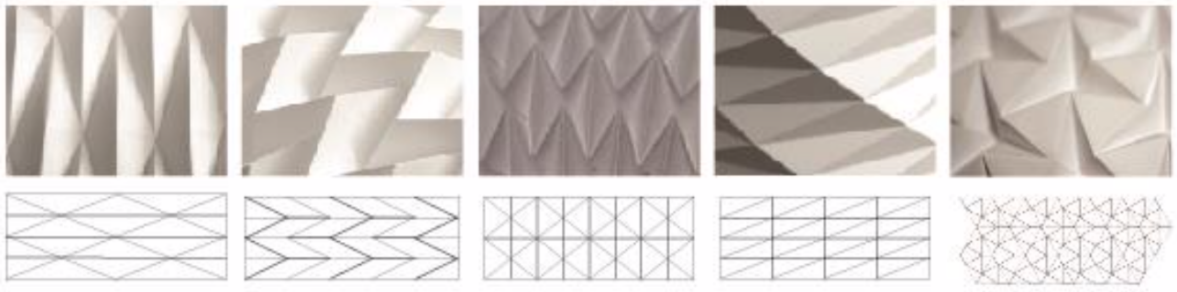

Figure 7.20: Origami concepts which are used as a baseline for the calculations of the foldability of MLI. Taken from [30]

Folding mechanics is a complex branch and various folding techniques could be used to physically fold or bend a material. In general, bending, folding and wrinkling are all the result of localized buckling on a surface. In order to fold a material, wrinkling occurs which then transitions into further folding of the material. [31] In general it is a combination of bending, in which both tension and compression above and below the neutral axis of bending takes place respectively, and in which the compression area results in buckling. This is visualized in Figure 7.21.

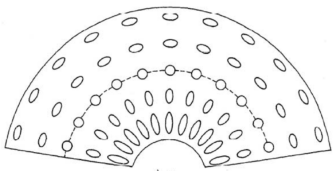

Figure 7.21: Bending of a material causes tensile stresses above the neutral line and compressive stress below the neutral line. At the neutral line, there is no material stress

The ability for a material to bend depends on several factors:

1. Bending stiffness (resistance to bending)
2. Radius of curvature [63]
3. Applied force (stress) to initiate the bend

The bending stiffness of MLI needs to be calculated first. MLI can be modelled as a thin plate consisting of multiple layers. The bending stiffness of a plate composed of N perfectly bonded layers of linear, elastic,

homogeneous, and isotropic material is [104] :

$$D_N = \frac{E(Nt_{MLI})^3}{12\left(1-\nu^2\right)} = N^3 \cdot \frac{Et_{MLI}^3}{12\left(1-\nu^2\right)} = N^3 \cdot D \tag{7.5}$$

The bending stiffness D is also referred to as the flexural rigidity and is analogous to flexural stiffness (= EI). In which N is the number of layers, t is the thickness of one layer and ν is the Poisson ratio. It can be seen that the bending stiffness increases with every added layer to the third power: $D_N \sim N^3$. This is also concluded in [31]. For a composite material like the MLI lay-up, equivalent material parameters based on the rule of mixtures need to be taken into account, as was also the case to calculate the bulk conductivity for example. Now, not the mass fraction, but the volume fraction is taken into account. As the area itself is equal for both Kapton and Dacron, the volume of both materials is only dependent on the thickness of their individual layers. The individual thicknesses of Kapton (shield) and Dacron (spacer) are 0.013 mm and 0.16 mm respectively.

Furthermore the total thickness of ONE layer (in m and not mm) is equal to:

$$t_{MLI,1L} = t_{Kapton} + t_{Dacron} = (13+160)\cdot 10^{-6} = 173 \cdot 10^{-6}\text{m} \tag{7.6}$$

Evaluating the bending stiffness equation, Equation 7.5 with the composite values of Table 3.4 results in the following bending stiffness of MLI as a function of the number of layers N:

$$D_N = N^3 \cdot \frac{Et_{MLI,1L}^3}{12\left(1-\nu^2\right)} = N^3 \cdot \frac{2.92\cdot 10^9 \cdot (173\cdot 10^{-6})^3}{12\cdot(1-0.40^2)} = N^3 \cdot 0.0015 \tag{7.7}$$

Furthermore relating the stress, strain and applied moment to each other that hold for the pure bending of a plate with a thickness over width ratio of in general 0.1 or less:

$$\begin{aligned} \sigma_x = \frac{E}{\left(1-\nu^2\right)}\epsilon_x \;\&\; \sigma_x = -\frac{M_z y}{I_{zz}} \rightarrow \\ M_z = -\frac{E}{1-\nu^2}\cdot\epsilon_x \cdot I_{zz} = -\frac{E}{1-\nu^2}\cdot\frac{-y}{\rho}\cdot I_{zz} \end{aligned} \tag{7.8}$$

In this equation, σ_x is the stress in Pa, ϵ_x is the strain, M_z is the induced moment on the MLI layer in Nm, I_{zz} is the area moment of inertia in m^4, y is the distance from the neutral line to any other position in the cross-section in m and ρ is the radius of curvature in m. When the plate is not bent the radius of curvature is infite, when the plate is slightly bent the radius of curvature is large and when the plate is significantly bent the radius of curvature is small. The radius of curvature and neutral axis of a plate/beam is schematized in Figure 7.22. Also, the strain ϵ_x for a bending plate/beam is defined as: $\epsilon_x = -\frac{y}{\rho}$.

It can be seen that at when this distance is zero $y = 0$, no strain is present, since this is the neutral line at which **no** tension or compression takes place as mentioned earlier. For the maximum strain y is maximal and equal to half the thickness of the MLI: $y_{max} = \frac{1}{2}t_{MLI,1L}$.

Realising that for the MLI (flat plate) the area moment of inertia is:

$$I_{zz} = \frac{1}{12}bt_{MLI,1L}^3 \tag{7.9}$$

In this equation b is the width of the plate in m. Substituting this area moment of inertia I_zz and the maximum distance from the neutral line y_max in the moment equation, Equation 7.8:

$$M_z = \frac{E}{1-\nu^2}\cdot\frac{0.5t_{MLI,1L}}{\rho}\cdot\frac{bt_{MLI,1L}^3}{12} = \frac{1}{2}\cdot D_N \cdot t_{MLI,1L}\frac{b}{\rho} = \frac{1}{2}\cdot N^3 \cdot \frac{Et_{MLI,1L}^4}{12\left(1-\nu^2\right)}\frac{b}{\rho} \tag{7.10}$$

It can be seen that the requirement moment to bend the MLI depends on:

1. The number of MLI layers
2. The radius of curvature of the bend
3. The Young's modulus of the MLI
4. The Poisson ratio of the MLI

5. The width of the MLI (simply the amount of area exposed to folding)

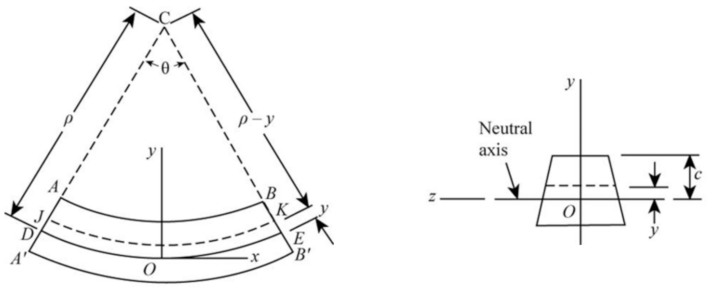

Figure 7.22: Radius of curvature ρ and neutral axis schematized

According to Equation 7.10, MLI can always be folded for any given number of layers and any given radius of curvature, however this just changes the bending moment that has to be applied to the MLI to fold it up. However, at some point with a too low radius of curvature or too many layers of MLI the bending moment M_z becomes simply too large and will then exceed the yield point, meaning that the MLI will plastically deform. This is not wanted as plastic deformations do not recover to their elastic state and are thus permanent. This has unwanted effects on the prestress which decreases as well as negatively alter the thermal shielding performance. Therefore the bending moment of Equation 7.10 is substituted back in the first equation of Equation 7.8 to get the stress of bending:

$$\sigma_x = \frac{M \cdot y}{I_{zz}} = \frac{\frac{0.25N^3 E t_{MLI,1L}^5 b}{12\rho(1-\nu^2)}}{\frac{1}{12} b t_{MLI,1L}^3} = \frac{0.25N^3 E t_{MLI,1L}^2}{\rho(1-\nu^2)} \rightarrow \frac{4\sigma_x(1-\nu^2)}{E t_{MLI,1L}^2} = \frac{N^3}{\rho} \tag{7.11}$$

Evaluating this equation for the yield strength of MLI: the yield strength of Kapton is around 69 MPa at 23 ° C and 41 MPa at 200 ° C, [29], and the yield strength of Dacron is 80 MPa. [43]. Since the baffle is deployed and the MLI unfolded during LEOP in which high temperatures are to be expected, a conservative value for the yield strength of 41 MPa for Kapton is assumed. For safety- and conservative reasons this lowest yield point of 41 MPa is also chosen for the evaluation instead of a rule of mixtures value.

For a yield point of 41 MPa, equivalent Poisson ratio ν of 0.40, equivalent Young's modulus E of 2.92 GPa and a thickness of MLI of $173 \cdot 10^{-6}$ m the following properties can be calculated for various number of MLI layers: minimum radius of curvature, packing thickness and stowed volume due to added packing thickness. The packing thickness changes the stowed radial lengths of the booms $L_{parallel}$ and $L_{diagonal}$: it is simply added to the stowed length of the radial booms. See Table 7.22 for the overview.

Table 7.22: Number of layers of MLI, corresponding minimum radius of curvature (bending radius) in order to avoid that the yield strength of MLI is exceeded, packing thickness and corresponding stowed volume based on the added packing thickness of MLI. All related to the foldability of MLI **when folded once**

Number of MLI Layers N	**Minimal Radius of Curvature** ρ **[m]**	$\frac{N^3}{\rho}$	**Packing Thickness** [m]	**Stowed Volume** [m^3]
1	$6.34 * 10^{-7}$	1.58	1.9	0.86
2	$5.08 * 10^{-6}$	1.58	11.1	0.89
3	$1.71 * 10^{-5}$	1.58	35.5	0.97
4	$4.06 * 10^{-5}$	1.58	82.7	1.14
5	$7.93 * 10^{-5}$	1.58	160.3	1.44
6	$1.37 * 10^{-4}$	1.58	275.8	1.96
7	$2.18 * 10^{-4}$	1.58	436.9	2.82

As can be seen in Table 7.22 the ratio between $\frac{N^3}{\rho}$ remains equal: 1.58. It can also be seen that the radius of curvature determines the packing efficiency of the MLI: it scales to the third power. Because of this, the stowed volume also increases immensely. The maximum number of MLI layers to conform to the $\leq 1.5\ m^3$ requirement is 5. The packing thickness is visualized in Figure 7.23.

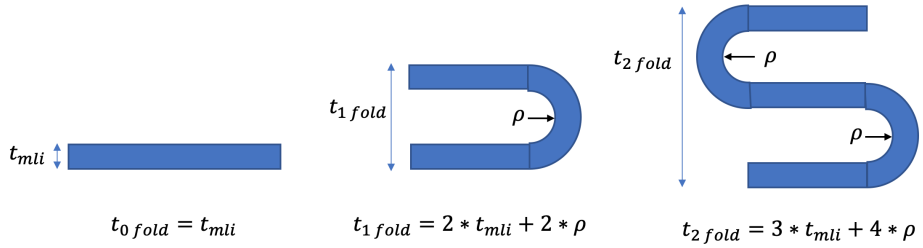

Figure 7.23: Packing thickness (which determines the packing efficiency) as a function of the number of MLI layers used, for 0, 1 and 2 folds.

From this figure it can be concluded that the packing thickness when folding MLI n_{folds} times is a function of the number of folds and the number of MLI layers used:

$$t_{\text{packing}}(n_{folds}, N) = (1 + n_{folds}) \cdot (N \cdot t_{Kapton} + (N+1) \cdot t_{Dacron}) + 2 \cdot n_{folds} \cdot \frac{N^3}{1.58} \tag{7.12}$$

In this equation, the radius of curvature is substituted by $\rho = \frac{N^3}{1.58}$ and the total MLI thickness t_{MLI} is substituted by: $t_{MLI} = N \cdot t_{Kapton} + (N+1) \cdot t_{Dacron}$, so that the packing thickness merely depends on the number of folds and the number of MLI layers. Equation 7.12 is also used to calculate the packing thickness for various number of MLI layers in Table 7.22.

It can be concluded that a maximum of 5 layers of MLI can be used to still conform to the $\leq 1.5\ m^3$ threshold stowed volume requirement. This conclusion will also be used for the MLI trade-off in Chapter 8.

7.8. Iterative Mechanical Design

7.8.1. Updated Stowed and Deployed Volume

Table 7.23: Updated stowed and deployed volume of both the baffle and full DST - with and without addition of MLI (5 layers)

Updated Stowed & Deployed Volume $[m^3]$		
$V = 2 \cdot (1+\sqrt{2}) \cdot W^2 \cdot H$ $W = \sqrt{L^2_{parallel} + L^2_{diagonal} - 2 \cdot L_{parallel} \cdot L_{diagonal} \cdot \cos(45°)}$		
Parameter	**Value**	**Comment**
Stowed Volume (Requirement: $\leq 0.75\ m^3$ (goal) $\leq 1.5\ m^3$ (threshold))		
$V_{\text{Stowed Baffle, without MLI}}$	0.71	Baffle volume without MLI. $W = 0.4075$ m, $H = 0.884$ m.
$V_{\text{Stowed Baffle, with MLI}}$	1.20	Baffle volume with MLI (5 layers). $W = 0.530$ m, $H = 0.884$ m.
$V_{\text{Stowed DST, without MLI}}$	0.85	Total stowed volume of the DST is bounded by stowed height of spider to the bottom of the interface housing:1.0625 m instead of 0.884 m. Stowed radius (width) is bounded by only the baffle, so 0.4075 m remains.
$V_{\text{Stowed DST, with MLI}}$	1.44	Total stowed volume of the DST is bounded by stowed height of spider to the bottom of the interface housing:1.0625 m instead of 0.884 m. Stowed radius (width) is bounded by only the baffle, so 0.530 m remains.
Deployed Volume		
$V_{deployed}$	7.50	Deployed baffle volume with MLI (5 layers). $W = 0.7659$ m, $H = 2.65$ m.

The stowed and deployed volume have to be updated so that it conforms to the volume of an octagonal baffle. In Table 7.23 the baffle volume and DST volume are summarized. These are not similar as is explained in Table 7.23. Also, when adding MLI, the stowed volume increases as well. The maximum of 5 MLI layers is added, as this still conforms to the 1.5 m^3 stowed volume threshold requirement: Section 7.7.

The stowed volume of the entire DST is 0.85 m^3 without MLI and 1.44 m^3 with MLI and thus in both cases exceeds the stowed volume goal requirement of 0.75 m^3, but does not exceed the stowed volume threshold requirement of 1.5 m^3, which is fine.

The total volume deployment ratio of the baffle only- and entire DST respectively are:

$$R_{\text{Volume Baffle}} = \frac{7.50}{1.20} \approx 6.3 \;\&\; R_{\text{Volume DST}} = \frac{7.50}{1.44} \approx 5.2 \tag{7.13}$$

7.8.2. Changing Cross-Section of Booms

A trade-off between different telescopic boom cross-sections is made, of which the trade-off criteria are strength, weight, manufacturability and deployment characteristics. Strength and weight are often combined into one strength/weight factor, since we are interested in the bending strength of the booms per unit weight of material. The strength is related to the area moment of inertia of the boom, thus depending on the cross-section. The weight depends on the area, as the length and density of the booms will be the same: $m = \rho \cdot V = \rho AL$.

Telescopic booms could consist of various cross-sections, each yielding in a different strength/weight ratio. In this section, two cross-sections are considered: a hollow cylindrical (default) - and hollow square cross-section.

An overview of the area moment of inertia and area of both these cross-sections is given in Table 7.24.

Cross-Section Shape	**Area Moment of Inertia**	**Area**
Hollow cylindrical	$\frac{\pi}{4} \cdot (r_{out}^4 - r_{in}^4)$	$\pi \cdot (r_{out}^2 - r_{in}^2)$
Hollow square	$\frac{1}{12} \cdot (b_{out}^4 - b_{in}^4)$	$b_{out}^2 - b_{in}^2$

Table 7.24: Area moment of inertia and area calculation for both a hollow square- and cylindrical cross-section

For equal stiffness, the difference in area is calculated. Since there are four unknowns and two equations, some numbers have to be assumed, and therefore the strength to weight ratio differs for various telescopic booms. The different values for the areas (relating to the weight of the booms) for similar stiffness values for the hollow cylindrical and square cross-sections are summarized in Table 7.25.

It can be seen in Table 7.25 that a hollow square cross-section yields lower area (so lower mass) for the same stiffness as the hollow cylindrical cross-section. This means that the same stiffness performance, and thus the same eigenfrequencies, are reached for less mass of material. The corresponding mass savings are summarized in Table 7.26.

Telescopic Boom Number	**Dimensions** [mm]	**Area Moment of Inertia** I_{xy} $[mm^4]$	**Area** A $[mm^2]$	**Strength to Weight** $\frac{I_{xy}}{A}$ $[mm^2]$
Hollow Cylindrical Cross-Section.				
1	$r_{out} = 10$ & $r_{in} = 9$	2700.98	56.69	47.64
2	$r_{out} = 8$ & $r_{in} = 7$	1331.25	47.12	28.25
3	$r_{out} = 6$ & $r_{in} = 4$	816.81	62.83	13.00
Hollow Square Cross-Section.				
1	$B_{out} = 20$ & $B_{in} = 18.9$	2700.98	42.81	63.10
2	$B_{out} = 16$ & $B_{in} = 14.92$	1331.25	33.39	39.87
3	$B_{out} = 12$ & $B_{in} = 10.23$	816.81	39.35	20.76

Table 7.25: Area moment of inertia, area calculation and strength to weight ratio for both a hollow square- and cylindrical cross-section

Telescopic Boom Number	**Mass Savings Square Cross-Section vs. Cylindrical Cross-Section**
1	$(1 - \frac{42.81}{56.69}) * 100\% = 24.5\%$
2	$(1 - \frac{33.39}{47.12}) * 100\% = 29.1\%$
3	$(1 - \frac{39.35}{62.83}) * 100\% = 37.4\%$

Table 7.26: Mass savings when using a square cross-section for the telescopic booms.

Visualizing this in Figure 7.24 shows that the hollow square cross-section has more than twice as much area to add a deployment actuation system: $10.23 \cdot 10.23 = 104.7\ mm^2$ instead of $\frac{\pi}{4} \cdot 8^2 = 50.3\ mm^2$.

Furthermore, there is a larger clearance between the telescopic elements when using hollow square cross-section (1.45/1.46 mm) instead of 1 mm for the circular tubes.

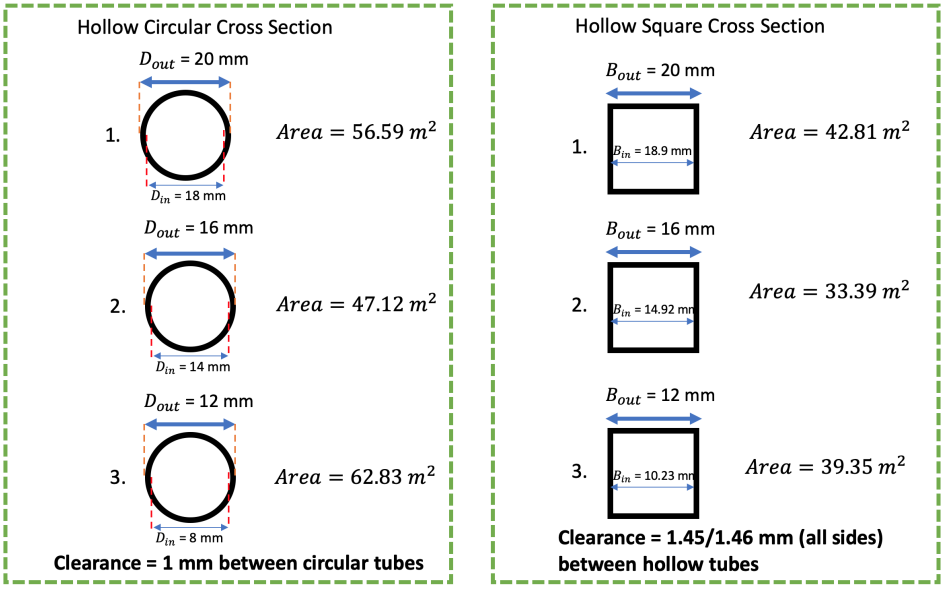

Figure 7.24: Hollow cylindrical- vs square cross-section for a 3-telescopic tube system. The hollow square cross-section has a better bending strength / weight ratio, since for equal bending strengths the areas for all three booms is much lower.

The trade-off criteria are strength to weight ratio, manufacturability and deployment characteristics. All criteria are in favor of the hollow square cross-section, therefore it is not needed to perform an AHP trade-off study:

1. A hollow square cross-section yields a higher bending strength to weight ratio, meaning that for the same area moment of inertia and thus same bending stiffness ($k = \frac{3EI}{L^3}$) can be achieved with less volume of material → less $M_{mechanical}$ mass, meaning more room for $M_{thermal}$
2. A hollow square cross-section prevents rotation along axial direction due the nature of its shape. When wanting to prevent rotation for a hollow cylinder, rails have to be added (like for the Telescopic Tubular Mast designed by Northrop Grumman [73]), which complicates the manufacturing process as well as.
3. Since the area of material is lower for a hollow square shape, more area is left for the addition of a deployment actuation system: 104.7 instead of 50.3 mm^2
4. More clearance is left between all sides of a hollow square cross-section than for a hollow cylindrical one: 1.45/1.46 mm instead of 1 mm clearance

To conclude, the hollow square cross-section is chosen. The mass of the baffle structure therefore has to be updated: from 3.90 kg to 2.73 kg.

The mass of the baffle structure decreases from 3.90 kg to 2.73 kg due to the change from hollow cylindrical cross-section to hollow cubical cross-section, for equal stiffness.

Note that since the area moment of inertia has stayed the same, the stiffness is also the same. Only, the results will even be more benificial since the mass decreases.

7.9. Preliminary Deployment Actuation System Choice

Based on the first order requirement of force needed to deploy the system, a proper deployment actuation system can be chosen that can deliver this force. Criteria that drive this actuator choice are:

1. Force needed to deploy shall be at least 0.9 N, see Section 7.5.2.

2. Added mass shall not exceed the total baffle mass requirement of 15 kg
3. Volume requirement: actuation system shall fit within the hollow square telescopic boom with smallest dimensions: 10.23 mm by 10.23 mm = 104.7 mm^2
4. Heritage

Based on all these criteria, the STEM actuation system seems to be a good fit which adheres to all requirements of which an explanation is given below.

Deployment Force The NANO STEM has "a maximum push force of 50 lbs at limit load." [47]. This is equal to a 22.7 kg push "force". This is well suitable for the boom structure, as its current mass is only 3.95 kg. The 50 lbs pound force translate to a 222.5 N force at limit load (since the pound force takes into account gravitational acceleration of the Earth). This is well above the minimum force requirement of 0.9 N and thus sufficient.

Volume
The diameter of a STEM boom varies from 6.52 mm,[4], to 7 mm. [92] This fits perfectly within the 8 mm diameter constraint. The STEM boom is visualized in Figure 7.25, taken from [92].

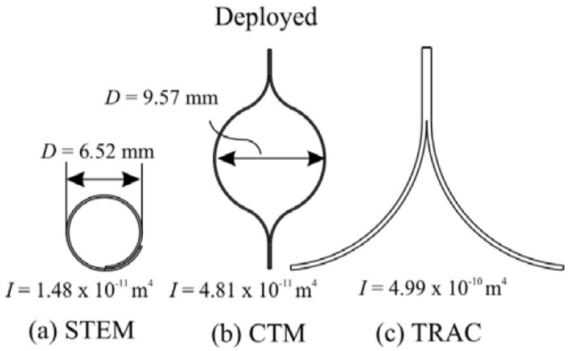

Figure 7.25: Strain energy based deployment actuation systems

Heritage
Furthermore, STEM has tremendous heritage. It will be used for the JWST to deploy its Sun-shield (with similar lay-up of material as the DST baffle MLI lay-up), developed by Northrop Grumman. This company has designed, developed, manufactured, tested and implemented many variations of STEM booms in different satellite programs. Next to the JWST, the Hubble Space Telescope, ISIS Mast Deployer, Mars Pathfinder Rover Ramps and FalconSat 3 Gravity Gradient Boom are satellites that have all used STEM booms. Northrop Grumman has a complete list of STEM flight heritage, in which the above mentioned satellites, including many others, are listed: [47]

Also, the NANO STEM actuator is "Useful as an antenna, cubesat deployable, instrument boom, boom to drive a telescopic mast". [47] This means that it could very well be used for our baffle telescopic deployment system. Northrop Grumman also uses a STEM actuation system to deploy its own Telescopic Tubular Mast, [73], concluding that it is indeed a good choice to use a STEM actuation system.

Mass
The mass of the NANO STEM actuator is "0.36 lb deployer + 0.025 lb/ft STEM". [47] In SI units, this is equal to a 0.163 kg deployer + 0.0372 kg/m STEM. When applying the NANO STEM actuator in one boom, the mass will be equal to the mass of the deployer plus the mass of the STEM boom, which depends on the total length needed for deployment. The total length of STEM boom needed in radial direction is equal to the deployed radial length of 795 mm for the parellel boom and 766.6 mm for the diagonal boom. For the axial direction the length is 2650 mm.

Assuming that it only one actuator is needed for radial direction and only one in axial direction (since it is a 2DOF system), this results in a total mass of:

$$M_{actuator} = M_{actuator,radial} + M_{actuator,axial} = 2 \cdot 0.163 + 0.0372 \cdot (0.795 + 2.650) = 0.454\,\text{kg} \tag{7.14}$$

Of which $M_{actuator,radial} = 0.163 + 0.0372 \cdot 0.795 = 0.193$ kg and $M_{actuator,axial} = 0.163 + 0.0372 \cdot 2.65 = 0.262$ kg.

For reliability reasons and to conform to the requirement that all single point of failures should be eliminated by redundant components, BAF-SYS-02-03, and active elements of mechanism such as actuators shall be redundant, BAF-SYS-03, it is chosen to **quadruple** the amount of NANO STEM actuators: 4 actuators to control the radial deployment and 4 actuators to control the axial deployment. This quandruples the mass value of Equation 7.14: $4 \cdot 0.454 = 1.816$ kg. Four radial- and axial actuators, making it a total of 8 actuators, yields a redundant design and half of the axial booms- and radial booms are actuated in this case.

7.10. Updated Eigenfrequencies

There are two changes to the mechanical design that change the stowed and deployed eigenfrequency: the addition of the deployment actuation mass and the change from hollow cylindrical cross-section to hollow square cross-section, which only influences the mass of the system and not the stiffness. For the stowed state the critical eigenfrequency is that of the radial configuration and for the deployed state it is the axial configuration. This has already been explained before.

The NANO STEM actuator that is being used to deploy the telescopic boom structure has a mass of 0.163 kg per deployer + 0.0372 kg/m STEM. Since the deployer itself is attached to the interface housing or close to it, it does not contribute to the radial eigenfrequency analysis. Also, the same holds for the axial eigenfrequency analysis: the mass of the deployer itself does not contribute to the eigenfrequency analysis as it is attached at the base of the axial booms. However, the distributed mass of the deployed STEM boom itself of 0.0372 kg/m does apply.

Stowed Eigenfrequency

The radial configuration is the critical configuration for the stowed eigenfrequency so this one will be analytically calculated. The axial actuators influence the radial eigenfrequency a lot, since these will be a attached in the axial booms of the telescopic structure. This means that the mass of the 4 axial actuators have to be added as a distributed mass at the tip of the radial booms: the full mass of that of the axial actuators (thus deployer + STEM boom).

Additionally, the mass of the radial actuation system of **only** the NANO STEM boom of 0.0372 kg/m has to be added, since the mass of the radial deployer is attached to the interface housing and NOT to the tip of the radial boom. Therefore, the mass of the radial actuator deployer of 0.163 kg does not contribute to the eigenfrequency behavior.

Deployed Eigenfrequency

For the deployed eigenfrequency the axial configuration is crucial and most stringent. The equivalent mass for the axial configuration consists of the distributed weight of the booms = $0.2427 \cdot M_{\text{Axial Booms}}$, the distributed weight of MLI = $0.2427 \cdot M_{\text{MLI}}$, the full mass of the truncated cone $M_{\text{Truncated Cone}}$ and distributed mass of the actuation system $0.2427 \cdot 4 \cdot 0.0372 \cdot 2.65$.

Table 7.27: Results updated eigenfrequencies - both stowed and deployed

Parameter	Requirement	Analytical Result
Ver. 1. Modal Analysis - Stowed Configuration		
First Eigenfrequency [Hz]	≥ 100	107.7
Ver. 4/5/6. Modal Analysis - Deployed Configuration		
First Eigenfrequency [Hz]	≥ 0.9	4.8

It can be concluded that for the entire baffle system, both including mechanical- and thermal mass, the stowed eigenfrequency is 107.7 Hz and thus ≥ 100 Hz and the deployed eigenfrequency is 4.8 Hz and thus ≥ 0.9 Hz. Therefore all eigenfrequencies conform the their structural eigenfrequency requirements.

7.11. Summary Mechanical Design and Performance

In this section the mechanical performance will be summarized as well as its mass budget and impact on the thermal design. The mechanical design will iteratively change the thermal design in Chapter 8.

7.11.1. Mass Budget after Mechanical Design

Table 7.28: Mass budget after preliminary mechanical design has been established

Mass Calculation	
Sub-System	**Mass (kg)**
MLI	1.96
Truncated Cone M2	2.766
Baffle Structure	2.73
Deployment Actuation System	1.816
Total Mass	9.272
Safety Margin	25%
Total Mass Including Safety Margin	11.59
Mass Thermal System $M_{thermal}$	5.91
Mass Mechanical System $M_{mechanical}$	5.68
Mass Requirement	15

As can be seen in Table 7.28, the total mass including safety margin of 25 % is 11.59 kg after the mechanical design has been established. This includes both the thermal system mass $M_{thermal}$ (MLI shield + truncated cone mass for stray-light purposes) and mechanical system mass $M_{mechanical}$ (baffle structure + deployment actuation system). Note that the mass of the baffle structure is precisely known, but the mass of the deployment actuation system is still quite uncertain and only based on literature. Also note that for the individual thermal- and mechanical mass, $M_{thermal}$ and $M_{mechanical}$, the uncertainty margin of 25 % is added as well.

7.11.2. Mechanical Performance

The mechanical performance is summarized here.

Table 7.29: Mechanical performance of the telescopic boom structure versus the inflatable structure as designed by E. Korhonen and the requirements

Parameter	**Requirement**	**Telescopic Boom Structure**	**Inflatable Structure (E. Korhonen)**
Mass [kg]	15	11.59	23.6
Stowed Volume Baffle Only [m^3]	0.75 (goal) / 1.5 (treshold)	1.2	0.71
Stowed Volume Entire DST [m^3]	0.75 (goal) / 1.5 (treshold)	1.44	1.8
Deployed Volume Entire DST [m^3]	-	7.50	10.2
Stowed Eigenfrequency [Hz]	≥ 100 Hz	107.7	Unknown. Likely ≈ 0 Hz
Deployed Eigenfrequency [Hz]	≥ 0.9 Hz	4.8	0.92
Quasi-Static 30g Load: Maximum Von Mises Stress [Pa]	$\leq 2 \cdot 10^9$ (Tensile Strength)	$1.39 \cdot 10^8$	Unknown
Quasi-Static 30g Load: Buckling Load Multiplier [-] **BAF-SYS-07-03**	≥ 2	237 (minimal)	Unknown

1. The axial configuration is not the critical/determining configuration in **stowed** state, but is in the **deployed** state, because in deployed state the length increases from 0.884 m to 2.65 m and this drastically detoriates the eigenfrequency, as the stiffness scales with the length to the power 3: $k = \frac{EI}{L^3}$. In stowed configuration the radial configuration is the critical configuration yielding a lower eigenfrequency, mainly due the addition of mass of MLI, truncated cone **and axial boom mass** as distributed point masses on all 8 radial booms at the end of the booms.

7.11.3. Effect of Mechanical Design Choices on Thermal Design

In Chapter 6 the effect of the thermal design choices on the mechanical deployment system was made. However, now that the mechanical deployment system is worked out in further detail, this retroactively changes the thermal design again. Obviously this makes sense as the nature of design is an iterative process.

The effect of the mechancial design choices from this chapter on the thermal design is, again, roughly displayed in the N2 diagram in Figure 4.3. To sum up:

1. Due to the shape of the telescopic boom system, the thermal shield shape changes as well: from a cylindrical to an **octagonal** shape. Therefore, the new shape has to be verified again.

2. The nominal temperatures and temperature gradients of the mechanical baffle structure (telescopic booms) can be simulated and analyzed. The temperature gradients cause thermo-elastic deformations, which cause stresses in the booms and might influence the deployment

3. The mechanical mass $M_{mechanical}$ is now defined: 5.68 kg. This sets a mass constraint on the numbers of MLI layers that can be used for the shield, which results in a proper trade-off for the numbers of MLI to be used.

4. The truncated cone as defined earlier has to be changed so that it fits the octagonal shape. New thermal analyses have to be made to show what the best shape is of the truncated cone.

The above mentioned influences on thermal design will be implemented in the full thermal-mechanical design integration, Chapter 8 and an overview is schematized in Figure 7.26.

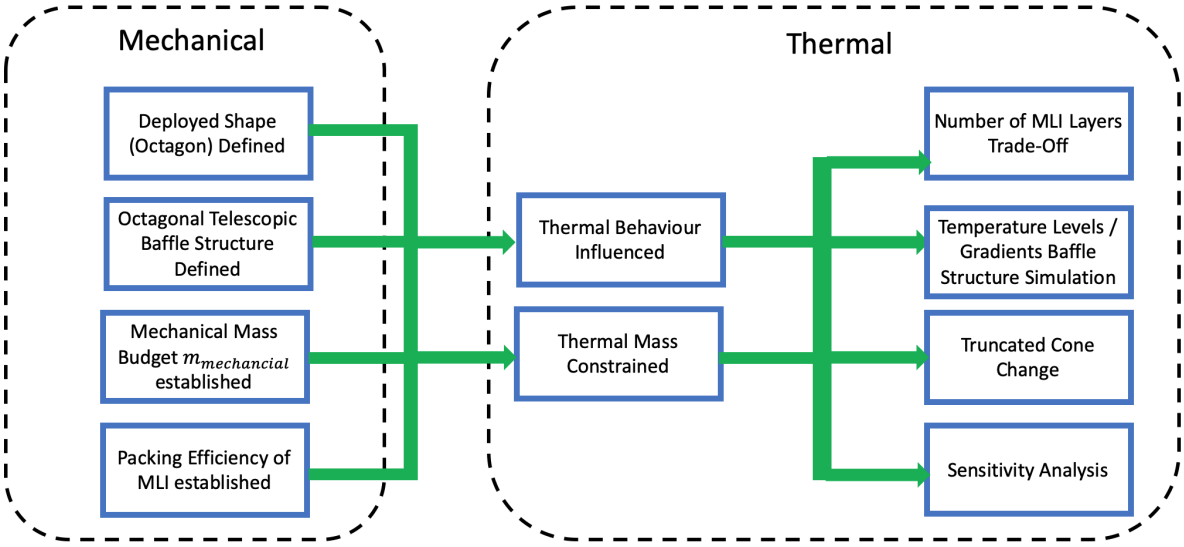

Figure 7.26: Influence of the thermal design on the mechanical design. These thermal design choices are input to start the mechanical design process, Chapter 7

8

Iterative Thermal Mechanical System Integration

After both the thermal- and mechanical design have been matured, a proper iterative integration needs to happen. Based on Figure 7.26, the following iterative design processes have to be performed within this section.

Table 8.1: Summarized iterative design processes for this chapter. The identifier for each process starts with IDP (Iterative Design Process)

Iterative Design Process (IDP)
IDP 1. New deployed octagonal shape **without truncated cone** has to be thermally verified, since the thermal results of Chapter 6 were that of a cylindrical baffle
IDP 1.1 Telescopic baffle structure can be integrated in thermal design **without addition of a truncated cone**. Investigate best placement: MLI inside or outside of telescopic booms by simulating and analyzing the nominal temperatures and temperature gradients of the telescopic structure.
IDP 1.2 Thermal performance of MLI for octagonal shape **without addition of a truncated cone** can be calculated. This serves as input for the MLI trade-off.
IDP 2. MLI trade-off. Possible since mass of deployment system $M_{mechanical}$ is now defined (5.68 kg) and the packing efficiency of MLI is calculated. Both set constraints on the numbers of MLI layers that can be used.
IDP 3. New deployed octagonal shape **with truncated cone** has to be thermally verified. The truncated cone as defined earlier has to be changed so that it fits the octagonal shape.
IDP 3.1 Investigate the best lay-up of the truncated cone (aspect angle, coating) that results in best thermo-elastic result
IDP 3.2 Telescopic baffle structure integrated in thermal design **with addition of a truncated cone**. Investigate if performance increases with addition of truncated cone. Also investigate temperature effects on telescopic deployment: temperature gradients result in thermo-elastic deformations and corresponding stresses in the booms. It is analyzed if this negatively influences the deployment
IDP 4. Sensitivity analysis of the deployed thermal configuration for both the nominal temperatures and the thermo-elastics.
IDP 5. Additional solutions to decrease the temperature gradients

The updated thermal analyses can be performed. As stated at the beginning of this chapter, the new octagonal shape has to be verified again in ESATAN-TMS. Additionally, the number of MLI layers has to be updated and a proper trade-off can be made since the mass of the mechanical system $M_{mechanical}$ is established.

8.1. IDP 1: Thermal Analysis - Octagonal Shape Without Truncated Cone

The cylindrical thermal model made in ESATAN-TMS has to be updated to the octagon shape due to the mechanical deployment system. This will change the thermal behavior, in terms of a change in thermal performance objective as well as nominal temperatures. Most importantly, the effective emissivity and conductivity change based on different exposed areas and temperature levels of the inner- and outer layer of the baffle. In Figure 8.1 the updated octagonal shape is displayed.

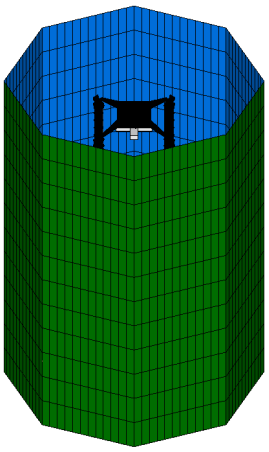

Figure 8.1: Thermal model of the octagonal shape without truncated cone

Number of layers	Effective Emissivity	Effective Conductivity
1	0.04241	0.24578
2	0.02997	0.17367
3	0.02446	0.14174
4	0.02118	0.12272
5	0.01894	0.10974
6	0.01728	0.10016
7	0.01600	0.09271

Figure 8.2: Updated values for the effective emissivity and conductivity as a function of the number of layers of MLI. Updated for the octagonal shape, without addition of a truncated cone as displayed in Figure 8.1

A very important remark is that the effective emissivity and conductivity change due to different exposed areas and a probable change in temperature levels of the inner- and outer layer of MLI. Therefore, thermal analyses have to be performed for **updated** values of effective emissivity and conductivity.

The updated values of MLI are calculated using the Doenecke method, [26], similar to Section 6.5.1. The calculations are performed in MATLAB of which the corresponding code is shown in Appendix **??**. The effective emissivity and conductivity values for 1-7 layers of MLI are shown in Figure 8.2. More layers than 7 will exceed the mass budget of 15 kg for the baffle and are therefore not taken into account. See Appendix F for the complete overview of the thermal results for 1 layer up to 7 layers. Here, only the conclusion of those analyses per layer is shown.

The relation between the effective emissivity and number of layers is now:

$$\epsilon_{eff} = 0.0424 \cdot N^{-0.501} \tag{8.1}$$

8.1.1. IDP 1.1: Thermal Performance Baffle Telescopic Structure - Without Truncated Cone

For the modelling, simulation and analysis of the thermo-mechanical behaviour of the telescopic boom structures, it is important to state the assumptions:

Table 8.2: Summarized iterative design processes for this chapter. The identifier for each process starts with IDP (Iterative Design Process)

Telescopic Boom Structure - Thermal Assumptions
Assumption 1. Telescopic booms have little to no conductive interface to each other (minimal interface contact point) → worst case modelled where no conduction takes place
Assumption 2. Telescopic booms can be modelled on the inside or outside of the MLI. When placed on the inside, it will interact with the DST sub-systems, and shall also use the MagicBlack coating to prevent stray-light entering the optical path. When placed on the outside, it can be coated with a low absorptance, high emittance coating to not absorb much Solar flux. Both options are modelled and simulated.

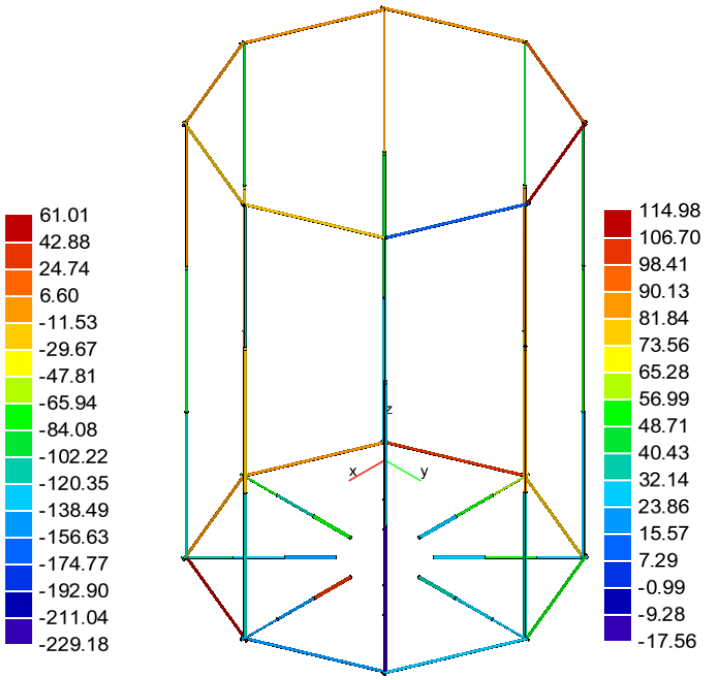

Figure 8.3: Thermal model including baffle telescopic boom structure, placed outside of the MLI

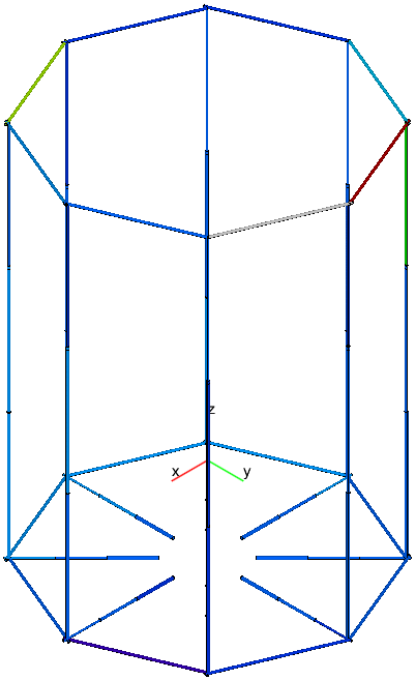

Figure 8.4: Thermal model including baffle telescopic boom structure, placed inside of the MLI. The telescopic booms are made red for better visibility

Table 8.3: Results of inside and outside placement of the baffle structure

Placement of Baffle Structure	**Argumentation/Comment**
Modelling Properties	
Baffle structure inside (MLI outside)	Coating: MagicBlack: to prevent stray-light entering the optical path. Material: M55J (properties in Table 7.14)
Baffle structure outside (MLI inside)	Coating: FEP/VDA as it has a low absorptance/high emittance. Material: M55J (properties in Table 7.14)
Results Inside-Outside Placement	
Baffle structure inside (MLI outside)	Better temperature distribution of all booms: The maximum temperature of the upper support telescopic boom is 115.0 ° C, while the minimum temperature is -17.6 ° C. Blue colored booms (Figure 8.3): average temperature of around 10 ° C. Maximum temperature of 115.0 ° C is that of the structural support boom on the top, and only holds for this single boom as can also be seen in Figure 8.5. This is likely to be decreased when a truncated cone is added (Section 8.3.2.)
Baffle structure outside (MLI inside)	Maximum temperature is 61.0 ° C and the minimum temperature is -229.2 ° C: significantly higher difference in max/min temperatures than when the MLI is modelled outside of the baffle. Temperature levels widely spread out for various booms (not consistent): see Figure 8.4

Because of the argumentation in Table 8.3, it is chosen to attach the MLI on the outside, so that the baffle structure is placed on the inside and is shielded by the MLI it is meant to hold. A further conclusion of these temperature levels of the telescopic booms is given after it is integrated with the truncated cone, Section 8.3.2.

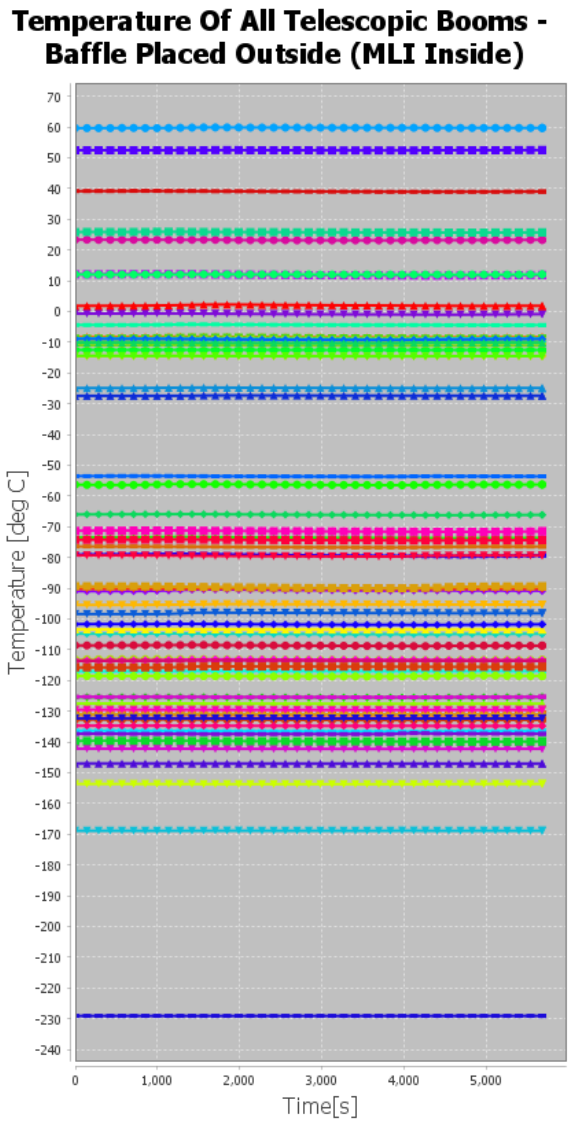

Figure 8.5: Thermal model including baffle telescopic boom structure, placed outside of the MLI

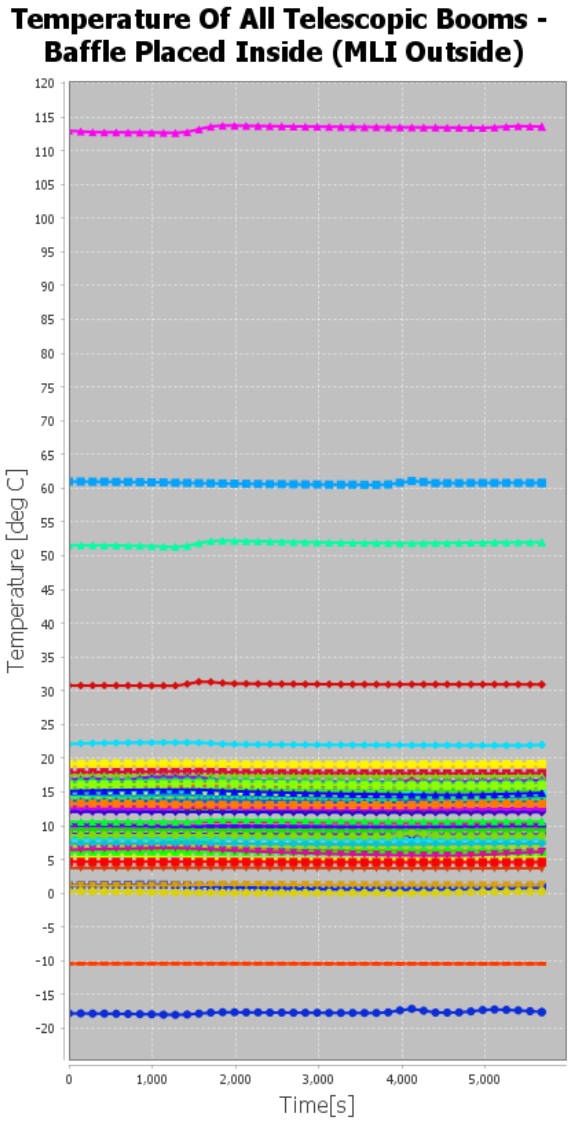

Figure 8.6: Thermal model including baffle telescopic boom structure, placed inside of the MLI. The telescopic booms are made red for better visibility

Table 8.4: Difference between the actual athermal value (translation only) and the requirement, which is the value that it should have for that particular number of MLI in order to meet the in-orbit drift budget of 2 µm, based on Equation 4.3. The difference should be 0 or lower, since then the system is athermalized and the translation of the booms and rods conforms to the in-orbit drift budget of 2 µm. Tabular form

Translation					
Number Of MLI Layers	A. $\Delta T_{booms,avg}$	B. $\Delta T_{rods,avg}$	C. $(\frac{\Delta T_{booms,avg}}{\Delta T_{rods,avg}})_{actual}$ (= A/B)	D. $(\frac{\Delta T_{booms,avg}}{\Delta T_{rods,avg}})_{required}$	Δ (= C - D)
1	3.5	0.4	9.5	≤ 5.4	4.2
2	3.0	0.3	8.9	≤ 5.7	3.3
3	2.8	0.3	8.7	≤ 5.9	2.8
4	2.6	0.3	8.4	≤ 6.0	2.3
5	2.5	0.3	8.3	≤ 6.2	2.1

8.1.2. IDP 1.2: Thermal Performance MLI Layers

In-Orbit Translation Drift Budget (2 µm)

Since for every added layer of MLI the change in temperature of the rods, $\Delta T_{rods,avg}$ decreases, the value

for $(\frac{\Delta T_{booms,avg}}{\Delta T_{rods,avg}})_{required}$ increases (see Equation 4.3), resulting in a less tight athermalisation requirement. Furthermore, for every added layer of MLI the $\Delta T_{booms,avg}$ also decreases, even more than the $\Delta T_{rods,avg}$. This means that the fraction $(\frac{\Delta T_{booms,avg}}{\Delta T_{rods}})_{actual}$ decreases for increasing number of MLI layers. Since the actual value decreases and the requirement increases for every added MLI layer, there is a point in which both the actual and requirement value are equal, resulting in a difference between them of 0. The values for 1 - 5 layers of MLI is shown in Table 8.4. These values are plotted in Figure 8.7.

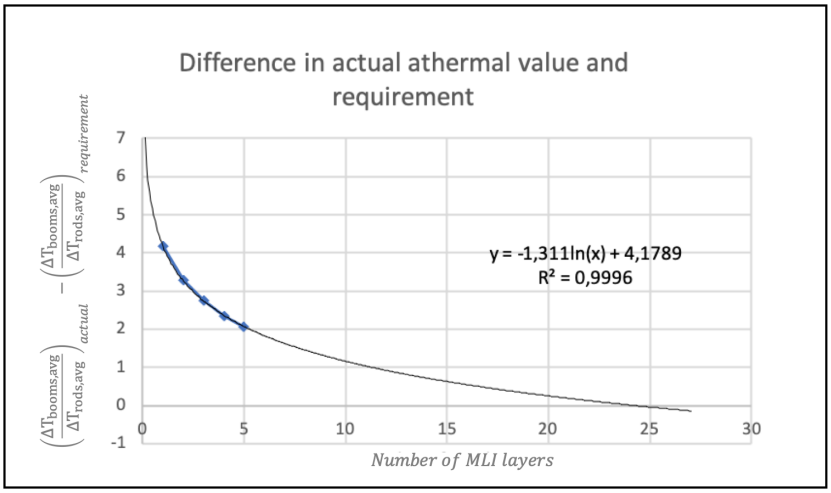

Figure 8.7: Difference between the actual athermal value (translation only) and the requirement, which is the value that it should have for that particular number of MLI in order to meet the in-orbit drift budget of 2 µm, based on Equation 4.3. The difference should be 0 or lower, since then the system is athermalized and the translation of the booms and rods conforms to the in-orbit drift budget of 2 µm.
Figure form

A trend-line can be established which gives a good algebraic fit to the data points. The following logarithmic function is used to fit the data points with a R^2 close to 1:

$$(\frac{T_{booms,avg}}{T_{rods,avg}})_{actual} - (\frac{T_{booms,avg}}{T_{rods,avg}})_{requirement} = \Delta = -1.311 \cdot \ln(N) + 4.1789 \tag{8.2}$$

In this equation, N is the number of MLI layers. To conform to the translational in-orbit drift budget of 2 µm, this Δ value should be zero, since then the actual fraction between the gradient of the booms and rods is equal to the requirement. Reverse engineering the number of MLI layers needed to meet the requirement:

$$N = e^{\frac{\Delta - 4.1789}{-1.311}} = e^{\frac{-4.1789}{-1.311}} \approx 24 \tag{8.3}$$

From Equation 8.3 it becomes clear that around 24 layers of MLI have to be chosen in order to make the system athermal so that the translational in-orbit drift budget of 2 µm is met.

Since the R^2 is 0.9996, which is a near-perfect estimation of a trend-line (R^2 of 1 is perfect), the trend-line equation, Equation 8.2, can be used for statistical evaluation with a high confidence level.

When looking at only the gradients in the booms and the corresponding elongation:

Table 8.5: Booms only

Translation of booms only		
Number Of MLI Layers	A. $\Delta T_{booms,avg}$	$(\Delta T_{booms,avg})_{required}$
1	3.5	≤ 1.4
2	3.0	≤ 1.4
3	2.8	≤ 1.4
4	2.6	≤ 1.4
5	2.5	≤ 1.4

For these values a similar trend-line can be established with a minimum deviation to the data points (R^2 close to 1). The following exponential function appears that matches to the data points in Equation 8.5:

$$\Delta T_{booms,avg} = -0.625 \cdot \ln(N) + 3.4765 \tag{8.4}$$

The requirement is that $\Delta T_{booms,avg}$ is less or equal than 1.416 to meet the in-orbit drift budget of 2 µm, when only the booms are taken into account. Again reverse engineering this to find the required amount of MLI layers:

$$N = e^{\frac{\Delta T_{booms,avg} - 3.4765}{-0.625}} = e^{\frac{1.416 - 3.4765}{-0.625}} \approx 27 \tag{8.5}$$

As can be seen in Equation 8.5 the required amount of MLI layers to make the elongation of only the booms adhere the 2 µm requirement is 27. This is close to the 24 layers for an athermal system, which included also the aluminium rods. Up next the rotational budget is checked:

In-Orbit Rotational Drift Budget (6 µrad)
The rotational budget is already met for all number of MLI layers, see the values of these analyses in Table 8.6, and Appendix F for the detailed version.

Table 8.6: Difference between the actual thermo-elastic value (rotation only) and the requirement, which is the value that it should have for that particular number of MLI in order to meet the in-orbit drift budget of 6 µrad. Tabular form

Rotation				
Number Of MLI Layers	$T_{boom,max} - T_{boom,min}$	$T_{boom,max} - T_{boom,min}$ requirement	$T_{rod,max} - T_{rod,min}$	$T_{rod,max} - T_{rod,min}$ requirement
1	0.7	≤ 2.3	0.2	≤ 0.3
2	0.6	≤ 2.3	0.2	≤ 0.3
3	0.6	≤ 2.3	0.2	≤ 0.3
4	0.5	≤ 2.3	0.2	≤ 0.3
5	0.5	≤ 2.3	0.2	≤ 0.3

Coatings
Since the maximal- and minimal nominal temperatures of all sub-systems as well as the baffle itself adheres to the thermal requirements, the chosen SiOx/VDA/Kapton coating remains.

Now, a proper MLI trade-off can be made, since the thermal performance of different numbers of MLI has been established in this section. This is input for the different criteria of the next section.

8.2. IDP 2: Trade-Off MLI

Table 8.7: Criteria for the trade-off of the numbers of MLI

MLI Trade-Off Criteria
Thermal Performance
Mass
Structural Integrity
Mechanical Folding Reliability
Debris Mitigation Reliability

8.2.1. Thermal Performance

It was found in Section 8.1 that the required number of MLI layers to make the booms adhere the 2 µm in-orbit drift budget is 27. Also, for the complete athermal system including the rods, the required amount of MLI layers is 24. However, there is not enough mass budget for 24 layers of MLI, since the mass budget for MLI depends on the mass budget requirement that shall not be exceeded (15 kg) as well as the structural integrity.

However, as was found in Equation 8.2, the thermal performance increases with increasing number of MLI layers, so this shall be maximized, given that the mass budget is adhered to and that the structural stowed eigenfrequency is ≥ 100 Hz.

8.2.2. MLI Mass Budget

The tight mass budget of 15 kg does not allow to use 24-27 layers of MLI. Based on the fully detailed mechanical design and thermal design, the total mass including 25% mass uncertainty margin is 11.59 kg. See Table 7.28. The MLI mass that is included in this value is 1.96 kg. Updating this value means that the maximum MLI mass budget is:

$$\begin{aligned}(M_{MLI} + M_{truncated,cone} + M_{baffle,structure} + M_{actuation}) \cdot 1.25 \leq 15\text{kg} \rightarrow \\ M_{MLI} = \frac{15}{1.25} - 2.77 - 2.73 - 1.82 = 4.69\text{kg}\end{aligned} \tag{8.6}$$

Note that this is an optimistic value despite the 25 % mass uncertainty, since additional fixation and mounting methods are not yet taken into account. The maximum amount of MLI layers that can be used to not exceed the 4.69 kg budget is **10** layers, since the MLI mass with 10 layers is 4.48 kg and that of 11 layers already is 4.89 kg.

However, the mass budget of 15 kg may not be leading the mass budget allocation for MLI, since from a structural integrity point of view the mass of MLI is important to be controlled as a too high MLI mass leads to a too low eigenfrequency. This is explained in the next section.

8.2.3. Structural Integrity (Eigenfrequency)

The eigenfrequency of the system is an important requirement that has to be adhered to in order to guarantee successfull launch survival as well as survival of operations. Both BAF-MEC-03-04 and BAF-MEC-07-06-03-1 eigenfrequency requirements have to be met. For the stowed eigenfrequency the radial configuration as defined in Chapter 7 is most stringent, but for the deployed configuration the axial configuration is most stringent due to its extreme increase in height.

First, it is calculated if 10 layers of MLI (maximum number of layers to conform to the ≤ 15 kg mass budget) results in a too low eigenfrequency. If so, the MLI mass needs to decrease. The results for 10 layers, as well other number of layers is summarized in Table 8.8.

Table 8.8: Results eigenfrequencies for MLI trade-off. Both stowed and deployed

Number of MLI layers [-]	**MLI Mass** [kg]	**Stowed Eigenfrequency** [Hz]	**Deployed Eigenfrequency** [Hz]
10 (maximum mass budget for ≤ 15 kg)	4.48	94.2	4.4
9	4.07	96.0	4.5
8	3.66	98.0	4.5
7	3.25	100.1	4.6
6	2.84	102.4	4.7
5	2.43	104.8	4.7

It can be seen in Table 8.8 that 10 layers of MLI with a MLI mass of 4.48 kg results in a too low first stowed eigenfrequency: 94.2 Hz which is < 100 Hz (requirement). Therefore, the MLI mass needs to decrease. The maximum number of MLI layers that can be used to conform to the ≥ 100 Hz budget is **7** layers.

The conclusion is that a maximum of **7** layers can be used to ensure the structural integrity. However, as attachment methods are not yet defined but do add mass to the system, the number of layers might decrease even more to 6 or 5 layers. Therefore, these eigenfrequencies for these number of MLI layers are also summarized in the same table.

8.2.4. Mechanical Folding Reliability

An important consideration for reliable deployment is the reliability of the mechanical folding. The question is what the optimal number of layers is to ensure reliable deployment of the MLI. From this it was concluded that MLI can be folded, **only** when the radius of curvature is not lower than the minimum bending radius (radius of curvature). Increasing the minimum bending radius also increases the stowed volume the baffle can reach, and therefore the optimal number of MLI layers can be deduced that still conforms to the stowed volume threshold requirement. This is summarized in Table 8.9

Table 8.9: Number of layers of MLI, corresponding minimum radius of curvature (bending radius) in order to avoid that the yield strength of MLI is exceeded, packing thickness and corresponding stowed volume based on the added packing thickness of MLI. All related to the foldability of MLI **when folded once**

N* of MLI Layers N	**Minimal Radius of Curvature** ρ **[m]**	$\frac{N^3}{\rho}$	**Packing Thickness** [m]	**Stowed Volume** [m^3]
1	$6.34 * 10^{-7}$	1.58	1.9	0.86
2	$5.08 * 10^{-6}$	1.58	11.1	0.89
3	$1.71 * 10^{-5}$	1.58	35.5	0.97
4	$4.06 * 10^{-5}$	1.58	82.7	1.14
5	$7.93 * 10^{-5}$	1.58	160.3	1.44
6	$1.37 * 10^{-4}$	1.58	275.8	1.96
7	$2.18 * 10^{-4}$	1.58	436.9	2.82

The conclusion is that a maximum of 5 layers can be used for the MLI to ensure that the stowed volume threshold requirement of 1.5 m^3 is met, as the packing thickness of MLI increases to the third power with increasing number of layers.

Furthermore, several comparable satellites can be used to verify the mechanical folding reliability. The most relevant one is the JWST, which consists of five Sun shield layers with similar lay-up of material as was discussed in the author's literature study: Kapton E with aluminium coating and doped-silicon as an additional coating for the hottest outer layer. [3] As the JWST also deploys five layers of aluminized Kapton it can be concluded that five layers is the best option.

8.2.5. Debris Mitigation Reliability

Debris penetration is important to take into account, especially since the baffle is the exterior shield of the DST. Also debris is located in mostly high inclination orbits, so important to take into consideration for the DST with an orbital inclination of 97.4 degrees.

MLI with less than 5 layers (constraint due to packing thickness) will most likely be pentrated by medium sized debris: "a 0.06 g/cm2 thermal blanket is easily penetrated by a 0.4 mm diameter aluminum spherical projectile impacting normal to the blanket at 7 km/s. This blanket consists of an outer layer of glass-teflon fabric (referred to as beta-cloth) followed by 20 layers of aluminized Mylar and a 0.05 mm thick Mylar back cover." [18]

However, the JWST also uses 5 Sun-shields with roughly the same material lay-up as discussed above. Its Sun-shield was also tested on hypervelocity impacts: "Hypervelocity impact tests up to 12 kilometers per second of meteoroid-like sand particles were performed on tensioned, irradiated membrane material at extreme hot and cold temperatures at Auburn University's Hypervelocity Impact Facility. The durability of the thin coatings was also demonstrated under representative ground handling and packaging/deployment environments. The strength and durability of membrane seaming joints and other design features were also tested under irradiated, extreme temperature environments, as was the resistance to tearing of the Kapton E. The materials passed all the tests." [15] From this source it is not stated what the outcome was of the hypervelocity impact tests, only that all materials passed all the tests. Passing such a hypervelocity test most likely still includes possible debris penetrations, only not resulting in catastrophic tears such that the thermal shielding performance did not degrade to a catastrophic extend.

It is hard to predict how many layers of MLI are needed for the DST to mitigate debris impacts, but it can at least be concluded that the debris impact can be mitigated with increasing number of layers. Therefore, the maximum number of MLI layers should be chosen that still conforms to the mass-, structural- and maximum packing thickness requirements: 5 layers.

As mentioned in the literature section of this thesis, a solution to mitigate orbital debris is the addition of a Whipple shield or stuffed Whipple shields. These seem promising as they have been extensively tested and have been used on satellites in the past such as the ISS . The simplest Whipple shield is a single wall Whipple shield which only consists of a thin bumper spaced a distance (stand-off) from the MLI. NASA considers aluminium of 2 mm thickness to be used as the thin bumper for the Whipple shield. [17] [18]. If a single wall Whipple shield of 2 mm aluminium is used for the octagonal baffle, an added mass to be expected is:

$$M_{whipple} = 8 \cdot H \cdot W \cdot t \cdot \rho = 8 \cdot 2.65 \cdot 0.7659 \cdot 0.002 \cdot 2780 = 90.3\text{kg} \tag{8.7}$$

This tremendously exceeds the mass budget of the entire baffle, as well as the DST and consequently is not

taken into account. However, it might be possible that the thickness of the Whipple shield can be lowered but this depends on the debris mitigation performance and thus needs to be optimized. This is left as a recommendation.

8.2.6. Conclusion MLI Trade-Off

5 layers of MLI are chosen for the following reasons:

1. A maximum of 5 layers of MLI can be used to conform to the $\leq 1.5\ m^3$ stowed volume threshold requirement. This is based on the maximum packing thickness of MLI with 5 layers when folded once (origami is often folded once but at different locations). Additionally, the JWST also uses 5 aluminized Kapton layers of MLI, meaning that this serves as a good reference case.

2. 5 layers of MLI fits well within the mass budget. The maximum number of layers of MLI to fit within the mass budget allocated for MLI (4.67 kg) was calculated to be **10**. Five layers, with a mass of 2.43 kg, therefore leaves room for additionall mass of hardware for attachments and interface points that are not designed yet.

3. The added mass of the 5 layers of MLI conforms to the stowed structural eigenfrequency requirement of $\geq$ 100 Hz: 104.7 Hz. Also the deployed eigenfrequency of 4.7 Hz is $\geq$ 0.9 Hz (requirement). The maximum number of MLI layers that can be used to still conform to the $\geq$ 100 Hz requirement is **7** layers.

4. Within the above mentioned constraints, the number of layers should be maximized to increase the thermal performance. More layers of MLI results in a better shielding of the instruments from external heat fluxes and lower thermal gradients. For an athermal system 24 layers of MLI are needed but due to the above mentioned reasons this is not feasible. Therefore, it is still best to choose the maximum number of layers that can be used to conform to the structural-, mass- and packing thickness requirements, which is 5 layers.

5. Within the above mentioned constraints, the number of layers should be maximized to increase the debris mitigation reliability. More layers results in a better shielding performance for debris and micro-asteroids. Although it is hard to say if the DST baffle will survive debris and micro-asteroids with 5 MLI layers, it can definately be concluded that its impact will reduce with increasing MLI layers as for every layer impact energy is absorbed.

The nominal temperatures of the octagonal shape with 5 layers of MLI, yet without addition of a truncated cone, is summarized in Table 8.10, and the corresponding thermo-elastic deformations are summarized in Table 8.11.

Table 8.10: Thermal parameters of octagonal shape - No truncated cone - 5 layers of MLI. Chosen in trade-off

Nominal Temperatures.				
Sub-System	**Max Temp. (° C)**	**Min Temp. (° C)**	**Requirement**	**Reference**
M2	15.2	15.0	$-20°C < T < 50°C$	BAF-T-01-03
Spider	0.3	-2.9	$-20°C < T < 50°C$	BAF-T-01-03
PMSS	8.5	5.6	$-20°C < T < 50°C$	BAF-T-01-03
M1	12.1	12.0	$-20°C < T < 50°C$	BAF-T-01-03
Top Hinge	14.0	0.4	$-20°C < T < 50°C$	BAF-T-01-03
Booms	6.5	4.1	$-20°C < T < 50°C$	BAF-T-01-03
Baffle Bottom Outside Avg	125	-100	$-250°C < T < 177°C$	BAF-T-02-01
Baffle Bottom Inside Avg	34	-17	$-250°C < T < 177°C$	BAF-T-02-01
Baffle Side Outside Avg	20	-69	$-250°C < T < 177°C$	BAF-T-02-01
Baffle Side Inside Avg	20	-22	$-250°C < T < 177°C$	BAF-T-02-01
Baffle Outside Max-Min	140	-70	$-250°C < T < 177°C$	BAF-T-02-01
Baffle Inside Max-Min	28	-26	$-250°C < T < 177°C$	BAF-T-02-01
Temperature Gradients				
Thermal Objective Terms	**Value**	**Requirement**	**Unit**	**Reference**
$\Delta T_{booms,avg}$	2.6	≤ 1.4	° C	Table 4.4
$\Delta T_{rods,avg}$	0.3	≤ 0.96	° C	Table 4.4
1. $\frac{\Delta T_{booms,avg}}{\Delta T_{rods,avg}}$	8.3	≤ 6.2. Perfect athermal = 1.483	-	Table 4.4
2. $T_{boom,max} - T_{boom,min}$	0.5	≤ 2.3	° C	Table 4.4
3. $T_{rod,max} - T_{rod,min}$	0.2	≤ 0.3	° C	Table 4.4
Thermal Design Objective (1+2+3)	8.9	-	° C	-

The thermo-elastic deformations due to the baffle with 5 layers of MLI without truncated cone are stated in Table 8.11:

Table 8.11: Thermo-elastic deformations of the octagonal baffle with 5 layers of MLI and without the addition of a truncated cone. Based on linear thermo-elastics.

	In-Orbit Drift Budget (requirement)	**Thermo-Elastic Deformation Booms**	**Thermo-Elastic Deformation Rods**	**|Athermalized M2|**
Translation	2 µm	3.5 µm	0.6 µm	2.9 µm
Rotation	6 µrad	1.3 µrad	3.2 µrad	1.9 µrad

8.3. IDP 3: Thermal Analysis - Octagonal Shape With Truncated Cone

The truncated cone near M2 is added in this section. A truncated cone as a shape was concluded as a good rule of thumb for stray-light mitigation for Cassegrain telescopes in specific: [97]. Since the baffle shape is octagonal instead of cylindrical, the shape also changes. However, it is still being referred to as a truncated cone. The purpose of adding a truncated cone is threefold:

1. Creating a more stable thermal environment to conform to the in-orbit drift budget. The translational term is crucial, since its requirement is not yet met. In particular decreasing the $\Delta T_{booms,avg}$ so that also $\frac{\Delta T_{booms,avg}}{\Delta T_{rods,avg}}$ will be decreased.
2. Decreasing temperatures of telescopic boom structure (especially the 115.0 ° C of the upper support structure) and therefore serving as a second layer of insulation for the telescopic boom structures
3. Baseline for mitigating stray-light

See Table 6.16 for the full overview of requirements for the truncated cone based on literature and Chapter 4. These thermo-optical reflectance requirements set a tight budget on which coatings can be used that

adhere to the high absorptivity requirement in both UR and IR regime. The absorptivity shall be ≤ 0.07 and the emissivity shall be ≤ 0.02. A flat reflector coating therefore has to be chosen. According to the NASA Solar Absorptance and Thermal Emittance of Some Common Spacecraft Thermal-Control Coatings, [48], only Vapor Deposited Silver (VDS) adheres to these requirements, as it has an absorptivity of 0.04 and emittance of 0.02. Furthermore, VDS was also considered for the JWST telescope mirror coatings for the same reflectance criteria. However, protected gold was eventually chosen as it yields a more robust design. [56] VDA almost adheres to the requirements: it has an absorptivity of 0.08 and emittance of 0.02.

The problem with VDS is that it can outgas, as was already seen in the outer coating trade-off in Chapter 6. The proposed solution is an added layer of Silicon Oxide to prevent outgassing. However, this is similar to having a SiOx/VDA/Kapton lay-up as was chosen for the MLI outer coating. Therefore, from a pragmatic point of view, both pure VDS and SiOx/VDA/Kapton are the only options for the coating of the truncated cone.

Furthermore, one of the requirements is that the aspect angle of the baffle shall be ≤ 35 deg. Therefore, only discrete angles between 0 and 35 degrees are evaluated: 0, 10, 20, 30 and 35 degrees.

The only two design parameters that are going to be used are the angle of impact and the outer coating for absorption/reflection criteria. The shape is already determined, since it has to conform to the octagonal shape of the deployment mechanism. The thickness and material of the baffle is driven by the mass budget. The thickness and material determine the specific heat and mass of the material, but as the absorption of the truncated cone in IR and UV spectrum is very low (0.02 and 0.04 for VDS and 0.14 and 0.17 for SiOx/VDA/Kapton), not much heat will be absorped and therefore little influence on the thermal system is expected. However, the sensitivity to this is tested in the sensitivity analysis of Section 8.4. The material of the truncated cone is designed to be the same as the baffle structure: M55J with the same properties as of Table 7.14.

The truncated cone as designed in ESATAN-TMS is shown in Figure 8.8 and the implementation of this truncated cone in the octagonal baffle for different aspect angles (0 degrees flat and 35 degrees maximum) is shown in Figure 8.9 and 8.10.

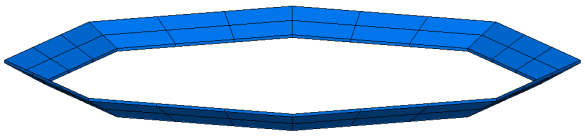

Figure 8.8: Visualization of the truncated cone near M2, used for both stray-light mitigation and improvement of the thermal stability to conform to the thermo-elastic in-orbit drift budgets

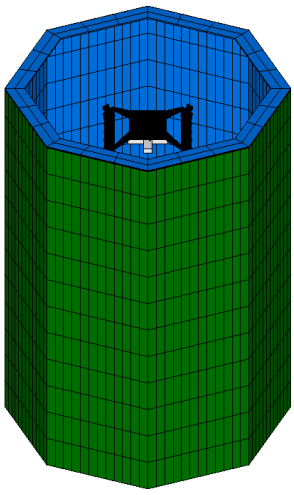

Figure 8.9: Thermal model of the octagonal shape with truncated cone: 0 degrees (flat) angle

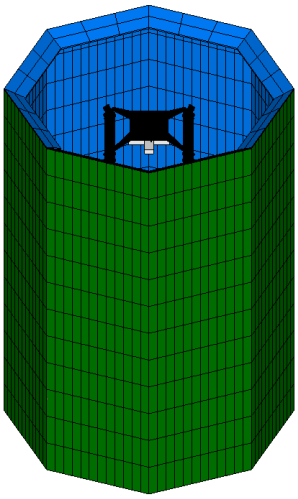

Figure 8.10: Thermal model of the octagonal shape with truncated cone: 35 degrees angle

With the defined truncated cone based on the mechanical design and the thermal requirements taken from the BELA mission [91] as stated at the beginning of Section 8.3 the thermal analyses can be run. A

distinction is yet again made between the nominal temperatures of the DST sub-systems and the thermo-elastics. The thermo-elastic results are first discussed, as these are crucial to meet the in-orbit drift budgets, while the nominal temperatures are not expected to change much.

8.3.1. IDP 3.1: Truncated Cone Lay-Up Investigation

The best lay-up in terms of aspect angle and coatings of the truncated cone is analyzed in this section. The results are benchmarked based on their thermo-elastic performance. The reason being is that the nominal temperatures of the DST sub-systems are not as sensitive to changes in the design as the temperature gradients. Also, the temperature gradient requirements are still not met. Therefore, the temperature gradients have to be decreased, possibly by the addition of a truncated cone.

Table 8.12: Thermo-elastics with and without the addition of a truncated cone. With addition of a truncated cone, two coatings and 5 different aspect angles are analyzed.

Translation					
Without Truncated Cone (See Table 8.10)					
Layers of MLI	A. $\Delta T_{booms,avg}$	B. $\Delta T_{rods,avg}$	C. $(\frac{\Delta T_{booms,avg}}{\Delta T_{rods,avg}})_{actual}$ (= A/B)	D. $(\frac{\Delta T_{booms,avg}}{\Delta T_{rods,avg}})_{required}$	Δ (= C - D)
5	2.5	0.3	8.3	≤ 6.2	2.1
With Truncated Cone. Also 5 layers of MLI (conclusion of MLI trade-off)					
Angle	A. $\Delta T_{booms,avg}$	B. $\Delta T_{rods,avg}$	C. $(\frac{\Delta T_{booms,avg}}{\Delta T_{rods,avg}})_{actual}$ (= A/B)	D. $(\frac{\Delta T_{booms,avg}}{\Delta T_{rods,avg}})_{required}$	Δ (= C - D)
Coating = Vapor Deposited Silver					
0	2.5	0.3	8.6	≤ 6.5	2.3
10	2.4	0.3	8.1	≤ 6.2	1.9
20	2.6	0.3	9.3	≤ 6.6	2.7
30	2.5	0.3	9.5	≤ 6.9	2.6
35	2.5	0.3	9.7	≤ 7.0	2.7
Coating = SiOx/VDA/Kapton					
0	2.4	0.3	8.7	≤ 6.7	2.0
10	2.3	0.3	8.3	≤ 6.6	1.7
20	2.4	0.3	9.2	≤ 7.0	2.2
30	2.3	0.2	9.3	≤ 7.2	2.1
35	2.4	0.3	9.4	≤ 7.1	2.3

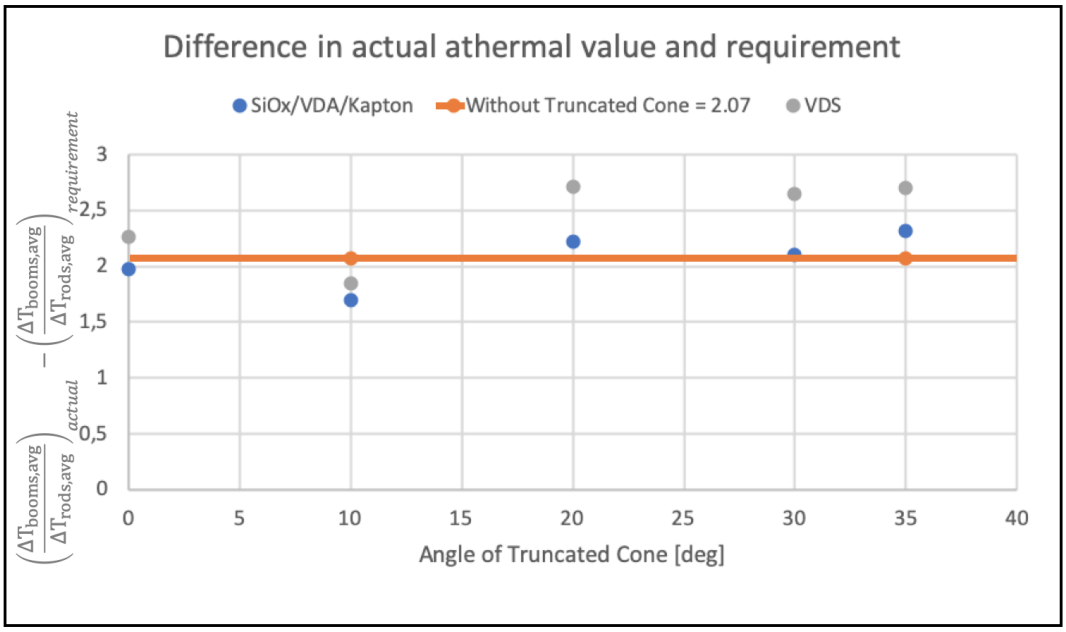

Figure 8.11: Result of shape optimization as a function of different angles of the truncated cone in blue and the reference baffle without truncated cone in orange: Difference between the actual ahtermal value (translation only) and the requirement, which is the value that it should reach to meet the in-orbit drift budget of 2 µm.

Table 8.13: Nominal temperatures and temperature gradients of octagonal shape with truncated cone (10 degrees aspect angle + SiOx/VDA/Kapton coating) and 5 layers of MLI

Nominal Temperatures.				
Sub-System	**Max Temp. (° C)**	**Min Temp. (° C)**	**Requirement**	**Reference**
M2	14.2	14.0	$-20°C < T < 50°C$	BAF-T-01-03
Spider	2.8	0.2	$-20°C < T < 50°C$	BAF-T-01-03
PMSS	8.7	6.1	$-20°C < T < 50°C$	BAF-T-01-03
M1	12.7	12.7	$-20°C < T < 50°C$	BAF-T-01-03
Top Hinge	12.8	0.0	$-20°C < T < 50°C$	BAF-T-01-03
Booms	6.8	4.5	$-20°C < T < 50°C$	BAF-T-01-03
Baffle Bottom Outside Avg	125	-100	$-250°C < T < 177°C$	BAF-T-02-01
Baffle Bottom Inside Avg	34	-16	$-250°C < T < 177°C$	BAF-T-02-01
Baffle Side Outside Avg	20	-67	$-250°C < T < 177°C$	BAF-T-02-01
Baffle Side Inside Avg	21	-19.5	$-250°C < T < 177°C$	BAF-T-02-01
Baffle Outside Max-Min	140	-70	$-250°C < T < 177°C$	BAF-T-02-01
Baffle Inside Max-Min	30	-22	$-250°C < T < 177°C$	BAF-T-02-01
Baffle Telescopic Structure	42.1	1.0	$T_{M55J,max} = 104°C$	[67]
Temperature Gradients				
Thermal Objective Terms	**Value**	**Requirement**	**Unit**	**Reference**
$\Delta T_{booms,avg}$	2.3	≤ 1.4	° C	Table 4.4
$\Delta T_{rods,avg}$	0.3	≤ 0.96	° C	Table 4.4
1. $\frac{\Delta T_{booms,avg}}{\Delta T_{rods,avg}}$	8.3	≤ 6.6. Perfect athermal = 1.483	-	Table 4.4
2. $T_{boom,max} - T_{boom,min}$	0.6	≤ 2.3	° C	Table 4.4
3. $T_{rod,max} - T_{rod,min}$	0.2	≤ 0.3	° C	Table 4.4
Thermal Design Objective (1+2+3)	9.1	-	° C	-

It can be seen in Table 8.12 and Figure 8.11 that the thermo-elastic performance only increases when adding a truncated cone under a 10 degree aspect angle. Also, the SiOx/VDA/Kapton outperforms the VDS coating from a thermal-mechanical perspective. For this best result, the nominal temperatures of the DST sub-systems are analysed. All nominal temperature requirements are met. Note that in the nominal temperature table also the nominal temperature limits of the baffle telescope are summarized. This result is touched upon in Section 8.3.2

The corresponding thermo-elastic deformations for the baffle with 5 layers of MLI and addition of a 10 ° SiOx/VDA/Kapton coated truncated cone are summarized in Table 8.14. Again, the in-orbit rotational drift budget is met but not the translational in-orbit drift budget. This will be further improved later in this thesis.

Table 8.14: Thermo-elastic deformations of the octagonal baffle with 5 layers of MLI and with the addition of a truncated cone. Based on linear thermo-elastics.

	In-Orbit Drift Budget (requirement)	**Thermo-Elastic Deformation Booms**	**Thermo-Elastic Deformation Rods**	**|Athermalized M2|**
		Without Truncated Cone		
Translation	2 µm	3.5 µm	0.6 µm	2.9 µm
Rotation	6 µrad	1.3 µrad	3.2 µrad	1.9 µrad
		With Truncated Cone		
Translation	2 µm	3.2 µm	0.6 µm	2.7 µm
Rotation	6 µrad	1.5 µrad	4.1 µrad	2.6 µrad

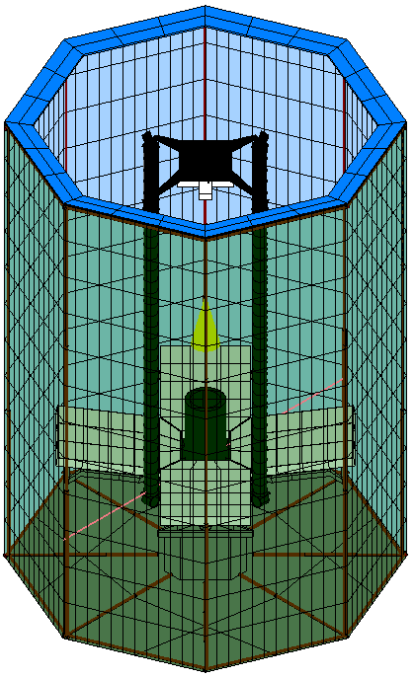

Figure 8.12: Thermal model of baffle telescopic boom structure, placed inside of the MLI and with addition of the 10 degrees aspect angle truncated cone with SiOx/VDA/Kapton coating

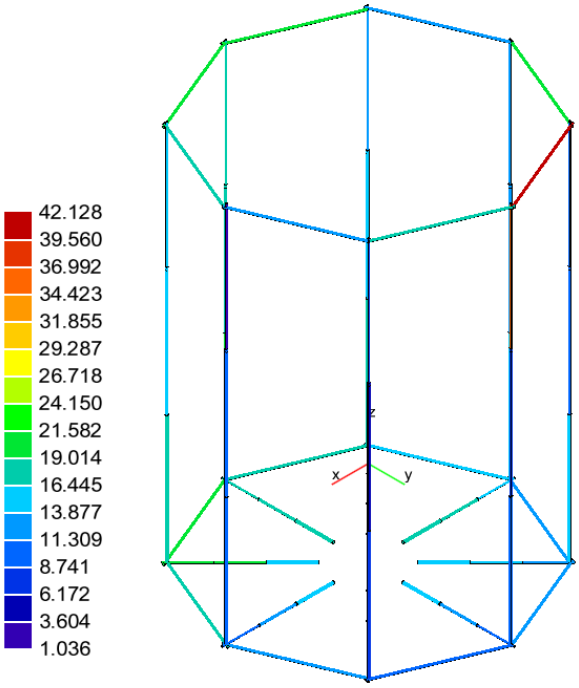

Figure 8.13: Nominal temperature result of the telescopic booms. The temperatures are much better than without the addition of a truncated cone

8.3.2. IDP 3.2: Thermal Performance Baffle Telescopic Structure - With Truncated Cone

The octagonal telescopic structure was already modelled in ESATAN-TMS and analysed in Section 8.1.1 for the baffle without the addition of a truncated cone. It was concluded that it is best to place the baffle structure on the inside of the MLI, so that the MLI is placed outside of the baffle structure and can therefore simultaneously shield the structure and DST sub-systems at the same time. However, since the baffle structure is placed on the inside, the coating shall adhere to the stray-light requirement that all hardware in the line of sight to the optical elements have a highly absorptive coating to prevent reflected stray-light entering the optical path. Therefore, its coating is MagicBlack with an absorptivity of 0.93 and emissivity of 0.84. This brings

about that it absorbs most of the impinged Solar- and Albedo flux due to its high absorptivity and IR flux due to its high emissivity. Especially the booms that are not shielded by the MLI, such as the uppor support structures. For this reason, the temperature of one of the upper support structure is high: 115.0 ° C. This temperature can be decreased due to the presence of the truncated cone. The truncated cone will, additional to mitigating stray-light and decreasing the thermal gradients in the booms and rods, also serve as a second layer of insulation to decrease the telescopic boom structure temperatures. See Figure 8.12 for the DST baffle model with baffle structure placed inside of the MLI (MLI outside) and truncated cone. The truncated cone is that of most optimized configuration: 10 degrees aspect angle and SiOx/VDA/Kapton coating.

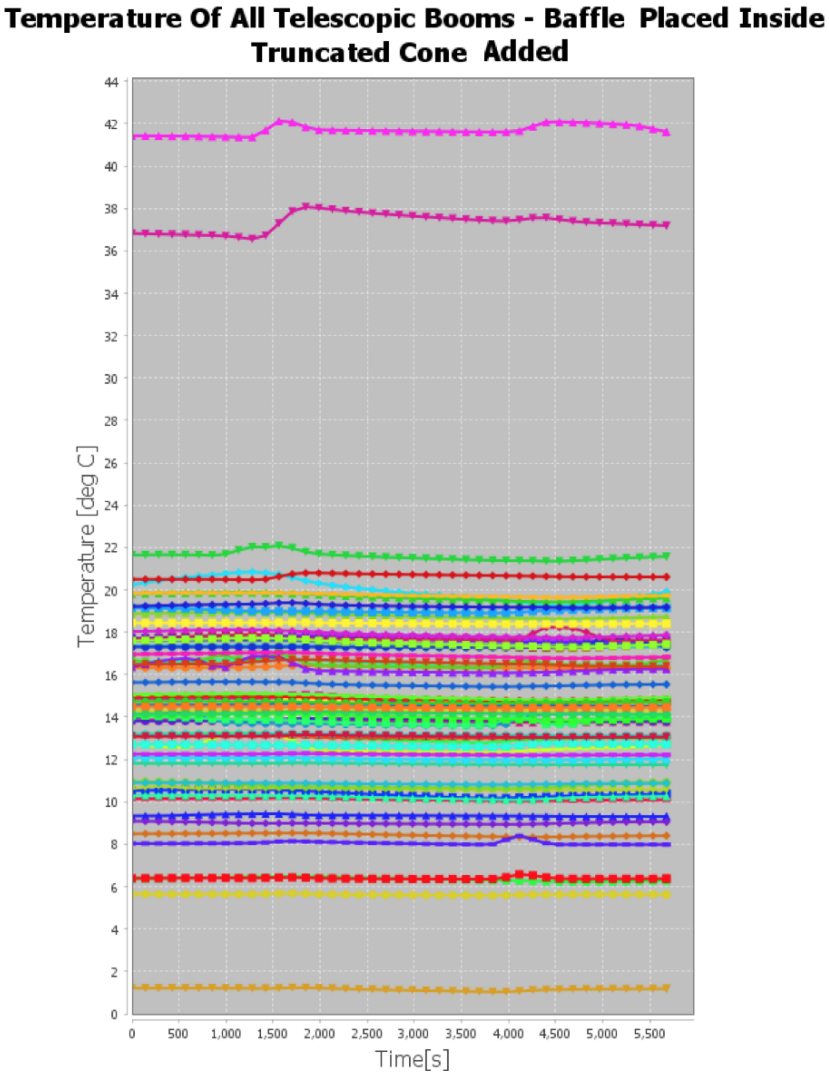

Figure 8.14: Corresponding temperature levels plotted as a function of time for one orbital period for all telescopic boom structures.

General Conclusion Nominal Temperatures Baffle Structure

Much change is visible in the temperature levels of the baffle telescopic boom structure. The maximum temperature of the upper support structure decreases from 114.7 ° C to 42.1 ° C and the minimum temperature increases from -17.6 ° C to 1.0 ° C. The total difference between maximum and minimum temperature therefore decreases from 132.5 ° C to 41.1 ° C.

From a thermal-mechanical point of view, the maximum service temperature of M55J carbon fibre is dependent on the glass transition temperature (T_g) in which a change of state is apparent. For epoxy-based composites the glass transition temperature lies around 100 to 180 ° C, and above 250 ° C charring takes place for epoxy. As M55J is an epoxy-based composite, similar temperature rule of thumbs apply as well. More research shows that for 36%-M55J-140 GSM the maximum service temperature is 104 ° C. [67] Therefore, the maximum temperature of 42.1 ° C conforms to this maximum service temperature.

Furthermore, it was stated in 7.5.2 that Delrin-Acetal might be used as a coating for the inner telescopic booms to reduce friction, as it is often used for applications in which low friction is required. It was concluded that Delrin-Acetal is not useful to use for the complete baffle structure, as it has a too low $\frac{E}{\rho}$ which would yield in low eigenfrequencies. However, it could be used as an inner coating, but this is left as a recommendation. The only objective statement that can be made in this section however is that if Delrin-Acetal is used as a coating, it has to adhere to specific temperature limits: -40 ° C to +120 ° C. [28] It can be concluded from the nominal temperatures of the baffle structure that this temperature requirement is met, as the maximum temperature of the baffle structure is 42.1 ° C and the minimum temperature is around 1 ° C. So, the recommendation that Delrin-Acetal can be used holds.

Temperature Effects on Telescopic Deployment

As can be seen there is a small temperature gradient for various telescopic booms. The maximum gradient as can be seen from Figure 8.14 is around 2 ° C. This will cause a change in area due to thermo-elasticity, which brings about stresses. As M55J is used, which is a CFRP with a negative CTE, the area will shrink. This is actually an advantage, since when the area of the boom shrinks, the area margin/clearance between telescopic booms becomes larger which results in a better deployability of the baffle as the contact and thus the friction decreases. However, the clearance shall not be too high since this will decrease the eigenfrequencies.

The worst case is that one outer telescopic boom experiences a temperature gradient of 2 ° C and thus a decrease in area, while its inner telescopic boom does not experience any gradient so its area stays the same. The change in area due to this temperature gradient of 2 ° C of the outer boom is given by Equation 8.8:

$$\Delta A = A \cdot \alpha_A \Delta T = A \cdot \alpha_L \cdot \Delta T \tag{8.8}$$

M55J has a linear CTE of $\alpha_L = -1.1 \cdot 10^6 /^\circ$ C, and in the worst case that the temperature gradient applies for the boom with largest area (42.79 m^2 for a hollow cubical cross-section with an outer width of 20 mm and inner width of 18.9 mm according to 7.24), the change in area becomes:

$$\Delta A = A \cdot \alpha_L \cdot \Delta T = 42.79 \cdot -1.1 \cdot 10^6 \cdot 2 \cdot 2 = -0.000188276 \text{m}^2 \tag{8.9}$$

The area will thus shrink from 42.79 to 42.79 - 0.000188276 = 42.7898 m^2 This leads to different outer width/inner width. If the outer width remains the same (20 mm), then the inner width changes slightly:

$$B_{in,expansion} = \sqrt{-1 \cdot (42.898 - 400)} = 18.900005 \text{mm} \tag{8.10}$$

This change in inner width is extremely small and thus it can be concluded that the clearance between the booms does barely change. This then does not complicate the deployment. However, the temperature gradient still results in stresses. Assuming that M55J is an isotropic material, then the corresponding stress in the boom in worst case due to the 2 ° C is:

$$\sigma = E \cdot \epsilon = E \cdot \alpha_L \cdot \Delta T = 5.4 \cdot 10^{11} \cdot -1.1 \cdot 10^6 \cdot 2 = -1.19 \text{MPa} \tag{8.11}$$

In which E is the Young's modulus and from Chapter 7 it is known that for M55J this is equal to $5.4 \cdot 10^{11}$ Pa. The result is a negative stress value of -1.19 MPa, meaning that it is a compressive stress, which is logical as the CTE is negative. The compressive strength of -1.19 MPa is well below the compressive strength of 880 MPa and therefore these temperature gradients doe not cause any issue for the M55J baffle structure.

8.3.3. Conclusion Truncated Cone

As can be seen in Figure 8.11 and Table 8.12, adding a truncated cone is **not** very helpful in making creating a more stable thermal environment to conform to the 2 µm budget. In fact, only under an angle of 10 degrees, both coatings yield a slightly decreasing value for the difference in actual athermal value and the requirement: 1.7 for SiOx/VDA/Kapton and 1.9 instead of 2.1 for the model without the truncated cone.

Also, SiOx/VDA/Kapton is a slightly better coating to use from a thermo-elastics point of view than VDS, but it does not adhere to the thermo-optical stray-light requirements stated in the beginning since its absorptivity and emissivity is too high. However, it does prevent outgassing while nominal VDS does not.

The difference in maximum and minimum temperature of the aluminium rods of the spider, $\Delta T_{rods,avg}$ in general decreases with increasing impact angle of the truncated cone. This is probably due to the fact that IR radiation, which is diffuse radiation and therefore impacts from various angles, is prevented from direct reflection off the inner layer of MLI.

Also, according to Table 8.13, the inner temperature of the baffle sides are +30 to -26 ° C when adding the truncated cone under an aspect angle of 10 degrees with a SiOx/VDA/Kapton coating. This gradient of 30–22 = 52 ° C is lower than without the truncated cone (see Table 8.10): 28–26 = 54 degrees. This is a small gradient change of 2 ° C, but as the temperatures of the inner layer of the baffle are the determining radiative heat source ($Q = \sigma AT^4$) to the DST sub-systems (additional to the IR and Albedo flux from Earth) this is already beneficial. The same can be concluded from the inner bottom layer in which a difference of 1 ° C gradient is noted when using a truncated cone.

Contrary to the thermal gradients that correspond to the thermo-elastic deformations, much change is visible in the temperature levels of the baffle telescopic boom structure. The maximum temperature of the upper support structure decreases from 115.0 ° C to 42.1 ° C and the minimum temperature increases from -17.6 ° C to 1. ° C. The total difference between maximum and minimum temperature therefore decreases from 132.5 ° C to 41.1 ° C. This maximum temperature conforms to the maximum service temperature of M55J, which is found to be 104 ° C. Also, the thermo-elastics of the baffle structure due to a maximum gradient of 2 ° C result in low compressive stresses around -1.19 MPa, well below the 880 MPa compressive strength limit. Also, since M55J has a negative CTE, the booms shrink instead of expand. This does not harm the deployment, but only gives and advantage as more clearance will be present between the booms and thus less friction. Temperature effects on the baffle structure therefore do not play a role.

The real question is: is it worth it to add a truncated cone? Based on the thermal results it is not, since it merely adds mass of around 2.77 kg which also decreases the eigenfrequencies of the system in both stowed and deployed state without increasing the thermal stability. In fact it is also possible to add more layers of MLI whilst getting rid of the truncated cone to get the same thermal perspective when adding a truncated cone with 10 degrees impact angle and SiOx/VDA/Kapton coating.

The amount of MLI layers needed to get the same thermal performance as when adding the truncated cone with 10 degrees impact angle and SiOx/VDA/Kapton coating can be calculated using Equation 8.3:

$$N = e^{\frac{\Delta - 4.1789}{-1.311}} = e^{\frac{1.702 - 4.1789}{-1.311}} \approx 6.6 \rightarrow 7 \tag{8.12}$$

Thus, not 5 layers, but 7 layers of MLI is needed to get to the same thermal result. As 2 additional layers of MLI only lead to an increase of mass of 0.865 kg while the truncated cone weighs 2.766 kg it can quickly be realised that adding more layers of MLI is a better solution than adding a truncated cone.

However, adding a truncated cone is very useful to decrease the temperature levels of the baffle telescopic boom structures and to mitigate stray-light, as the primary function of the truncated cone is to mitigate stray-light. A truncated cone as a shape was also proposed by [97]. However, this functionality still has to be analysed and modelled.

Therefore, the truncated cone is useful and remains. The mechanical design including thermal results brings about a good first baseline for another student to start a stray-light analysis. The complicating factor of designing a stray-light cone that also deploys is one that is being accounted for in this thesis. As a recommendation once the stray-light analysis is made, a new trade-off between impact angle and coatings should be made that includes both stray-light results and thermo-elastic results. This is added as a recommendation. The sensitivity analysis as part of the next section also contains the truncated cone.

8.4. IDP 4: Thermal Sensitivity Analysis

A sensitivity analysis is crucial at this stage as there are still many design uncertainties. A preliminary sensitivity analysis was already performed for the thermal model in Section 6.7, but for this final sensitivity analysis the truncated cone is also added as it will be part of the baffle for stray-light purposes. The baffle height and width are also added as sensitivity parameters.

The parameters that are uncertain and also have a big impact on the thermal performance can be deduced from the analytical equations from Section 6.2. Based on that equation, the mass, specific heat and the ΔQ are driving the transient response. ΔQ is defined as the difference between the absorbed heat per node minus the total radiative heat coupling from that node to space: $\Delta Q = Q_{tot,n+1} - R_{tot,n+1}$ in which n is the time step. Both of these parameters are stated in Equation 6.13 and 6.14. In these equations it can be seen that $R_{tot,n+1}$ depends on the emissivity values of all surfaces, the effective emissivity/ conductivity of the MLI and several Gebhart factors which depend on geometrical parameters and emissivities. Additionally, for contacting surfaces not only radiation but also conduction is crucial. Since the conductive coupling $GL = \frac{k}{AL}$ scales linearly with the conductivity of the material, the conductivity of MLI material is taken into account

as well. The absorbed heat per node is dependent on the area and absorptivity (for Solar/Albedo heat flux) and emissivity (For IR flux) of that node. Furthermore, the mass depends on the density and volume of the MLI material. The volume depends on the thickness, width and height of the material (radius for cylindrical shape, but the sensitivity analysis is now performed for the chosen octagonal shape). Therefore, all these parameters are used for the sensitivity analysis.

In Table 8.15 the parameters are summarized that are input for the sensitivity analysis.

Table 8.15: Sensitivity analysis input parameters, including uncertainty margins and corresponding hot and cold worst cases

Parameter	**Uncertainty Margin**	**Worst Hot Case**	**Worst Cold Case**	**Nominal Value**	**Worst Hot Case Value**	**Worst Cold Case Value**
MLI						
Effective Conductivity [$\frac{W}{K}$]	25%	High	Low	0.1097	0.137	0.082
Effective Emissivity [-]	25%	High	Low	0.01894	0.0237	0.014
Density [$\frac{kg}{m^3}$]	20%	Low	High	146	116.8	175.2
Specific Heat [$\frac{J}{kgK}$]	15%	Low	High	1117.5	949.9	1285.1
Conductivity [$\frac{W}{mK}$]	20%	Low	High	0.1275	0.102	0.153
Inner Coating α [-]	5%	High	Low	0.93	0.977	0.884
Inner Coating ϵ [-]	5%	High	Low	0.84	0.882	0.798
Outer Coating α [-]	15%	High	Low	0.19	0.219	0.162
Outer Coating ϵ [-]	15%	Low	High	0.14	0.119	0.161
Thickness [mm]	35%	Low	High	0.7812	1.055	0.508
Baffle Height [mm]	0.5%	High	Low	2650	2663	2637
Baffle Width [mm]	1%	High	Low	765.9	758	774
Truncated Cone						
Density [$\frac{kg}{m^3}$]	20%	Low	High	1911	1528.8	2293.2
Specific Heat [$\frac{J}{kgK}$]	15%	Low	High	711.8	605.0	818.6
Conductivity [$\frac{W}{mK}$]	20%	Low	High	155.6	124.5	186.7
Coating ϵ [-]	15%	Low	High	0.14	0.119	0.161
Coating α [-]	15%	High	Low	0.19	0.219	0.162

Most of the uncertainty margins for each parameter from Table 8.15 are explained in Section 6.7 of Chapter 6, such as the effective conductivity/emissivity, MLI bulk density, specific heat and conductivity and absorptivity and emissivity of the inner and outer coating. However, the MLI thickness, baffle height and width and truncated cone bulk material and properties are not explained yet. Therefore, these remaining parameters are explained below.

MLI Thickness: Uncertainty Margin Rationale

The thickness does not vary much. The thickness does not change the through thickness radiative- nor conductive coupling (GL and GR), since no bulk calculation is performed here. The thickness only changes the in-plane conductivity GL values, as it has a linear relationship with the mass of the baffle and is linearly proportional to the number of layers of MLI. As the effective emissivity with an uncertainty margin of 25% is also linked to the number of layers of MLI, an uncertainty margin for the thickness can be calculated: the uncertainty margin for the effective emissivity is 25 %, meaning that the nominal value of 0.1894 increases to 0.023675 in the worst hot case. Matching this to the number of layers of MLI for the worst hot case using Equation 8.1, but then reverse engineered as shown in Equation 8.13:

$$N = (\frac{\epsilon_{eff}}{0.0424})^{\frac{-1}{0.501}} = (\frac{0.023675}{0.0424})^{\frac{-1}{0.501}} = 3.2 \tag{8.13}$$

Therefore, the uncertainty margin for the MLI thickness is $1 - \frac{3.2}{5} = 36\%$. This will be rounded of to a MLI thickness uncertainty margin of 35 %.

Baffle Heigth and Width: Uncertainty Margin Rationale

The geometrical height and width values depend on the deployment accuracy and reliability. For a telescopic boom system, the deployment accuracy is high as it contains a locking mechanism that locks all three booms in fixed position with high accuracy. For the booms of the octagonal shape an accuracy offset of no more than

± 10 mm is expected. This leads to an uncertainty margin for the baffle height of

$$H_{uncertainty} = (\frac{2660}{2650} - 1) \cdot 100\% \approx 0.38\% \tag{8.14}$$

And for the baffle width W, in which the $L_{parallel}$ and $L_{diagonal}$ are also increased with 10 mm from 795 to 805 mm and 766.6 to 776.6 mm respectively:

$$\begin{aligned} W = \sqrt{L_{parallel}^2 + L_{diagonal}^2 - 2 \cdot L_{parallel} \cdot L_{diagonal} \cdot \cos(45°)} \rightarrow \\ W_{uncertainty} = \frac{W_{increased}}{W_{old}} = (\frac{773.0}{765.9} - 1) \cdot 100\% \approx 0.93\% \end{aligned} \tag{8.15}$$

So to be conservative, the uncertainty margin of the baffle height is taken as 0.5 % and that of the baffle width is 1 %.

Truncated Cone Bulk Material and Coating Properties: Uncertainty Margin Rationale
The truncated cone has been thermally modelled in Section 8.3. In this section it was concluded that type of coating influences the thermo-elastics of the DST as well as the aspect angle. However, there is little to no uncertainty in the aspect angle, since this angle is fixed and is **not** deployed: the aspect angle in both stowed and deployed configuration is 10 degrees as can also be seen in Figure 7.19.

Therefore, only the bulk material and the coating are prone to uncertainties due to the same reasons as the change in bulk material properties / thermo-optical coating properties for the MLI. For this reason the same uncertainty margin is used: 15% for the emissivity and absorptivity of the coating and the specific heat, as well as 20% for the bulk density and conductivity.

8.4.1. Nominal Temperatures Sensitivity Analysis

The nominal temperatures of the DST are important to adhere to their nominal temperature requirement BAF-T-01-03 and BAF-T-02-01, even in the worst hot and cold cases.

In Table 8.16 it can be concluded that in both worst cases the temperature requirements are met. In the worst hot case, the maximum temperature of the baffle is that of the outside bottom: 167 ° C, which is well below the 177 ° C requirement. The lowest temperature, which is the case for the worst cold case, is also that of the outside of the MLI bottom: -105 ° C, which is far above the minimum temperature of -250 ° C to which aluminized Kapton can be continously exposed (BAF-T-01-03). All DST sub-systems are well within the $-20°C < T < 50°C$ range. The worst hot and cold cases are therefore not crucial for the nominal temperature levels, but are expected to influence the gradients in the booms and rods a lot, which influences the thermo-elastis of the athermalisation system. The thermo-elastics sensitivity analyis results is shown below and these are the results for the same worst hot and cold models as for the nominal temperatures from Table 8.16.

8.4.2. Thermo-Elastics Sensitivity Analysis

For the thermo-elastics, a sensitivity analysis is also made. The same sensitivity input, Table 8.15, is used as for the nominal temperatures. The only difference now are the requirements: the requirements change as well for the sensitivity analysis to take into account the worst case that the CTE of the booms/rods change, as well as their lengths/widths. Their nominal parameters were summarized in Table 4.4 but are summarized here again for convenience: Table 8.17. In this new table, the worst case requirements for the thermal gradients are also summarized of which the values are explained below.

Worst Case CTE: Uncertainty Margin Rationale
The CTE in worst case increases as then the total deformation increases too. For a CFRP, the CTE can increase due to fabric skewness, stacking sequence uncertainty, fiber and void volumes, layup angle, thermal cycling, temperature dependance and material viscoelasticity. [52] The CTE is also different for CFRP in different directions: axial or transverse. However, the axial deformation and thus axial CTE is of interest in this thesis as the axial in-orbit drift budget is smallest (2 µm). Based on research where the expected CFRP is compared to the measured CTE, a difference of 24% was measured. This value will be used as a worst case value, but rounded off to 30%. This leads to a CTE in worst case of $-1.04 \cdot 10^{-6}$ m/mK. [39] Aluminium is more predictable than CFRP: the CTE of aluminium could go up to $25.3 \cdot 10^{-6}$ m/mK for an exposure temperature up to 200 ° C and for a particiular aluminium alloy based on NIST data. [49]

Table 8.16: Nominal Temperatures exposed to worst cases as established with a sensitivity analysis. The latest, best version of the baffle is taken

Nominal Case.				
Sub-System	**Max Temp. (° C)**	**Min Temp. (° C)**	**Requirement**	**Reference**
M2	14.2	14.0	$-20°C < T < 50°C$	BAF-T-01-03
Spider	2.8	0.2	$-20°C < T < 50°C$	BAF-T-01-03
PMSS	8.7	6.1	$-20°C < T < 50°C$	BAF-T-01-03
M1	12.7	12.7	$-20°C < T < 50°C$	BAF-T-01-03
Top Hinge	12.8	0.0	$-20°C < T < 50°C$	BAF-T-01-03
Booms	6.8	4.5	$-20°C < T < 50°C$	BAF-T-01-03
Baffle Bottom Outside Avg	125	-100	$-250°C < T < 177°C$	BAF-T-02-01
Baffle Bottom Inside Avg	34	-16	$-250°C < T < 177°C$	BAF-T-02-01
Baffle Side Outside Avg	20	-67	$-250°C < T < 177°C$	BAF-T-02-01
Baffle Side Inside Avg	21	-19.5	$-250°C < T < 177°C$	BAF-T-02-01
Baffle Outside Max-Min	140	-70	$-250°C < T < 177°C$	BAF-T-02-01
Baffle Inside Max-Min	30	-22	$-250°C < T < 177°C$	BAF-T-02-01
Worst Hot Case.				
Sub-System	**Max Temp. (° C)**	**Min Temp. (° C)**	**Requirement**	**Reference**
M2	21.4	21.2	$-20°C < T < 50°C$	BAF-T-01-03
Spider	8.2	4.8	$-20°C < T < 50°C$	BAF-T-01-03
PMSS	22.8	18.6	$-20°C < T < 50°C$	BAF-T-01-03
M1	26.3	26.2	$-20°C < T < 50°C$	BAF-T-01-03
Top Hinge	18.2	5.0	$-20°C < T < 50°C$	BAF-T-01-03
Booms	16.1	12.8	$-20°C < T < 50°C$	BAF-T-01-03
Baffle Bottom Outside Avg	150	-90	$-250°C < T < 177°C$	BAF-T-02-01
Baffle Bottom Inside Avg	51	-5	$-250°C < T < 177°C$	BAF-T-02-01
Baffle Side Outside Avg	40	-56	$-250°C < T < 177°C$	BAF-T-02-01
Baffle Side Inside Avg	36	-13	$-250°C < T < 177°C$	BAF-T-02-01
Baffle Outside Max-Min	167	-59	$-250°C < T < 177°C$	BAF-T-02-01
Baffle Inside Max-Min	46	-16	$-250°C < T < 177°C$	BAF-T-02-01
Worst Cold Case.				
Sub-System	**Max Temp. (° C)**	**Min Temp. (° C)**	**Requirement**	**Reference**
M2	11.0	10.7	$-20°C < T < 50°C$	BAF-T-01-03
Spider	-0.9	-3.3	$-20°C < T < 50°C$	BAF-T-01-03
PMSS	-1.2	-3.1	$-20°C < T < 50°C$	BAF-T-01-03
M1	3.3	3.3	$-20°C < T < 50°C$	BAF-T-01-03
Top Hinge	8.5	-4.0	$-20°C < T < 50°C$	BAF-T-01-03
Booms	0.5	-1.3	$-20°C < T < 50°C$	BAF-T-01-03
Baffle Bottom Outside Avg	100	-110	$-250°C < T < 177°C$	BAF-T-02-01
Baffle Bottom Inside Avg	20	-22	$-250°C < T < 177°C$	BAF-T-02-01
Baffle Side Outside Avg	1	-78	$-250°C < T < 177°C$	BAF-T-02-01
Baffle Side Inside Avg	12	-23	$-250°C < T < 177°C$	BAF-T-02-01
Baffle Outside Max-Min	117	-83	$-250°C < T < 177°C$	BAF-T-02-01
Baffle Inside Max-Min	22	-26	$-250°C < T < 177°C$	BAF-T-02-01

Worst Case Length and Width: Uncertainty Margin Rationale

The length of the booms and rods barely change in worst case, as an aluminium rod of 0.0907 m can be accurately manufactured. The same holds for CFRP with a nominal length of 1.7657 m.

However, the width between the booms and between the rods are more likely to change in a worst case scenario due to mounting technique errors. For a worst case, the width decreases as then the rotation angle

becomes larger and the maximum allowed thermal gradient becomes lower. A difference of 5% is taken. This leads to a change in $L_{\text{Width Booms}}$ from 0.54 m to 0.513 m and $L_{\text{Width Rods}}$ from 0.11 to 0.1045 m.

The corresponding thermo-elastic deformations are summarized in the tables below. The thermo-elastic deformations for the nominal case were already calculated and are summarized in Table 8.14, but are again summarized below in Table 8.19 so that comparison between the nominal, worst hot case and worst cold case is easier.

As can be seen in Table 8.18, the thermo-elastics in translation are much better for the worst cold case than that of the nominal case. In fact, based on the requirement for athermalization that states that $\frac{\Delta T_{\text{booms,avg}}}{\Delta T_{\text{rods,avg}}}$ should be below 2.5 to conform to the in-orbit drift budget of 2 µm is met. The reason for this is that the effective emissivity and conductivity have decreased with 25%, which is the effect of an increasing number of MLI layers. It was already concluded that increasing the number of MLI layers improves the thermo-elastic stability since more MLI layers yields a lower difference in actual athermal value and required athermal value, see Table 8.4 and figure 8.7. However, for the worst cold case, the different in thermal gradient amongst the rods is high: 4.1 ° C, meaning that one rod has a larger gradient and thus deforms more than other rods. The corresponding maximum rotation angle is 89.9 µrad, which exceeds the 6 µrad budget by a great margin. The athermalized result is also not within the budget. The 4.1 ° C difference in temperature gradient of the rods is likely the effect of the lower baffle height for the worst cold case.

As can be concluded the nominal case performs quite well, as only the boom temperature gradient exceeds its budget. If this temperature gradient is lowered than the in-orbit drift budgets will all be met. The rotation budget is already met. However, in the worst cases the thermal gradients are lower than their requirements. For all cases this results in too large deformations that can not even accounted for using athermalization.

Therefore, several solutions are proposed to decrease the thermal gradients and hence the thermo-elastic deformations.

Table 8.17: Worst case thermo-elastic requirements used for the calculation of the performance in both the worst hot- and cold case (sensitivity analysis). The nominal thermo-elastic requirements are shown in Figure 4.4

Worst Case Requirements		
Parameter	**Booms**	**Rods**
Length [m]	1.7657	0.0907
α [m/mk]	$1.04 * 10^{-6}$	$25.3 * 10^{-6}$
L_{width} [m]	0.513	0.1045
Thermal Requirements		
Translation: L_{max} = 2 µm		
$\Delta T_{max} = \frac{\Delta L_{max}}{\alpha * L}$ [° C / K]	1.1	0.87
$(\frac{\Delta T_{booms,avg}}{\Delta T_{rods,avg}})_{perfect,athermal}$ [-]	1.250	
$(\frac{\Delta T_{booms,avg}}{\Delta T_{rods,avg}})_{upper,boundary}$ [-]	$1.250 \cdot (\frac{+0.87}{\Delta T_{rods,avg}} + 1)$	
$(\frac{\Delta T_{booms,avg}}{\Delta T_{rods,avg}})_{lower,boundary}$ [-]	$1.250 \cdot (\frac{-0.87}{\Delta T_{rods,avg}} + 1)$	
Rotation: β_{max} = 6 µrad		
$\Delta T_{max} = \frac{\tan(\beta) \cdot L_{width}}{\alpha * L_0}$ [° C / K]	1.7	0.3

These worst case requirements as summarized in Table 8.17 are applied to the worst hot- and cold case.

Table 8.18: Temperature gradients for thermo-elastics for the nominal, worst hot- and worst cold case

Nominal Case				
Thermal Objective Terms	**Value**	**Requirement**	**Unit**	**Reference**
$\Delta T_{booms,avg}$	2.3	≤ 1.4	° C	Table 4.4
$\Delta T_{rods,avg}$	0.3	≤ 0.96	° C	Table 4.4
1. $\frac{\Delta T_{booms,avg}}{\Delta T_{rods,avg}}$	8.3	≤ 6.6. Perfect athermal = 1.483	-	Table 4.4
2. $T_{boom,max} - T_{boom,min}$	0.6	≤ 2.3	° C	Table 4.4
3. $T_{rod,max} - T_{rod,min}$	0.2	≤ 0.3	° C	Table 4.4
Thermal Design Objective (1+2+3)	9.1	-	° C	-
Worst Hot Case				
Thermal Objective Terms	**Value**	**Requirement**	**Unit**	**Reference**
$\Delta T_{booms,avg}$	3.3	≤ 1.1	° C	Table 8.17
$\Delta T_{rods,avg}$	0.4	≤ 0.87	° C	Table 8.17
1. $\frac{\Delta T_{booms,avg}}{\Delta T_{rods,avg}}$	8.6	≤ 4.2. Perfect athermal = 1.250	-	Table 8.17
2. $T_{boom,max} - T_{boom,min}$	0.8	≤ 1.7	° C	Table 8.17
3. $T_{rod,max} - T_{rod,min}$	0.2	≤ 0.3	° C	Table 8.17
Thermal Design Objective (1+2+3)	9.7	-	° C	-
Worst Cold Case				
Thermal Objective Terms	**Value**	**Requirement**	**Unit**	**Reference**
$\Delta T_{booms,avg}$	1.8	≤ 1.1	° C	Table 8.17
$\Delta T_{rods,avg}$	0.85	≤ 0.87	° C	Table 8.17
1. $\frac{\Delta T_{booms,avg}}{\Delta T_{rods,avg}}$	2.1	≤ 2.5. Perfect athermal = 1.250	-	Table 8.17
2. $T_{boom,max} - T_{boom,min}$	0.5	≤ 1.7	° C	Table 8.17
3. $T_{rod,max} - T_{rod,min}$	4.1	≤ 0.3	° C	Table 8.17
Thermal Design Objective (1+2+3)	6.6	-	° C	-

Table 8.19: Thermo-elastic deformations of the octagonal baffle with 5 layers of MLI and with the addition of a truncated cone. Nominal case.

	In-Orbit Drift Budget (requirement)	**Thermo-Elastic Deformation Booms**	**Thermo-Elastic Deformation Rods**	**|Athermalized M2|**
Nominal Case				
Translation	2 µm	3.2 µm	0.6 µm	2.7 µm
Rotation	6 µrad	1.5 µrad	4.1 µrad	2.6 µrad
Worst Hot Case				
Translation	2 µm	6.1 µm	0.9 µm	5.2 µm
Rotation	6 µrad	2.3 µrad	4.6 µrad	1.7 µrad
Worst Cold Case				
Translation	2 µm	3.3 µm	2.0 µm	1.3 µm
Rotation	6 µrad	1.6 µrad	89.9 µrad	88.3 µrad

8.5. IDP 5: Solutions To Decrease Thermo-Elastic Deformations

There are multiple solutions to ensure that the in-orbit drift budgets (both translation and rotation) are met. These solutions can roughly be divided into three categories:

Table 8.20: Solutions to decrease the thermo-elastic deformations so that the in-orbit drift budgets are met

Solutions to Decrease Thermo-Elastic Deformations
Sol 1. Change other DST sub-systems
Sol 2. Change the DST baffle: Active Thermal Control (ATC) addition
Sol 3. Change the orbital configuration

8.5.1. Sol 1: Change Other DST Sub-Systems

Sub-systems can be changed as well in detail, however this is out of the scope of this thesis. Therefore, only preliminary conclusions can be made about changing properties of not the baffle itself, but of other sub-systems. These properties could be the lengths of the SMSS booms, their coatings or their coefficients of thermal expansion.

The CTE's were chosen as such that it might result in an athermalized system. However, in this thesis it was found out that athermalization is not possible with the current design of the sub-systems. The CTE's could be altered, but the CFRP CTE is already at its minimum (lower CTE's than $0.8 \cdot 10^{-6}$ m/mK are practically not possible). The length of the booms cannot be lowered, as this would yield a too small distance between M1 and M2. The minimum boom length is $1.7657 - 0.0907 = 1.675$, which would still result in a thermo-elastic translation of $1.675 \cdot 0.8 \cdot 10^{-6} \cdot 2.294 = 3.07 \mu m$. This still exceeds the 2 µm budget. The coatings can also not be changed, as stray-light has to be mitigated, thus the highly absorptive MagicBlack coating has to remain.

The only conclusion is thus to decrease the thermal gradients by either actively controlling the temperature of the booms/rods or actively controlling the temperature levels of the baffle. As the design of the baffle is the focus of this thesis, the temperature levels of the baffle are recommended to be controlled, so that the inner sub-systems are also controlled. This is discussed in the next section.

8.5.2. Sol 2: Change the DST Baffle: Active Thermal Control Addition

The baffle can only influence the heat supply from external heat sources to the sub-systems such as the SMSS booms and rods and other M2 support structures. It was discovered that these external heat sources are hard to control due to the presence of a Solar eclipse, which causes the temperature gradients in the system and hence the deformations that do not conform to the budgets. A solution is to apply Active Thermal Control (ATC) to the inner layer of the baffle.

Active Thermal Control (ATC)

As was already concluded, the transient temperature profile of the inner layer of MLI determines the thermal stability of DST sub-systems that are placed inside the baffle. If the temperature gradient of the MLI layer can be stabilized, it will have positive effects on the temperature gradients of the sub-systems. Designing an active thermal control system is out of the scope of this thesis, however a first analysis can be made in which the temeprature of the inner MLI layer is controlled.

The temperature of the inside of MLI can be controlled by means of a thermistor or thermostat, in which the temperature is monitored. If the temperature drops below a certain treshold (or exceeds the upper treshold), then heat will be added due to dissipation of a heater. The full design of such a heater and its implementation in the DST is taken as recommendation, but a first order analysis is made here.

Based on research in the theory chapter, Chapter 3, several active thermal control methods were summarized that might be useful for the DST. Since deployability needs to be one of the main characteristics of these active thermal control hardware, only DST feasible active thermal control systems are summarized. Due to simplicity for now, the Polyimide Thermofoil Heater is taken for a first order analysis, as it has some positive characteristics [70]:

1. Can be embedded in Kapton (so good to combine with the DST baffle MLI)
2. The heater is flexible with a minimum bending radius of 0.8 mm, so can be used for deployment
3. Can be used under extreme temperature conditions: -200 to +200 ° C.

4. High power density of 0 - 10 $\frac{W}{cm^2}$ (depending on service temperature and mounting technique)

The Polymide Thermofoil heater is displayed in 3.4 in Chapter 3. The power density depends on the service temperature and the mounting technique. For the nominal case, the inner temperature of the MLI is 21 to -19.5 ° C, as was concluded in table 8.16. Based on the power density graph, Figure 3.5, the average ideal power density then is around 5 $\frac{W}{cm^2}$, assuming an Epoxy mounting method (orange line). However, as the power density depends on the resistance, this ideal power density decreases, to a value of 2.8 $\frac{W}{cm^2}$. [70]

This 2.8 $\frac{W}{cm^2}$ power density holds for an effective area of 101.5 cm^2, for 1 heater. When 8 individual heaters are applied for every octagonal side of the baffle, then an actual power of 287 W is used for every side. [71] This 287 W power dissipation is applied as a boundary condition to the inner layer of MLI as a heat load / unit area and is controlled through the use of a thermostat, which measures the temperature of the inside layer of MLI and actuates the Polymide Thermofoil heater once the temperature exceeds the boundary temperatures. The boundary temperature limits are taken to be +22 ° C and +15 ° C. Therefore, an actively controlled 287 W Polymide Thermofoil heater is used and switched on when the inner MLI temperature is below +15 ° C and switched off when the temperature is above +22 ° C using proportional control.

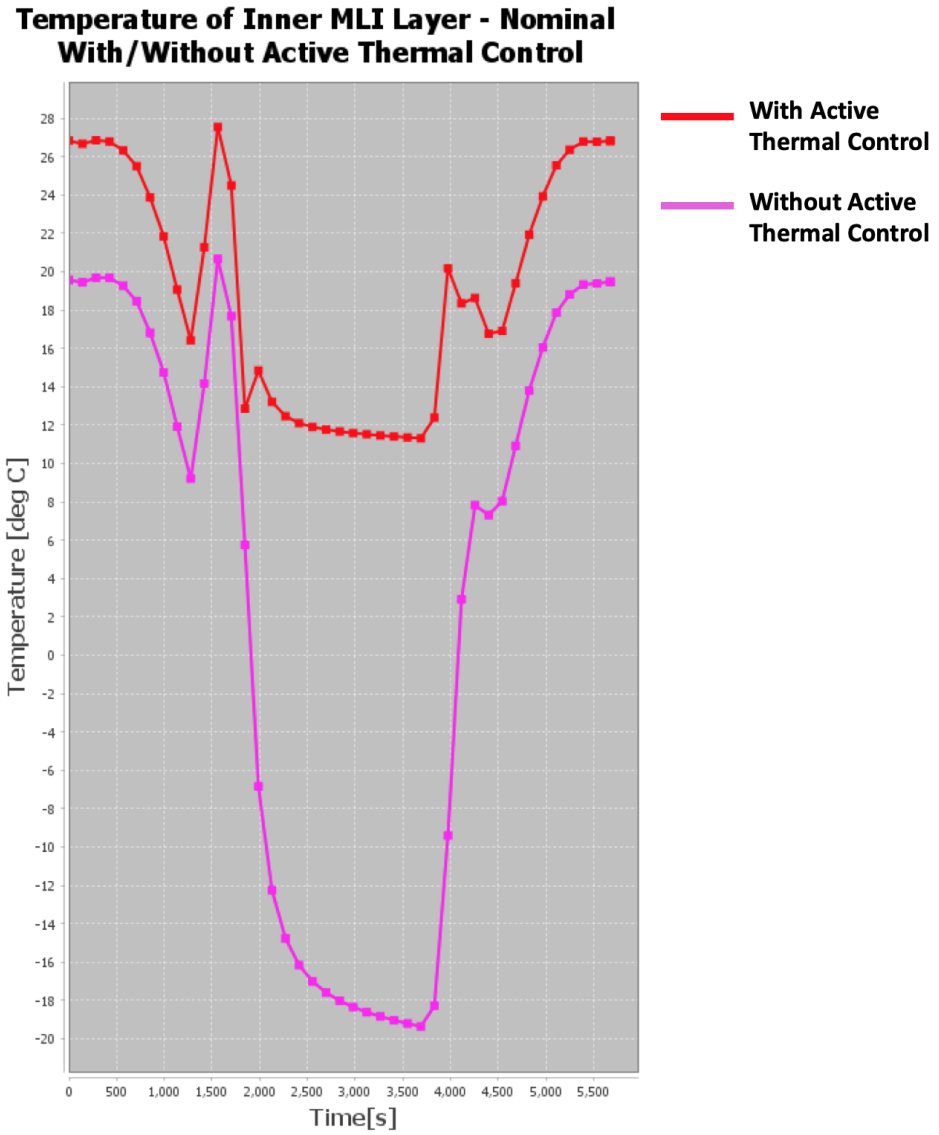

Figure 8.15: Temperature profile of the inner layer of MLI **with and without** addition of active thermal control. With active thermal control in red and without active thermal control in purple. Active thermal control: an actively controlled 287 W Polymide Thermofoil heater, switched on when temperature is below +15 ° C and switched off when temperature is above +22 ° C.

Table 8.21: Temperature gradients for thermo-elastics for both with active thermal control and without active thermal control. Without active thermal control is the nominal case of a 2.65 m height octagonal baffle with SiOx/VDA/Kapton outer coating, 5 layers of MLI and a truncated cone with aspect angle of 10 degrees.

Without Active Thermal Control				
Nominal Case				
Thermal Objective Terms	**Value**	**Requirement**	**Unit**	**Reference**
$\Delta T_{booms,avg}$	2.3	≤ 1.4	° C	Table 4.4
$\Delta T_{rods,avg}$	0.3	≤ 0.96	° C	Table 4.4
1. $\frac{\Delta T_{booms,avg}}{\Delta T_{rods,avg}}$	8.3	≤ 6.6. Perfect athermal = 1.483	-	Table 4.4
2. $T_{boom,max} - T_{boom,min}$	0.6	≤ 2.3	° C	Table 4.4
3. $T_{rod,max} - T_{rod,min}$	0.2	≤ 0.3	° C	Table 4.4
Thermal Design Objective (1+2+3)	9.1	-	° C	-
With Active Thermal Control				
Nominal Case				
Thermal Objective Terms	**Value**	**Requirement**	**Unit**	**Reference**
$\Delta T_{booms,avg}$	0.6	≤ 1.5	° C	Table 4.4
$\Delta T_{rods,avg}$	0.1	≤ 0.96	° C	Table 4.4
1. $\frac{\Delta T_{booms,avg}}{\Delta T_{rods,avg}}$	3.9	≤ 11.0. Perfect athermal = 1.483	-	Table 4.4
2. $T_{boom,max} - T_{boom,min}$	1.0	≤ 2.3	° C	Table 4.4
3. $T_{rod,max} - T_{rod,min}$	0.2	≤ 0.3	° C	Table 4.4
Thermal Design Objective (1+2+3)	5.0	-	° C	-
Worst Hot Case				
Thermal Objective Terms	**Value**	**Requirement**	**Unit**	**Reference**
$\Delta T_{booms,avg}$	0.9	≤ 1.1	° C	Table 8.17
$\Delta T_{rods,avg}$	0.2	≤ 0.87	° C	Table 8.17
1. $\frac{\Delta T_{booms,avg}}{\Delta T_{rods,avg}}$	5.1	≤ 7.3. Perfect athermal = 1.250	-	Table 8.17
2. $T_{boom,max} - T_{boom,min}$	1.0	≤ 1.7	° C	Table 8.17
3. $T_{rod,max} - T_{rod,min}$	0.3	≤ 0.3	° C	Table 8.17
Thermal Design Objective (1+2+3)	6.3	-	° C	-
Worst Cold Case				
Thermal Objective Terms	**Value**	**Requirement**	**Unit**	**Reference**
$\Delta T_{booms,avg}$	0.5	≤ 1.1	° C	Table 8.17
$\Delta T_{rods,avg}$	0.1	≤ 0.87	° C	Table 8.17
1. $\frac{\Delta T_{booms,avg}}{\Delta T_{rods,avg}}$	4.3	≤ 10.2. Perfect athermal = 1.250	-	Table 8.17
2. $T_{boom,max} - T_{boom,min}$	0.7	≤ 1.7	° C	Table 8.17
3. $T_{rod,max} - T_{rod,min}$	0.1	≤ 0.3	° C	Table 8.17
Thermal Design Objective (1+2+3)	5.1	-	° C	-

The temperature profile of the inner layer of MLI with the addition of active thermal control can be found in Figure 8.15. This is compared to the inner temperature profile of MLI without active thermal control, which is displayed in the same figure.

It can be seen from Figure 8.15 that applying ATC is very useful to decrease the gradient of the transient temperature profile of the inner layer of MLI. Its maximum temperature is 28 ° C and minimum around 12 ° C. This gradient is better than without active thermal control: 21 ° C to -19.5 ° C. This will therefore have a huge impact on the temperature gradients of the inner sub-systems, as well as the related thermo-elastic

deformations. The thermal gradients are summarized in Table 8.21 and the corresponding thermo-elastic deformations, both translation and rotation, are summarized in Table 8.22.

Table 8.22: Thermo-elastic deformations of the octagonal baffle with 5 layers of MLI and with the addition of a truncated cone. Nominal case.

	In-Orbit Drift Budget (requirement)	**Thermo-Elastic Deformation Booms**	**Thermo-Elastic Deformation Rods**	**|Athermalized M2|**
Without Active Thermal Control				
Nominal Case				
Translation	2 µm	3.2 µm	0.6 µm	2.7 µm
Rotation	6 µrad	1.5 µrad	4.1 µrad	2.6 µrad
With Active Thermal Control				
Nominal Casel				
Translation	2 µm	0.8 µm	0.3 µm	0.5 µm
Rotation	6 µrad	2.7 µrad	4.0 µrad	1.3 µrad
Worst Hot Case				
Translation	2 µm	1.3 µm	0.4 µm	0.9 µm
Rotation	6 µrad	2.7 µrad	5.1 µrad	2.4 µrad
Worst Cold Case				
Translation	2 µm	0.7 µm	0.3 µm	0.5 µm
Rotation	6 µrad	2.1 µrad	2.3 µrad	0.2 µrad

The conclusion is that ATC is very useful to decrease the thermal gradients of the sub-systems, in both the nominal design case and the the worst cases. The worst cold case again is even better than the nominal case. The reason for this is that in the cold case the effective emmisivity and conductivity of MLI decreases with 25%, which is the same effect of applying more layers of MLI. It was already concluded that more MLI layers decreases the thermal gradients and thus increases the thermal performance. So, as in all cases ATC works, it is highly recommended that this is worked out in further detail.

8.5.3. Sol 3: Change the Orbital Configuration

The DST currently operates in a SSO at 500 km altitude, 0 eccentricity, 97.4 ° inclination and LMT of 10:30 AM. The result of this orbit is an eclipse time of 37 % of the total orbital period. The eclipse is what causes the temperature gradients, as the heat flux drops an order of magnitude as was found during the analytical thermal solution, Section 6.2. This drop in heat flux, and resulting thermal gradients, can be mitigated by choosing a different orbital configuration that yields less eclipse time or no eclipse time at all.

Dusk-Dawn Orbit

A dusk-dawn orbit is also a SSO orbit, meaning that the same altitude, eccentricity and inclination can be used. However, its LMT is not 10:30 AM but 18:00 / 6:00 AM/PM. This means that the Solar beta angle β is always 90 degrees and therefore a dusk-dawn orbit never experiences an eclipse. This results in almost zero thermal gradients in the DST, which is highly benificial for the thermo-elastics. Additionally, it provides a constant Solar illumination so also a constant power source for the solar panels.

Changing the orbital configuration is however not an easy solution as it alters the entire mission envelope and objective of which Earth regions the customer wants to observe. Therefore, this is merely taken as a recommendation to change the thermal performance only as it will affect the optical performance.

8.5.4. Optimal Solution

The most optimal solution to decrease the thermo-elastics of the system, and thus conforming to the in-orbit drift budgets of 2 µm maximum translation of M2 and 6 µrad maximum rotation of M2, is to apply ATC. It was already concluded that when heaters are applied on the inside of layer of MLI, the temperature of the inner layer of MLI can be controlled precisely and therefore also the influence on the sub-systems of which the booms and rods are part of. With the addition of heaters, the budgets are met as can be seen in Table 8.22. Changing the DST-subsystems and the orbital configuration are not ideal, as both drastically influence the mission, as well as the structural integrity of other sub-systems. Therefore, applying active thermal control is a good solution.

9

Final Design Description

This chapter contains a detailed final design description of the baffle after thermal-mechanical system integration. Note that the performance of this design is not stated in this chapter, but in the conclusion: Chapter 10.

9.1. General Design Input and Assumptions

General design input and assumptions are enumerated below and explained thereafter.

1. The baffle as part of DST operates in a circular Sun-Synchronous Orbit (SSO) at an altitude of 500 km, 97.4 ° inclination and 10:30 AM LMT.

2. The in-orbit drift budget is the most stringent budget for the M2 to be met to ensure for optical stability

3. The thermo-elastic budget is assumed to be equal to the in-orbit drift budget for the time periods that both budgets hold

9.1.1. Orbit: Rationale

A Sun-Synchronous Orbit was already chosen based on the mission objective. To summarize: A SSO gives the advantage of having a nearly constant illumination angle (constant Solar beta angle) because the RAAN rotates with an angular velocity of 360 ° / 365.2422 days, same as the orbital period of the Earth around the Sun. This thus results in a constant illumination angle on the Earth when pictures are taken and a nearly constant passage time of the same spot on Earth. Additionally, it results in a constant source of power for solar panels (still have to be designed). The inclination of 97.4 ° is chosen as this results in a perfect SSO orbit for an orbital altitude of 500 km.

The altitude choice of 500 km stems from D. Dolkens' preliminary opto-mechanical design, and is chosen because a multitude of Earth observation space telescopes (like the ANT-1, ANT-2 and ARCTIC-1) have been operating around the altitude range of 443 - 550 km. [23]

The LTDN of 10:30 AM is chosen because it offers the best trade-off between coverage of a large portion of Europe, as well as avoiding the Sun glint effect that would play a role with a LTDN of 12:00 AM. Sun glint is the specular reflection of sunlight off the flat surface of the sea and is worst when the telescope senses the surface with the same angle as the reflection angle with the flat sea surface. Therefore, Sun glint is worst at a LTDN of 12:00 AM, but Europe coverage is best at 12:00 AM. To avoid Sun glint while still maintaining sufficient Europe coverage a LTDN of 10:30 AM is chosen. [51] Further literature research on cloud coverage shows that a LTDN of 10:30 AM presents less cloud coverage than a LTAN of 1:30 PM, which is also better. [1]

9.1.2. Critical Budget and System: Rationale

The M2 is observed to be the most critical system at the beginning of this thesis, since:

1. For the M2 and SMSS, no active optical system that controls the 6DOF of the M2 based on actuation commands is present, unlike for the M1

2. The spider of the SMSS is least protected by the baffle and therefore a highly critical system that needs thermal control

3. The length of the SMSS deployed CFRP booms make it thermally sensitive, since thermo-elastic elongations are linearly related to the length of the booms.

4. As analyzed by T. van Wees, [102], the thermo-elastic translation in Z-direction of M2 is > 2.23 µm and exceeds the in-orbit drift budget in best case scenario of a reflected baffle and no orbital eclipse

The critical budget that M2 shall adhere to is the in-orbit drift budget and not the deployment/coarse alignment budget or stability budget. The in-orbit drift budget holds for the entire period that the DST is able to image, which is the Sunlit period of 3566 s (Δt_{drift}). The coarse alignment budget holds for the period when the DST is in Eclipse: 2102 s (Δt_{coarse}). The stability budget only applies during image acquisition, of which the duration of it is currently in the order of one second. [76]. Therefore, the stability budget is not exposed to a large period of time in which thermal gradients can build up, which is the case for only the in-orbit drift budget and coarse/deployment budgets. The reason why the in-orbit drift budget is more stringent than the deployment/coarse alignment budget is because the temperature gradients, that is the difference between maximum and minimum temperature of the M2 athermalized system (booms and rods), are equal for both budgets. This is despite the fact that Δt_{drift} and Δt_{coarse} are different. This is visualized in Figure 5.3. Since the thermal gradients and thus the corresponding thermo-elastic deformations are equal for both budgets, the most stringent budget has to be adhered to. This is the in-orbit drift budget with a maximum translation requirement of 2 µm and 6 µrad rotation versus the deployment/coarse alignment budget with a maximum translation requirement of 10 µm and 100 µrad rotation.

Furthermore it is assumed that the in-orbit drift budget is completely devoted to thermo-elastic deformations due to temperature gradients. This is to a great extent correct as thermo-elastic deformations are one of the main sources of operational deformations due to the Eclipse. Other deformations are the result of e.g. vibrations and flutter but are assumed to be less severe than thermo-elastic deformations.

9.2. Final Thermal Design

1. Octagonal shape with height of 2.65 m and width of each octagonal side of 0.7654 m.

2. Passive Thermal Control (PTC) consisting of:

   (a) MLI:

      i. 5 layers of aluminized Kapton with a total thickness of $1.03 * 10^{-3}$ m
      ii. Thickness aluminized Kapton (shield) of 0.013 mm
      iii. Thickness of Dacron net of 0.16 mm per layer
      iv. Bulk density of 146 $\frac{kg}{m^3}$
      v. Bulk specific heat of 1117.5 $\frac{J}{kgK}$
      vi. Bulk conductivity of 0.1275 $\frac{W}{mK}$
      vii. MLI mass of 2.431 kg (5 layers)

   (b) Coatings:

      i. Outer coating of 2 mil SiOX/VDA/Kapton with absorptivity of 0.19 and emissivity of 0.14, leading to an $\frac{\alpha}{\epsilon} = \frac{0.19}{0.14} = 1.36$.
      ii. Inner coating is 2 mil Magic Black with absorptivity of 0.93 and emissivity of 0.84, leading to an $\frac{\alpha}{\epsilon} = \frac{0.93}{0.84} = 1.11$.
      iii. Truncated cone near M2 for both stray-light mitigation and reflection of critical IR/Albedo flux from the Earth, made from M55J with mass of 2.667 kg, aspect angle of 10 %, thickness of 1 mm and SiOx/VDA/Kapton coating that adheres to the truncated cone requirements

3. Preliminary Active Thermal Control (ATC) consisting of:

   (a) 8 individual 287 W Polymide Thermofoil heater, applied to each octagonal inner layer of MLI. Switched on when inner baffle temperature is below +15 ° C and switched off when inner baffle temperature is above + 22 ° C

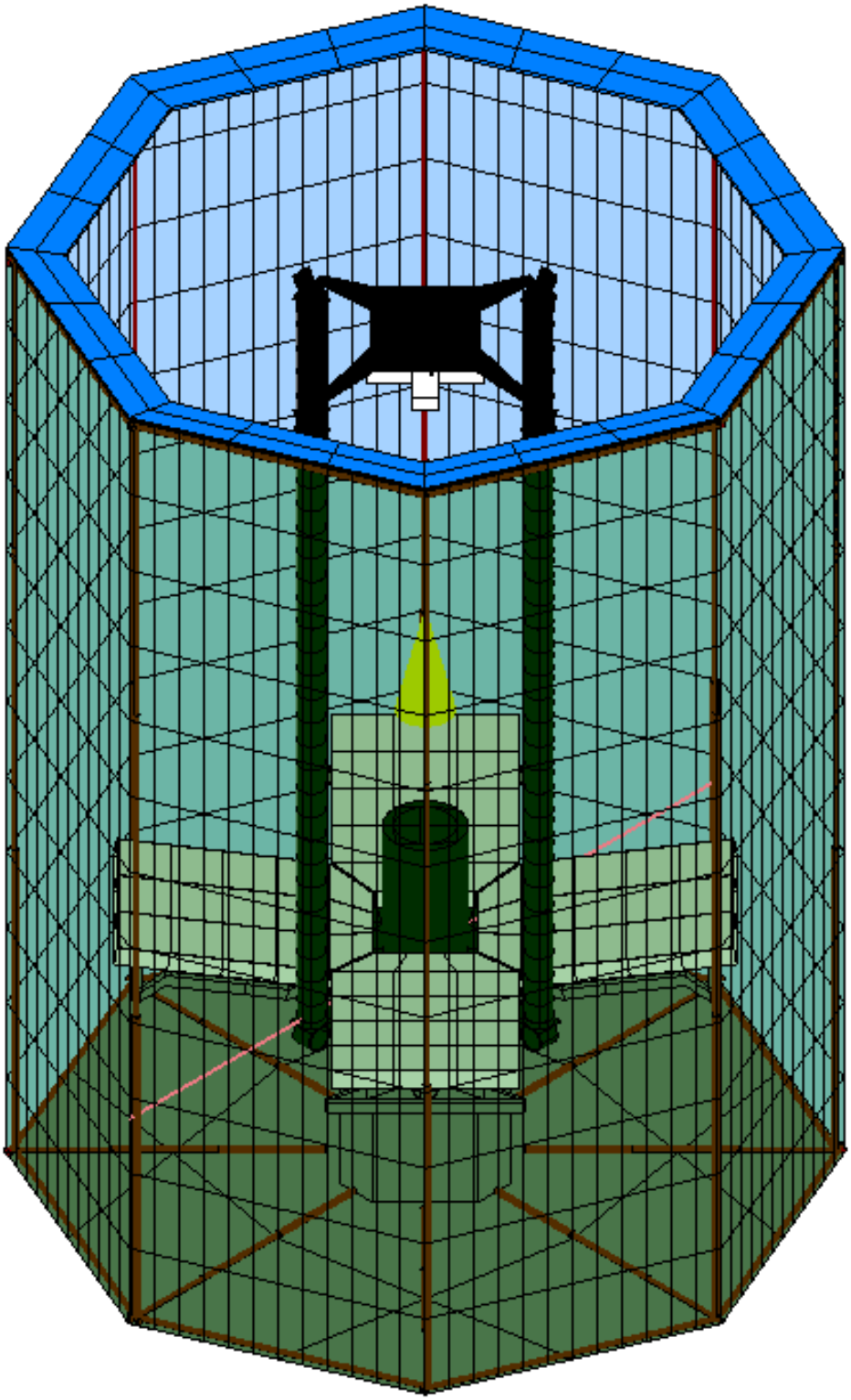

Figure 9.1: Final design of the baffle as visualized in **deployed** configuration. The baffle sides are made transparent for visibility reasons, but are obviously not transparent in operations. In red, the baffle telescopic structure can be seen.

9.2.1. Shape: Rationale

An octagonal shape is eventually chosen as this is the result of the mechanical telescopic boom structure design. An octagonal shape is a polygonized cylindrical shape, and a cylindrical shape was chosen and preferred over a cubical shape, since its thermal performance is better: it yields a lower value for the thermal performance objective, evaluated for different outer coatings: 24.2 ° C instead of 38.3 ° C for a black copper outer coating with $\frac{\alpha}{\epsilon} = 1.56$, 23.7 ° C instead of 37.9 ° C for an $\frac{\alpha}{\epsilon} = 1.81$ and 23.4 ° C instead of 24.0 ° C for aluminized Kapton as the outer coating with an $\frac{\alpha}{\epsilon} = 3$. This means that the gradients of the booms and rods are lower for a cylindrical shape than for a cubical shape.

Additionally, the mechanical performance of a cylindrical shape, polygonized to an octagonal shape, is better: it saves $1 - \frac{3.77}{3.14} = 16.7\%$ mass in best case scenario when the cubical baffle is 45 degrees rotated, has a higher eigenfrequency of 1.53 Hz than 1.27 Hz according to E. Korhonen [58] and is worked out in detail by E. Korhonen which results in more available information and comparison of mechanical models.

9.2.2. Height and Width: Rationale

There exists a quadratic relationship between the baffle height and the thermal performance. This is evaluated in both ESATAN-TMS as well as analytically for a cylindrical baffle using view factor data. The view factor data for the inner surface of a baffle to itself and to the baffle bottom also shows a quadratic relationship. Several heights were evaluated in the trade-off between 2.5 m and 2.9 m, since for a minimum height of 2.5 m the baffle barely covers the spider and is thus the boundary of baffle protection, and the maximum height of 2.9 m is evaluated as a decrease in thermal performance was already witnessed as the maximum nominal temperature of M2 is ° C and thus exceeds the -20 to +50 ° C requirement as stated in BAF-T-01-03. Therefore, these boundaries are not optimal. The best performing heights are 2.65 and 2.725 m. A baffle height of 2.65 m is chosen as it yields the best thermal performance: lower thermo-elastic athermalized rotation of the M2 of 69 µrad instead of 125.83 µrad for a 2.725 m baffle height, it saves mass, increases structural eigenfrequencies $\frac{k_{eq}}{M_{eq}}$ as its stiffness increases and mass decreases and less deployment force is needed to deploy a baffle with 2.65 m height with respect to 2.725 m height. Furthermore, this heigth is lower than the 3.060 m that E. Korhonen designed.

The polygonized radius of the cylinder must be minimized to avoid heat flow from different angles to enter the interior of the baffle. The larger the radius, the more heat can enter the baffle. The constraint to the minimal radius is the allowed clearance between the DST sub-systems (mainly M1) and the baffle. The requirement is that there is a minimum clearance of 200 mm between M1 and any point of the baffle in deployed configuration - BAF-SYS-18. Given that the arc length of M1 is 750 mm, this leads to a minimum polygonized radius of 950 mm, which leads to 1000 mm radius when taking an extra margin of safety into account.

9.2.3. MLI Lay-Up: Rationale

MLI is modelled as a surface with two layers (inside and outside) with effective emissivity and conductivity, to take into account perforations, stand-offs, temperature levels of layers and debris penetrations and based on empirical data. This modelling choice is validated by N. van de Pas and early Fokker Space documents [20]. The bulk materials are calculated using the rule of mixtures for composites, as MLI is a composite consisting of a shield material (aluminized Kapton) and a spacer layer (Dacron).

5 layers of MLI have been chosen based on the following design rationale:

1. The foldability of MLI is analyzed and use is made of the structural theory of the bending of beams. An analytical expression has been established in which the minimum radius of curvature and the thickness of the layers (which depends on the number of MLI layers that is used) are related to the Yield point of the material. In other terms, in order to not plastically deform the MLI (so to stay below the Yield point), the ratio between the cube of the number of layers N and the radius of curvature ρ shall not exceed $\frac{N^3}{\rho} = 1.58$. Therefore, increasing the number of layers immensely increases the radius of curvature as well, which consequently increases the packing thickness. Based on the maximum stowed treshold volume requirement of 1.5 m^3, a maximum of 5 layers of MLI can be used, which results in a MLI packing thickness of 160.3 mm and a total DST stowed volume of 1.44 m^3. Increasing the number of layers further will result in exceeding values for the packing thickness (6 MLI layers already gives a packing thickness of 275.8 mm) with a DST stowed volume of 1.96 m^3, which exceeds the 1.5 m^3 stowed treshold volume requirement.

Additionally, the JWST also uses 5 aluminized Kapton layers of MLI, meaning that this serves as a good reference case.

2. 5 layers of MLI fits well within the mass budget. The maximum number of layers of MLI to fit within the mass budget allocated for MLI (4.668 kg) was calculated to be **10**. Five layers, with a mass of 2.431 kg, therefore leaves room for additionall mass of hardware for attachments and interface points that are not designed yet.

3. The added mass of the 5 layers of MLI conforms to the stowed structural eigenfrequency requirement of ≥ 100 Hz. The maximum number of MLI layers that can be used to not exceed the budget of 3.271 kg in order to meet the eigenfrequency requirement is **7** layers.

4. Within the above mentioned constraints, the number of layers should be maximized to increase the thermal performance. More layers of MLI results in a better shielding of the instruments from external heat fluxes and lower thermal gradients. For an athermal system 24 layers of MLI are needed but due to the above mentioned reasons this is not feasible. Therefore, it is still best to choose the maximum number of layers that can be used to conform to the structural-, mass- and packing thickness requirements, which is 5 layers.

5. Within the above mentioned constraints, the number of layers should be maximized to increase the debris mitigation reliability. More layers results in a better shielding performance for debris and micro-asteroids. Although it is hard to say if the DST baffle will survive debris and micro-asteroids, it can definately be concluded that its impact will reduce with increasing MLI layers as for every layer impact energy is absorbed.

9.2.4. Outer Coating: Rationale

The outer coating does not influence the thermal gradients much, meaning that from a thermo-elastic deformation point of view no significant change is visible. However, the outer coating does significantly influence the nominal temperatures of the DST sub-systems. Since BAF-T-01-03 states that all DST sub-system temperatures within the baffle shall be between -20 to +50 ° C, an outer coating with an $1 < \frac{\alpha}{\epsilon} < 3$ shall be chosen. The optimum is an $\frac{\alpha}{\epsilon} \approx 2$ to account for sensitivities and uncertainties in the system. The best coating that conforms to all requirements, including worst hot- and cold cases, is SiOx/VDA/Kapton with an $\frac{0.19}{0.14} = 1.36$: it shows very good thermo-optical properties that remain stable throughout its operational lifetime (no change in EOL vs BOL), it is resistant against AO, since it erodes uniformly, with minor differences in its thermo-optical - and radiative properties. It also prevents outgassing, is easily embedded in MLI and has flight heritage.

9.2.5. Inner Coating: Rationale

The inner coating remains the same as E. Korhonen's design: MagicBlack with an $\frac{\alpha}{\epsilon} = \frac{0.93}{0.84} = 1.11$. The reason for this is that the inner coating shall absorb as much heat flux, both external and internal, to prevent stray-light interfering with the optical system. For this reason, a non-reflective coating must be chosen with high absorptance and emittance.

9.2.6. Truncated Cone: Rationale

There are 4 main requirements for the truncated cone design: aspect angle ≤ 35 degrees, emissivity and absorptance ≤ 0.02 and 0.07 respectively, added mass shall not exceed the 15 kg baffle mass requirement and truncated cone shall be deployable.

The truncated cone has changed based on the mechanical design and therefore the lay-up, mass and ideal aspect angle also have changed as is explained in Chapter 8. To summarize: a truncated cone is added for three reasons: (i) A truncated cone as a shape was concluded as a good rule of thumb for stray-light mitigation for Cassegrain telescopes in specific: [97], (ii) to decrease the thermal gradients in the SMSS athermalized system and (iii) to decrease the temperature levels of the baffle telescopic booom structures. Different than for the cylindrical baffle, an octagonal truncated cone for the new octagonal baffle barely decreases the thermal gradients of the SMSS. Only for an aspect angle of 10 degrees the difference between actual athermal translation ratio and requirement ratio decreased from 2.0707 to 1.702 for the SiOx/VDA/Kapton coating.

SiOx/VDA/Kapton is chosen as a coating for the truncated cone as it yields the lower thermal gradients than Vaporized Deposited Silver (VDS) and it prevents outgassing while the previously chosen VDS does not.

However, it does have exceeding values for the absorptivity and emissivity 0.19 and 0.14 respectively, but this is something that a future student has to iterate on when performing a proper stray-light analysis.

The material and thickness are driven by the mass budget and define the truncated cone mass and specific heat. To get a high stiffness to weight ratio M55J is used, same as for the baffle structure. The thickness is chosen to be minimal: 1 mm to yield low mass. As the coatings are highly reflective, little heat flux is absorbed and thus the thickness has low influence on the thermal performance.

9.2.7. Active Thermal Control: Rationale

Based on the thermal performance, of which the conclusion is presented in Section 10.1.1, it is concluded that the M2 cannot be made athermal based on merely Passive Thermal Control (PTC), thus merely consisting of MLI and appropriate coatings and a truncated cone, as the thermo-elastic deformations exceed the in-orbit drift budgets for M2 of 2 µm translation and 6 µrad rotation. Several methods were investigated to decrease the thermo-elastic deformations.s These solutions are: changing the DST sub-systems, changing the DST baffle by applying ATC and changing the orbital configuration.

Changing the DST sub-systems yield the following options: decrease the CTE's of the booms/rods, decrease the length or their coatings. The CFRP CTE is already at its minimum (lower CTE's than $0.8 \cdot 10^{-6}$ m/mK are practically not possible), thus not possible to change. The length of the booms cannot be lowered, as this would yield a too small distance between M1 and M2. The minimum boom length is $1.7657 - 0.0907 = 1.675$, which would still result in a thermo-elastic translation of $1.675 \cdot 0.8 \cdot 10^{-6} \cdot 2.294 = 3.07 \mu m$, which still exceeds the 2 µm budget. Therefore changing these sub-systems does not yield in an athermalized system.

Changing the orbital configuration is an option that could be applied. A dusk-dawn orbit could be used since it does not experience any eclipse, which is also a SSO and can have the same orbital parameters as the current orbital configuration. The only change is that the 10:30 AM LMT changes to 18:00 / 6:00 AM/PM. As this changes the complete mission objective and changes the Earth coverage. For these reasons, this is merely taken as a recommendation to upper management.

The most optimal solution is concluded to be the application of Active Thermal Control, as this lowers all gradients so that the in-orbit drift budgets of M2 are met. For a first order analysis, 8 Polyimide Thermofoil heaters with a dissipative power of 287 W are used on each inner octagonal surface, as these heaters can be embedded in Kapton, are flexible with a minimum bending radius of 0.8 mm, can be used under extreme temperature conditions of -200 to +200 ° C and have a high power density. More about the performance in Section 10.1.1.

9.3. Final Mechanical Design

The final mechanical design, that is the design of the deployable baffle structure, is summarized below including explanation on what these choices are based.

1. Octagonal telescopic deployment system using prismatic joints (no hinges), consisting of hollow square telescopic booms
2. Deployment ratio in axial configuration and radial configuration is 3.
3. Biggest telescopic boom has outer width of 20 mm and inner width of 18.9 mm. Smallest telescopic boom has outer width of 12 mm and inner width of 10.23 mm.
4. Material of baffle structure is M55J CFRP
5. Telescopic octagonal truncated cone added, made of M55J CFRP
6. 8 NANO STEM actuation systems (4 for radial deployment and 4 for axial deployment) chosen

9.3.1. Telescopic Deployment Concept: Rationale

A telescopic deployment system is chosen, and performs better than the inflatable deployment system as was concluded from the AHP trade-off, due to lower mass and stowed volume, greater structural integrity (higher eigenfrequencies in both stowed and deployed configuration), higher deployment reliability as it consists of less failure modes than the inflatable baffle and higher flexibility as it is rigid and stray-light hardware can easily be added. The actual performance values are summarized in Section 7.11.2 below.

Four different telescopic boom conceps were also investigated: *Concept 1.* a completely rigid telescopic boom concept, *concept 2.* a mid-side hinge concept, *concept 3.* a concept that uses telesopic booms as well as

mid-and side hinges and *concept 4.* a concept consisting of side hinges. Using the AHP trade-off method, *concept 1* scores best due to lower mass as it is a 2-DOF system while the others are ≥ 8-DOF systems and hence need more than 8 actuation systems, lower deployment complexity, highest stowed and deployed stiffness due to its rigidity in both states and highest flexibility as vanes/truncated cones can easily be added since the rigidity of the shape is the same in both stowed and deployed configuration.

The telescopic booms are based on the Telescopic Tubular Mast designed by Northrop Grumman, [73], since this telescopic structure is also deployed using spring based STEM booms.

9.3.2. Deployment Ratio: Rationale

The deployment ratio in both axial and radial deployment is 3, meaning that 3 telescopic booms are used for both configurations. The largest booms are the axial booms: 0.884 m in length, which then gives a deployed height of $3 \cdot 0.884 = 2.65$ m. The radial booms are seperated into parallel radial booms and diagonal radial booms, as these need to be attached to the interface housing which has different dimensions for both geometries. The parallel radial booms have a length of 0.256 m and the diagonal radial booms have a length of 0.265 m. These lengths are chosen such that in stowed configuration, the height of the baffle is 0.884 m and the radial lengths are 0.256 and 0.265 m, leading to a total radius measured from the centerline of the interface housing of 0.5 m for both parallel and radial booms. However, it was found out during deployment that the stowed configuration can only be 0.5324 m in radial direction. The height remains at 0.884 m. This does not have a negative impact on the stowed volume, since the maximum stowed volume including 5 layers of MLI of the entire DST is 1.44 m^3 and still conforms to the maximum stowed volume threshold requirement of 1.5 m^3. The deployed radius of parallel and diagonal radial booms are 0.795 m and 0.7666 m respectively, and the height 2.65 m. This results in a deployed distance of 1 m from both measured from the center of the interface housing, which was set as the requirement based on thermal performance (for a cylindrical shape). This is schematized in Figure 7.3. The corresponding deployed volume of the DST is 7.5 m^3.

9.3.3. Telescopic Boom Material: Rationale

CFRP M55J is chosen since based on eigenfrequency analysis the material needed to be have a $\frac{E}{\rho} > 1.0 \cdot 10^8 \ \frac{m^2}{s^2}$ in order to conform to the stowed eigenfrequency requirement of ≥ 100 Hz. For this reason a high-modulus CFRP material is chosen. To conclude the reasons why M55J is chosen: (i) high modulus material meaning high Young's modulus and low density, which results in an increase in structural integrity and decrease in mass simultaneously (ii) prevents cold welding since cold welding only takes place for metallic materials. Cold welding is crucial to prevent for a telescopic boom system, since if cold welding happens, the baffle cannot deploy. (iii) M55J has a negative CTE, meaning that due to temperature gradients the boom does not expand but contract. This therefore does not hinder the deployment and no extra clearance between the telescopic elements is needed. Finally, (iv) M55J is used in Aerospace industry applications and therefore has space heritage.

9.3.4. Hollow Square Cross-Section: Rationale

During the iterative mechanical design process, it was found out that a hollow square cross-section can yield the same stiffness as a hollow cylindrical cross-section, but for a lower area. This therefore decreases mass of the entire baffle from 3.90 kg to 2.73 kg. To summarize all benefits of a hollow-square cross-section:

1. A hollow square cross-section yields a higher bending strength to weight ratio, meaning that for the same area moment of inertia and thus same bending stiffness ($k = \frac{3EI}{L^3}$) can be achieved with less volume of material → less $M_{mechanical}$ mass, meaning more room for $M_{thermal}$

2. A hollow square cross-section prevents rotation along axial direction due the nature of its shape. When wanting to prevent rotation for a hollow cylinder, rails have to be added (like for the Telescopic Tubular Mast designed by Northrop Grumman [73]), which complicates the manufacturing process as well as.

3. Since the area of material is lower for a hollow square shape, more area is left for the addition of a deployment actuation system: 104.7 instead of 50.3 mm^2

4. More clearance is left between all sides of a hollow square cross-section than for a hollow cylindrical one: 1.45/1.46 mm instead of 1 mm clearance

9.3.5. Boom Cross-Section Dimensions: Rationale

Given that the cross-section has changed from a hollow cylinder to a hollow square, the dimensions (biggest telescopic boom has outer width of 20 mm and inner width of 18.9 mm and smallest telescopic boom has outer width of 12 mm and inner width of 10.23 mm) yield the same area moment of inertia and thus same stiffness as for an equivalent hollow circular cross-section with outer diameter of 20 mm, inner diameter of 18 mm (largest boom) and 12 mm and 8 mm outer-inner diameter respectively for the smallest boom. It can be seen that due the outer width and outer radius are the same, but the inner width and inner radius are not: for the hollow square cross-section less area is needed which yields more clearance between all sides of the hollow square cross-section (already concluded above).

9.3.6. Actuation System: Rationale

The NANO STEM booms are used for the actuation of the baffle structure. In total 8 NANO STEM booms are used: 4 for the radial deployment and 4 for the axial deployment, leading to a total mass of 1.816 kg. In theory only 2 NANO STEM booms are sufficient (1 axial and radial deployment), but due to redundancy reasons and increase in reliability, the amount of actuators is quadrupled to conform to BAF-SYS-02-03. The force needed for deployment has preliminarily established to be 0.9 N. The NANO STEM boom can deliver a 222.5 N force, which definately meets the requirement. It 1.816 kg also does not exceed the mass budget, it has space heritage as it has been used on the Hubble Space Telescope and Mars Pathfinder and will be used for the JWST Sun-shield deployment to name a few and it fits within the 10.23 x 10.23 mm inner width of the smallest hollow square telescopic boom as its diameter is merely 6.52 mm.

10

Conclusion & Recommendations

This chapter aims at making a conclusive statement about the design and performance, answering the research question proposed in the beginning of this thesis and stating recommendations for the future.

10.1. Conclusion Design and Performance

10.1.1. Final Thermal Performance

In this section conclusive remarks about the thermal performance are made.

1. Nominal Temperatures of Baffle and DST Sub-Systems

The final nominal temperatures of the baffle and DST sub-systems without addition of ATC are summarized in Table 10.1. ATC is not added for the overview of the nominal temperatures, as ATC will only further increase the stability of the nominal temperatures and does not effect the nominal temperatures.

It can be concluded from the results in this table that all nominal temperature requirements are met. This is because all DST sub-system temperatures are between -20 ° C and +50 ° C (BAF-T-01-03 requirement). Furthermore, the maximum temperature of the MLI of the baffle is 140 ° C. In the worst hot case, this temperature increases from 140 to 167 ° C as was found out during a sensitivity analysis (see Table 8.16). The maximum tempeature of 167 ° C still conforms to the maximum MLI temperature requirement of 177 ° C. The minimum MLI temperature (in worst cold case) is -110 ° C and conforms to the > -250 ° C requirement (BAF-T-02-01 requirement).

Furthermore, the temperatures of the baffle telescopic structure are in the range of 1.0 to 42.1 ° C, which are lower than the 104 ° C maximum operating temperature of M55J. Namely, the maximum service temperature of M55J, which is the material of the baffle structure and octagonal truncated cone, is based on research: 104 ° C, as for epoxy-based composites the glass transition temperature in general lies around 100-180 ° C. [67]

Finally, it was found that the addition of a truncated cone drastically reduces the temperature levels of the telescopic baffle structure: the maximum temperature decreases from 115.0 ° C to 42.1 ° C due to merely adding an octagonal truncated cone, and the lowest temperature increases from -17.6 ° C to +1.0 ° C. Therefore, a truncated cone is definitely an added value to the baffle design.

2. Temperature Gradients of Current Baffle Design

For the translation, the temperature gradient in the SMSS booms exceeds the 1.4 ° C requirement. The temperature gradient in the rods is fine, but the final athermalized result does not comply to the requirement since $\frac{\Delta T_{booms,avg}}{\Delta T_{rods,avg}} = 8.3$ and exceeds the 6.6 requirement ratio. The consequence of this is that the athermalized translation due to temperature gradients is 2.7 µm and hence exceeds the 2 µm budget. This is also explained in the thermo-elastics bullet point 3 below.

For the rotation, the temperature gradients in both booms and rods conform to the temperature gradient requirement, resulting in a rotation that is below 6 µrad for the booms, rods and complete athermalized M2 system.

With the addition of a truncated cone, the temperature gradients still do not conform to the in-orbit drift budget. Only for a 10 degree aspect angle, the athermalized temperature gradients are lowered: 2.9 to 2.7 µm

translation, but > still 2 µm.

Table 10.1: Temperature data corresponding to the iterated DST baffle with improved properties for the boom. For **Temperature Gradients**: Those in red are not acceptable, since these gradients cause thermo-elastic deformations well above the requirements, see Table 10.2

Nominal Temperatures.				
Sub-System	**Max Temp. (° C)**	**Min Temp. (° C)**	**Requirement**	**Reference**
M2	14.2	14.0	$-20°C < T < 50°C$	BAF-T-01-03
Spider	2.8	0.2	$-20°C < T < 50°C$	BAF-T-01-03
PMSS	8.7	6.1	$-20°C < T < 50°C$	BAF-T-01-03
M1	12.7	12.7	$-20°C < T < 50°C$	BAF-T-01-03
Top Hinge	12.8	0.0	$-20°C < T < 50°C$	BAF-T-01-03
Booms	6.8	4.5	$-20°C < T < 50°C$	BAF-T-01-03
Baffle MLI Bottom Outside Avg	125	-100	$-250°C < T < 177°C$	BAF-T-02-01
Baffle MLI Bottom Inside Avg	34	-16	$-250°C < T < 177°C$	BAF-T-02-01
Baffle MLI Side Outside Avg	20	-67	$-250°C < T < 177°C$	BAF-T-02-01
Baffle MLI Side Inside Avg	21	-19.5	$-250°C < T < 177°C$	BAF-T-02-01
Baffle MLI Outside Max-Min	140	-70	$-250°C < T < 177°C$	BAF-T-02-01
Baffle MLI Inside Max-Min	30	-22	$-250°C < T < 177°C$	BAF-T-02-01
Baffle Telescopic Structure	42.1	1.0	$T_{M55J,max} = 104°C$	[67]
Temperature Gradients				
Thermal Objective Terms	**Value**	**Requirement**	**Unit**	**Reference**
$\Delta T_{booms,avg}$	2.3	≤ 1.4	° C	Table 4.4
$\Delta T_{rods,avg}$	0.3	≤ 0.96	° C	Table 4.4
1. $\frac{\Delta T_{booms,avg}}{\Delta T_{rods,avg}}$	8.4	≤ 6.6. Perfect athermal = 1.483	-	Table 4.4
2. $T_{boom,max} - T_{boom,min}$	0.6	≤ 2.3	° C	Table 4.4
3. $T_{rod,max} - T_{rod,min}$	0.2	≤ 0.3	° C	Table 4.4
Thermal Design Objective (1+2+3)	9.1	-	° C	-

Table 10.2: Thermo-elastic deformations after iterative process: cylindrical baffle with height of 2.65 m, outer coating of SiOx/VDA/Kapton, discretized booms and improved thermal properties and addition of truncated cone.

	In-Orbit Drift Budget (requirement)	**Thermo-Elastic Deformation Booms**	**Thermo-Elastic Deformation Rods**	**|Athermalized M2|**
Baseline 1. Without Baffle				
Translation [µm]	2	32.4	42.1	9.7
Rotation [µrad]	6	8.3	928.3	920.1
Baseline 2. E. Korhonen design				
Translation [µm]	2	5.4	2.2	3.2
Rotation [µrad]	6	35.9	44.9	9.1
Final Design Without Active Thermal Control (ATC)				
Nominal Case				
Translation [µm]	2	3.2	0.6	2.7
Rotation [µrad]	6	1.5	4.1	2.6
Final Design With Active Thermal Control (ATC)				
Nominal Case				
Translation [µm]	2	0.8	0.3	0.5
Rotation [µrad]	6	2.7	4.0	1.3
Worst Hot Case				
Translation [µm]	2	1.3	0.4	0.9
Rotation [µrad]	6	2.7	5.1	2.4
Worst Cold Case				
Translation [µm]	2	0.7	0.3	0.5
Rotation [µrad]	6	2.1	2.3	0.2

It can thus be concluded that the passive baffle **without** Active Thermal Control (ATC) conforms to the nominal temperature requirements, but does not ensure that the temperature gradients conform to their requirements. For this reason ATC is added to the passive thermal-mechanical design. The thermo-elastic de-

formations of the DST M2 system due to the baffle with addition of ATC are summarized in *3. Final Thermo-Elastic Verification* below.

Furthermore, conclusive remarks about the temperature gradients in the baffle telescopic structure can be made. A temperature gradient of only 2 ° C in the telescopic structure has been simulated in ESATAN-TMS. In the worst case this results in a compressive thermal stress of -1.19 MPa, which is well below the critical compressive strength of 880 MPa for M55J. The 2 ° C gradient results in a shrinkage of the cross-sectional area due to the negative CTE of CFRP. This even increases the clearance between the booms which facilitates the deployment. However, the clearance has been observed to not decrease the structural integrity of the telescopic structure.

3. Final Thermo-Elastic Verification
The thermo-elastics of the M2 system are the result of the thermal gradients, mentioned under the aforementioned second bullet point. In Table 10.2 the thermo-elastic performance of baseline 1, 2 and the designed system (with and without ATC) is summarized. The results are also explained in the text below.

Without a baffle (baseline 1) the athermalized M2 system translates 9.7 µm and rotates 920.1 µrad, both exceeding the in-orbit drift budgets tremendously (especially rotation-wise). This proves the necessity of implementing a baffle.

The previously designed baffle by E. Korhonen and analyzed by T. van Wees (baseline 2), [58] [102], also exceeds both the translation- and rotation in-orbit drift budget: 3.2 µm and 9.1 µrad respectively. Note that this is for the best case scenario in which perfect athermalization is assumed, meaning that the rotation of the booms is counteracted by the rotation of the rods: 44.9 µrad - 35.9 µrad = 9.1 µrad. There is a great uncertainty in this statement as well. This means that in the worst case scenario both rotations go about the same rotation axis, resulting in the addition of the rotations. This would result in a total M2 rotation of 80.8 µrad.

The final designed baffle in this thesis without ATC yields a better thermo-elastic performance than both baseline 1 and 2: athermalized translation and rotation of 2.7 µm and 2.6 µrad. The rotation is within the 6 µrad budget (even in worst case when the rotations are added: 5.6 µrad), but the translation exceeds the budget. For this reason, ATC is deemed to be crucial to meet all in-orbit drift budgets.

For the final designed baffle with ATC the thermo-elastic deformations are all within the in-orbit drift budget. This also holds for the worst hot- and cold cases. ATC consists of 8 flexible Polymide Thermofoil heaters embedded in the Kapton of MLI and actively controlled by thermostats between +15 and +22 ° C. The Polymide Thermofoil heaters are therefore recommended to be used in a baffle. Next to the improved thermal performance of the baffle, the heaters are flexible, can be used under extreme temperature conditions and have a high power density which lead to a generation of 287 W of power for only a 7.6 x 15.2 cm heater. It is actively controlled by thermostats and applied to each octagonal surface of the inner baffle layer, since the transient temperature profile of the inside of the baffle determines the thermal gradients of the DST subsystems like the M2 and SMSS.

The conclusion of applying active thermal control is that active thermal control is very useful to decrease the thermal gradients of the sub-systems, in both the nominal design case, as well as the worst cases. Therefore, it is highly recommended that this is worked out in further detail.

10.1.2. Final Mechanical Performance

The final mechanical performance is summarized in Table 10.3 below:

Table 10.3: Mechanical performance of the telescopic boom structure versus the inflatable structure as designed by E. Korhonen and the requirements

Parameter	**Requirement**	**Telescopic Boom Structure**	**Inflatable Structure (E. Korhonen)**
Mass [kg]	15	12.19	23.6
Stowed Volume Baffle Only [m^3]	0.75 (goal) / 1.5 (treshold)	1.2	0.71
Stowed Volume Entire DST [m^3]	0.75 (goal) / 1.5 (treshold)	1.44	1.8
Deployed Volume Entire DST [m^3]	-	7.5	10.2
Stowed Eigenfrequency [Hz]	≥ 100 Hz	104.8	Unknown. Likely ≈ 0 Hz
Deployed Eigenfrequency [Hz]	≥ 0.9 Hz	4.7	0.92
Quasi-Static 30g Load: Maximum Von Mises Stress [Pa]	$\leq 1.3 \cdot 10^9$ (M55J Tensile Strength with 1.5 safety factor)	$1.39 \cdot 10^8$	Unknown
Quasi-Static 30g Load: Buckling Load Multiplier [-] **BAF-SYS-07-03**	≥ 2	237 (minimal)	Unknown

The deployable telescopic boom system meets all mechanical requirements, while the inflatable structure does not, as can be seen in Table 10.3.

10.1.3. Final Mass Budget

Table 10.4: Mass budget after preliminary thermal design has been established

Mass Calculation	
Sub-System	**Mass (kg)**
MLI	2.43
Truncated Cone M2	2.77
Baffle Structure	2.73
Deployment Actuation System	1.82
Total Mass	9.75
Safety Margin	25%
Total Mass Including Safety Margin	12.19
Mass Thermal System $M_{thermal}$	6.50
Mass Mechanical System $M_{mechanical}$	5.69
Mass Requirement	15

As can be seen in Table 10.4, the final total mass including safety margin of 25 % is 12.19 kg, which is well below the 15 kg requirement. Other stray-light hardware and mounting techniques still have to be added, but enough mass margin is left for this.

10.2. Compliance to Requirements

The research question proposed in Chapter 2 is going to be answered within this section, as it consists of the compliance to the requirements:

> *Which modifications are required to the existing thermal-mechanical design of the baffle to create a stable thermal environment such that the related thermal-mechanical budgets are met?* Consequently, the overall design shall comply with the functional, characteristic and constraint requirements.

The previous version of the thermal-mechanical design of the inflatable baffle exceeded all the in-orbit thermo-elastic budgets so a stable thermal environment could not be created with this previously designed baffle. Furthermore, the mass, stowed volume and stowed eigenfrequency all did not meet their requirements as summarized in Table 10.3. This means that structural integrity during LEOP cannot be guaranteed and that the entire DST becomes too large and heavy in stowed configuration. Furthermore, its deployment reliability

Table 10.5: Compliance to requirements used for this MSc thesis as summarized in Chapter 4

Compliance to Requirements		
Requirement ID	**Compliance**	**Comment**
	Survive Launch	
BAF-MEC-03-01/02/03	Compliant	$\sigma_{30g} = 1.39 \cdot 10^8 < 1.3 \cdot 10^9$ Pa (M55J tensile strength with safety factor)
BAF-MEC-03-04	Compliant	$\omega_{n,stowed} = 104.8 > 100$ Hz requirement
BAF-T-01	TBD	No thermal analysis of stowed configuration made yet
M2-T-01	Compliant	Worst case without a baffle: T < 373 K.
	Succesfull Deployment	
BAF-MEC-04	TBD	Further deployment analysis required
BAF-MEC-04-03	TBD	Further deployment analysis required
BAF-MEC-04-04-02-01	Compliant	> 200 mm clearance between M1 and baffle guaranteed
BAF-MEC-04-05-01	Compliant	Baffle deploys before M1/M2
	Perform Operations	
BAF-T-01	Compliant	Only when ATC is added
BAF-T-01-01	Compliant	All DST temperatures between 253-323 K.
BAF-T-01-02 & BAF-T-02-02	Compliant	BOL/EOL same for SiOx/VDA/Kapton + sensitivity analysis made
BAF-O-01	TBD	Full stray-light analysis still needs to be performed. However, truncated cone + coatings already implemented
BAF-O-01-01	Compliant	MagicBlack inner coating
	Survive OPS & Space Environment	
BAF-MEC-07-01	Compliant	-
BAF-MEC-07-02	TBD	5 layers MLI likely not sufficient for debris survival
BAF-MEC-07-03	Compliant	All materials TML of < 1 % and CVCM of < 0.01 %.
BAF-MEC-07-04	Compliant	SiOx/VDA/Kapton resistant to AO
BAF-MEC-07-04-01	TBD	Verification after manufacturing only
BAF-T-02	Compliant	All temperature requirements met
BAF-T-02-01	Compliant	Baffle MLI -250<T<177 °C.
BAF-MEC-07-06-01	Compliant	$\omega_{n,deployed,telescopic} \approx 5 \cdot \omega_{n,deployed,inflatable}$
BAF-MEC-07-06-02	TBD	Flutter TBA but likely compliant as $\omega_{n,deployed} \approx 5 \cdot \omega_{n,deployed,inflatable}$
BAF-MEC-07-06-03	Compliant	$\omega_{n,deployed,telescopic} \approx 5 \cdot \omega_{n,deployed,inflatable}$
BAF-MEC-07-06-03-01	Compliant	$\omega_{n,deployed,telescopic} = 4.72$ Hz > 0.9 Hz Hz
M2-T-02	Compliant	$T_{booms,deployed} \approx 280$ K < 473 K
	Cost	
BAF-SYS-01	TBD	The total DST cost requirement is unknown.
	Safety	
BAF-SYS-02	TBD	Mainly determined by debris impacts, so debris accumulation analyses TBA
BAF-SYS-02-01	Compliant	SPOF = actuators
BAF-SYS-02-02	TBD	Detailed deployment TBA
BAF-SYS-02-03 / BAF-SYS-03	Compliant	Redundant STEM actuators added
BAF-SYS-04	Compliant	Materials conform to ECSS standards (MLI standards)
BAF-SYS-05	Compliant	Thermal performance can be tested in TVC / TBC and mechanical performance (deployment) can be tested in 0g environment (parabolic flight)
BAF-SYS-06	Compliant	5 degrees temperature calculation uncertainty margin and 25 % mass uncertainty taken into account
BAF-SYS-07-03	Compliant	Buckling safety factor of 2 applied
	Regulations	
BAF-SYS-08/09	TBD	-
	Flexibility	
BAF-SYS-10	Compliant	Flexibility to accommodate modifications of requirements imposed on the TCS and deployement system added: rigid deployment
BAF-SYS-11	Compliant	Flexibility to offer design trimming capabilities added to accommodate late requirement updates: rigid deployment
	Constraints	
BAF-SYS-12	Compliant	Stowed volume 1.44 < 1.5 m^3
BAF-SYS-13	Compliant	Passive systems in stowed configuration, no power needed
BAF-SYS-14	TBD	No solar panels added yet, so TBA
BAF-SYS-15-01	Compliant	Deployed volume 7.5 m^3, fits well within LSS
BAF-SYS-16	Compliant	Total baffle mass 12.18 < 15 kg
BAF-SYS-17	TBD	Support structure TBA in full detail.
BAF-SYS-18	Compliant	All materials available (MLI lay-up, M55J, coatings)

is low as the inflation sequence consists of many failure modes, such as timely inflation in all booms, correct pressurization of the aluminium laminate and venting of the gas.

Therefore, several modifications are required to be made to the existing thermal-mechanical design to create a stable thermal environment so that the related thermo-mechanical budgets are met. To further ensure that the functional, characteristic and constraint requirements are met, an overview of the compliance to each requirement is summarized in Table 10.5.

The modifications to the existing design consist of a completely new mechanical deployment system. It is composed of a new geometry with a different deployment ratio, different CFRP material (M55J), new actuation system (STEM booms) and based on telescopic booms. It meets all the structural requirements as summarized in Table 10.3.

Furthermore, the baffle has been optimized for thermal stability using Passive Thermal Control methods. This includes the investigation of what the best height, radius and shape as well as the MLI lay-up and coating choice is. Additinally, a truncated cone is added. The addition of a truncated cone is proven to be useful for stray-light mitigation for Cassegrain telescopes in specific as a rule of thumb: [97], decreasing the thermal gradients in the SMSS athermalized system and decreasing the temperature levels of the baffle telescopic booom structures. Decreasing the temperature levels is also benificial to decrease the rate of potential outgassing, as outgassing increases with increasing temperature. The final thermal design, including the rationale of every design choice, is summarized in the Final Design Description chapter: Chapter 9.

It was found that an optimized PTC baffle does conform to the nominal temperature requirements, but does not conform to the in-orbit drift budgets that are important to guarantee optical stability. This holds for the entire PTC baffle, including truncated cone. It is therefore concluded that a stable thermal environment based on athermalization of the SMSS cannot be achieved with merely Passive Thermal Control as the effect of the eclipse is too strong.

For these reasons, Active Thermal Control (ATC) is concluded to be of crucial importance to meet the in-orbit drift budgets for M2 of 2 μm and 6 μrad so that the optical stability is guaranteed. Namely, even in the worst case (as analyzed with a sensitivity analysis) the maximum athermalized translation is 0.9 μm and 2.4 μrad, both conforming to the in-orbit drift budget requirements. Active Thermal Control is based on 8 flexible Polymide Thermofoil heaters as they can be embedded in Kapton of the MLI, are flexible, can be used under extreme temperature conditions and have a high power density which leads to a generation of 287 W of power for only a 7.6 x 15.2 cm heater. It is actively controlled by thermostats and applied to each octagonal surface of the inner baffle layer, since the transient temperature profile of the inside of the baffle determines the thermal gradients of the DST sub-systems like the M2 and SMSS. Controlling the operation of the ATC system between +15 and +22 ° C already provides a thermal stability of the M2 optical mirror that cannot be provided with merely an optimized Passive Thermal Control (PTC) baffle as the decrease in external Solar flux due to Eclipse is too large. Furthermore, uncertainties in the design that are not accounted/simulated for can be controlled by ATC and thermal fluctuations become less stringent so a margin in the budgets become available for structural on-board vibrations and flutter.

With the addition of ATC to the current passively optimized PTC baffle, it is guaranteed that the in-orbit drift budgets, that are most stringent, are met. This holds for the nominal case, but also for the worst hot- and cold cases. It is therefore feasible, at a preliminary level, to design a deployable baffle that creates a stable thermal environment to maintain in-orbit alignment and consequently guarantee the optical performance while imaging. This enables the next generation of high resolution Earth observation space telescopes at reducing cost.

10.3. Recommendations and Future Work

General

1. The remaining requirements in the Appendix that are not used for this thesis need to be verified.

Thermal

1. Continue the ATC design. A preliminary thermal analysis has already been performed using 287 W Polymide Thermofoil heaters applied to the inner MLI side, which showed promising results. However, it must be investigated whether this degrades the optical performance (stray-light). This is therefore a good option to be worked out by a future MSc student that also works on the stray-light analysis.

2. A recommendation is made to change the orbital configuration to a SSO Dusk-Dawn orbit, which results in no eclipse. However, this must be discussed with the optical team as this has direct implications on the Earth coverage.

3. The stowed configuration of the entire DST including baffle should be modelled in ESATAN and simulations should be performed. This is not done in this thesis, since the operational performance (thermo-elastics) at this stage was more crucial

4. Verification of analysis by testing in a Thermal Vacuum test chamber. This is crucial to validate the current thermal design (especially the effective emissivity/conductivity) and to verify the thermal requirements.

5. Adding Solar panels to the thermal model

6. Modelling and simulating post-deployment wrinkle formation of MLI, which could result in local hotspots.

Mechanical

1. Buckling investigation of STEM booms during deployment

2. Design of debris mitigation hardware, such as an additional Whipple shield. The preliminary mass estimate of a single wall Whipple shield for the DST baffle is 92.8 kg, so therefore it is recommended that this is optimized

3. Include attachment methods: truncated cone to the baffle structure and baffle to the interface housing

4. Design a locking mechanism for the telescopic tubes

5. Find out if Delrin-Acetal can be used as a coating for the inner sides of the telescopic booms, since this material is often used for low-friction applications. It already adheres to the temperature requirements (40 ° C to +120 ° C), so Delrin-Acetal might potentially be a good coating to reduce friction in the telescopic booms.

6. Flexible Body Dynamics analysis for the axial deployment

Thermal-Mechanical

1. Using preliminary thermo-elastic calculations as input for proper thermo-elastic calculation using SINAS: thermal nodes have to be mapped with mechanical FEM nodes to produce a thermo-mechanical FEM model used for thermo-elastic FEM calculations

Optical

1. A stray-light analysis should be made using the current thermal-mechanical design of the baffle

2. An updated trade-off between impact angle and coatings of the truncated cone should be made that includes both stray-light results and thermo-elastic results.

Bibliography

[1] Antonio Ciccolella - ESA. Mission analysis aspects for earth observations missions. URL `https://www.summerschoolalpbach.at/docs/2010/lectures/Ciccolella.pdf`.

[2] A Anvari, F Farhani, and KS Niaki. Comparative study on space qualified paints used for thermal control of a small satellite. 2009.

[3] J.W. Arink. Ae4020 literature study - literature review on the continuation of the thermo-mechanical design of the baffle. 2018.

[4] Jeremy Banik and Thomas Murphey. Performance validation of the triangular rollable and collapsible mast. 2010.

[5] J.W. Lopes Barreto. Deployable space telescope: Optimal boom design for high precision deployment of the secondary mirror. Master's thesis, Technische Universiteit Delft, 2017.

[6] Randall F Barron and Gregory F Nellis. *Cryogenic heat transfer*. CRC press, 2016.

[7] Janet L Barth. Space and atmospheric environments: from low earth orbits to deep space. In *Protection of Materials and Structures from Space Environment*, pages 7–29. Springer, 2004.

[8] Samuel B Batdorf, Murry Schildcrout, and Manuel Stein. Critical stress of thin-walled cylinders in axial compression. 1947.

[9] Cynthia A Belk, Jennifer H Robinson, Margaret B Alexander, William J Cooke, and Steven D Pavelitz. Meteoroids and orbital debris: effects on spacecraft. 1997.

[10] W Keith Belvin, Marco Straubel, W Keats Wilkie, Martin E Zander, Juan M Fernandez, and Martin F Hillebrandt. Advanced deployable structural systems for small satellites. 2016.

[11] Gabi Ben-Dor, Anatoly Dubinsky, and Tov Elperin. *High-Speed Penetration Dynamics: engineering models and methods*. World Scientific, 2013.

[12] ER Benton and EV Benton. Space radiation dosimetry in low-earth orbit and beyond. *Nuclear Instruments and Methods in Physics Research Section B: Beam Interactions with Materials and Atoms*, 184 (1-2):255–294, 2001.

[13] G. D. Boreman. Modulation transfer function in optical and electro-optical systems. *SPIE Press*, 2001.

[14] HD Burns. Outgassing test for non-metallic materials associated with sensitive optical surfaces in a space environment. Technical report, MSFC-SPEC-1443.

[15] Rob Gutro NASA's Goddard Space Flight Center. Super-tough sunshield to fly on the james webb space telescope. URL `https://www.nasa.gov/topics/universe/features/jwst_toughshield.html`. Accessed: 2019-07-15.

[16] Craig J Chivatero, Aleck L Lee, and J Keith Kalinowski. Contamination analysis for a hubble space telescope observation of venus. In *Optical System Contamination V, and Stray Light and System Optimization*, volume 2864, pages 127–137. International Society for Optics and Photonics, 1996.

[17] Eric Christiansen and Dana Lear. Micrometeoroid and orbital debris environment and hypervelocity shields. 2012.

[18] Eric L Christiansen and Dana M Lear. Toughened thermal blanket for micrometeoroid and orbital debris protection. *Procedia Engineering*, 103:73–80, 2015.

[19] Emilio Chuvieco. *Earth observation of global change: The role of satellite remote sensing in monitoring the global environment*. Springer, 2008.

[20] M. Coesel and N. Pennings. Background for thermal modeling of multi layer insulation blankets. *arXiv preprint arXiv:1110.3193*, 1993.

[21] coolcodea. 116. lighting in 3d – specular lighting. URL https://coolcodea.wordpress.com/2013/09/30/116-lighting-in-3d-specular-lighting/. Accessed: 2018-12-18.

[22] M. Corvers. Design of a primary mirror deployment mechanism for a deployable space telescope. Master's thesis, 2018.

[23] D.Dolkens. A deployable telescope for sub-meter resolutions from microsatellite platforms. Master's thesis, Technische Universiteit Delft, 2015.

[24] D.Dolkens. Design and optimization of a deployable telescope for earth observation applications. Master's thesis, Technische Universiteit Delft, 2018.

[25] Joyce Dever, Bruce Banks, Kim de Groh, and Sharon Miller. Degradation of spacecraft materials. In *Handbook of environmental degradation of materials*, pages 465–501. Elsevier, 2005.

[26] Jochen Doenecke. Survey and evaluation of multilayer insulation heat transfer measurements. Technical report, SAE Technical Paper, 1993.

[27] M Donabedian, DG Gilmore, JW Stultz, GT Tsuyuki, and EI Lin. Insulation. *Spacecraft thermal control handbook*, 1:161–205, 2002.

[28] DuPont. Delrin® acetal resin, . URL https://www.dupont.com/products-and-services/plastics-polymers-resins/thermoplastics/brands/delrin-acetal-resin.html. Accessed: 2019-08-04.

[29] DuPont. Dupont kapton® hn polyimide film, . URL https://www.dupont.com/content/dam/dupont/products-and-services/membranes-and-films/polyimde-films/documents/DEC-Kapton-HN-datasheet.pdf. Accessed: 2019-07-12.

[30] Max W Durney and Alan D Pendley. Method of designing fold lines in sheet material, October 21 2008. US Patent 7,440,874.

[31] Yuri Ebata. Bending, wrinkling, and folding of thin polymer film/elastomer interfaces. 2013.

[32] Sunday C Ekpo and Danielle George. A system engineering analysis of highly adaptive small satellites. *IEEE Systems Journal*, 7(4):642–648, 2012.

[33] ECSS Secretariat ESA-ESTEC. Space engineering - verification guidelines. URL http://everyspec.com/ESA/download.php?spec=ECSS-E-10-02C.047796.pdf. Accessed: 2019-01-21.

[34] Peter Potapov et al. Mapping the world's intact forest landscapes by remote sensing. *Ecology and Society*, 13(2), 2008. ISSN 17083087. URL http://www.jstor.org/stable/26267984.

[35] JR Fekete and JN Hall. Design of auto body: Materials perspective. In *Automotive Steels*, pages 1–18. Elsevier, 2017.

[36] MM Finckenor and D Dooling. Multilayer insulation material guidelines. 1999.

[37] Peter Fortescue, Graham Swinerd, and John Stark. *Spacecraft systems engineering*. John Wiley & Sons, 2011.

[38] Xavier Gabrion, Vincent Placet, Frédérique Trivaudey, and Lamine Boubakar. About the thermomechanical behaviour of a carbon fibre reinforced high-temperature thermoplastic composite. *Composites Part B: Engineering*, 95:386–394, 2016.

[39] Hota VS GangaRao, Narendra Taly, and PV Vijay. *Reinforced concrete design with FRP composites*. CRC press, 2006.

[40] Peter Giesen and Erik Folgering. Design guidelines for thermal stability in optomechanical instruments. In *Optomechanics 2003*, volume 5176, pages 126–135. International Society for Optics and Photonics, 2003.

[41] David G Gilmore, JC Lyra, and JW Stultz. Heaters. *Spacecraft Thermal Control Handbook*, 1:223–245, 2002.

[42] DG Gilmore, WK Stuckey, and M Fong. Thermal surface finishes. *Spacecraft Thermal Control Handbook, 2nd ed.; Gilmore, DG, Ed*, pages 139–159, 2002.

[43] GoodFellow. Polyethylene terephthalate (polyester, pet, petp) material information. URL `http://www.goodfellow.com/E/Polyethylene-terephthalate.html`. Accessed: 2019-07-12.

[44] Yann Goueffon, Laurent Arurault, Catherine Mabru, Claire Tonon, and Pascale Guigue. Black anodic coatings for space applications: study of the process parameters, characteristics and mechanical properties. *Journal of Materials Processing Technology*, 209(11):5145–5151, 2009.

[45] Dr.-Ing. Christian Gritzner. Why do some space telescopes have to be cooled? URL `https://www.dlr.de/en/desktopdefault.aspx/tabid-5170/8702_read-17203/8702_page-3/`. Accessed: 2019-03-13.

[46] E Grossman and I Gouzman. Space environment effects on polymers in low earth orbit. *Nuclear Instruments and Methods in Physics Research Section B: Beam Interactions with Materials and Atoms*, 208: 48–57, 2003.

[47] Northrop Grumman. Stem products and programs. URL `https://www.northropgrumman.com/BusinessVentures/AstroAerospace/Products/Documents/pageDocs/STEM_Hardware_Programs.pdf`. Accessed: 2019-07-18.

[48] John H Henninger. Solar absorptance and thermal emittance of some common spacecraft thermal-control coatings. Technical report, NATIONAL AERONAUTICS AND SPACE ADMINISTRATION WASHINGTON DC, 1984.

[49] Peter Hidnert and HS Krider. Thermal expansion of aluminum and some aluminum alloys. *Journal of research of the national bureau of standards*, 48(3):209–220, 1952.

[50] Tom Irvine. Bending frequencies of beams, rods, and pipes. *Compare*, 500(s 50), 2012.

[51] Christopher R Jackson and Werner Alpers. The role of the critical angle in brightness reversals on sunglint images of the sea surface. *Journal of Geophysical Research: Oceans*, 115(C9), 2010.

[52] Robert R Johnson, Murat H Kural, and George B Mackey. Thermal expansion properties of composite materials. Technical report, LOCKHEED MISSILES AND SPACE CO INC SUNNYVALE CA, 1981.

[53] Pratistha Kansakar and Faisal Hossain. A review of applications of satellite earth observation data for global societal benefit and stewardship of planet earth. *Space Policy*, 36:46–54, 2016.

[54] Robert Karam. *Satellite thermal control for systems engineers*. American Institute of Aeronautics and Astronautics, 1998.

[55] Gabriel Karpati, Tupper Hyde, Hume Peabody, and Matthew Garrison. Resource management and contingencies in aerospace concurrent engineering. In *AIAA SPACE 2012 conference & exposition*, page 5273, 2012.

[56] Ritva A Keski-Kuha, Charles W Bowers, Manuel A Quijada, James B Heaney, Benjamin Gallagher, Andrew McKay, and Ian Stevenson. James webb space telescope optical telescope element mirror coatings. In *Space Telescopes and Instrumentation 2012: Optical, Infrared, and Millimeter Wave*, volume 8442, page 84422J. International Society for Optics and Photonics, 2012.

[57] E.A. Korhonen. Ae4020 literature study - deployable space telescope. 2018.

[58] E.A. Korhonen. Design of a deployable baffle for the deployable space telescope. Master's thesis, 2019.

[59] H Koskinen, E Tanskanen, R Pirjola, A Pulkkinen, C Dyer, D Rodgers, P Cannon, JC Mandeville, D Boscher, and A Hilgers. Space weather effects catalogue. *ESA Space Weather Study (ESWS)*, (2.2), 2001.

[60] A. Krikken. Design of the secondary mirror support structure for the deployable space telescope. Master's thesis, 2018.

[61] J.M. Kuipers. Dst systems engineering revision december 2018. 2018.

[62] Norbert Adolph Lange et al. Lange's handbook of chemistry/editor, john a. dean; formerly compiled and edited by norbert adolph lange. page 2807–2758.

[63] Carlye Lauff, Timothy W Simpson, Mary Frecker, Zoubeida Ounaies, Saad Ahmed, Paris von Lockette, Rebecca Strzelec, Robert Sheridan, and Jyh-Ming Lien. Differentiating bending from folding in origami engineering using active materials. In *ASME 2014 International Design Engineering Technical Conferences and Computers and Information in Engineering Conference*, pages V05BT08A040–V05BT08A040. American Society of Mechanical Engineers, 2014.

[64] Rene Laureijs, J Amiaux, S Arduini, J-L Augueres, J Brinchmann, R Cole, M Cropper, C Dabin, L Duvet, A Ealet, et al. Euclid definition study report. *arXiv preprint arXiv:1110.3193*, 2011.

[65] GR Liu. A step-by-step method of rule-of-mixture of fiber-and particle-reinforced composite materials. *Composite structures*, 40(3-4):313–322, 1997.

[66] Tianyu Liu, Quan Sun, Jieru Meng, Zhengqiang Pan, and Yanzhen Tang. Degradation modeling of satellite thermal control coatings in a low earth orbit environment. *Solar Energy*, 139:467–474, 2016.

[67] MatWeb Material Property Data LLC. Cytec (solvay group) cycom® 950-1 epoxy prepreg unidirectional tape with 36 URL `http://www.matweb.com/search/datasheet.aspx?matguid=2a8492fb7a944588957aa57fdda20b3e`. Accessed: 2019-07-02.

[68] Shengnan Lu, Dimiter Zlatanov, and Xilun Ding. Approximation of cylindrical surfaces with deployable bennett networks. *Journal of Mechanisms and Robotics*, 9(2):021001, 2017.

[69] G.van Marrewijk. Aberration correction system for a deployable space telescope. Master's thesis, 2018.

[70] Minco. Polyimide thermofoiltm heaters. thin, flexible heating solutions from -200 to 200°c, . URL `https://www.minco.com/~/media/WWW/Resource%20Library/Heaters/Polyimide%20Thermofoil%20Heater%20Tech%20Spec.ashx`. Accessed: 2019-08-05.

[71] Minco. Thermofoiltm solutions for heating, . URL `http://www.temflexcontrols.com/pdf/hs202a.pdf`. Accessed: 2019-08-05.

[72] Kim K. de Groh Miria M. Finckenor. Space environmental effects. URL `https://www.nasa.gov/sites/default/files/files/NP-2015-03-015-JSC_Space_Environment-ISS-Mini-Book-2015-508.pdf`. Accessed: 2018-11-27.

[73] Mehran Mobrem and Chris Spier. Design and performance of the telescopic tubular mast. In *Aerospace Mechanisms Symposium*, 2012.

[74] NASA. Chapter 5. systems engineering technical reviews. URL `https://nodis3.gsfc.nasa.gov/displayCA.cfm?Internal_ID=N_PR_7123_001A_&page_name=Chapter5#_Toc159347530`. Accessed: 2018-12-17.

[75] Michael Ohadi and Jianwei Qi. Thermal management of harsh-environment electronics. In *Microscale Heat Transfer Fundamentals and Applications*, pages 479–498. Springer, 2005.

[76] S. Pepper. Design of a primary mirror fine positioning mechanism for a deployable space telescope. Master's thesis, 2018.

[77] MJ Persky. Review of black surfaces for space-borne infrared systems. *Review of Scientific Instruments*, 70(5):2193, 1999.

[78] Vincent L Pisacane. *Fundamentals of space systems*. Johns Hopkins University/Appli, 2005.

[79] Juan Reveles, Mike Lawton, Vincent Fraux, and Vinoth Gurusamy. The development of a low mass extendible composite boom for small satellite applications. 2015.

[80] Warren M Rohsenow, James P Hartnett, Young I Cho, et al. *Handbook of heat transfer*, volume 3. McGraw-Hill New York, 1998.

[81] John J Scialdone and Carroll H Clatterbuck. Four space application material coatings on the long-duration exposure flight (ldef). 1992.

[82] ECSS Secretariat. Ecss space engineering-fracture control. Technical report, Technical Report ECSS-E-ST-32-01C, ESA, 2008.

[83] ECSS Secretariat. Ecss space engineering-structural general requirements. Technical report, Technical Report ECSS-E-ST-32C , ESA, 2008.

[84] ECSS Secretariat. Ecss space engineering-thermal control general requirements. Technical report, Technical Report ECSS-E-ST-31C, ESA, 2008.

[85] ECSS Secretariat. Ecss space engineering-space environment. Technical report, Technical Report ECSS-E-ST-10-04C, ESA, 2008.

[86] ECSS Secretariat. Ecss space engineering-structural factors of safety for spaceflight hardware. Technical report, Technical Report ECSS-E-ST-32-10 , ESA, 2009.

[87] ECSS Secretariat. Ecss space product assurance-materials, mechanical parts and processes. Technical report, Technical Report ECSS-Q-ST-70C , ESA, 2009.

[88] ECSS Secretariat. Ecss space engineering-mechanisms. Technical report, Technical Report ECSS-E-ST-33-01C , ESA, 2009.

[89] ECSS Secretariat. Ecss space engineering-space engineering materials. Technical report, Technical Report ECSS-E-ST-32-08C , ESA, 2014.

[90] ECSS Secretariat. Ecss space engineering-explosive subsystems and devices. Technical report, Technical Report ECSS-E-ST-33-11C , ESA, 2017.

[91] Karsten Seiferlin, Sumita Chakraborty, Kurt S Gunderson, Josef Fischer, Benjamin Luthi, Daniele Piazza, Martin Rieder, Martin Sigrist, Nicolas Thomas, and Thomas Weigel. Design and manufacture of a lightweight reflective baffle for the bepicolombo laser altimeter. *Optical engineering*, 46(4):043003, 2007.

[92] Stefano Seriani and Paolo Gallina. A storable tubular extendible member (stem) parallel robot: Modelization and evaluation. *Mechanism and Machine Theory*, 90:95–107, 2015.

[93] AK Sharma. Surface engineering for thermal control of spacecraft. *Surface engineering*, 21(3):249–253, 2005.

[94] C Sickinger and E Breitbach. Ultralightweight deployable space structures. In *4th Internationalconference on thin-walled structures*, 2004.

[95] Edward M Silverman. Space environmental effects on spacecraft: Leo materials selection guide, part 1. 1995.

[96] Emma A Taylor, MK Herbert, BAM Vaughan, and JAM McDonnell. Hypervelocity impact on carbon fibre reinforced plastic/aluminium honeycomb: comparison with whipple bumper shields. *International Journal of Impact Engineering*, 23(1):883–894, 1999.

[97] V Yu Terebizh. Optimal baffle design in a cassegrain telescope. *Experimental Astronomy*, 11(3):171–191, 2001.

[98] Anders Thorseth. Ledmet report: Simulation and correction of stray light in spectrometers. 2018.

[99] J-M Ting, C Tang, and P Lake. Vapor grown carbon fiber reinforced aluminum matrix composites for enhanced thermal conductivity. *MRS Online Proceedings Library Archive*, 551, 1998.

[100] INC TORAY CARBON FIBERS AMERICA. Torayca m55j data sheet, technical data sheet no. cfa-017. URL `https://www.toraycma.com/file_viewer.php?id=5096`. Accessed: 2019-06-12.

[101] AK Van der Vegt and LE Govaert. Polymeren. *Tc*, 186:75, 2005.

[102] T.T.D. van Wees. Thermal modelling and analysis of the deployable space telescope. 2019.

[103] M.G.S. Voorn. Testing the secondary mirror support structure of the deployable space telescope. Master's thesis, 2018.

[104] Bin Wang, Zhancheng Li, Chunhui Wang, Stefano Signetti, Benjamin V Cunning, Xiaozhong Wu, Yuan Huang, Yi Jiang, Haofei Shi, Seunghwa Ryu, et al. Folding large graphene-on-polymer films yields laminated composites with enhanced mechanical performance. *Advanced Materials*, 30(35):1707449, 2018.

[105] Ting Wang, Hongsheng Zhang, Hui Lin, and Chaoyang Fang. Textural–spectral feature-based species classification of mangroves in mai po nature reserve from worldview-3 imagery. *Remote Sensing*, 8(1): 24, 2015.

[106] James R Wertz. Orbit and constellation design. *Space mission analysis and design(2 nd edition)(A 95-23902 05-12), Torrance, CA/Dordrecht, Netherlands, Microcosm, Inc./Kluwer Academic Publishers, 1995,*, pages 157–195, 1995.

[107] Xu Zeshui and Wei Cuiping. A consistency improving method in the analytic hierarchy process. *European journal of operational research*, 116(2):443–449, 1999.

Appendices

A

Input Thermal Analyses ESATAN-TMS

Table A.1: Input for ESATAN-TMS, mainly based on Orbit Definition and Assumption, Section 3.1

Parameter	Value	Units
Environment		
Sun-Planet System		
Planet Radius	6371000	m
Gravitational Acceleration	9.798	$\frac{m}{s^2}$
Sun Planet Distance	148453932600	m
Solar Declination	0	degrees
Sun's Right Ascension	0	degrees
Orbital Precession	0	degrees/s
Sun Radius	$695800 \cdot 10^3$	m
Celestial Body Image	Earth	-
Sun Specific		
Sun Temperature	5778	K
Solar Constant Override	0	$\frac{W}{m^2}$
Sun Rays	Parallel Rays	-
Sun Distance Override	0	m
Planet Albedo		
Method	Uniform	-
Albedo	0.306	-
Planet Temperature		
Method	Uniform	-
Temperature	254.3	K
Infra-Red Emissivity	1	-
Orbit		
Ellipse		
Eccentricity	0	-
Semi-Major Axis	6871000	m
Altitude of Apogee	500000	m
Altitude of Perigee	500000	m
Inclination	97.4	degrees
Right Ascension	-22.5	degrees
Argument of Periapsis	0	degrees
Arc		
Initial True Anomaly	0	degrees
Final True Anomaly	360	degrees
Positions		
Angle Gap	20	degrees
Number of Positions	18	-
True Anomalies Vector	-	degrees
Eclipse Entry Exit Points	Off	
Pointing		
Primary Pointing		
Pointing Vector	[0.0, 0.0, 1.0]	-
Pointing Direction	NADIR	-
Secondary Pointing		
Pointing Vector	[0.0, 1.0, 0.0]	-
Pointing Direction	NORMAL TO ORBIT	-
User Defined Movement		
Phi/Psi/Omega	0.0	degrees
Phi/Psi/Omega Rotation Rate	0	degrees/s
Spacecraft Movement		
Type	None	-

B

DST N2 Interface

The N2 (N-squared) diagram gives an overview of the interfaces between different sub-systems in terms of inputs and outputs. The N2 diagram is a type of functional analysis to map the architecture of the DST and is useful to find relations between the sub-systems that influence each other.

Figure B.1: DST N2 interface map to functionally analyse the DST architecture. Developed as a group work package in the DST Systems Engineering Budgets document, revision december 2018, [61].

C

Full List of Baffle Requirements

Table C.1: Baffle functional requirements: Survive AIT, Maintain Stowage, Launch Survival and Successful Deployment.

ID	Description
Survive AIT	
BAF-MEC-01	The baffle shall survive assembly, handling, transport and testing in both stowed and deployed configuration.
Maintain Stowage	
BAF-MEC-02	The baffle shall maintain in stowed configuration until deployment is initiated.
BAF-MEC-02-01	The baffle's HDRM mechanism shall be able to hold the baffle in stowed configuration until deployment is initiated.
BAF-MEC-02-02	The baffle's HDRM mechanism shall be capable to survive the stowed configuration until deployment is initiated.
BAF-MEC-02-02-01	The baffle including HDRM shall mitigate the effect of creep in stowed configuration, such that it shall not result in consequential damage to the equipment or other spacecraft components.
BAF-MEC-02-02-02	Storage conditions shall not cause any degradation to the thermal hardware.
Survive Launch	
BAF-MEC-03	The baffle shall survive the launch in stowed configuration.
BAF-MEC-03-01	The baffle shall survive a quasi-static load of 30g applied simultaneously to the x- and y- axes in the launcher coordinate frame in the stowed configuration during launch.
BAF-MEC-03-02	The baffle shall survive a quasi-static load of 30g applied simultaneously to the x- and z- axes in the launcher coordinate frame in the stowed configuration during launch.
BAF-MEC-03-03	The baffle shall survive a quasi-static load of 30g applied simultaneously to the y- and z- axes in the launcher coordinate frame in the stowed configuration during launch.
BAF-MEC-03-04	The baffle shall have a minimum first eigenfrequency of 100 Hz in stowed configuration during launch.
BAF-MEC-03-04	The stowed baffle shall survive a heat flux of 1135 $\frac{W}{m^2}$ immediately after separation of the fairing.
Successful Deployment	
BAF-MEC-04	The baffle shall deploy succesfully.
BAF-MEC-04-01	The HDRM shall initiate the deployment of the baffle upon actuation command.
BAF-MEC-04-02	The baffle booms shall have a minimum bending stiffness of TBD N/m.
BAF-MEC-04-03	The baffle shall survive deployment.
BAF-MEC-04-03-01	The baffle shall survive local- and global buckling loads.
BAF-MEC-04-03-02	The baffle shall survive deployment shocks and vibrations.
BAF-MEC-04-03-03	The baffle shall deploy in TBD s within the acceleration range of TBD $\frac{\mathrm{m}}{\mathrm{s}^2}$.
BAF-MEC-04-03-04	The baffle shall mitigate the creation of hot-spots such that it shall not result in consequential structural- or thermal damage that does not conform to the operational requirements.
BAF-MEC-04-03-05	The baffle shall survive mechanism heat dissipation.
BAF-MEC-04-04	The baffle shall achieve a deployed configuration that conforms to the operational requirements with a position accuracy of TBD m.
BAF-MEC-04-04-01	The HDRM shall be provided with a regular mechanical end stop to limit the motion
BAF-MEC-04-04-02	The baffle geometry shall not obstruct any telescope elements and not interfere with the optical performance
BAF-MEC-04-05	The baffle shall not impede the deployment of the primary- and secondary mirror.
BAF-MEC-04-05-01	The baffle shall deploy before the primary- and secondary mirror

Table C.2: Baffle functional requirements: Perform Operations, Survive OPS and Space Environment.

ID	Description
Perform Operations	
BAF-T-01	The baffle shall create a stable thermal environment.
BAF-T-01-01	The temperatures within the baffle shall have a temporal temperature stability of TBD K/s or below.
BAF-T-01-02	The temperatures within the baffle shall have a spatial temperature uniformity / thermal gradient of 0.1 mK/m or below.
BAF-T-01-02-01	The material of the inner layer of the baffle shall have a conductivity of at least TBD $\frac{W}{mK}$ or higher in axial direction.
BAF-T-01-03	The temperatures within the baffle shall remain within a stability bandwith of 297-299 K.
BAF-T-01-04	The baffle shall maintain its operational functionality in both extreme cases of BOL- and EOL optical material properties.
BAF-O-01	The baffle shall mitigate stray-light in deployed configuration.
BAF-O-01-01	The internal layer of the baffle shall absorb at least 90 % of incident radiation in both UV- and IR wavelength spectra.
BAF-O-01-02	The baffle shall apply two truncated trones near primary mirror and secondary mirror.
Survive OPS & **Space Environment**	
BAF-MEC-07	The baffle shall survive the operations- and space environment in deployed configuration.
BAF-MEC-07-01	The operational loads shall be added to the in-orbit loads.
BAF-MEC-07-02	The baffle shall survive the impact of medium sized debris, $1 < d < 100$mm.
BAF-MEC-07-02-01	The worst crack-like defect in the part shall not grow to such an extent that the minimum specified performance is no longer assured within a specified safe life interval, using a design life factor of at least 4. [82]
BAF-MEC-07-02-02	For metallic materials the maximum sustained stress-intensity factor Kmax, shall not exceed the threshold stress-intensity factor for stress-corrosion cracking KISCC.
BAF-MEC-07-02-03	The failure of the item shall not result in the release of any part or fragment which can create a catastrophic or critical hazard.
BAF-MEC-07-02-04	The fatigue analysis for metallic parts shall be replaced by a crack growth analysis using an equivalent initial crack size of a = c = 0,125 mm (corner or surface crack), and demonstrating no failure after four (4) times the service life.
BAF-MEC-07-02-05	For metallic, composite, bonded and sandwich enclosures it shall be verified that the loose item does not penetrate or fracture the enclosure with a safety factor of 1,5 on its kinetic energy.
BAF-MEC-07-02-06	The maximum tensile stress based on net cross-sectional area in the part at limit load shall be no greater than 30 percent of the ultimate tensile strength for the metal used.
BAF-MEC-07-02-07	Low-risk fracture items are shown to possess acceptable resistance to crack growth from potential initial defects caused by machining, assembly, and handling, by demonstrating that assumed initial surface cracks of 3 mm depth and 6 mm length and corner cracks of 3 mm radius from holes and edges do not grow to failure in less than four complete service lifetimes.

Table C.3: Baffle functional requirements: Survive OPS and Space Environment continued.

ID	Description
Continued: Survive OPS & Space Environment	
BAF-MEC-07-03	The materials to be used for the baffle shall limit outgassing to a TML of < 1 % and CVCM of < 0.01 %.
BAF-MEC-07-04	The baffle shall be resistant against AO and plasma/ionizing radiation.
BAF-MEC-07-04-01	The baffle shall make use of a protective outer coating that is resistant to AO.
BAF-MEC-07-04-02	The baffle shall be electrically bonded (grounded) to the S/C bus to avoid electrical charging.
BAF-T-02	The baffle shall survive the thermal operational- and environmental loads in deployed configuration.
BAF-T-02-01	The baffle shall survive extreme hot and cold temperatures between -250 ° C and +177 ° C respectively.
BAF-MEC-07-05-02	The baffle shall avoid heat fluxes due to plume interaction due to the firing of thrusters during ABM and AOC.
BAF-T-02-02	The baffle shall survive the thermal loads both with BOL- and EOL optical properties.
BAF-MEC-07-05-04	The baffle design shall use the parameters for operational orbits, as specified by ECSS-E-ST-31C, Section 4.1.4.
BAF-MEC-07-06	The baffle shall survive the mechanical operational- and environmental loads in deployed configuration.
BAF-MEC-07-06-01	The baffle shall survive on-board vibrations of TBD due to the reaction wheel in deployed configuration.
BAF-MEC-07-06-02	The baffle shall mitigate the effect of thermal flutter in deployed configuration.
BAF-MEC-07-06-03	The baffle shall survive vibration fatigue due to on-board vibrations and thermal flutter
BAF-MEC-07-06-03-01	The baffle shall have a minimum first eigenfrequency ≥ 0.9159 Hz in deployed configuration.
BAF-MEC-07-06-03-02	The baffle shall have a structural bending damping factor of TBD.

Table C.4: Baffle characteristic requirements

ID	Description
BAF-SYS-01	The total cost of the baffle shall be no more than TBD over the mission lifetime of the DST.
BAF-SYS-02	The baffle shall have an operational expected lifetime of 5 years.
BAF-SYS-02-01	All single point of failure modes of the baffle and its sub-components shall be identified.
BAF-SYS-02-02	The baffle shall have a MTBF of at least 5 years for single point of failure components.
BAF-SYS-02-03	All single point of failures should be eliminated by redundant components.
BAF-SYS-03	Active elements of mechanisms, such as sensors, motor windings, brushes, actuators, switches and electronics, shall be redundant if a mechanism is is not completely redundant.
BAF-SYS-04	The baffle shall use space qualified parts, materials and procesess (PMP).
BAF-SYS-05	The baffle shall be designed such that conformance to performance requirements can be demonstrated by thermal analyses and thermal test.
BAF-SYS-06	Verification by analysis shall take into account uncertainties
BAF-SYS-07	The baffle shall be designed using factors of safety (FoS) conform with ECSS-E-ST-32-10.
BAF-SYS-07-01	The baffle shall use a minimum yield stress safety factor (FoS) of 1.25 for standard metallic materials
BAF-SYS-07-02	The baffle shall use a minimum ultimate stress safety factor (FoS) of 1.5 for standard metallic materials
BAF-SYS-07-03	The baffle shall use a minimum buckling safety factor (FoS) of 2 for standard metallic materials
BAF-SYS-07-04	The baffle shall use a minimum fatigue safety factor (FoS) of 4 for standard metallic materials
BAF-SYS-08	The baffle shall not use any ITAR controlled components or technologies
BAF-SYS-09	The baffle shall not comply with national and international regulations during AIT activities, launch, operations and EOL.
BAF-SYS-10	The baffle design shall incorporate flexibility to accommodate modifications of requirements imposed on the TCS during the project development phase
BAF-SYS-11	The baffle design shall incorporate flexibility to offer trimming capabilities to accommodate late requirement updates.

Table C.5: Baffle constraint requirements

ID	Description
BAF-SYS-11	The volume of the baffle shall not exceed 1.5 m^3 (threshold) / 0.75 m^3) (goal) when in stowed configuration.
BAF-SYS-12	The stowed baffle shall not require any power during launch
BAF-SYS-13	The operational functionality of the baffle, as well as the ability to survive the operations and space environment shall be compatible with the power- and radiation exchange of the solar panels.
BAF-SYS-14	The baffle and its HDRM shall be compatible with operation on ground in ambient and thermal vacuum conditions.
BAF-SYS-15	The baffle in deployed configuration should fit inside a TV/TB chamber to allow for thermal testing.
BAF-SYS-15-01	The maximum volume of the baffle in deployed configuration should conform to the usable volume of a medium-sized vacuum chamber from ESA: 0.85 mm diameter and 1.5 m by 1.9 m long.
BAF-SYS-16	The mass of the entire baffle including deployment mechanism shall not exceed 15 kg
BAF-SYS-17	The baffle shall be properly attached to the instrument housing, such that it gives structural support.
BAF-SYS-18	The baffle shall be manufacturable with compliance to the availability of parts and materials.
BAF-SYS-19	the baffle shall have a clearance of 200 mm in deployed configuration between M1 and any point of the baffle.

D

Detailed Trade-off Descriptions

In this chapter detailed textual overviews are given of the two main mechanical trade-offs made in Chapter 7. In two subsequent sections, the trade-off between the telescopic- and inflatable concepts and the trade-off between different telescopic concepts are explained.

I. Telescopic versus Inflatable Concepts

In this section a detailed textual description of the trade-off between the telescopic and inflatable concepts is made. This is the full description which is roughly summarized in Table 7.4.

Stowed Volume

The stowed volume is most important, since this is a mission requirement and is the main driver behind developing a Deployable Space Telescope: the volume of the instrument in stowed configuration shall not exceed $0.73 m^3$ (goal)/ $1.5 m^3$ (threshold). Unlike the mass requirement, this stowed volume requirement directly affects the baffle, since the baffle is the outer shield which drives the stowed volume budget.

The inflatable concept exceeds both the goal and treshold stowed volume requirement, since it has a stowed volume of 1.8 m^3. The telescopic boom can be made compact to adhere to the threshold stowed volume requirement by finding the right values for axial- and radial deployment ratio, while still maintaining proper structural integrity. Based on preliminary calculations (these are also performed in the next sections) using an extra safety margin of 25 % to account for packing of the MLI and other uncertainties, a stowed volume of $\pi \cdot R^2 \cdot H \cdot S_{margin} = \pi \cdot 0.5^2 \cdot 0.955 \cdot 1.25 = 0.94 m^3$ is calculated. It is doable to design a telescopic boom structure concept to stay within the stowed volume treshold requirement. This stowed volume is approximately twice as good as for the inflation concept. Therefore, the telescopic concept scores twice as high on the stowed volume criteria: 66.6% versus 33.4 %.

Mass

Mass, similar to the stowed volume, is of utter importance, since this is also a mission requirement. Note that the mission requirement states the mass requirement of the entire satellite, but a mass budget for the baffle sub-system can be deduced from this. The mass criterion is less important than the stowed volume requirement, since there is no direct relation with the mass budget allocated for the baffle and the entire mass budget of the satellite. The 15 kg requirement was taken as a baseline, but can be altered to a higher value if possible, if the mass budgets of the other sub-systems allow.

The inflatable concept exceeds the mass budget of 15 kg as it has a total mass of 23.6 kg, mainly due to the addition of the pressure system (valves, CGG, etcetera). The telescopic boom concept can be designed such that it does meet the mass budget, since the radius and thickness of tubes can be designed to conform the budgets (also taking into account manufacturability). A preliminary mass calculation, see Table 7.8, shows that a boom mass of around 6 kg can be established. Taking into account an uncertainty margin of 50 % for the deployment actuation system and attachment methods, a mass of 9 is calculated. With the mass of MLI of 1.96 kg and truncated cone of 1.61 kg, the 15 kg can still be met. Therefore, the telescopic boom structure scores better on this criterion: $\frac{1}{\frac{23.6}{15}+1}$ = 63.8% and the inflatable concept has a scoring weight of 1 - 0.638 = 0.362 %.

Deployment Complexity/Reliability
Deployment complexity is also tremendously important, since the more complex the deployment is, the more failure modes are present in the deployment. The aim should be to design a (passive) system with the least amount of failure modes possible to increase the reliability of deployment and the survival upon it. This ensures that BAF-MEC-04 and BAF-MEC-04-03 will be met with greater certainty.

The inflatable concept consists of four CGG's , a filter and a valve. Furthermore, the gas has to be vented after the baffle is inflated. This brings about many failure modes and a complex inflation process. The telescopic system is fairly easy compared to the inflatable concept, as it is already rigid in stowed configuration. The deployment itself can be done by spring based actuators, which have proven flight heritage. The complexity in this deployment is the HDRM initiation. The telescopic concept has less failure modes and therefore has a higher scoring weight factor: assumed to be 66.6% for the telescopic concept and 33.4 % for the inflatable concept.

Deployed Stiffness
Deployed stiffness is of importance, since this characterizes the deployed structural integrity of the baffle system. The stiffer the baffle in deployed configuration is, the better it is resistant to thermal flutter, vibrations due to external forces and moments (reaction wheel for example), buckling and shocks as a result of deployment. For an overview, see the N2 diagram, 4.3. Deployed stiffness is almost equally important to stowed stiffness, but is deemed slightly more critical than the stowed stiffness, since the stowed stiffness only effects the multi-axial 30G quasi-static load requirement to survive launch, whereas the deployed stiffness affects the entire 5 year operational period. Obviously, both are important, since if the stowed structure structurally fails due to the 30G launch loads, there will be no mission.

The deployed stiffness of the telescopic boom concept is likely to be higher than that of the inflatable concept since the stiffness and corresponding eigenfrequencies of the inflatable concept depend on how well the rigidization of the aluminium layer occurs. Also, because the wall thickness of the Aluminium-Kapton-Aluminium layer is very thin: 63 µm. Furthermore, the telescopic boom system is already rigid in stowed configuration and the transition from stowed to deployed stiffness is based on an increase in effective length and effective center of gravity of booms and it is based on the locking mechanism of the booms. This is stiffer than the inflatable concept and therefore has a higher scoring weight factor: assumed to be 75% for the telescopic concept and 25 % for the inflatable concept.

Deployment Control
Deployment control is important as well and quite similar to deployment complexity. However, a design can be complex in and of itself, but can at the same time be highly controlled.

The deployment control at this stage for both concepts is assumed to be roughly equal, since for the inflatable concept the control depends the inflation process in which it is not known if inflation will occur at the same velocity in all booms or if some booms inflate faster than others which create momentum change. A very important remark to be made is that the success of the inflatable concept depends on the ability of the system to be rigidized correctly due to pressurization, so that the deployed stiffness, as well as pre-tension of the MLI, conforms to the designed values. The same thought can be applied to the telescopic boom concept, as its actuation system (a strain energy based spring for example) does not have fully controllable deployable characteristics. The deployment of a multitude of actuation systems depend on the HDRM of which not much info is available at this moment. Furthermore, the telescopic boom system can jam due to friction, but local friction can also occur in the inflation concept due to viscosity effects. Since there are roughly equal advantages and disadvantages for both system in terms of deployment control, the scoring weights for both concepts are equal: 50%.

Stowed Stiffness
As said above, the stowed stiffness is almost equally important as deployed stiffness, since the multi-axial 30G quasi-static launch load has to be survived during launch, otherwise the mission would fail.

The telescopic structure is way stiffer, as it is already rigid in stowed configuration. The stowed configuration is also stiffer than its deployed configuration, as the booms are telescopic so it has an even higher area moment of inertia (I_{xyz}) when the booms are stowed and tucked in. The inflatable concept has little stiffness, almost zero as it is not rigidized yet in stowed configuration. Therefore the telescopic structure has a way higher scoring weight: 90% versus 10% for the inflatable concept.

Flexibility
Flexibility is quite important too but not of most importance, since adding flexibility to design is a characteristic requirement (BAF-SYS-09/10). Offering design trimming capabilities for late requirement updates is a nice addition, but even with a design which has no built-in flexibility, the design can still be the most robust and reliant design. However, in a later stage, design iterations are most likely needed to take into account stray-light analyses.

The telescopic concept is more flexible for future addition of stray-light hardware (optimized cones/-vanes) as it has a rigid configuration in both stowed and deployed configuration. This is not the case for the inflatable system, meaning that stray-light cones or vanes or other optimized stray-light mitigation systems (if added in the future) also have to be inflated and rigidized in the future. Therefore, the telescopic concept scores better on this criteria as well: 80% versus 20 %.

Heritage
Feasibility of the deployment system based on heritage is something that normally is of great importance to any mission. That is why COTS systems are normally reliable and economically attractive. However, for the baffle, the individual mechanical criterion are deemed more important than the potential heritage, since the other mechanical criteria can be modelled and verified through analysis above, which gives objective feedback on whether or not the designed mechanical deployment mechanism is able to deploy properly and if it can survive launch- and operational loads. Especially, because a baffle that serves as a heat shield and stray-light mitigation device has not been designed before. Therefore, heritage is taken as the least important scoring criteria.

Heritage is taken to be equal for both concepts: 50% scoring factor for both.

II. Trade-Off Multiple Telescopic Concepts

In this section a detailed textual description of the trade-off between multiple telescopic concepts is made. This is the full description which is roughly summarized in Table 7.9.

Stowed Volume
The stowed volume of concept 2 is worst as it does not meet the stowed volume goal requirement of 0.75 m^3. Namely, the support structure in the middle is not telescopic, but only consists of a mid-hinge. This makes that the support structure, and hence the entire baffle structure cannot be fully stowed. This can also be seen in Figure 7.5. All other three concepts perform equally well on the stowed volume criteria, since they all meet the stowed goal requirement of 0.75 m^3 since concept 1, 3 and 4 all consist of telescopic booms for the support structure. The corresponding scoring weight of all concepts to the stowed volume criterion is then 4.6% for concept 2, while concept 1, 3 and 4 score 31.8 %. All based on the AHP method. The consistency ratio is 0 %, meaning perfectly consistent scoring weight factors.

Mass
Mass of the baffle structure itself for all concepts is roughly equal. However, the actuation system that is needed to actuate the deployment is not. Concept 1 is a 1-DOF system in radial direction so in theory only 1 actuation system is needed to deploy in this degree of freedom, whereas concept 4 is a 8-DOF system in radial direction (all radial booms need to be actuated) and concept 2 and 3 are both also minimally 8-DOF systems. Concept 2 and 3 probably need more actuation systems than 8, as the mid-hinge need to be controlled too. All these extra actuation systems add tremendous mass and based on this, concept 1 scores best followed by concept 4 and then concept 2 and 3 as last. Concept 2 and 3 score equally bad. Concept 1, 2, 3 and 4 score 56.8, 8.8, 8.8 and 23.8 % respectively.

Deployment Complexity/Reliability
Deployment complexity/reliability relates to the failure modes of the system. More failure modes means less reliable system and often is the result of a too complex system. Concept 2 and 3 are by far more complex to deploy due to the extra degree of freedom of the mid-hinge. This results in more than 8 actuators as already discussed above and thus a decrease in reliability. The mid-hinge is therefore not a reliable addition and for concept 2 and 3 score equally bad in terms of deployment complexity. Concept 1 could only have 1 actuation system in theory, while concept 4 needs 8. If the actuation system of concept 1 fails, then the whole baffle

fails to deploy. This can easily be modified by adding another actuator. This was also concluded by prof. dr. ir. J.L. Herder, since sliding of prismatic joints brings about friction, normally due to both the normal force due to gravity and inertia. The normal force is almost zero in space, since micro-gravity is in the order of magnitude of $9.8 \cdot 10^{-6} \frac{m}{s^2}$. However, inertia is still present due to the presence of mass and its distribution. However, the lack of deployment reliability due to friction caused by inertia, could be mitigated by using a multitude of distributed actuation systems. This will also be applied since it results in redundancy and increase in deployment reliability. In that case when one actuator fails, the whole baffle can still be deployed by the other non-failing actuator as the complete structure is rigid and consists of only 1 DOF. However, if one actuation system fails for concept 4, then the other 7 work but the designed octagonal shape cannot be reached no more, as it is an 8-DOF structure in radial direction. Therefore, concept 4 needs all 8 actuation systems to work, while for concept 1 only need 1 to work.

This means that concept one scores best, followed by concept 4 and concept 2/3 (equally bad). This is the same scoring weight as for the mass so the same weight factors are used: Concept 1, 2, 3 and 4 score 56.8, 8.8, 8.8 and 23.8 % respectively.

Deployed/Stowed Stiffness
Concept 1 does not contain any hinges: its configuration remains the same for stowed and deployed state. It consists of 1 telescope for the support structure and two telescopes (3 booms) for the radial direction. Concept 2 also consists of two telescopes in radial direction, but a hinge in the middle and sides without telescope for the support. A telescopic structure in the middle instead of three hinges yields a higher stiffness and thus higher eigenfrequency. Concept 1 is thus better than concept 2. Concept 3 contains both telescope and 3 hinges for the support structure. So this is worse than concept 2. Concept 4 only has the two side hinges, so better stiffness than concept 2 and 3. However, worse than concept 1 since concept 1 only has 1 telescopic boom for the support. The best scoring concept is concept 1 followed by concept 4, concept 2 and concept 3: 56.5, 11.8, 5.5 and 26.2 % respectively.

Deployment Control
Concept 1 has a lower deployment controllability than concept 4, since for concept 4 every boom just needs to be actuated and no friction in the support structure is present due to the side-hinge. Concept 2 and 3 are again equally bad due to the presence of the mid-hinge. The best scoring concept is concept 4 followed by concept 1, concept 2/3: 20.8, 8.9, 8.9 and 61.4 % respectively.

Flexibility
Flexibility is important for later addition of truncated cones/vanes or other stray-light mitigation hardware. Concept 1 has the same shape/configuration both stowed and deployed configuration due to its rigidity, meaning that additional hardware can easily be added. Therefore, concept 1 scores best, followed again by concept 4, followed by concept 2/3 (equally bad again).

The best scoring concept is concept 1 followed by concept 4, concept 2/3: 61.4, 8.9, 8.9 and 20.8 % respectively.

Heritage
The heritage for all concepts is equal since telescopic booms and hinges, so both prismatic- and revolute joints, have been used before in both the space industry as other engineering industries. The scoring weight for all concepts is therefore 25%.

E

Structural Calculations

In this chapter, several structural calculations are derived. The formulas for the equivalent stiffness, mass and corresponding eigenfrequency are derived that are used to verify and cross-check the modal results from ANSYS, as well as the comparison of strength vs weight of cross-sections of different shapes.

I. Equivalent Stiffness of Deployed Telesopic Booms

First off, the deployed telescopic structure is being analysed

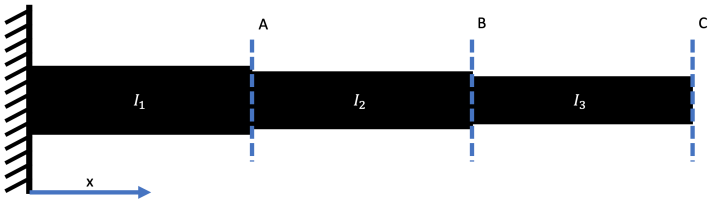

Figure E.1: Schematization of 3 telescopic booms in deployed configuration. As each boom has a different geometry and area their area moment of inertia's change and the stiffness is thus different.

In Figure E.1 the telescopic boom structure is visualized in which A is the length of the largest outer boom, $B-A$ is the length of the middle boom and $C-B$ is the length of the smallest telescopic boom, all in m. I_A, I_B and I_C are their respective area moment of inertias in m^4. The equivalent stiffness can be calculated using:

$$k_{eq} = \frac{F}{\gamma_{eq}} \tag{E.1}$$

In which F is the applied force in N and γ_{eq} the equivalent bending deflection at the tip of the telescopic booms. For this we need to calculate the equivalent bending deflection, which is related to the bending angle.

The bending angle θ at the tip of the total deployed beams can be written as:

$$\theta = \int_0^C \frac{M(x)}{EI(x)}dx = \int_0^A \frac{M(x)}{EI_A}dx + \int_A^B \frac{M(x)}{EI_B}dx + \int_B^C \frac{M(x)}{EI_C}dx \tag{E.2}$$

In this equation $M(x)$ is the applied moment as a function of the measured distance from the base, E and the Young's modulus of the material in Pa. The applied moment as a function of measured base distance is:

$$M(x) = F(L-x) \tag{E.3}$$

Substituting these equations:

$$\theta = \int_0^C \frac{F(L-x)}{EI(x)}dx = \int_0^A \frac{F(L-x)}{EI_A}dx + \int_A^B \frac{F(L-x)}{EI_B}dx + \int_B^C \frac{F(L-x)}{EI_C}dx \tag{E.4}$$

Evaluating this for the first beam:

$$\int_0^A \frac{F(L-x)}{EI_A}dx = \frac{F(Lx-0.5x^2)}{EI_A} + c_1 \tag{E.5}$$

Furthermore, the deflection is simply the integral of the bending angle over the length. Evaluating the bending deflection of just the first beam:

$$\gamma_A = \int_O^A \theta dx = \int_0^A (\frac{F(Lx-0.5x^2)}{EI_A} + c_1)dx = \frac{F(0.5Lx^2 - \frac{1}{6}x^3)}{EI_A} + c_1 x + c_2 \tag{E.6}$$

The constant terms c_1 and c_2 dissapear when evaluating the integral for a defined domain. For the first beam again:

$$\gamma_A = [\frac{F(0.5Lx^2 - \frac{1}{6}x^3)}{EI_A}]_0^A = \frac{F(0.5LA^2 - \frac{1}{6}A^3)}{EI_A} \tag{E.7}$$

The same formulas can be applied to calculate γ_B:

$$\gamma_B = [\frac{F(0.5Lx^2 - \frac{1}{6}x^3)}{EI_B}]_A^B = \frac{F(0.5LB^2 - \frac{1}{6}B^3)}{EI_B} - \frac{0.5FA^2(L - \frac{1}{3}A)}{EI_B} \tag{E.8}$$

And γ_C:

$$\gamma_C = [\frac{F(0.5Lx^2 - \frac{1}{6}x^3)}{EI_C}]_B^C = \frac{F(0.5LC^2 - \frac{1}{6}C^3)}{EI_C} - \frac{0.5FB^2(L - \frac{1}{3}B)}{EI_C} \tag{E.9}$$

So:

$$\gamma_{eq,tot} = \gamma_A + \gamma_B + \gamma_C = \frac{FA^2(3L-A)}{6EI_A} + \frac{FB^2(3L-B)}{6EI_B} - \frac{FA^2(3L-A)}{6EI_B} + \frac{FC^2(3L-C)}{6EI_C} - \frac{FB^2(3L-B)}{6EI_C} \tag{E.10}$$

The equivalent stiffness than becomes:

$$k_{eq} = \frac{F}{\gamma_{eq}} = \frac{1}{16E}[A^2(3L-A)\cdot(\frac{1}{I_A} - \frac{1}{I_B}) + B^2(3L-B)\cdot(\frac{1}{I_B} - \frac{1}{I_C}) + C^2(3L-C)\cdot\frac{1}{I_3}] \tag{E.11}$$

F

Thermal Analyses - Detailed

I. Chapter 5: Various Heights

I.1. Height = 2.5 m

Table F.1: Cylindrical Baffle - Height of 2.5 m

Nominal Temperatures.				
Sub-System	**Max Temperature (° C)**	**Min Temperature (° C)**	**Requirement**	**Reference**
M2	11.0	6.8	$-20°C < T < 50°C$	BAF-T-01-03
Spider	21.5	10.5	$-20°C < T < 50°C$	BAF-T-01-03
PMSS	42.5	30.5	$-20°C < T < 50°C$	BAF-T-01-03
M1	36.7	36.6	$-20°C < T < 50°C$	BAF-T-01-03
Top Hinge	27.0	6.0	$-20°C < T < 50°C$	BAF-T-01-03
Booms	33.9	16	$-20°C < T < 50°C$	BAF-T-01-03
Temperature Gradients				
Thermal Objective Terms	**Value**	**Requirement**	**Unit**	**Reference**
$\Delta T_{booms,avg}$	18.4	≤ 1.4	° C	Table 4.4
$\Delta T_{rods,avg}$	10.1	≤ 0.96	° C	Table 4.4
1. $\frac{\Delta T_{booms,avg}}{\Delta T_{rods,avg}}$	1.8	Between 1.3 - 1.6. Perfect athermal = 1.483	-	Table 4.4
2. $T_{boom,max} - T_{boom,min}$	8.7	≤ 2.3	° C	Table 4.4
3. $T_{rod,max} - T_{rod,min}$	28.1	≤ 0.3	° C	Table 4.4
Thermal Design Objective (1+2+3)	38.6	-	° C	-

I.2. Height = 2.65 m

Table F.2: Cylindrical Baffle - Height of 2.65 m

Nominal Temperatures.				
Sub-System	**Max Temperature (° C)**	**Min Temperature (° C)**	**Requirement**	**Reference**
M2	26.5	25.9	$-20°C < T < 50°C$	BAF-T-01-03
Spider	21.5	12.7	$-20°C < T < 50°C$	BAF-T-01-03
PMSS	48.0	36.0	$-20°C < T < 50°C$	BAF-T-01-03
M1	40.3	40.2	$-20°C < T < 50°C$	BAF-T-01-03
Top Hinge	26.3	9.0	$-20°C < T < 50°C$	BAF-T-01-03
Booms	36.0	18.0	$-20°C < T < 50°C$	BAF-T-01-03
Temperature Gradients				
Thermal Objective Terms	**Value**	**Requirement**	**Unit**	**Reference**
$\Delta T_{booms,avg}$	18.2	≤ 1.4	° C	Table 4.4
$\Delta T_{rods,avg}$	2.8	≤ 0.96	° C	Table 4.4
1. $\frac{\Delta T_{booms,avg}}{\Delta T_{rods,avg}}$	6.5	Between 1.0 - 2.0 . Perfect athermal = 1.483	-	Table 4.4
2. $T_{boom,max} - T_{boom,min}$	5.2	≤ 2.3	° C	Table 4.4
3. $T_{rod,max} - T_{rod,min}$	4.3	≤ 0.3	° C	Table 4.4
Thermal Design Objective (1+2+3)	16.1	-	° C	-

I.3. Height = 2.725 m

Table F.3: Cylindrical Baffle - Height of 2.725 m

Nominal Temperatures.				
Sub-System	**Max Temperature (° C)**	**Min Temperature (° C)**	**Requirement**	**Reference**
M2	32	28.7	$-20°C < T < 50°C$	BAF-T-01-03
Spider	22.0	12.5	$-20°C < T < 50°C$	BAF-T-01-03
PMSS	46.5	35.0	$-20°C < T < 50°C$	BAF-T-01-03
M1	40.9	40.8	$-20°C < T < 50°C$	BAF-T-01-03
Top Hinge	28.0	9.0	$-20°C < T < 50°C$	BAF-T-01-03
Booms	40.0	22.0	$-20°C < T < 50°C$	BAF-T-01-03
Temperature Gradients				
Thermal Objective Terms	**Value**	**Requirement**	**Unit**	**Reference**
$\Delta T_{booms,avg}$	18.2	≤ 1.4	° C	Table 4.4
$\Delta T_{rods,avg}$	3.4	≤ 0.96	° C	Table 4.4
1. $\frac{\Delta T_{booms,avg}}{\Delta T_{rods,avg}}$	5.3	Between 1.1 - 1.9. Perfect athermal = 1.483	-	Table 4.4
2. $T_{boom,max} - T_{boom,min}$	3.8	≤ 2.3	° C	Table 4.4
3. $T_{rod,max} - T_{rod,min}$	7.1	≤ 0.3	° C	Table 4.4
Thermal Design Objective (1+2+3)	16.2	-	° C	-

I.4. Height = 2.9 m

Table F.4: Cylindrical Baffle - Height of 2.9 m

Nominal Temperatures.				
Sub-System	**Max Temperature (° C)**	**Min Temperature (° C)**	**Requirement**	**Reference**
M2	52.3	50.3	$-20°C < T < 50°C$	BAF-T-01-03
Spider	27.1	17.3	$-20°C < T < 50°C$	BAF-T-01-03
PMSS	48.0	36.0	$-20°C < T < 50°C$	BAF-T-01-03
M1	42.5	42.4	$-20°C < T < 50°C$	BAF-T-01-03
Top Hinge	29.3	12.5	$-20°C < T < 50°C$	BAF-T-01-03
Booms	42.3	25.0	$-20°C < T < 50°C$	BAF-T-01-03
Temperature Gradients				
Thermal Objective Terms	**Value**	**Requirement**	**Unit**	**Reference**
$\Delta T_{booms,avg}$	17.6	≤ 1.4	° C	Table 4.4
$\Delta T_{rods,avg}$	4.1	≤ 0.96	° C	Table 4.4
1. $\frac{\Delta T_{booms,avg}}{\Delta T_{rods,avg}}$	4.3	Between 1.1 - 1.8. Perfect athermal = 1.483	-	Table 4.4
2. $T_{boom,max} - T_{boom,min}$	7.4	≤ 2.23	° C	Table 4.4
3. $T_{rod,max} - T_{rod,min}$	8.9	≤ 0.3	° C	Table 4.4
Thermal Design Objective (1+2+3)	20.6	-	° C	-

II. Chapter 7: Octagonal Shape Without Truncated Cone

II.1. One Layer of MLI

Table F.5: Octagonal shape - No truncated cone - 1 layer of MLI

Nominal Temperatures.				
Sub-System	**Max Temperature (° C)**	**Min Temperature (° C)**	**Requirement**	**Reference**
M2	14.8	14.5	$-20°C < T < 50°C$	BAF-T-01-03
Spider	-0.4	-3.9	$-20°C < T < 50°C$	BAF-T-01-03
PMSS	9.4	5.3	$-20°C < T < 50°C$	BAF-T-01-03
M1	12.9	12.9	$-20°C < T < 50°C$	BAF-T-01-03
Top Hinge	13.5	-1.5	$-20°C < T < 50°C$	BAF-T-01-03
Booms	5.8	2.4	$-20°C < T < 50°C$	BAF-T-01-03
Baffle Bottom Outside Avg	120	-90	$-250°C < T < 177°C$	BAF-T-02-01
Baffle Bottom Inside Avg	49	-23	$-250°C < T < 177°C$	BAF-T-02-01
Baffle Side Outside Avg	25	-57	$-250°C < T < 177°C$	BAF-T-02-01
Baffle Side Inside Avg	22	-28	$-250°C < T < 177°C$	BAF-T-02-01
Baffle Outside Max-Min	127	-60	$-250°C < T < 177°C$	BAF-T-02-01
Baffle Inside Max-Min	35	-32	$-250°C < T < 177°C$	BAF-T-02-01
Temperature Gradients				
Thermal Objective Terms	**Value**	**Requirement**	**Unit**	**Reference**
$\Delta T_{booms,avg}$	3.5	≤ 1.4	° C	Table 4.4
$\Delta T_{rods,avg}$	0.4	≤ 0.96	° C	Table 4.4
1. $\frac{\Delta T_{booms,avg}}{\Delta T_{rods,avg}}$	9.5	≤ 5.4. Perfect athermal = 1.483	-	Table 4.4
2. $T_{boom,max} - T_{boom,min}$	0.6	≤ 2.3	° C	Table 4.4
3. $T_{rod,max} - T_{rod,min}$	0.2	≤ 0.3	° C	Table 4.4
Thermal Design Objective (1+2+3)	10.4	-	° C	-

II.2. Two Layers of MLI

Table F.6: Octagonal shape - No truncated cone - 2 layers of MLI

Nominal Temperatures.				
Sub-System	**Max Temperature (° C)**	**Min Temperature (° C)**	**Requirement**	**Reference**
M2	15.0	14.7	$-20°C < T < 50°C$	BAF-T-01-03
Spider	-0.1	-3.5	$-20°C < T < 50°C$	BAF-T-01-03
PMSS	8.9	5.3	$-20°C < T < 50°C$	BAF-T-01-03
M1	12.6	12.5	$-20°C < T < 50°C$	BAF-T-01-03
Top Hinge	13.5	-0.7	$-20°C < T < 50°C$	BAF-T-01-03
Booms	6.1	3.0	$-20°C < T < 50°C$	BAF-T-01-03
Baffle Bottom Outside Avg	120	-98	$-250°C < T < 177°C$	BAF-T-02-01
Baffle Bottom Inside Avg	37	-20	$-250°C < T < 177°C$	BAF-T-02-01
Baffle Side Outside Avg	23	-62	$-250°C < T < 177°C$	BAF-T-02-01
Baffle Side Inside Avg	21	-26	$-250°C < T < 177°C$	BAF-T-02-01
Baffle Outside Max-Min	133	-62	$-250°C < T < 177°C$	BAF-T-02-01
Baffle Inside Max-Min	32	-29	$-250°C < T < 177°C$	BAF-T-02-01
Temperature Gradients				
Thermal Objective Terms	**Value**	**Requirement**	**Unit**	**Reference**
$\Delta T_{booms,avg}$	3.0	≤ 1.4	° C	Table 4.4
$\Delta T_{rods,avg}$	0.3	≤ 0.96	° C	Table 4.4
1. $\frac{\Delta T_{booms,avg}}{\Delta T_{rods,avg}}$	8.9	≤ 5.7. Perfect athermal = 1.483	-	Table 4.4
2. $T_{boom,max} - T_{boom,min}$	0.6	≤ 2.3	° C	Table 4.4
3. $T_{rod,max} - T_{rod,min}$	0.2	≤ 0.3	° C	Table 4.4
Thermal Design Objective (1+2+3)	9.7	-	° C	-

II.3. Three Layers of MLI

Table F.7: Octagonal shape - No truncated cone - 3 layers of MLI

Nominal Temperatures.				
Sub-System	**Max Temperature (° C)**	**Min Temperature (° C)**	**Requirement**	**Reference**
M2	15.1	14.9	$-20°C < T < 50°C$	BAF-T-01-03
Spider	0.1	-3.3	$-20°C < T < 50°C$	BAF-T-01-03
PMSS	8.7	5.4	$-20°C < T < 50°C$	BAF-T-01-03
M1	12.3	12.3	$-20°C < T < 50°C$	BAF-T-01-03
Top Hinge	13.6	-0.3	$-20°C < T < 50°C$	BAF-T-01-03
Booms	6.2	3.5	$-20°C < T < 50°C$	BAF-T-01-03
Baffle Bottom Outside Avg	120	-100	$-250°C < T < 177°C$	BAF-T-02-01
Baffle Bottom Inside Avg	36	-17	$-250°C < T < 177°C$	BAF-T-02-01
Baffle Side Outside Avg	21	-65	$-250°C < T < 177°C$	BAF-T-02-01
Baffle Side Inside Avg	20	-24	$-250°C < T < 177°C$	BAF-T-02-01
Baffle Outside Max-Min	138	-65	$-250°C < T < 177°C$	BAF-T-02-01
Baffle Inside Max-Min	30	-28	$-250°C < T < 177°C$	BAF-T-02-01
Temperature Gradients				
Thermal Objective Terms	**Value**	**Requirement**	**Unit**	**Reference**
$\Delta T_{booms,avg}$	2.8	≤ 1.4	° C	Table 4.4
$\Delta T_{rods,avg}$	0.3	≤ 0.96	° C	Table 4.4
1. $\frac{\Delta T_{booms,avg}}{\Delta T_{rods,avg}}$	8.7	≤ 5.9. Perfect athermal = 1.483	-	Table 4.4
2. $T_{boom,max} - T_{boom,min}$	0.6	≤ 2.3	° C	Table 4.4
3. $T_{rod,max} - T_{rod,min}$	0.2	≤ 0.3	° C	Table 4.4
Thermal Design Objective (1+2+3)	9.4	-	° C	-

II.4. Four Layers of MLI

Table F.8: Octagonal shape - No truncated cone - 4 layers of MLI

Nominal Temperatures.				
Sub-System	**Max Temperature (° C)**	**Min Temperature (° C)**	**Requirement**	**Reference**
M2	15.2	15.0	$-20°C < T < 50°C$	BAF-T-01-03
Spider	0.2	-3.1	$-20°C < T < 50°C$	BAF-T-01-03
PMSS	8.5	5.4	$-20°C < T < 50°C$	BAF-T-01-03
M1	12.2	12.1	$-20°C < T < 50°C$	BAF-T-01-03
Top Hinge	13.8	0.0	$-20°C < T < 50°C$	BAF-T-01-03
Booms	6.4	3.8	$-20°C < T < 50°C$	BAF-T-01-03
Baffle Bottom Outside Avg	125	-100	$-250°C < T < 177°C$	BAF-T-02-01
Baffle Bottom Inside Avg	34	-18	$-250°C < T < 177°C$	BAF-T-02-01
Baffle Side Outside Avg	20	-66	$-250°C < T < 177°C$	BAF-T-02-01
Baffle Side Inside Avg	20	-24	$-250°C < T < 177°C$	BAF-T-02-01
Baffle Outside Max-Min	140	-70	$-250°C < T < 177°C$	BAF-T-02-01
Baffle Inside Max-Min	29	-26	$-250°C < T < 177°C$	BAF-T-02-01
Temperature Gradients				
Thermal Objective Terms	**Value**	**Requirement**	**Unit**	**Reference**
$\Delta T_{booms,avg}$	2.6	≤ 1.4	° C	Table 4.4
$\Delta T_{rods,avg}$	0.3	≤ 0.96	° C	Table 4.4
1. $\frac{\Delta T_{booms,avg}}{\Delta T_{rods,avg}}$	8.4	≤ 6.0. Perfect athermal = 1.483	-	Table 4.4
2. $T_{boom,max} - T_{boom,min}$	0.51	≤ 2.3	° C	Table 4.4
3. $T_{rod,max} - T_{rod,min}$	0.17	≤ 0.3	° C	Table 4.4
Thermal Design Objective (1+2+3)	9.1	-	° C	-

II.5. Five Layers of MLI

Table F.9: Thermal parameters of octagonal shape - No truncated cone - 5 layers of MLI. Chosen in trade-off

Nominal Temperatures.				
Sub-System	**Max Temperature (° C)**	**Min Temperature (° C)**	**Requirement**	**Reference**
M2	15.2	15.0	$-20°C < T < 50°C$	BAF-T-01-03
Spider	0.3	-2.9	$-20°C < T < 50°C$	BAF-T-01-03
PMSS	8.5	5.6	$-20°C < T < 50°C$	BAF-T-01-03
M1	12.1	12.0	$-20°C < T < 50°C$	BAF-T-01-03
Top Hinge	14	0.4	$-20°C < T < 50°C$	BAF-T-01-03
Booms	6.5	4.1	$-20°C < T < 50°C$	BAF-T-01-03
Baffle Bottom Outside Avg	125	-100	$-250°C < T < 177°C$	BAF-T-02-01
Baffle Bottom Inside Avg	34	-17	$-250°C < T < 177°C$	BAF-T-02-01
Baffle Side Outside Avg	20	-69	$-250°C < T < 177°C$	BAF-T-02-01
Baffle Side Inside Avg	20	-22	$-250°C < T < 177°C$	BAF-T-02-01
Baffle Outside Max-Min	140	-70	$-250°C < T < 177°C$	BAF-T-02-01
Baffle Inside Max-Min	28	-26	$-250°C < T < 177°C$	BAF-T-02-01
Temperature Gradients				
Thermal Objective Terms	**Value**	**Requirement**	**Unit**	**Reference**
$\Delta T_{booms,avg}$	2.5	≤ 1.4	° C	Table 4.4
$\Delta T_{rods,avg}$	0.3	≤ 0.96	° C	Table 4.4
1. $\frac{\Delta T_{booms,avg}}{\Delta T_{rods,avg}}$	8.3	≤ 6.2. Perfect athermal = 1.483	-	Table 4.4
2. $T_{boom,max} - T_{boom,min}$	0.5	≤ 2.3	° C	Table 4.4
3. $T_{rod,max} - T_{rod,min}$	0.2	≤ 0.3	° C	Table 4.4
Thermal Design Objective (1+2+3)	8.9	-	° C	-